UNIVERSITY OF NOTTINGHAM

Institute of Engineering Surveying and Space Geodesy

The University of Nottingham

GPS/GALILEO SIMULATION FOR REDUCED DYNAMIC LEO SATELLITE ORBIT DETERMINATION

by

Ashraf Mohamed Ahmed FARAH
BSc (Hons.), MSc (Assiut University, EGYPT)

Thesis submitted to the University of Nottingham for
the degree of Doctor of Philosophy

May 2004

ABSTRACT

Global Navigation Satellite Systems (GNSS) have an endless number of applications in industry, science, military, transportation and recreation & sports. Two systems are currently in operation namely GPS (the USA Global Positioning System) and GLONASS (the Russian GLObal NAvigation Satellite System), and a third is planned, the European satellite navigation system GALILEO. The potential performance improvements achievable through combining these systems could be significant and expectations are high. Computer software can be used to simulate the overall process of GNSS (signal transmission and reception) and produce realistic simulated GNSS measurements. Using such simulated measurements, current and future GNSS systems and possible new applications of GNSS can be investigated. Thus data simulation is the perfect research tool in GNSS fields.

Oceanography, is one application of GNSS, which requires position determination with a high accuracy. LEO satellites are used to measure the precise height of the sea surface for studying the dynamics of the world's oceans. Achieving maximum benefit from the altimetric data collected by LEO satellites requires a radial orbit accuracy of 10 cm or better. It is in determining this orbit where GNSS may be utilised. GPS already delivers high quality position information for LEO satellite orbits such as Topex/Poseidon (1992- present). However LEO satellite orbits determination can still benefit from using GPS combined with GALILEO as there will be more visible satellites and a higher quality of measurements. Investigation of LEO satellite orbit determination using GPS or GALILEO or both systems requires GPS and GALILEO

measurements. Due to the lack of real GALILEO measurements, as the system is still in development, the simulation of GPS and GALILEO measurements is required. In order to generate realistic simulated GPS and GALILEO data, the errors, which predominate in GNSS measurements, must be accurately modelled.

During this research, it has been shown that it is possible to generate realistic simulated GPS data through the more realistic simulation of the ionospheric, tropospheric and multipath delays. Models with a high spatial resolution have been implemented to simulate the real behaviour of the ionosphere and troposphere. The behaviour of the resulting simulated GPS data is shown to follow the behaviour of real GPS data with a strong agreement. It has also been possible to generate GALILEO simulated data through modifying the simulation software using the GALILEO Design technical specifications. The potential impact of using GPS and GALILEO on LEO satellite orbit determination could be investigated on Topex/Poseidon mission which real GPS data was available from the beginning of this study. The performance of GPS, GALILEO, combined GPS/GALILEO and combined GPS-modernised/GALILEO constellations have been investigated in relation to the reduced dynamic orbit determination of the LEO satellite Topex/Poseidon. It can be concluded that the GALILEO constellation will provide high quality real time LEO satellite orbits compared with GPS. GALILEO constellation will provide slightly better quality real time LEO satellite orbits over the combined GPS-present/GALILEO constellation. However the best quality real time LEO satellite orbits will result from the combined GPS-modernised/GALILEO constellation.

ACKNOWLEDGEMENTS

Praise be to ALLAH the most gracious the most merciful, for the bless of finishing this research after almost four years of hard work. I'm very grateful to the Egyptian government and the authorities of South Valley University, Egypt for providing me this chance to get my Ph.D. degree from the University of Nottingham, United Kingdom. The Egyptian embassy in London through her Educational Bureau has paid my tuition fees and provided my living allowance. I appreciate the support provided by the director and the staff of the Educational Bureau.

I am indebted to my research supervisors Prof. Terry Moore and Dr. Chris J Hill from The IESSG, The University of Nottingham for the advice, support and encouragement I have received from them throughout this research. Deep gratitude to all members of IESSG staff and Ph.D. students for their help and support. Special gratitude to Dr. Caroline Noakes for her effort in proof reading the script of the thesis and her valuable comments about it.

The services of the Natural Environment Research Council (NERC) British Isles GPS archive Facility (BIGF), www.bigf.ac.uk, in providing archived GPS data to this project, are gratefully acknowledged.

I am grateful to my wife and lovely daughter "*Rahma*" for the support and encouragement during this tough period of our life.

ACRONYMS AND ABBREVIATIONS

AIUB	Astronomical Institute, University of Bern, Switzerland.
A-S	Anti-Spoofing.
AVISO	Archiving, Validation and Interpretation of Satellites Oceanographic data.
Bernese	Bernese GPS postprocessing software.
BIH	Bureau International de l'Heure.
BIPM	International Bureau of Weights and Measures.
C/A	Coarse-Acquisition code.
CIO	Conventional International Origin.
CODE	Centre for Orbit Determination in Europe.
COSPAS-SARSAT	International Satellite System for Search and Rescue.
CSR	Texas Center for Space Research.
CTRS	Conventional Terrestrial Reference System.
DATSIM	DATa SIMulator software.
DME	Distance Measuring Equipment.
DORIS	Doppler Orbitography and Radio-positioning Integrated by Satellites tracking system.
EF	Earth Fixed Frame.
EGNOS	European Geo-stationary Navigation Overlay Service.
GAS	GPS Analysis Software package.
GAST	Greenwich Apparent Sidereal Time.
GEM	Goddard Earth Model.
GIM's	Global Ionospheric Maps.
GLONASS	Russian GLObal NAvigation Satellite System.
GMDSS	Global Maritime Distress and Safety System.
GMST	Greenwich Mean Sidereal Time.
GNSS	Global Navigation Satellite System.
GPS	Global Positioning System.
GSFC	Goddard Space Flight Center Space Geodesy Branch, University of Texas.
IAU	International Astronomical Union.

ICAO	International Civil Aviation Organization.
IERS	International Earth Rotation Service.
IESSG	Institute of Engineering Surveying and Space Geodesy.
IF	Inertial Frame.
IGS	International GPS Service.
IONEX	IONosphere map EXchange format.
IRI	International Reference Ionosphere model.
ITRF	International Terrestrial Reference Frame.
JGM	Joint Gravity Model.
JPL	Jet Propulsion Laboratory.
JTIDS/ MTIDS	Joint Tactical Information Distribution Systems/Multifunction Information Distribution System.
LEO	Low Earth Orbit.
PRARE	Precise Range And Range Rate Equipment tracking system.
RIM's	Receiver Integrity Monitors.
RMS	Root Mean Square.
RNSS	Radio-Navigation Satellite Systems.
SA	Selective Availability.
SLR	Satellite Laser Ranging.
T/P	Topex/Poseidon LEO-satellite.
TBC	To Be Confirmed.
TBD	To Be Determined.
TDB/TDT	Barycentic Dynamical Time/ Terrestrial Dynamical Time.
TEC	Total Electron Content.
USNO	United State Naval Observatory.
USSA	United States Standard Atmospheres.
UTC	Universal Time Coordinated.
WAAS	Wide Area Augmentation System.
WADGPS	Wide Area Differential GPS.
WGS-84	World Geodetic System-1984.

Contents

List of Figures

List of Tables

CHAPTER 1

Introduction

There are many applications of Global Navigation Satellite Systems (GNSS) in fields such as, industry (Agriculture, Mapping & Geographical Information System (GIS) Data Collection, Public Safety, Surveying and Telecommunications), military (Intelligence & Target Location, Navigation and Weapon Aiming & Guidance), science (Archeology, Atmospheric sciences, Environmental, Geodesy, Geology & Geophysics, Oceanography and Wildlife), transportation (Aviation, IVHS (Intelligent Vehicular Highway Systems) & Fleet Tracking, Marine and Space) and recreation & sports (Land, Sea and Air).

All these applications are solely dependent on GPS (the USA Global Positioning System) at the present time. As these applications are developing and becoming more widely used, mankind is becoming increasingly reliant on GPS services. Thus the assured continuous availability of these services is required. The availability of these services can be enhanced through the use of more than one GNSS. Making the need for GALILEO, another GNSS interoperable with GPS, inevitable. In this thesis's text, the term GALILEO will refer to the European satellite navigation system and is not an acronym.

Simulation is a crucial research tool for present and future GNSS systems. Using computer sciences to develop software which simulates the behaviour of a present (GPS) or future system (GALILEO), new scenarios and applications for present systems can be tested at low cost and the behaviour of future systems (GALILEO) can be explored. Testing the behaviour of such simulation software against the behaviour of present systems (GPS) gives confidence in the findings for future systems.

Different techniques for simulating multi-component GNSS systems are varying in application and complexity. Examples of such techniques are:

1- Service Volume Simulators (SVS) used to give the overall view of the performance levels seen by the user such as the GALILEO Integrity Performance Assessment (GIPA) project (Werner et al., 2001).

2- End-to-End simulators which simulate every aspect of the GNSS system (ground control, space and user segments), may work in real-time and have the ability of testing hardware, such as the GalileoSat System Simulation Facility (GSSF) (Pidgeon et al., 2000) and the NavSim simulation software (Engler et al., 2001).

3- GNSS measurements Simulators, also called Raw Data Generators simulate only one aspect of GNSS systems which is the measurements that would be made by a user receiver for a particular GNSS system, such as SATNAV Toolbox simulator (SATNAV, 1998) developed by GPSoft LLC, University of Calgary simulator (Lou, 2000), Bernese GPS data simulation software

(Hugentobler et al., 2001) and the IESSG-DATa SIMulator (DATSIM) software which is the scope of study for this thesis.

The DATa SIMulator (DATSIM) is the IESSG's in-house developed software used for simulating GPS data. The accuracy of the GPS simulated data depends mainly on the accuracy of the models used to simulate the various types of errors contained in the GPS measurements such as ionospheric delay, tropospheric delay and multipath. The more realistic the error models, the more realistic the simulated data. The software has already been used to successfully simulate GPS data in previous projects (Ashkenazi et al., 1994; 1996; 1997).

Oceanography is one field of application of GNSS systems. Low Earth Orbit (LEO) satellites are used to measure the precise height of the sea's surface when studying the dynamics of the circulation of the world's oceans. Achieving maximum benefit from the altimetric data collected by LEO satellites requires a radial orbit accuracy of 10 cm or better. It is in the determination of those orbits that GNSS systems can play a key role. The two significant LEO missions in this field are Topex/Poseidon (1992-present) and Jason-1 (2001-present).

The main objectives of this research were:

- To improve the performance of the DATSIM software through implementation of more realistic models for simulating the most predominate environmental errors in GPS measurements, namely
    - the ionospheric delay error

- the tropospheric delay error
- the multipath delay error.

- To generate more realistic simulated GPS data.
- To generate simulated GALILEO data through modifying the DATSIM software.
- To investigate the performance of the GPS, GALILEO, combined GPS/GALILEO and combined GPS-modernised/GALILEO constellations in respect of LEO satellite orbit determination (specifically Topex/Poseidon) using GPS and GALILEO simulated data.

This research has resulted in the following software developments:

1. The implementation of an accurate model for simulating the ionospheric delay within DATSIM software based on IGS-GIM's (International GPS Service - Global Ionospheric Maps) which describes the ionosphere's variable behaviour to a high level of accuracy with a reasonable computational time when compared with other available models.
2. The implementation of the EGNOS (European Geo-stationary Navigation Overlay Service) model for simulating the tropospheric delay within DATSIM software, which shows good behaviour compared with IGS-tropospheric estimates and other available tropospheric models.
3. The implementation of an algorithm based on the theory of Gaussian random fields that allows the simulation of the small-scale regional variations within the ionosphere and troposphere resulting in high spatial variation models.

4. The implementation of a more realistic model for simulating the multipath delay within DATSIM software based on Gaussian colored noise.

From use of the improved simulation software in LEO satellite reduced dynamic orbit determination; the following conclusions can be drawn:

1. The GPS broadcast ephemeris error is a limiting factor in providing high quality real time LEO satellite orbits.
2. The GALILEO constellation will provide high quality real time LEO satellite orbits compared with GPS.
3. The GALILEO constellation will provide slightly better quality real time LEO satellite orbits over the combined GPS/GALILEO constellation.
4. The Combined GPS-modernised/GALILEO constellation will provide better quality real time LEO satellite orbits compared with GPS or GALILEO individually.

The thesis contains eight chapters, references section and eight appendices. Chapter 1 gives an introduction for the conducted research stating the objectives and outcomes of the research. Chapter 2 contains a brief description of the GPS system and its error sources. The GALILEO system design architecture and services are presented briefly in Chapter 3. Chapter 4 describes the method of GPS data simulation, detailing the structure of the DATSIM software and discussing the various implemented models through this research which used for simulating the most predominate errors in GPS measurements (ionosphere, troposphere and multipath) with some suggested techniques for improving the behaviour of such models. A comparison study of the

GPS data simulated using the new models with its counterpart using original models along with GALILEO simulated data and real GPS data is presented in Chapter 5 with some concluding remarks. Chapter 6 gives a brief review of the basics of GNSS satellite orbit determination, followed by a discussion of various techniques for LEO satellite orbit determination. Chapter 7 presents an investigation of the reduced dynamic orbit determination with different GNSS constellations (GPS, GALILEO, combined GPS-present/GALILEO and combined GPS-modernized/GALILEO) using different types of simulated data and different scenarios as well as some tests assessing the effect of the quality of GPS ephemeris data and the accuracy of the initial predicted orbit on the reduced dynamic solutions. A validating study is also revealed in Chapter 7 assessing the quality of reduced dynamic orbits using real GPS data and simulated GPS data. Chapter 7 also presents an orbit overlap study as well as some recommendations for real-time applications ending with concluding remarks. Chapter 8 contains the conclusions of the thesis and recommendations for future work. A references section followed with eight appendices discussing in detail various points encountered through the thesis. Appendix H contains some Publications based on the author's research.

CHAPTER 2

Global Positioning System Review

2.1 General Description

The Global Positioning System (GPS) is a satellite-based navigation system made up of a network of nominally 24 satellites placed into orbit by the U.S. Department of Defense. GPS was originally intended for military applications, but in the 1980s, the American government made the system available for civilian use. GPS works in any weather conditions, anywhere in the world, 24 hours a day. There are no subscription fees or setup charges to use GPS (NAVSTAR, 1996).

The NAVSTAR Global Positioning System is a space-based radio positioning and time-transfer system. GPS provides accurate Position, Velocity and Time (PVT) information to an unlimited number of suitably equipped, sea, air and space users. Passive PVT fixes are available worldwide in all-weathers in a worldwide

common coordinate system. Unfortunately, GPS contains some features, which limit the full accuracy of the service to authorized users only and preventing spoofing of the signals.

GPS consists of three major system segments; Space, Control and User. The current (05/07/2004) GPS constellation consists of 28 Block II/IIA/IIR satellites deployed in six orbital planes with an inclination of 55° (http://tycho.usno.navy.mil). Each satellite broadcasts Radio Frequency (RF) ranging codes and a navigation data message. The Control Segment consists of a network of monitoring and control facilities, which are used to manage the satellite constellation and update the satellite navigation data message. The User Segment consists of a variety of radio navigation receivers specifically designed to receive, decode, and process the GPS satellite ranging codes and navigation data messages.

The ranging codes broadcast by the satellites enable a GPS receiver to measure the transit time of the signals and thereby determine the range between each satellite and the receiver. The receiver also calculates the position of each satellite at the time the signals were transmitted from data in the navigation message, and uses this information together with the ranges to determine its own position. Each range measurement defines a sphere centered on a satellite and the point of intersection of these spheres defines the receiver position.

For GPS positioning, a minimum of four satellites are required to be simultaneously in view of the receiver, providing four range measurements, in

order that the receiver can calculate the three unknown coordinates of its position and a fourth parameter representing the user clock error.

2.2 System Overview

2.2.1 Space Segment

The Space Segment is designed to have a minimum of 24 satellites in semi-synchronous (approximately 12 hour) orbits. The satellites are arranged in six orbital planes with four satellites in each plane. The average orbit altitude is 20,200 kilometers above the surface of the earth. Satellites are positioned in the orbital planes so that four or more satellites with a good geometry relationship for positioning will normally be observed at every location on earth. GPS satellites transmit ranging signals on two L-band frequencies: L1 at 1575.42 MHz and L2 at 1227.60 MHz.

The satellite signals are transmitted using spread-spectrum technique with two different ranging codes: A Coarse/Acquisition code (C/A- code) of 1.023 MHz on L1 and a 10.23 MHz Precision code (P-code) on both L1 and L2. Either the P-code or the C/A- code can be used to determine the range between the satellite and the user. The P-code is normally encrypted to become the Y-code and is only available to authorized users. A 50 Hz navigation message is superimposed on both the C/A-code and the P(Y)-code, it includes satellite clock-bias data, satellite ephemeris data for the transmitting satellite, ionospheric signal-propagation correction data, and the satellite almanac (coarse orbital data) for the entire constellation (NAVSTAR, 1996).

2.2.2 Control Segment

The Control Segment consists of a Master Control Station (MCS) at Falcon Air Force Base (AFB) in Colorado Springs, USA, plus monitor stations and ground antennas at various locations around the world. The main processing facility for the control segment is the MCS, which monitors and manages the satellite constellation. Its functions include control of satellite manoeuvers, reconfiguration of redundant satellite equipment and regularly updating the navigation messages transmitted by the satellites. The monitor stations track all GPS satellites in view, collecting ranging data from each satellite. This information is sent to the MCS where the satellite ephemeris and clock parameters are estimated and predicted. The ground antenna is used to periodically upload the ephemeris and clock data to each satellite for re-transmission in the navigation message (NAVSTAR, 1996).

2.2.2.1 GPS Reference Time System

GPS measurements are intrinsically dependent on time. The measured time elapsed from when the signal leaves the satellite to when it reaches the receiver is used to compute the pseudo-range. The GPS system uses its own particular time scale, GPS time. The GPS time is an atomic time scale which has the same unit (seconds) as UTC (Coordinated Universal Time). GPS time was coincident with UTC on January 6, 1980. The relationship between UTC and GPS time is available in time bulletins of the USNO (United States Naval Observatory) and the BIPM (International Bureau of Weights and Measures) as well as the GPS satellite message (Seeber, 1993).

2.2.2.2 GPS Reference Frame

GPS uses the World Geodetic System WGS-84 reference frame to provide the basic frame of reference for the description of the satellite motion, the modelling of the observations, and the representation and interpretation of results in an Earth-centered, Earth-fixed system (Seeber, 1993). The origin and axes of WGS-84 were adopted from the Conventional Terrestrial System (CTS), which was defined by the former Bureau International de L'Heure (BIH) until (January 1, 1988) and is now defined by the International Earth Rotation Service (IERS). For more details of WGS-84 the reader is referred to NIMA (2002).

2.2.3 User Segment

The User Segment consists of receivers designed to receive, decode, and process the GPS satellite signals. These receivers can be stand-alone, integrated with or embedded into other systems. GPS receivers can vary significantly in design and function depending on their application e.g. navigation, accurate positioning, time transfer, surveying and attitude reference.

2.3 GPS Services

2.3.1 Precise Positioning Service

The Precise Positioning Service (PPS) is an accurate positioning, velocity and timing service but it is only available to authorized users and was intended for military purposes. The PPS uses the P-code on both frequencies L1 and L2, and the C/A code on L1 frequency. The PPS is specified to provide 16 metres

Spherical Error Probable (SEP) (3-D, 50%) positioning accuracy and 100 nanosecond Universal Coordinated Time (UTC) time transfer accuracy, this is approximately equal to 37 metres (3-D, 95%) and 197 nanosecond (95%) under typical system operating conditions (Kaplan, 1996).

Use of the PPS is controlled by two controlling features based on cryptographic techniques, namely Selective Availability (SA) and Anti-Spoofing (A-S). SA was used to reduce the accuracy of GPS positioning, velocity, and time to unauthorized users by introducing pseudo-random errors into the satellite signals. However, SA was reduced to zero on the second of May 2000. The A-S feature is activated on all satellites to negate potential spoofing of the ranging signals. This feature encrypts the P-code into the Y-code. Encryption keys are provided to PPS users, which allow them to remove the effects of SA (if it is there) and A-S and thereby attain the maximum accuracy of GPS.

2.3.2 Standard Positioning Service

The SPS service is available to all GPS users but it is a less accurate positioning and timing service. The level of SA was controlled to provide 100 metre (95%) horizontal accuracy which is approximately equal to 156 metres 3D (95%). The SPS can also achieve approximately 337 nanosecond, (95%) UTC time transfer accuracy. The SPS is primarily intended for civilian purposes. Thus it uses the C/A code on L1 frequency only. The performance of the SPS service improved greatly after SA was reduced to zero, giving a global average positioning domain accuracy of 33 metres 95% horizontal error and 73 metres 95% vertical error with time transfer accuracy of 40 nanoseconds 95% (GPS-SPS, 2001).

2.4 GPS Observations

There are two types of GPS observations: (i) pseudo-range, which is primarily used for navigation and (ii) carrier phase, used for high precision positioning applications.

2.4.1 Pseudo-range Observations

The time difference between the transmitted and received GPS signal, obtained via a code correlation process, multiplied by the speed of light in a vacuum gives the pseudo-range between the satellite and the receiver. As there are some errors in the synchronization of the satellite and receiver clocks with each other and with GPS time (§ 2.2.2.1), the resulting distance is called a "pseudo-range", not the true range.

The basic pseudo-range observation equation can be given as:

$$\rho = \rho_t + c(dT - dt) + d\rho_{ion} + d\rho_{trop} + \Delta(\rho), \qquad (2.1a)$$

where,

ρ : observed pseudo-range measurement,

ρ_t : true range,

c : speed of light in a vacuum,

dt : the offset of the satellite clock from GPS time,

dT : the offset of the receiver clock from GPS time,

$d\rho_{ion}$: ionospheric error,

$d\rho_{trop}$: tropospheric error,

$\Delta(\rho)$: pseudo-range noise and multipath.

The true range is a function of the receiver and the satellite positions. The satellite positions are obtained using the satellite ephemeris and the satellite clock correction parameters which are given in the broadcast navigation message. When the ionospheric and tropospheric errors are modelled properly, the only unknowns left are the receiver clock bias and the coordinates of the receiver position, so the observed pseudo-range measurement can be expressed as:

$$\rho = \rho_t + c(dT - dt) + \Delta(\rho) \tag{2.1b}$$

with $$\rho_t = \sqrt{(X^s - X_r)^2 + (Y^s - Y_r)^2 + (Z^s - Z_r)^2}\,, \tag{2.2}$$

where

(X^s, Y^s, Z^s) : the satellite coordinates,

(X_r, Y_r, Z_r) : the receiver coordinates.

As a result of equation (2.2) at least four satellites are required to provide four observations to solve for the four unknowns (three receiver position coordinates and one receiver clock bias). The un-modelled errors such as multipath and measurement noise are assumed to be random and are included as a residual term in a least squares solution.

2.4.2 Carrier Phase Observations

The carrier phase observable can be obtained by removing the code from the incoming signal. The approximate wavelengths of the carrier frequencies are 19 cm and 24 cm for LI and L2 respectively. The phase difference of the carriers can be accurately measured to better than 0.01 cycle, which with wavelength of about 20 cm equates to millimeter precision. As a result, it is possible to obtain very precise positioning using the carrier phase observable. The distance between the satellite and the receiver is obtained by measuring the fractional part of the carrier phase, plus the total number of cycles between the satellite and the receiver such that:

$$\lambda\Phi = \rho_t + c(dT - dt) - \lambda d\Phi_{ion} + \lambda d_{trop} - \lambda N + \Delta(\Phi), \qquad (2.3)$$

where

Φ : carrier phase measurements,

$d\Phi_{ion}$: ionospheric error on carrier measurements,

$d\rho_{trop}$: tropospheric error on carrier measurements,

λ : carrier wavelength,

N : integer ambiguity,

$\Delta(\Phi)$: carrier phase measurements noise and multipath.

The receiver is able to count the change in the number of cycles but not the number of cycles traveled through before the receiver starts to count the cycles, which is referred to as the 'integer ambiguity'. The integer ambiguity remains the same as long as the receiver phase lock loop is maintained. If the signal is lost,

resulting in a 'cycle slip', the integer ambiguity needs to be computed again. The cycle slip and integer ambiguity problems have been intensively studied in order to attempt to provide a high accuracy service, Ashkenazi et al. (1989), Walsh (1994) and Teunissen et al. (1995).

2.5 Error Sources

The GPS measurements are subject to three main types of errors; gross errors, systematic errors and random errors. Gross errors are those which are outliers in the observation model. The systematic errors must be removed from the observations to avoid introducing biases to the results. These errors have some physical or mathematical relationship with the measurements and can be modelled as additional terms in the observation equation, or eliminated by appropriate combinations of the observations. The random errors are the discrepancies remaining after the systematic errors and gross errors have been removed. The GPS systematic errors are described in the following sections according to their source.

2.5.1 Satellite Dependent Errors

- **Satellite Orbital Error**

The position of the satellite is required to form the GPS observation equations (see equation (2.2)). The satellite orbit information is provided through the broadcast ephemeris in the navigation message. The positions of the satellites are treated as known parameters during GPS data processing to solve for the unknown receiver position. Therefore any error in the satellite positions

propagates directly into the calculated coordinates of the receiver. The accuracy of the satellite position given in the broadcast ephemeris is in the range of (5 – 10) metres (Jefferson and Bar-Sever, 2000). Alternatively, more ephemeris data can be obtained for post-processing GPS measurements. The IGS offers different types of GPS ephemeris with different accuarcies. The accuracy of the IGS final precise ephemeris is estimated at approximately 5 cm (IGS, 2003) but is only available after a 13 days delay.

- **Satellite Clock Error**

GPS satellites carry both rubidium and caesium atomic frequency standards. The clocks are physically left to drift off the GPS time but their drift is monitored by the control segment. The clock error dt is included in the broadcast navigation message in the form of a second order polynomial such that:

$$dt = a_0 + a_1(t - t_{oc}) + a_2(t - t_{oc})^2, \tag{2.4}$$

Where,

t_{oc} is the reference epoch (seconds),

a_0 is the satellite clock time offset (seconds),

a_1 is the fractional satellite clock frequency offset (sec/sec),

a_2 is the fractional satellite clock frequency drift (ageing term) (sec/sec^2).

The size of the satellite clock bias without corrections is of the order of 7 ns, corresponding to 2.6 m in terms of range (IGS, 2003).

- **Relativistic Effects**

The satellite clock is affected by both special relativity and general relativity. The special relativity is due to the satellite's velocity, whereas the general relativity is due to the drift in the gravitational potential at the satellite's position relative to the gravitational potential at the Earth's surface. These effects are accounted for by offsetting the fundamental frequency of the receiver clocks (10.23 MHz) by 0.0045674 Hz (Baker, 1998).

2.5.2 Receiver Dependent Errors

- **Receiver Clock Error**

Most GPS receiver clocks are based on quartz oscillators and are inferior to those onboard the satellite. The receiver clock error which biases measurements with respect to GPS time are, however, removed when observations are differenced with respect to two satellites.

- **Antenna Phase Center Variations**

The phase center of an antenna is the electrical point to which the GPS satellite signal is referred and generally is not identical to the geometric center of the antenna. The offset is dependent on the elevation, azimuth and intensity of the satellite signal and is different for the L1 and the L2 observations (Hofmann-Wellenhof et al., 2000).

2.5.3 Signal Path Dependent Errors

GPS measurements are subject to errors when the signal passes through the earth's atmosphere which not only bends the ray, but also slows it (Dodson et al., 1992). The errors are due to two components: (i) the excess path length due to propagation delay and (ii) the excess path length due to bending, noting that the bending effect is usually not significant except at low elevation angles. In most geodetic purposes, these errors can be satisfactory modelled (Dodson, 1986). The propagation delay is estimated by the integral of the atmospheric refractive index along the signal path. The atmosphere can be considered as two distinct components, namely the ionosphere and the troposphere, which have different physical characteristics and should be modelled separately.

- **Ionospheric Errors**

The GPS signals are affected by the ionised medium when propagating through the ionosphere, which results in a frequency dependent non-linear dispersion of the signal. The relationship between the refractive index n, of the ionosphere and the frequency is given by (Dodson, 1986) as,

$$n = 1 \pm \frac{A_1 N_e}{f^2} + \text{higher order terms,} \tag{2.5}$$

where,

A_1 is a constant (40.3 if using S.I. units) (m^3/s^2)

N_e is the free electron density in the ionosphere (electron/m^3),

f is the frequency of the signal (Hz).

The sign $\pm$ in equation (2.5) is determined by which observable is considered. The ionosphere delays the GPS code signal resulting in, the observed range being too long and hence the positive sign is used. However, the ionosphere advances the carrier phase, resulting in the observed carrier phase range being too short and thus the negative sign is applied. The ionospheric delay error vary from tens of centimeters to tens of meters depending on the Total Electron Content (TEC) along the signal path through the ionosphere. Since the ionospheric delay is dependent on the signal frequency, the delay can be estimated through the combination of dual frequency observations.

- **Tropospheric Error**

The troposphere is not a dispersive medium at radio frequencies, unlike the ionosphere, so the use of the combination of dual frequency measurements to estimate the tropospheric delay cannot be applied. The tropospheric delay T_r^s (metres) is equivalent to the integral of the refractive index along the tropospheric signal path, which can be given as,

$$T_r^s = 10^{-6} \int_a^b N ds \quad , \tag{2.6}$$

where,

$N = (n-1) \times 10^6$, is the refractivity,

a and b define the limits of the troposphere boundary.

2.5.4 Cycle Slips and Multipath

A cycle slip is caused by the loss of lock in the phase-lock loop, generating a discontinuity in the accumulation of the integer number of cycles. Loss of lock may occur for many reasons: obstruction of the satellite signal, low signal-to-noise ratio (SNR) due to atmospheric disruption, multipath, high receiver dynamics and low satellite elevation, and receiver software failure (Hein, 1990). The cycle slips have to be detected and repaired to avoid any bias in the measurements.

The multipath effect is caused by the arrival of the signal at the receiver via more than one path due to the presence of reflecting surfaces near the receiver. Multipath can also occur due to reflections at the satellite itself during signal transmission. While both code and carrier measurements are affected by multipath, the effect on code is two orders of magnitude larger than on carrier phase observations (Seeber, 1993).

As multipath effects depend on the receiver's surrounding environment, there is no general model to correct for these effects. However, when the same environmental conditions exist, repetitive patterns can be found in many cases from day to day static observations. Possible ways to minimize multipath effects are: carefully chosen receiver sites, carefully designed antennas and accessories such as ground planes and choke rings.

2.6 Atmospheric Effects on GPS Observables

2.6.1 The Atmosphere

The atmosphere mainly composed of two layers namely the *ionosphere* and the *neutral atmosphere*, every layer has its own divisions and characteristics as illustrated in Figure 2.1 after (Shardlow, 1994).

2.6.1.1 The Ionosphere

The ionosphere is the upper layer of the atmosphere that extends from about 50 km to approximately 1000 km. Surprisingly the ionosphere makes up less than 1 % of the mass of the atmosphere above 100 km. Even though it is only contains a small fraction of atmospheric material, it is very important because of its influence on the passage of radio waves (GPS signals). Most of the ionosphere is electrically neutral, but when solar radiation strikes the chemical constituents of the atmosphere electrons are dislodged from atoms and molecule to produce the ionosphere plasma. This occurs on the sunlit side of the earth and only the shorter wavelengths of solar radiation are energetic enough to produce this ionisation. The presence of these charged particles makes the upper atmosphere an electrical conductor, which supports electric currents and affects radio waves. Various regions have been identified within the ionosphere each with its own characteristics. For more information about these regions and detailed characteristics of the ionosphere's regions, the reader is referred to Taylor (1961), Jursa (1985), Davis (1989), Kelly (1989), Hargreaves (1992) and Komjathy (1997).

Altitude (km)	Nomenclature		Characteristics
1000	**IONOSPHERE**		**Charged Particles (ions)** **Dispersive Medium** **Spatially Non-uniform**
50	**STRATOSPHERE**	**NEUTRAL ATMOSPHERE**	**Neutral Medium** **(Non-ionised)**
16	**Tropopause**		
8	**TROPOSPHERE**		**75 % of total molecular or gaseous mass of atmosphere** **water vapour content small but extremely variable**
1	**Boundary Layer**		

Figure 2.1: Atmosphere Classification (Shardlow, 1994).

2.6.1.2 The Neutral Atmosphere

This layer is the non-ionized layer of the atmosphere, ranging from the earth's surface to approximately 50 km above it. It consists of the boundary layer, the troposphere, the tropopause and the stratosphere.

2.6.1.2.1 The boundary layer

The boundary layer, is the lowest kilometer of the atmosphere and also the most active region since it experiences diurnal changes. The interactions with the earth's surface provide the atmosphere with both water vapour and heat exchange. These interactions drive the diurnal temperature cycle.

2.6.1.2.2 The Troposphere

The Troposphere ranges from zero to about 10 km in altitude including the boundary layer. It contains approximately 75% of the total molecular or gaseous mass of the atmosphere and virtually all of the water vapour and aerosols. There are no significant variations in the composition of dry air with latitude or with height (Smith and Weintraub, 1953). Although the water vapour content is small, it is extremely variable both in latitude and in height, but reduces to zero above 10 km (Hopfield, 1971).

2.6.1.2.3 The Tropopause

The tropopause is a region that is isothermal with altitude and it can be defined as the lowest level at which the lapse rate decreases to less than, or equal to 2^{o} C/km (provided that the average lapse rate of the 2 km layer above does not exceed 2^{o} C/km (Barry and Chorley, 1986). This layer is not constant in space or time,

because its maximum altitude at any point appears to be correlated with sea-level temperature and pressure.

2.6.1.2.4 The Stratosphere

This is the layer above the tropopause and it is ranging from 10 to 50 km in altitude. It contains much of the total atmospheric ozone. The temperature tends to increase with altitude in the stratosphere.

2.6.1.2.5 Terminology

In talking about GPS, the atmosphere is often divided provisionally into the ionosphere and the neutral atmosphere, following this division each of the two layers is modelled separately because of their different characteristics. The propagation delay experienced in the neutral atmosphere is often termed the tropospheric delay because 80 % of the delay can be attributed to the troposphere (Hopfield, 1971). So through the rest of this thesis the term tropospheric delay will refer to the propagation delay experienced in the lower 50 km of the atmosphere, i.e. the neutral atmosphere.

2.6.2 Radio Wave Propagation

The sun's electromagnetic radiation is a continuum that spans radio wavelengths through infrared, visible, ultraviolet, x-ray, and beyond. Photo ionisation process occurs when ultraviolet radiation interacts with upper atmospheric constituents to form an ionised layer called the ionosphere.

The ionosphere affects radio signals in different aspects depending on their frequencies, which range from extremely low (ELF) to extremely high (EHF) see

Figure 2.2. The ionosphere may act as an efficient reflector for frequencies below about 30 MHz, allowing radio communications to distances of many thousands of kilometres. Whereas radio signals on frequencies above 30 MHz usually penetrate the ionosphere and therefore are useful for ground–to-space communications. The ionosphere plays an essential role for many radio-wave navigation systems including terrestrial based system such as Loran-C and Omega and space-based systems (GPS, GLONASS and GALILEO). Omega navigation requires it, Loran tries to work around it, and GPS is hindered by it. Unlike the low-frequency radio transmissions used by terrestrial systems, GPS uses radio signals that pass through the ionosphere (see Figure 2.3). The ionosphere is neither homogenous in structure nor constant over time (Davis, 1989). Solar and geomagnetic activity affects the character of the ionosphere and, consequently, the proper function of navigation systems.

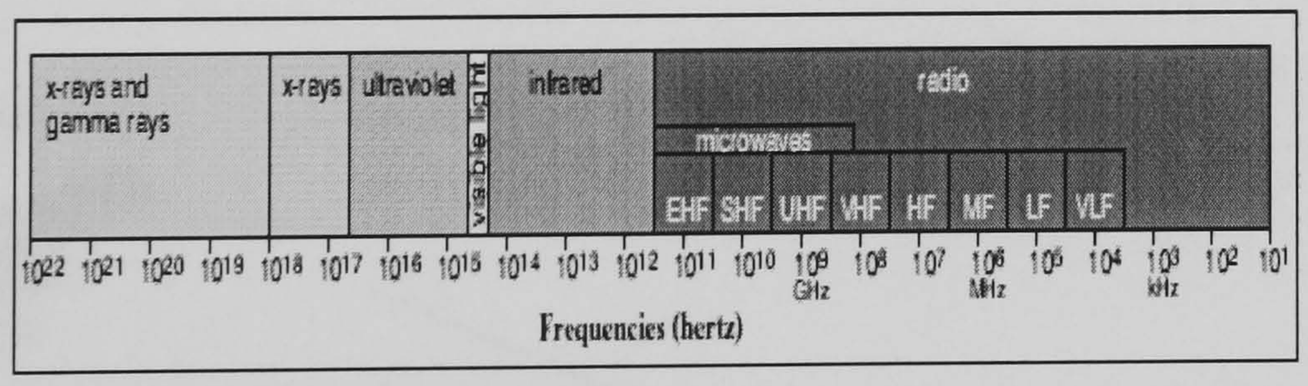

Figure 2.2: The electromagnetic spectrum includes x-rays, Visible light and radio waves (SEC, 2003).

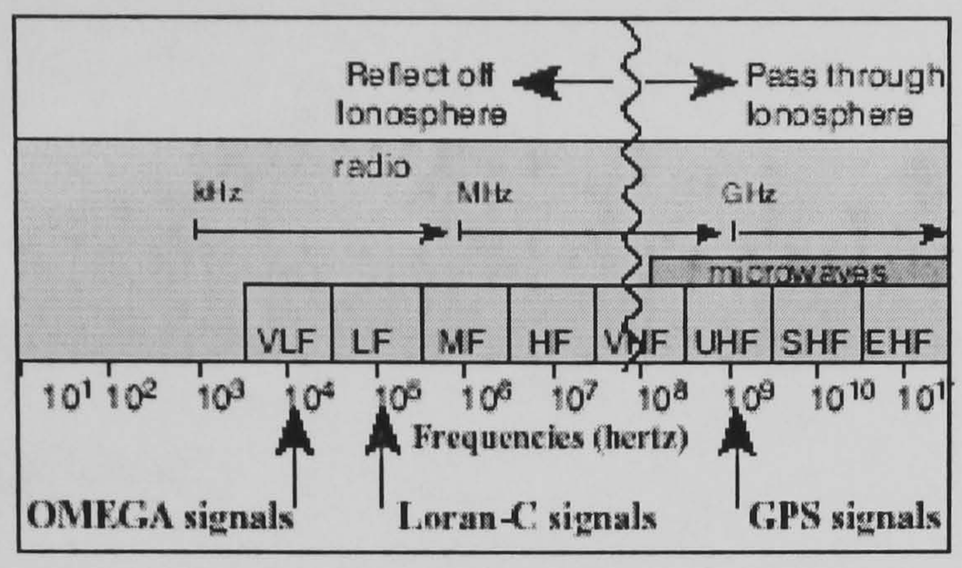

Figure 2.3: The Frequencies of the most common navigational systems (SEC, 2003).

2.6.3 Atmospheric Effects on GPS signals

Accurate GPS observables require the microwave signals to travel through the atmosphere in a geometrically straight line, but this is not the case. Due to the characteristics of the atmosphere, the signal faces two effects, bending and slowing in its way, see Figure 2.4.

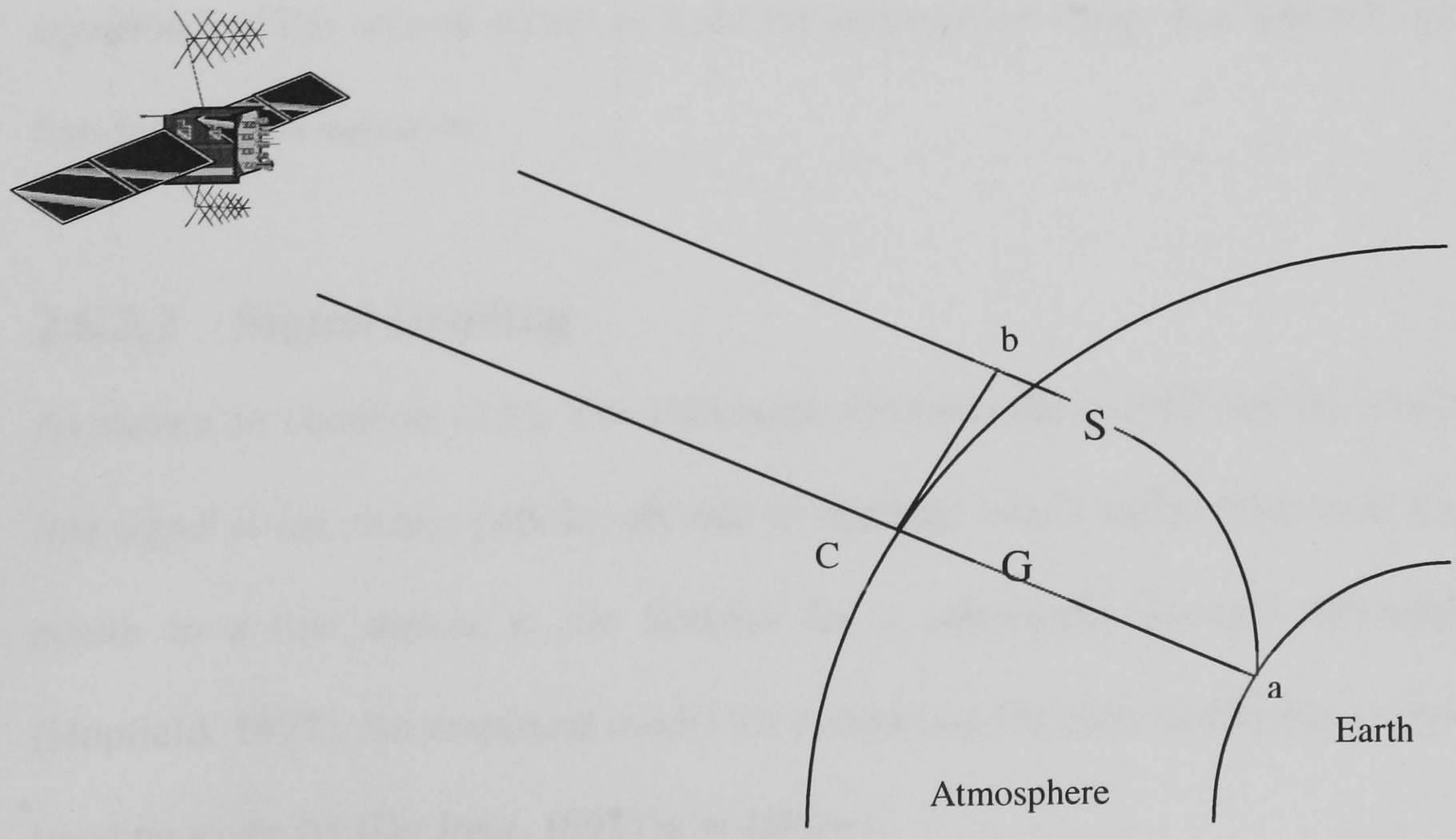

Fig. 2.4: GPS Signal Geometry (Shardlow, 1994).

The straight line geometrical distance, can be expressed as:

$$G = \int_a^c dG \quad , \tag{2.7}$$

and the minimum electrical path length , L (according to Fermat's principle) (Brunner, 1992) is given as:

$$L = \int_a^b n\, ds \quad , \tag{2.8}$$

where,

n : the varying refractive index of the atmosphere.

From the two equations (2.7) and (2.8), the excess path length will be,

$$L - G = \int_a^b (n - 1) ds + (S - G). \tag{2.9}$$

From equation (2.9), the atmospheric delay in the signal comes from two sources, the first source is due to signal bending which appears as the second term of the equation and the second source is from the propagation delay that appears as the first term of the equation.

2.6.3.2 Signal Bending

As shown in equation (2.9), The difference between the curved and the straight line signal is the excess path length due to bending, which varies from zero at the zenith to a few meters at the horizon for a spherically layered atmosphere (Hopfield, 1977). An empirical model for computing the path length due to signal bending given by (De Jong, 1991) is as follows,

$$b(\varepsilon) = \frac{1.92}{\varepsilon^2 + 0.6} \quad , \tag{2.10}$$

where, $b(\varepsilon)$ = Excess path length due to signal bending (m),

ε = Elevation of the satellite in degrees.

From this model, it was recommended using a cut-off elevation angle of [10-15°] for two benefits: the difficulty of modelling the troposphere at low elevation angles and the need for taking into account the effect of signal bending vanishes (De Jong, 1991).

2.6.3.2 Propagation Delay

The propagation delay can be expressed as,

$$\Delta S = 10^{-6} \int_a^b N ds \quad , \tag{2.11}$$

where, $N = (n-1) \times 10^6$

n : the refractive index of the atmosphere.

The propagation delay is considered to be the main source for the atmospheric delay. The propagation delays due to the ionosphere and the troposphere will now be discussed separately.

2.6.4 Ionospheric Effects on GPS

As shown in equation (2.5), the ionospheric delay is directly proportional to the free electron density in the ionosphere, and inversely proportional to the square of the frequency of the signal. An accurate estimate for the refractive index n depends on accurate knowledge of the free electron density along the signal path which is governed by the activity of the sun. Solar activity has an average period

of about 11 years, the last maximum solar activity was during 2000 (Thompson and Kunches, 2002). The ionospheric delay is considered one of the main sources for observable bias for single frequency GPS users. During the maximum ionospheric activity, the ionospheric delay could be of order 300 ns, which yields around 100 meters error in range (Newby and Langley, 1992).

2.6.4.1 Ionospheric Models

A range of ionospheric models have been developed, varying in accuracy, input data and computational complexity, so the choice between these different models depends on the circumstances of the user. An overview of the most well-known models is given below.

2.6.4.1.1 The Bent Model

The Bent model (Llewellyn and Bent, 1973) is an empirical worldwide algorithm, capable of accurately estimating the electron density profile and the associated delay along with directional changes of the wave due to refraction. Designed originally for ground-to-satellite communications, it can also be used for ground-to-ground or satellite-to-satellite communications. The required input data for the model consists of the satellite and station positions, time information, daily values of solar flux, and the 12-month running averages of solar flux and Zurich sunspot numbers. (Newby and Langely, 1992) found that Bent model could accounts for up to 80% of the total ionospheric delay, however this is a computationally demanding model requires regular updating of large amount of solar flux and Zurich sunspot numbers input data (not recommended for GPS Data simulation purposes).

2.6.4.1.2 The Klobuchar Model

The Klobuchar model (Klobuchar, 1982), was designed based on the Bent model, and is now considered the most widely used model due to its computational simplicity. The model is built on a simple cosine representation of the ionospheric delay, with a fixed phase-zero at 14.00 hours local time and a constant night time offset of 5 nanoseconds. The period and amplitude of the ionospheric delay are represented as third degree polynomials in local time and geomagnetic latitude. The eight time-varying coefficients of the two polynomials are broadcast in the GPS navigation message, and are updated daily. These coefficients are selected from 370 possible sets of constants by the GPS master control station and placed in the satellite upload message for downlink to the user. These coefficients are based on two parameters, day of the year and average solar 10.7-cm flux value (the solar flux density at 10.7cm wavelength) for the previous five days.

The model assumes an ideal smooth behaviour of the ionosphere, therefore any significant fluctuations from day to day will not be modelled properly. The accuracy of the model is limited to 50-60% of the total effect (Dodson, 1988). Under special circumstances, such as severe ionosphere activity at low elevations, the range error can be of order of 50 m (Newby et al., 1990).

2.6.4.1.3 The Klobuchar Model with CODE coefficients

CODE, the Center for Orbit Determination in Europe, acts as one of five so-called Ionosphere Associated Analysis Centers of the International GPS Service (IGS), currently generating ionospheric coefficients compatible with the Klobuchar model and the related algorithm as declared by the GPS ICD (Rockwell

International Corporation, 1993). This method takes advantage of global TEC map information in IONosphere map EXchange (IONEX) format (Schaer et al., 1998c) that is derived by the CODE analysis center. Based on a 60-day comparison study analyzing (root mean square) rms difference, the performance of the Klobuchar model with CODE-coefficients is better by roughly a factor of 1.5 than the Klobuchar model with GPS navigation message-coefficients with respect to the highly accurate-CODE final global TEC maps (Schaer, 2001). These CODE coefficients can be accessed via the internet.

2.6.4.1.4 The IRI Model

The International Reference Ionosphere (IRI) is an international project sponsored by the Committee on Space Research (COSPAR) and the International Union of Radio Science (URSI), which formed a working group in the late sixties to produce an empirical standard model for the ionosphere, based on all available data sources from the worldwide network of ionosondes. The IRI was developed by K. Rawer and others (Rawer, 1981). For given location, time and date with a safe range of altitude below 1000 Km, IRI describes many ionospheric variables, mainly the electron density and others. Several steadily improved editions of the model have been released, IRI-90 (Bilitza, 1990), IRI-95 (Bilitza et al., 1993) and IRI-2000 (Bilitza, 2001). The IRI-95 model can run via the Internet [http://nssdc.gsfc.nasa.gov/space/model/models/iri.html]. Tests have shown that the IRI-95 model performs better than the IRI-90 model in computing the ionospheric delay for the single-frequency altimeters (Urban, 1997).

2.6.5 Tropospheric Effects on GPS

The most widely used formula for tropospheric refractivity N is the Smith and Weintraub (1953) simplified two-term formula:

$$N = 77.6\frac{P}{T} + 3.73 \times 10^{5}\left(\frac{e}{T^{2}}\right), \tag{2.12}$$

where,

P : the total atmospheric pressure in (mbar),

T : temperature in Kelvin,

e : partial pressure of water vapour (mbar).

Two basic types of models exist that relate the parameters in equation (2.12) to either empirical Surface Meteorological (SM) measurements (*surface meteorological models*) or global standard atmospheres (*global empirical models*). Other considerations relate to the mapping function used to account for elevation angle dependent variations. Surface meteorological models, global empirical models and mapping functions will be discussed in the following sections.

2.6.5.1 Surface Meteorological models

These models are based on radiosonde profiles and relate the parameters of equation (2.12) to measurements taken at the ground surface. The most well known models are the Hopfield and Saastamoinen models. A description of these and some other models will follow.

2.6.5.1.1 Hopfield (1971)

This model was developed using a large number of sonde profiles recorded at a variety of geographical locations over a number of years. It is based on a single-

layer polytropic model atmosphere extending from ground level to approximately 40 km. The model gives the following expression for the zenith hydrostatic delay (the first term on the right-handed side of equation (2.12)),

$$S_{zh} = 10^{-6} K_1 \frac{P_s}{T_s}\left[\frac{h_h - h_s}{5}\right], \tag{2.13}$$

where,

K_1 : 77.61 (K/mbar),

P_s : surface pressure (mbar),

T_s : absolute surface temperature (K),

h_h : the height of the hydrostatic neutral atmosphere (km),

h_s : the station height above sea level (km).

The zenith wet delay is given by,

$$S_{zw} = 10^{-6}\left[(K_2 - K_1).\ 273 + K_3\right]\frac{e_s}{T_s}\ .\ \frac{h_w - h_s}{5}, \tag{2.14}$$

where,

K_2 : 71.6 (K/mbar),

K_1 : 77.61 (K/mbar),

K_3 : 3.747 x 10^5 (K^2/mbar),

e_s : surface partial water vapour pressure (mbar),

T_s : absolute surface temperature (K),

h_w : height of the wet troposphere (km),

h_s : the station height above sea level (km).

The hydrostatic component accuracy is approximately 7 mm, but the wet component is only accurate to 3-5 cm (Janes et al., 1989).

2.6.5.1.2 Saastamoinen (1973)

This model is based on two assumptions, the first that temperature in the troposphere changes linearly with altitude and remains constant in the stratosphere and the second that the decay of water vapour pressure in the troposphere follows the standard exponential form. The model gives the following expressions for the hydrostatic and wet components of the zenith delay respectively,

$$S_{zh} = 0.002276\, P_s \ , \tag{2.15}$$

$$S_{zw} = 0.002276\left[\frac{1255}{T_s} + 0.05\right] e_s \, . \tag{2.16}$$

The hydrostatic component accuracy is in the region of 2-3 mm. Similarly to the Hopfield model, the wet component accuracy is 3-5 cm (Saastamoinen, 1973).

2.6.5.1.3 The Black Model

Black, (1978) developed a model, which is a modification of the Hopfield model. The model uses constants to define water vapour in the refractivity model depending on season and latitude whereas Hopfield uses model uses relative humidity measurements to derive water vapour content. The model uses the following formula for the total zenith delay:

$$\Delta S_z = \Delta S_{zd} + \Delta S_{zw} \tag{2.17}$$

where the dry zenith delay ΔS_{Zd} is evaluated by

$$\Delta S_{Zd} = 2.343 \,.\, P_S\left[\frac{(T_S - 4.12)}{T_S}\right].\, I\left(h = h_d, \varepsilon\right), \tag{2.18}$$

and the wet zenith delay is evaluated by

$$\Delta S_{Zw} = K_w.\, I(h = h_w, \varepsilon\varepsilon\ ) \tag{2.19}$$

where

$$I(h,\varepsilon) = \left\{1 - \left[\frac{Cos(\varepsilon)}{1 + (1 - l_c).\dfrac{h}{r_s}}\right]^2\right\}^{-\frac{1}{2}},$$

ε = elevation angle (degree),

h = height above the geoid (m),

h_d = height of the dry troposphere above the geoid [148.98 . (T_s – 4.12)]

m above the station (hopfield, 1971),

h_w = height of the wet troposphere above the geoid , 13000 m,

K_w = constant dependent on latitude and season (Black, 1978),

r_s = distance from the centre of the earth to the station (m),

l_c = 0.85.

2.6.5.1.4 Marini Model

Marini, (1972) tried to express more accurately the elevation angle (ε) dependence of the delay by introducing the following continued-fraction form of the mapping function

$$Mapping\ Function\ (\varepsilon) = \frac{1}{\sin(\varepsilon) + \dfrac{a}{\sin(\varepsilon) + \dfrac{b}{\sin(\varepsilon) + \dfrac{c}{\sin(\varepsilon) + ...}}}} \tag{2.20}$$

where (a, b, c,.....etc) are the profile dependent coefficients for which Marini developed theoretical expressions. The following equation is the total delay evaluation formulae developed by Marini based on Saastamoinen's basic zenith delay formulae;

$$\Delta S(\varepsilon) = \frac{1}{f(\phi,h)} \cdot \frac{A+B}{\sin(\varepsilon)} \cdot \frac{B}{(A+B)(\sin(\varepsilon)+0.015)}, \tag{2.21}$$

where,

$$A = 0.002277 \,.\, \left[P_s + \left(\frac{1255}{T_s} + 0.05 \right) . e_s \right],$$

$$B = 2.644 \,.\, 10^{-6} \,.\, EXP[-0.14372 \,.\, h],$$

h = station height above sea-level (km),

ϕ = latitude,

$$f(\phi,h) = 1 - (0.0026 \,.\, \cos 2\phi) - (0.00031 \,.\, h).$$

2.6.5.2 Global Empirical Models

These models avoid the use of surface meteorological data and assume that the atmosphere behaves in a certain manner depending on the behaviour of the temperature, pressure, and humidity.

2.6.5.2.1 Bomford & Bernese Models

These models assume standard atmosphere and constant rates of change of meteorological data with height. For example, Bomford, (1975) uses the following values for the standard atmosphere at sea-level;

- Standard Temperature = 18° c
- Standard Pressure = 1013.25 mbars
- Standard relative humidity = 50%

The following relationships are then used to determine the meteorological values at the reference station height,

$$\frac{dP}{dh} = -0.119 \quad \text{mbars/metre,} \tag{2.22}$$

$$\frac{dT}{dh} = -0.0055 \quad C^{o}/\text{metre,} \tag{2.23}$$

$$\frac{de}{dh} = -\frac{e_0}{2700}\text{EXP}\left(\frac{-h}{2700}\right) \quad \text{mbars/metre} \tag{2.24}$$

where e_0 is an average sea-level value at that time and locality.

The Bernese software developers (Hugentobler et al., 2001) offer another set of values for the standard atmosphere at sea-level. Then the generated meteorological values are input into a surface meteorological model to evaluate the range correction for the GPS signal. It is obvious that the best obtained behaviour from surface tropospheric models will be gained through seeding the models with surface meteorological data such as (IGS- meteorological data) and not meteorological Data resulting from (Bomford & Bernese) models (§4.4.5).

2.6.5.2.2 Magnet Model

Magnet model is an example for global empirical models which only accounts for the hydrostatic delay and generates the pressure data using the station latitude, station height and julian day (Curley, 1988). The model generates its own surface pressure P_s, and uses it to calculate the hydrostatic delay using the Saastamoinen expression (equation (2.15)). P_s is given by,

$$P_s = [1015 - 1.75\cos(\phi)]e^{-h\chi}, \tag{2.25}$$

where,

$$\chi = 0.113 + 0.001h + 0.017\sin(\phi)[1.0 + 0.382\cos(0.0174(jd - 30))], \tag{2.26}$$

P_s : surface pressure (mbar),

ϕ : station latitude,

h : station height (km),

jd : julian day.

Then the delay value is mapped down to the target elevation angle using the following mapping function,

$$Mf_{dry}(\varepsilon) = \frac{1}{\sin(\varepsilon) + \frac{0.00143.\cos(\varepsilon)}{\sin(\varepsilon) + 0.0445.\cos(\varepsilon)}}. \tag{2.27}$$

2.6.5.3 Mapping Functions

A number of mapping functions have been developed in the last couple of decades such as: Lanyi (1984), Davis et al.(1985), Ifadis (1986), Santerre (1987), Herring

(1992) and Niell (1993). These mapping function vary in their dependent parameters. Some of them depend on surface meteorological measurements such as Davis et al. (1985), Ifadis (1986), however others depend only on station height, latitude and day-of-year such as Niell (1993). It was suggested that most of these mapping functions can provide satisfactory results when used for elevation angels above 15^0. However for high precision applications, the recommended mapping functions by (Mendes and Langley, 1994) are those of Lanyi (1984), Ifadis (1986), Herring (1992) and Niell (1993). A brief description will follow for Niell mapping function. For more information about different mapping functions, the reader is referred to (Baker, 1998).

2.6.5.3.1 Niell Mapping Function

Niell (1996) developed the following global mapping function,

$$Mapping\ Function\ (\varepsilon) = \frac{\left(\dfrac{1}{1+\dfrac{a}{1+\dfrac{b}{1+c}}}\right)}{\left(\dfrac{1}{\sin(\varepsilon)+\dfrac{a}{\sin(\varepsilon)+\dfrac{b}{\sin(\varepsilon)+c}}}\right)} \tag{2.28}$$

where,

ε : elevation angle,

a,b,c : coefficients interpolated from the USSA (United States Standard

Atmospheres) (Cole et al., 1965). Two different sets for the dry and wet tropospheric delay.

The Niell mapping function varies with station height, station latitude and day of year. It was developed to map to elevation angle down to 3° assuming azimuth symmetry. The Niell mapping function gives good global performance without the need for in situ meteorological measurements (Niell, 1996).

CHAPTER 3

GALILEO

3.1 Introduction

Satellite navigation, positioning and timing has already found widely spread applications in many fields (see Chapter 1). Presently these applications are all reliant on the American-owned GPS, a system principally designed for military use. As such, world-wide commercial users have no guarantee of the availability of GPS services and this can be a hindrance for the developments of non-military applications of satellite navigation technology.

Recently Europe has begun a two-phase program to develop its own interests in satellite navigation. The first phase, GNSS-1, was to develop the European Geo-stationary Navigation Overlay Service (EGNOS), which provides the integrity and Wide Area Differential GPS (WADGPS) services for both the GPS and GLONASS systems. The geo-stationary satellites are used to broadcast the integrity and WADGPS corrections to the users, and to provide extra pseudo-range observations (Penna et al., 2001). The second phase is to develop its own GNSS system named GALILEO, which will provide world-wide navigation services.

According to (GALILEO, 2002), GALILEO, the first satellite positioning and navigation system designed for civilian purposes, will be more advanced, more efficient and more reliable than GPS which is controlled by military administration and currently has a monopoly. GALILEO will also help to meet the radio navigation needs in future years to come which it is anticipated can not be satisfied with a single system.

There are at present two radio navigation satellite networks: the American GPS and the Russian GLONASS systems, however GLONASS is no longer fully operational. Both systems were designed for military purposes; however both provide low grade services to civilian users.

GPS has several major shortcomings as given below:

- The military character of GPS means that there is always a risk of civilian users being cut off in the event of a crisis.
- Reliability not dependable; with low coverage of regions in extreme latitudes, low signal penetration in dense areas and town centres.
- No integrity, as there are no warnings and no immediate information about errors and such signal interruptions can have disastrous consequences.
- A Canadian research body has highlighted the case of a plane affected by an unannounced signal interruption of over 1h20, aggravated by an initial positioning error of 200 km when re-established. The Icelandic aviation authorities have reported several transatlantic flights disturbed in the same way in their control zone. Also in the United States, civilian aircraft have suffered 20-

minute signal interruptions in three mid-American states (GALILEO, 2002).

- The report of the Volpe National Transportation Center commissioned by the US government clearly stressed a number of such shortcomings and even the GPS III project to improve the system, would not resolve all of them (Volpe, 2001).
- No guarantee and no responsibility, this being incompatible with the military objectives of the system-with all the implications that can be imagined in the event of an aviation accident or any other similar event.

In the light of such shortcomings of GPS, many studies have demonstrated the importance of GALILEO and its useful impact on Europe and the whole world (Galileo, 2002). On its own, GALILEO aims to offer better and constant positioning accuracy, offer superior reliability since it includes an integrity message and ensure genuine continuity of public service. Combined use of GALILEO, GPS and GLONASS should, therefor, increase the overall performance, availability, continuity and safety of services. It will also allow for worldwide acceptability of the exploitation and use of satellite navigation for the benefit of all users.

3.2 GALILEO SYSTEM ARCHITECTURE

The following sections give a brief description of the GALILEO system design architecture based on the technical documents available in (GALILEO, 2002) and (Javier B., 2001).

3.2.1 Global Component

- A constellation of 30 satellites in Medium-Earth Orbits (MEO) giving an adequate

worldwide coverage for the provision of the system's services. Each satellite will contain a navigation payload and a search and rescue transponder. The design constellation is expected to offer more visible satellite than GPS constellation (see Table 7.11 and Appendix B) as well as high quality ephemeris data (65cm RMS) (Lucas et al., 2000), (Provenzano et al., 2000).

- A ground segment managing the constellation of navigation satellites, controlling the functions of satellite orbit determination and clock synchronization and determining and disseminating the integrity information. It will also provide interfaces with service centres providing value-added commercial services and with the COSPAS-SARSAT ground segment for the provision of search and rescue services.

3.2.2 Regional Components

- Non-European Regional components, ground segments for integrity determination over these regions.
- EGNOS providing integrity and differential corrections for GPS and GLONASS through geo-stationary satellites.

3.2.3 Local Components

These local components are to provide special services such as increased accuracy, integrity time-to-alarm and signal acquisition/reacquisition for some classes of user who have requirements beyond those available from the global system. These local components can also provide other services like commercial data, additional navigation signals, mobile communication channels and enhanced positioning data in areas of poor signal reception.

3.3 User Segment

Consisting of different types of user receivers related to the different signals used to fulfil the various services offered by GALILEO.

3.4 Service Centres

These centres provide different functions such as information and warranty on performance, subscription and access key management, insurance, certification and commercial interfaces.

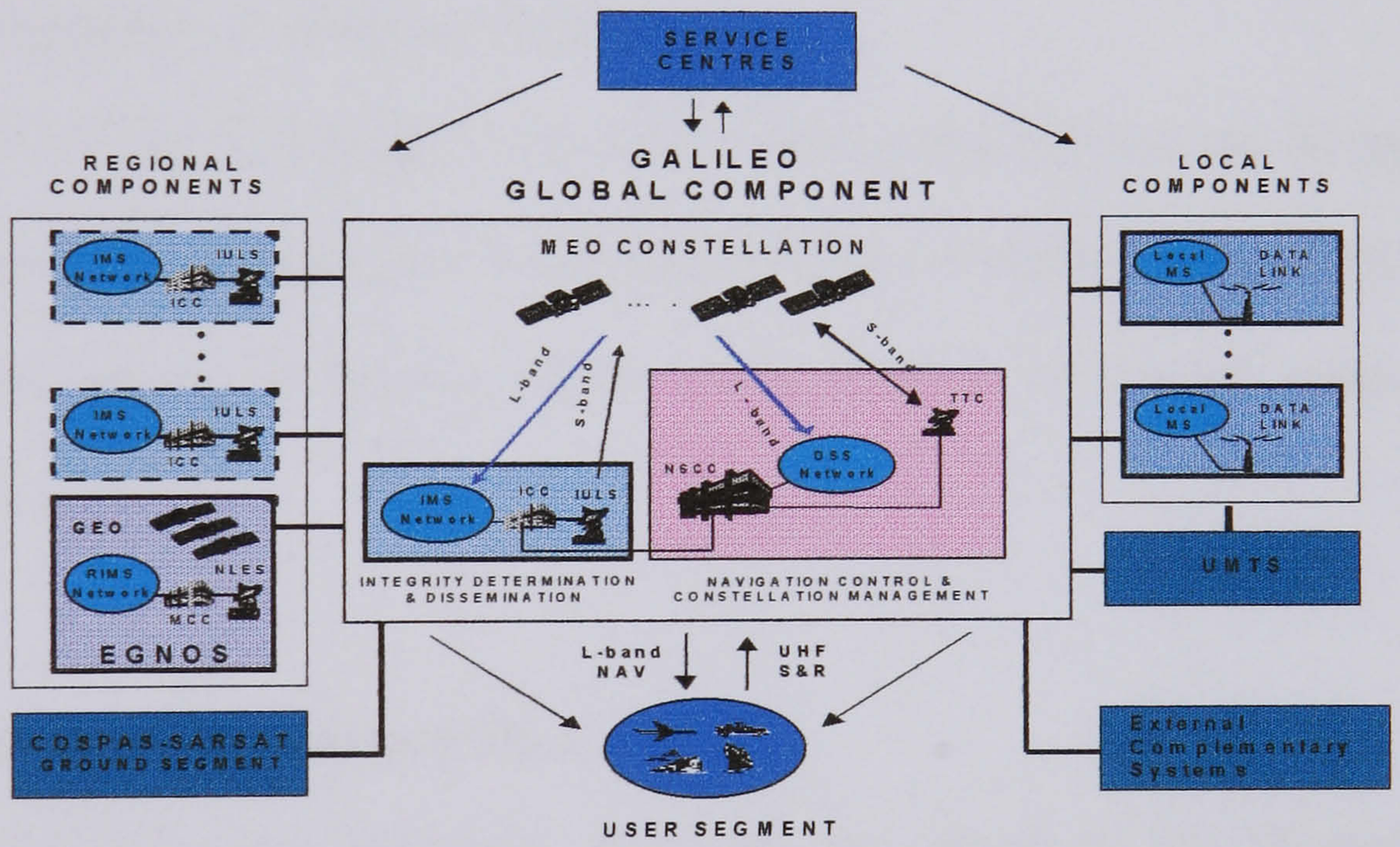

Figure 3.1: GALILEO System Architecture (GALILEO, 2002).

3.5 GALILEO CAPABILITIES

GALILEO services result from the combination of the system capabilities of each of the components and segments of the system architecture (see Figure 3.1). There are also services resulting from using other existing GNSS systems.

3.6 GALILEO Signals and Data

The GALILEO constellation will broadcast globally ten navigation signals supporting different services, namely open, commercial, safety-of-life and public regulated services. Each signal is composed of one or two ranging codes and navigation data as well as, integrity, commercial and search and rescue data depending on the type of the signal. Satellite-to-user distance measurements based on ranging codes and data are made in the GALILEO user's receiver.

3.6.1 Encryption & Service Denial

To control the access to GALILEO services, ranging codes and data can be open or encrypted. Encryption could be activated permanently or temporarily. GALILEO will also have the ability of denying access to its services to prevent misuse by unauthorized users.

3.7 Signal and Frequency Plan

The GALILEO frequency plan was discussed and agreed at the international Telecommunications Union (ITU) forums such as the World Radio-Communications Conference (WRC). The available spectrum which can be used for the development of Radio-Navigation Satellite Systems is shown in Figure 3.2.

In this figure, a number of frequency bands are identified for GALILEO. Out of the definition studies, four frequency bands have been retained for the setting up of the GALILEO signals. These are described below. A tentative allocation of the ten

GALILEO navigation signals into frequency bands has also been made on the basis of the transmission of four carriers, one for each frequency band.

- E5 and L5, covering the range 1164 MHz to 1215 MHz. Within this band, the use of 30 MHz of spectrum is being considered with the final selection of the centre frequency depending on interoperability issues with E5/L5, co-existence with other services such as DME (Distance Measuring Equipment), JTIDS/MTIDS (Joint Tactical Information Distribution Systems/Multifunction Information Distribution System) and on GALILEO autonomy requirements. The studies recommended a centre frequency of 1192 MHz. In E5/L5, an open signal for supporting the Open and Safety of Life Service can be included.

- E6, 1260 to 1300 MHz. Within this band, the use of 20 MHz of spectrum is being considered with a centre frequency of 1278.75 MHz, to accommodate the signals for the Public Regulated Service and the Open (Commercial-encrypted, TCAR(Three Carrier phase Ambiguity Resolution techniques)) Service.

- E2-L1-E1 covering the range 1561 to 1590 Mhz, with a centre frequency of 1575.42 MHz. This band would accommodate a signal for the Public Regulated Service and the Open and Safety of Life Service.

The GALILEO signal and frequency plan is defined to provide high performance, better ranging accuracies than GPS due to the chip rate relations between GPS and GALILEO signals (see Table 3.1). GALILEO signals will have the same center

frequencies as GPS signals on E5 (L5) and E2-L1-E1 (L1) to give GALILEO maximum interoperability with GPS.

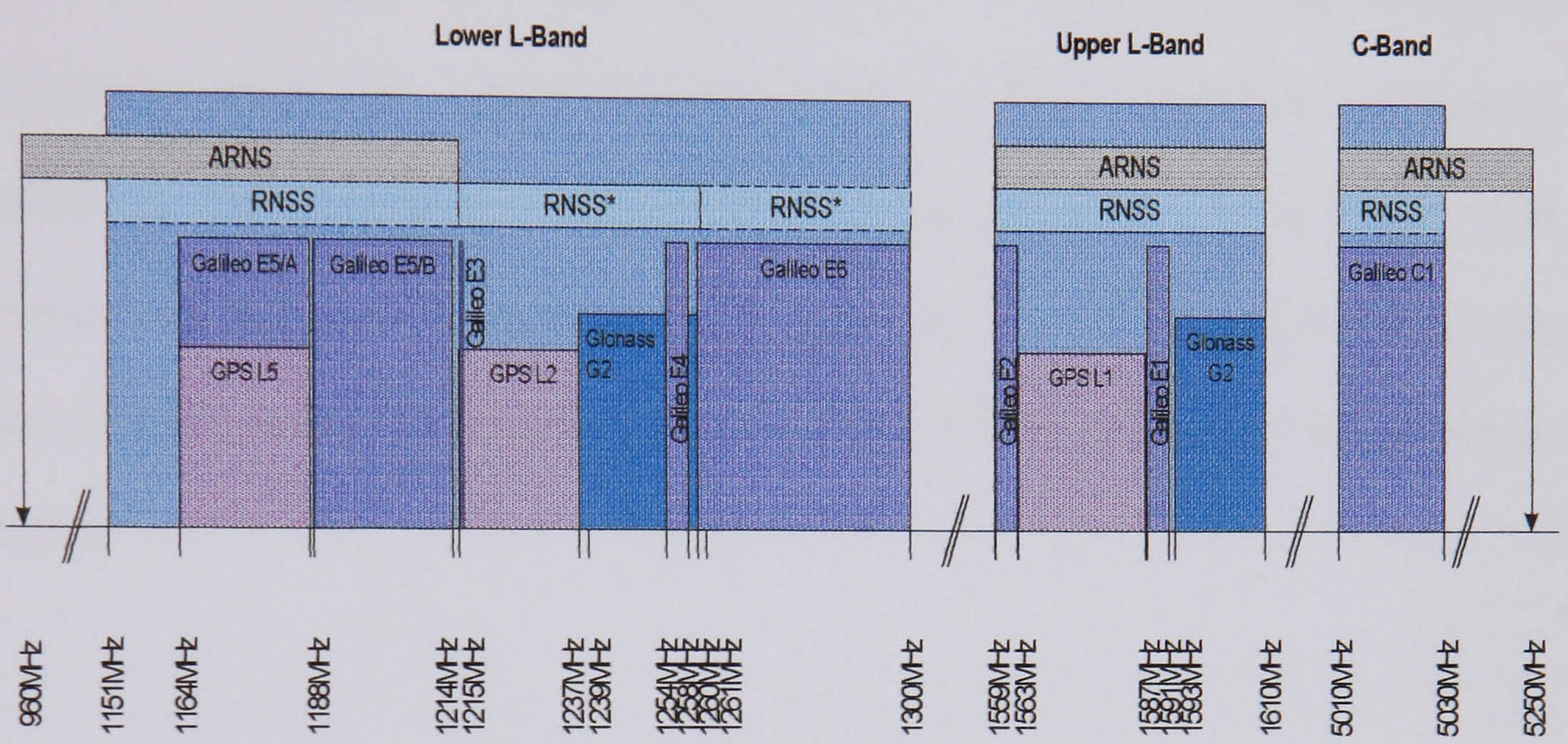

Figure 3.2: RNSS Frequency Spectrum (GALILEO, 2002).

Signal	Chip rate (Mcps)
GPS C/A-code	1.023
GALILEO E2L1E1	2.046
GALILEO E5AB	10.000
GALILEO E6	5.115

Table 3.1: Chip rate relation between GPS signals and GALILEO signals (GALILEO, 2002)

3.8 GALILEO Services

3.8.1 Open Service

The design open service provides positioning, navigation and timing signals that can be used free of charge. The target of this service is the mass-market navigation applications, such as vehicle-navigation and mobile telephone positioning applications. This service also provides a precise timing service (UTC) when used with receivers in fixed locations for applications such as network synchronization or scientific applications. The performance characteristics of this service are shown in table 3.2.

Open Service (positioning)			
Type of Receiver	Carriers	Single Frequency	Dual-Frequency
	Computes Integrity	No	
	Ionospheric Correction	Based on simple model	Based on dual-frequency measurements
Coverage		Global	
Accuracy (95%)		H: 15 m V: 35 m	H: 4 m V: 8 m
Integrity	**Alarm Limit**	Not Applicable	
	Time-To-Alarm		
	Integrity Risk		
Continuity Risk		8×10^{-6}/15 S	
Timing Accuracy wrt UTC/TAI		30 ns	
Certification Liability		No	No
Carriers		Three-Frequencies	
Availability		99.8 %	

Table 3.2: GALILEO Open Service performance characteristics (GALILEO, 2002).

3.8.2 Commercial Service

This service provides more advanced characteristics to the open service. These characteristics are related to the design of the signal, which supports, dissemination of encrypted value-added data in the open GALILEO signals, very precise local differential applications using the open signal overlaid with the Public Regulated Service signal on E6 and a pilot signal for supporting integration of GALILEO positioning applications and wireless communications networks. The performance of these services is dependent on the quality of the commercial data broadcast and on the performance of local components.

3.8.3 Safety of Life Service

This service's performance is compatible with the requirements of the Approach with Vertical Guidance (AVP-II) as defined by International Civil Aviation Organization (ICAO). Also the performance needs for other modes of transport (land, rail, maritime) are adequately covered through those requirements. A GALILEO service availability of over 99.9 % would make it usable as a stand-alone service. On the other hand combination of this service with the current GPS, augmented by EGNOS corrections, or with the future improved GPS and EGNOS integrity-only would support CAT-I performance and gives the ability of sole means availability. Amongst the other applications covered will be ship docking, train control, and advanced vehicle control.

Safety-of-Life Service			
Type of Receiver	Carriers	Three Frequencies	
	Computes Integrity	Yes	
	Ionospheric Correction	Based on dual-frequency measurements	
Coverage		Global	
		Critical level	Non-critical level
Accuracy (95%)		H: 4 m V: 8 m	H: 220 m
Integrity	**Alarm Limit**	H: 12 V : 20	H: 556 m
	Time-To-Alarm	6 seconds	10 seconds
	Integrity Risk	3.5×10^{-7} / 150 s	10^{-7} / hour
Continuity Risk		10^{-5} /15 s	10^{-4} / hour – 10^{-8} hour
Certification Liability		Yes	
Availability of Integrity		99.5 %	
Availability of accuracy		99.8 %	

Table 3.3: Service Performance for safety of life Service with the Satellite Navigation Signals only and without any other augmentations (GALILEO, 2002).

3.8.4 Public Regulated Service

The Public Regulated Service is provided on dedicated frequencies to provide greater continuity of service. It will be placed under the control of EU countries and used for public applications (police, civil protection, law enforcement), transport, telecommunications applications and economical or industrial activities with strategic importance. This service is robust, being interference resistant and also resistant to jamming and other accidental aggressions.

Public Regulated Service		
Type of Receiver	Carriers	Dual Frequencies
	Computes Integrity	Yes
	Ionospheric Correction	Based on dual-frequency measurements
Coverage		Global
Accuracy (95%)		H : 6.5 m V: 12 m
Integrity	**Alarm Limit**	H : 20 V: 35
	Time-To-Alarm	10 s
	Integrity Risk	3.5×10^{-7} / 150 s
Continuity Risk		10^{-5} / 15 s
Timing Accuracy wrt UTC/TAI		100 ns
Availability		99.5 %

Table 3.4: Service Performance for Public Regulated Service with the Satellite Navigation Signals only (GALILEO, 2002).

3.8.5 Navigation Services by Local Components

Using differential corrections provided by local components will provide positioning accuracy better than 1 metre for single frequency users. Local components could report integrity with a time to alarm of 1 second, also the local service providers will adapt the signal format to accommodate additional data.

The combination of the Three Carrier phase Ambiguity Resolution techniques (TCAR) with local components will provide users with positioning accuracy below 10 centimeters (GALLEO, 2002). The pilot signal provided with the open signal will enhance the performance of wireless telecommunications networks in difficult

environments, also pseudolites serving, as local stations will be used to increase the availability of the GALILEO service in a defined local area.

Type of Local Components	Broadcast of Differential corrections for Single or dual frequency users	Broadcast of Differential corrections for Triple-frequency Users (TCAR)	UMTS-assisted user position computation
Accuracy	< 1 m	< 10 cm	50 m (TBC)
Integrity Time to Alarm	1 s	1 s	Not applicable
Availability	High under open field-of-view condition	High under open field-of-view condition	Increased in urban canyons and for indoor applications

Table 3.5: Performance for Services combining Satellite and Local Component signals (GALILEO, 2002).

3.8.6 Search and Rescue Service

Search and Rescue Service will be coordinated with the current International Satellite System for Search and Rescue (COSPAS-SARSAT) service and compatible with both Global Maritime Distress and Safety System (GMDSS) and Trans European Transport Network guidelines. GALILEO will give the benefit of improving the time detection and the accuracy of location of distress beacons with respect to the current system performance for search and rescue. COSPAS-SARSAT will carry out the task of position determination for distress beacons on the basis of the signals and data provided by the GALILEO Search and Rescue Service. The position determination

will be enhanced from 5 Km for the current beacons, to less than 10 meters for advanced beacons equipped with GALILEO receivers.

Search and Rescue Service (SAR)	
Capacity	Each satellite shall relay signals from up to 300 simultaneous active beacons
Forward System Latency Time	The communications from beacons to S& R ground stations shall allow detection and location of a distress emission in less than 10 min. The latency time goes from beacon first activation to distress location determination
Quality of Service	Bit Error Rate < 10^{-5} for communication link : beacon to S & R ground station
Acknowledgment Data Rate	6 messages of 100 bits each, per minute
Coordination Messages Data Rate	18 messages of 420 bits each, per minute
Availability	> 99 %

Table 3.6: GALILEO service performance for Search and Rescue Service (GALILEO, 2002).

3.8.7 Navigation/Communication Service

This service is the combined use of GALILEO with other current wireless, terrestrial or satellite networks. This service is suitable for regulated applications requiring global and high availability and reliable position reporting which will be achieved by allowing the quasi-instantaneous transmission of short messages from users to a service centre and vice versa.

Navigation Related Communications Service (NRS) Characteristics	
Delivery Time	Delivery to recipient < 1 min. after sending (TBC)
Acknowledge	Acknowledge to sender < 1 min. after reception (TBC)
Error Notice	Error reported to sender < 5 min. after sending (TBC)
Capacity	TBD
Availability	> 99.5 %

Table 3.7: GALILEO service performance for N/C (GALILEO, 2002).

CHAPTER 4

GPS Data Simulation

4.1 Introduction

Simulation is a tool traditionally used in aspects of the conceptualization, design, development and testing of systems. More recently, there has been a move to systematically apply simulation throughout the life cycle of a system. Simulation, as a research tool was, and still is the best option for the analysis of endless scenarios at relatively no cost. Many scientific discoveries would not have been made without the use of simulation techniques, as field tests are often impractical.

In the last ten years dependence on GPS has become unavoidable in many aspects of every day life. As described in Chapter 1, GPS technology has many areas of applications that hold great expectations for terrestrial and space-based users as well. Some of these terrestrial expectations are safer air travel, improvements in search and rescue systems, improved Earthquake monitoring, tractor-trailer tracking and enhanced farming techniques.

GPS also has promising benefits for spacecraft and space systems such as significant reductions in spacecraft costs, improvements in spacecraft autonomy and new revolutionary scientific capabilities can be accomplished through the availability of this technology on the spacecraft of the future (Bauer et al., 1998). Consequently, there is a need for research tool that allows wider ranging of analysis of GPS to be undertaken without incurring high costs. Field tests often have difficulties in providing the varying test conditions required and always have significant costs associated with them, therefore the use of simulation techniques is a preferable choice.

Techniques for simulating multi-component GNSS systems are wide-ranging in complexity. Service Volume Simulators (SVS) are often used to give an overall view of the performance levels seen by the user such as GALILEO Integrity Performance Assessment (GIPA) project (Werner et al., 2001). For a more detailed analysis of the system, an End-to-End simulator may be used which simulates every aspect of the GNSS system including ground control, space and user segments. Such simulators may have the ability to work in real time and have the facility to test hardware in the loop such as the GalileoSat System Simulation Facility (GSSF) which is one of a number of ESA facilities designed to support the development of the GALILEO space, ground and user segments. GSSF is a software simulation tool that reproduces the functional and performance behaviour of the GALILEO system in order to support the definition, integration, validation, verification and operations of GALILEO (Pidgeon et al., 2000). It is often the case that only one aspect of the overall GNSS system needs to be analysed and thus simulation tools can be

developed for one particular part of the system. This thesis is concerned with the simulation of the measurements that would be made by a user receiver for a particular GNSS and the remainder of this section gives details of how such a measurement data simulator can be developed.

4.2 GPS Data Simulation

4.2.1 DATa SIMulator (DATSIM) software

The Institute of Engineering Surveying and Space Geodesy (IESSG) at the University of Nottingham has its own GPS DATa SIMulator (DATSIM) software which was developed as part of the GPS Analysis Software package (GAS) (Stewart et al., 2002).

DATSIM simulates GPS observations, including pseudo-range, carrier phase and Doppler measurements based on the following observation equations:

Pseudo-range:

$$P_1 = d + c(dt_r - dt_s) + a_1 d_{ion} + d_{trop} + d_{SA} + n_{p1} \quad \text{(L1)}, \quad (4.1)$$

$$P_2 = d + c(dt_r - dt_s) + a_2 d_{ion} + d_{trop} + d_{SA} + n_{p2} \quad \text{(L2)}. \quad (4.2)$$

Carrier Phase:

$$\Phi_1 = \frac{f_1}{c}\left(d + c(dt_r - dt_s) - a_1 d_{ion} + d_{trop} + d_{SA}\right) + N1 + n_{\Phi 1} \quad \text{(L1)}, \quad (4.3)$$

$$\Phi_2 = \frac{f_2}{c}\left(d + c(dt_r - dt_s) - a_2 d_{ion} + d_{trop} + d_{SA}\right) + N2 + n\Phi 2 \quad \text{(L2)}. \qquad (4.4)$$

where,

d the distance between satellite and receiver,

dt_r the receiver clock error,

dt_s the satellite clock error,

d_{ion} the difference between L1 and L2 ionospheric delays,

d_{trop} the tropospheric delay,

d_{SA} the SA dither error,

N_1 the L1 carrier phase ambiguity,

N_2 the L2 carrier phase ambiguity,

n_{p1} the measurement noise for L1 pseudo-range,

n_{p2} the measurement noise for L2 pseudo-range,

$n_{\Phi 1}$ the measurement noise for L1 carrier phase,

$n_{\Phi 2}$ the measurement noise for L2 carrier phase,

f_1 the carrier frequency for L1 observations,

f_2 the carrier frequency for L2 observations,

c the speed of light,

a_1 function of L1 frequency,

a_2 function of L2 frequency.

Doppler measurements being modelled as the first derivatives of the pseudo-range measurements.

The control flow chart of the DATSIM software is given in Figure 4.1. The input to the software includes the GPS satellite orbits and the receiver coordinates. For a mobile receiver, a file consisting of a set of coordinates representing the trajectory of the receiver is required. The coordinates of the receiver at any desired epoch are obtained by interpolation between the trajectory epochs. The software calculates the true range and range rate between the satellites and the receiver, generates different errors from various error models, and finally combines them to form the observations.

The simulated measurements time-tagged for each satellite in view are then written out to a file in a standardized format for each receiver. Some modifications have recently been made to allow the generation of simulated data from inertial sensors, specifically gyroscopes and accelerometers. The user can manipulate various errors in the observations in order to simulate particular environments. As well as simulated GPS data files for each receiver, the software also outputs files containing the different error sources, the simulated data files for the inertial sensors if required and a report file.

DATSIM contains various models for the different sources of error in GPS measurements (ionospheric delay, tropospheric delay, multipath, satellite clock error, receiver clock error, and measurement noise) and gives the user the flexibility to activate or deactivate the errors by switching the models on or off. Prior to the

Author's research, the DATSIM software has been used in a number of research projects at the IESSG and had already been tested to some extent against real data to show that realistic data can be generated with this simulator (Ashkenazi et al., 1997). (Ashkenazi et al., 1997) found that similar results can be obtained using simulate and real GPS tracking data for LEO satellite reduced dynamic orbit determination (Topex/Poseidon). The agreement was up to 0.11m, 0.25m, 0.08 and 0.22m for radial, along-track, across-track and total orbital errors respectively.

4.2.2 DATSIM: Original GPS Error Models

The DATSIM version before the effort of this research used the following mentioned models for different GPS errors. The satellite and receiver clock errors are simulated using polynomial functions, the coefficients of which are generated by the software. These coefficients are generated to be comparable with the observed behaviour of real clocks. Alternatively the satellite clock errors can be read from the ephemeris file or a clock data file generated during a previous run of DATSIM.

DATSIM simulated the ionospheric delay error, by using the Klobuchar model (§2.6.4.1.2) using ionospheric parameters extracted from the GPS navigation message. The accuracy of the Klobuchar model is limited to 50-60 % of the total effect (Dodson, 1988) as well as the model is incapable of showing the variable nature of the ionosphere with different geographical areas as it fits well for middle-latitude areas only.

DATSIM simulated the tropospheric delay error, by applying a global atmospheric model to generate local meteorological conditions, which are then used to calculate the delay on each measurement. Various tropospheric models were available in the software for the user to choose, including Hopfield (§2.6.5.1.1), Saastamoinen (§2.6.5.1.2) and magnet models (§2.6.5.2.2). Magnet model is a global empirical model that stands for the hydrostatic tropospheric delay only. Surface meteorlogical models (Hopfield and Saastamoinen) need surface meteorological data to give its best behaviour which is not recommended for simulation purposes. Using such models with atmospheric data generated using global atmospheric models limits its accuracy.

DATSIM simulated Multipath error using a model consisting of two parts; the first is Gaussian white noise and the second is single replica model. The model showed no correlation between different multipath time series as well as no elevation-angle dependent behaviour.

Measurement noise is also simulated within DATSIM and is modelled as Gaussian white noise with a mean of zero and a user specified standard error. Random integers are added to the carrier phase measurements as initial ambiguities. As an option, the software can also add random carrier-phase cycle slips to the data.

While the DATSIM software has been shown to produce realistic simulated data (Ashkenazi et al., 1997), there are still areas where improvements to the error models can be made, especially the environmental delay models (ionosphere delay, troposphere delay and multipath).

The following sections show how the author has improved the performance of DATSIM by implementing new, more accurate models to simulate the two major sources of errors for GPS measurements namely the ionospheric and tropospheric delays. Also a more realistic model for simulating the multipath effect is proposed.

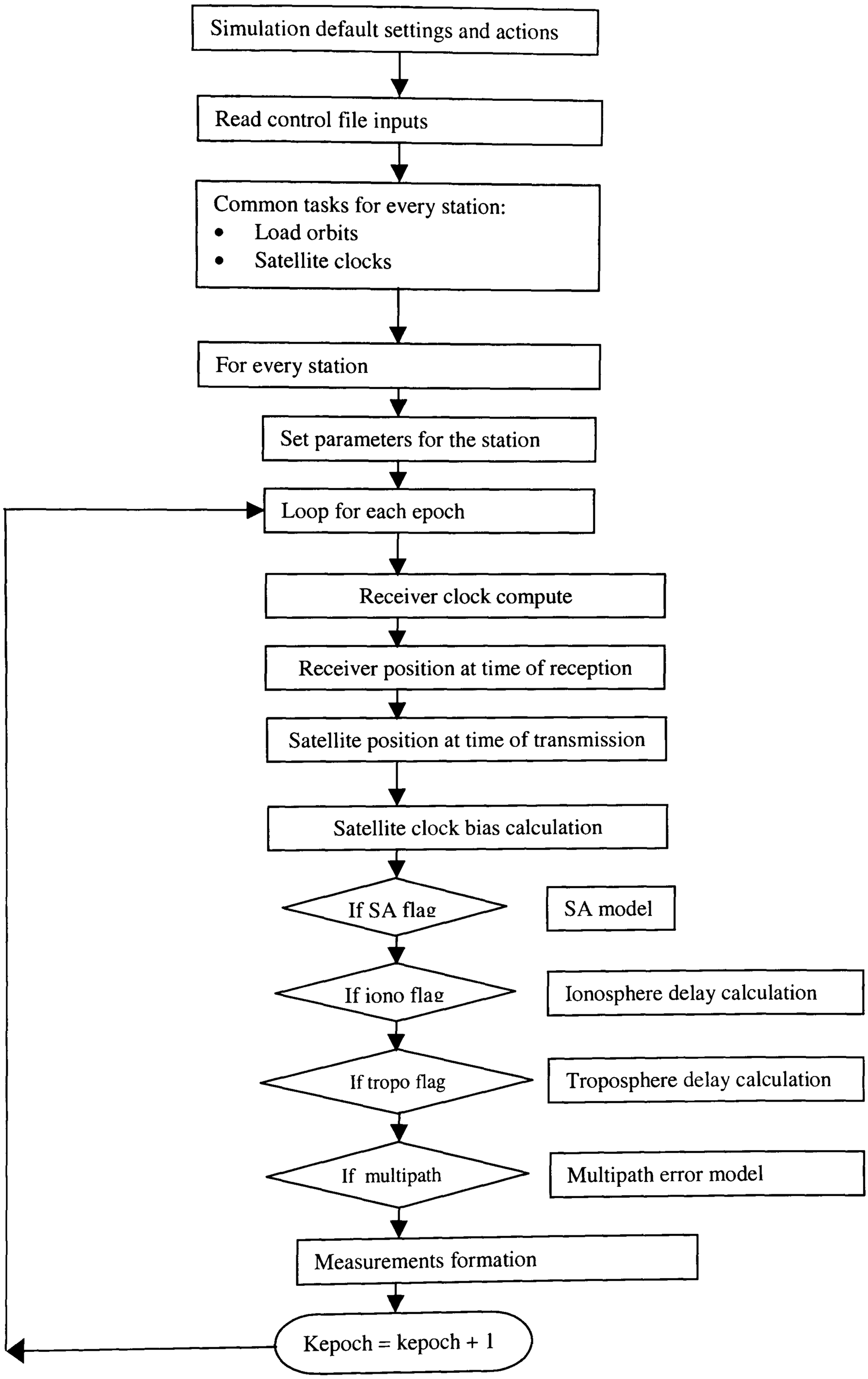

Figure 4.1: DATa SIMulator, (DATSIM) Control Flow Chart.

4.3 Simulation of Ionospheric Delay

4.3.1 Introduction

Now that SA, the intentional degradation of the accuracy of the single-frequency GPS position by the American DOD, has been turned to a zero level, the ionospheric error is considered to be the major source of potential range delay for single frequency users (Kunches and Klobuchar, 2001).

The ionospheric range delay on GPS signals can be simulated in different ways and the various options will be discussed in the following sections. A description of the current options within the simulator (DATSIM) is given along with their advantages and shortcomings and finally, a new method for simulating the ionospheric delay is proposed.

4.3.2 The Ionospheric Delay Simulation Techniques

The philosophy behind selecting a model to simulate the ionospheric delay from the GPS-simulation point of view stands on two main points:

- Firstly, the selected model is the model which gives the best description and visualization of the behaviour of the ionosphere or, in other words, the model which shows the variable ionospheric behaviour with different locations (latitudes & longitudes), with different times of the year and with different times of the day.
- Secondly, the selected model is the model, which computes the ionospheric delay to a high degree of accuracy, but with reasonable computation time and easy implementation. Obviously, the best-selected model will be the one, which

gives both of the two previous criteria.

Over the years, many models have been developed for modelling the ionospheric path delay, the drive behind these developments being the need for single frequency users to remove the delay from their measurements. These models can be used 'in reverse' for data simulation to add the ionospheric delay into the measurements. The models may be divided into two main categories:

- Firstly, state-of-the-art ionospheric models, which require updating regularly with hundreds of coefficients to fit the monthly average behaviour of ionospheric range delay to within a residual bias of approximately 10%. Typical models are the International Reference Ionosphere, (IRI) and the Bent model.
- Secondly, simple-computational models with an ideal description for the ionosphere's average behaviour but with other shortcomings such as, low accuracy in describing the variability of the ionospheric behaviour with different latitudes and times, low accuracy in computing the ionospheric delay and inability to model the ionosphere's significant changes from its average behaviour. A typical model is the well-known Klobuchar model for which coefficients are sent through the GPS navigation message.

4.3.2.1 State-of-the-art Model

One of the options for ionospheric delay simulation is to use a state-of-the-art ionospheric model, however the need for continuous updating of hundreds of

coefficients with tremendous penalty in computational complexity makes this option not recommended for simulation purposes.

4.3.2.2 The Klobuchar model

This is the most widely-known global model (reviewed in § 2.6.4.1.2), which uses the Ionospheric Corrections Algorithm (ICA) (Klobuchar, 1987) designed to account for approximately 50% (rms) of the ionospheric range delay. This is the standard correction used by virtually all-single frequency GPS receivers. The coefficients for this algorithm are transmitted as part of the satellite navigation message and are updated at least once every ten days by the GPS Master Control Facility, or more often if there are significant changes in the five-day running mean solar radio flux during the ten-day period. The ICA is limited to only 8 coefficients due to GPS navigation message length limitations.

This model has one main advantage, which is its simplicity and the low computation time but, it also has many shortcomings:

- Low accuracy for computing the ionospheric delay correction (50-60%) (Dodson, 1988)
- The algorithm does not properly represent the behaviour of the ionosphere in the near-equatorial region of the world, where the highest values of the ionospheric delay occur (Klobuchar, 1982).
- The algorithm is very poor in high latitude regions where the ionospheric variability is high due to auroral processes.
- The model is unable to represent the behaviour of the ionosphere when

the ionosphere differs by substantial amounts from its average behaviour.

4.3.2.3 The Klobuchar model with CODE-coefficients

The main idea of this model is to use the same Klobuchar model with new coefficients produced by CODE. This method takes advantage of high-quality global TEC map information in IONEX format that is routinely derived by this centre as final and rapid, as well as predicted products. A working study using this model has shown that these new CODE coefficients increase the accuracy of the Klobuchar model from 50% (with GPS-coefficients) to 75% of the total effect (Schaer, 2001). However the main shortcomings of the Klobuchar model remain unresolved i.e. the inability to represent the behaviour of the ionosphere in the near-equatorial latitudes, in the high latitudes and when the ionosphere exhibits major variations from its average behaviour.

4.3.3 The Proposed Model for Ionospheric Delay Simulation

After working with each of the previously mentioned models, the following new model was developed. The main idea was to implement a model which has the following attributes; high accuracy in computing the ionospheric delay, ability to represent the behaviour of the ionosphere in different circumstances and computational simplicity.

4.3.3.1 The Model Description

The new model is based on the assumption that the ionosphere has three main states of activity, quiet, medium, and active, depending on the value of the Sun Spot Number (SSN). SSN is a measuring tool for the activity of the solar cycle defined by

cool planet-sized areas on the sun where intense magnetic fieldline loops poke through the star's visible surface (Davis, 1989). The technique chosen to simulate the ionospheric delay for each activity case, is to use the high-quality global TEC map information in IONEX format derived by IGS-analysis centres such as the CODE analysis center. The data format adopted by the IGS analysis centers to provide the TEC information is the IONosphere map EXchange (IONEX) format (Schaer et al., 1998c).

CODE is one of five ionospheric associate analysis centers of the IGS, and currently produces global Total Electron Content (TEC) maps on a regular basis. These maps are derived from the double-differenced carrier phase measurements of the IGS tracking network.

IGS- based Global Ionospheric Maps (GIM's) describing the Earth's vertically integrated TEC are produced in three types at the CODE, a final, a rapid, and a predicted product. It is proposed to use the final product in the simulation model, which is derived from the, geometry-free linear combination of phase-leveled-to-code measurements (Komjathy, 1997) of about 140-150 globally distributed IGS ground stations and is available approximately three days after the observations. These global maps are represented by a spherical harmonic expansion of degree 12 and order 8 referenced to a solar-geomagnetic frame (the global TEC distribution is relatively stationary in that frame). Since June, 1998 the Ionosphere maps are given in an earth-fixed reference frame with a resolution of 5^{o}, 2.5^{o} in longitude and latitude respectively. The conversion of line-of-sight TEC to vertical TEC is done using a

single-layer model (see Figure 4.2) (Schaer, 1999). The time resolution of the maps is two hours. For more information about these TEC global maps, the reader is referred to Feltens and Schaer (1998), Schaer (1998a) and Schaer (1998b).

4.3.3.2 The Model Algorithm

The Simulation of the ionospheric delay using the suggested model based on IGS-GIM's involves three steps:

1- Extracting the value of TEC at the ionospheric pierce point (Fig. 4.2) at the required time using linear interpolation between two consecutive TEC maps.

2- Computing the zenith ionospheric delay using the extracted TEC value.

3- Converting the zenith ionospheric delay to the slant delay using a mapping function.

4.3.3.2.1 Extracting TEC Value

In order to compute the TEC value (E) as a function of geocentric latitude (β), longitude (λ) and universal time (t), the following linear interpolation formula between two consecutive TEC maps was used;

$$E(\beta,\lambda,t) = \frac{T(i+1)-t}{T(i+1)-Ti} E_i(\beta,\lambda) + \frac{t-Ti}{T(i+1)-Ti} E_{i+1}(\beta,\lambda) \qquad (4.5)$$

where, $T_i \le t < T_{i+1}$

A simple 4-point grid interpolation formula (Bivariate interpolation) (Schaer et al., 1998c) was used to compute the value of the $E_i(\beta,\lambda)$ using the nearest 4 TEC values which is adequate for the grid spacing used (2.5° in latitude, 5° in longitude) .

4.3.3.2.2 The Zenith Ionospheric Delay Computation

The Zenith ionospheric delay can be computed using the following simple equation (Seeber, 1993);

$$d_{ion} = (40.3) \cdot \frac{TEC}{f^2}, \tag{4.6}$$

where, d_{ion} = zenith ionospheric delay (m),

TEC = total electron content in TEC units (1x 10^{16} electron),

f = Frequency of the GPS signal (Hz).

4.3.3.2.3 The Slant Ionospheric Delay Computation

The slant ionospheric delay is evaluated by multiplying the zenith delay by the following mapping function (Schaer, 1999):

$$Mapping\ Function = \frac{1}{\cos Z'}, \tag{4.7}$$

where , $\sin Z' = \frac{R}{R+H} \sin Z$,

Z, Z` are the geocentric zenith distances of a satellite at the height of the GPS receiver and the single layer of the ionosphere, respectively,

H is the height of the single layer of ionosphere above the Earth mean surface (450 km),

R is the mean radius of the Earth (6371 km approximately).

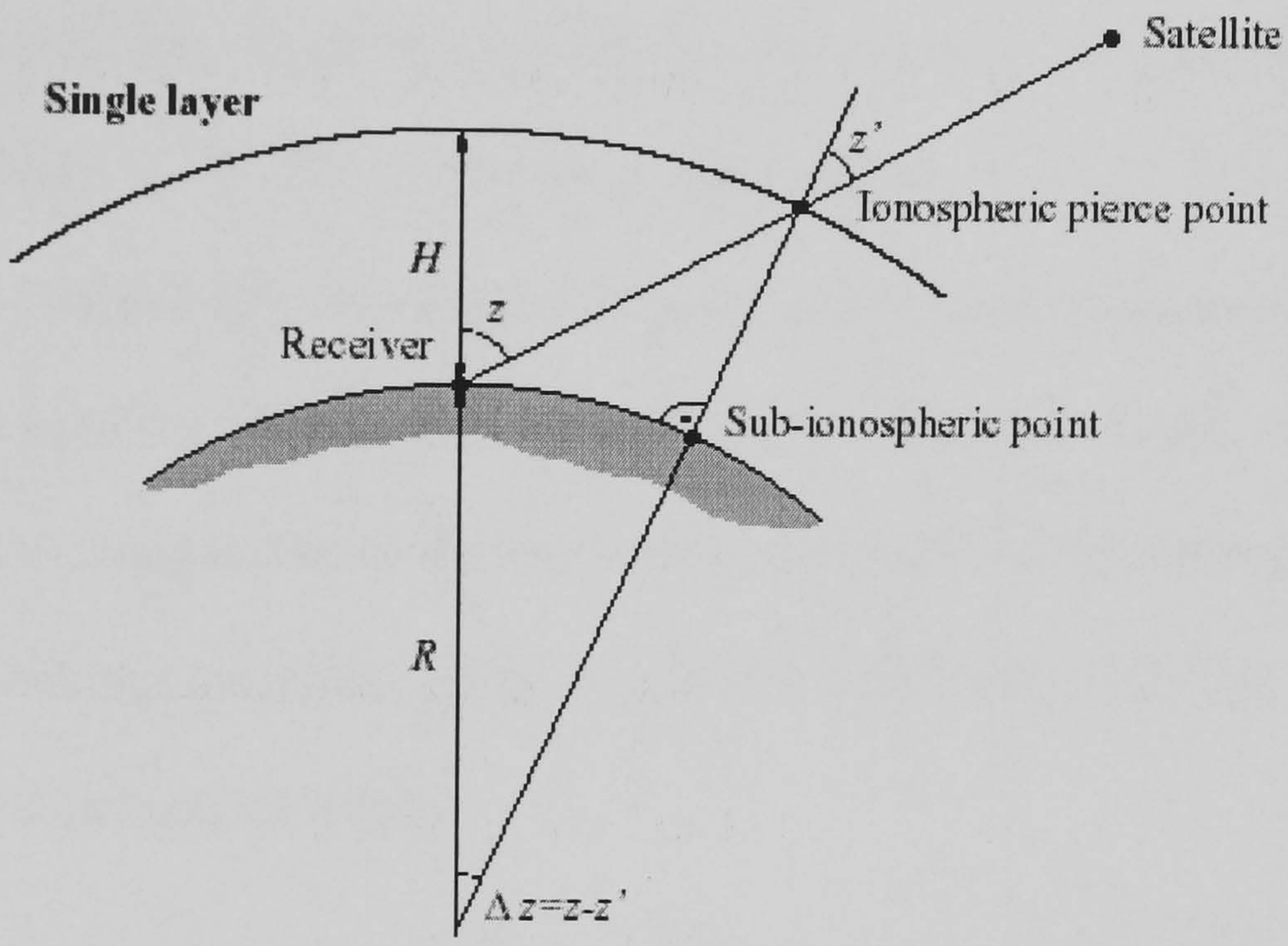

Figure 4.2: Description of the single-layer ionosphere model (Schaer, 1999).

4.3.3.3 Model Evaluation

The new model was tested against: the Klobuchar model with GPS coefficients and the Klobuchar model with CODE coefficients. The test involved producing global ionospheric zenith delay grid maps every two hours over a 24 hours period using each of the three models. The results were then assessed against the criteria given in §4.3.2. The date chosen for testing was the 10th of August 2001, which was an active ionospheric day (SSN = 99). The L1 frequency was used and the global TEC maps were obtained from CODE.

Figures 4.3, 4.4 and 4.5 show two-hourly snapshots of the Earth's zenithal ionospheric delay in meters for August 10, 2001 for each of the three models. This study's findings were presented in Farah (2002a), (2002b), (2003b).

4.3.3.4 Discussion

It can be concluded from Figure 4.3 that the Klobuchar model is a simplified model, its accuracy limited to 50-60% of the total effect shown in Figure 4.5. The model does not give a detailed description of the ionosphere behaviour particularly in high latitudes. The model is inaccurate in computing the ionospheric delay value at the equatorial regions compared with the new developed model as the difference reaches about 5 meter of zenith delay taking in mind that this difference will get larger with using lower cut-off elevation angles.

It can be seen from Figure 4.4 that the use of CODE coefficients in the Klobuchar model gives a better prediction of the ionospheric delay than using the same model with GPS broadcast coefficients. The accuracy of the Klobuchar model with CODE coefficients in the range of 75-85% of the total effect shown in Figure 4.5 (agree with (Schaer, 2001)). This yields the conclusion that the performance of the Klobuchar model with CODE coefficients is better than the same model with GPS coefficients by roughly a factor of 1.4 to 1.5 but the new CODE coefficients can't eliminate the main shortcoming of the Klobuchar model which is the model's inability to describe the ionosphere's behaviour in high and equatorial latitudes, and also when the ionosphere varies significantly from its average behaviour.

Figure 4.5 shows a more realistic description for the ionosphere behaviour that can be achieved using the newly developed model based on the IGS-GIM's. This is because:

- Firstly, it gives highly realistic behaviour in the estimation of the ionospheric delay comparing with the other two models as it is based on double-difference carrier phase measurements from IGS global tracking stations.
- Secondly, the new developed model gives a more realistic description of the global variation of the ionosphere's behaviour in different latitudes.

The newly developed model satisfies the previously mentioned criteria because it gives; high realistic behaviour in computing the ionospheric delay, more realistic detailed description for the ionosphere's behaviour whatever the latitudes or the time and finally it is very simple in computation process. Comparing the graphs in Figures 4.3, 4.4 and 4.5, the advantages of the new model can clearly be seen and the expected effect of the new model on the simulated data generated with DATSIM inferred. Selecting the new model based on IGS-GIM's for more realistic simulation of the ionospheric delay, which is the major source of error for GPS signals, will result in more realistic simulated GPS data.

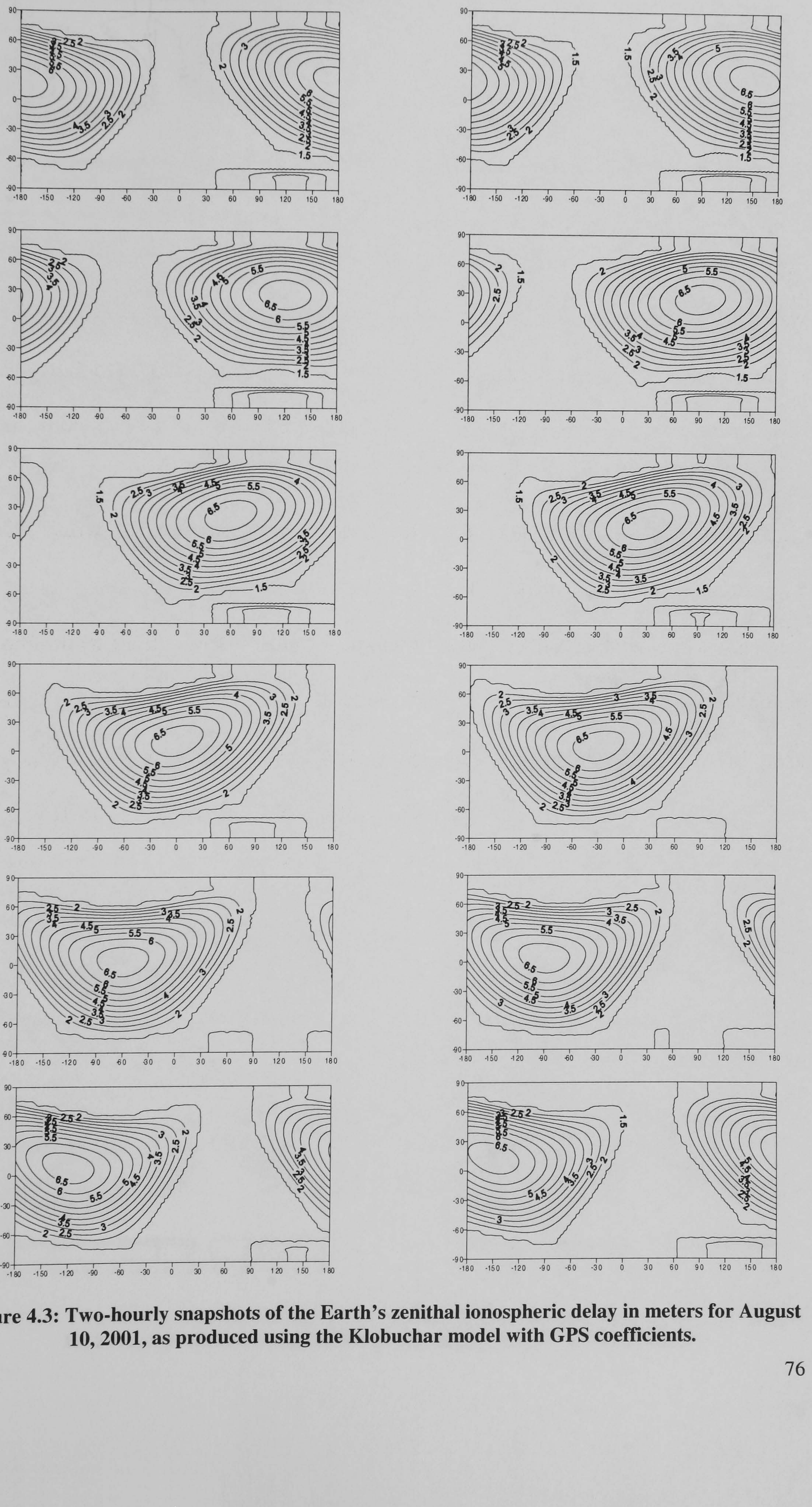

Figure 4.3: Two-hourly snapshots of the Earth's zenithal ionospheric delay in meters for August 10, 2001, as produced using the Klobuchar model with GPS coefficients.

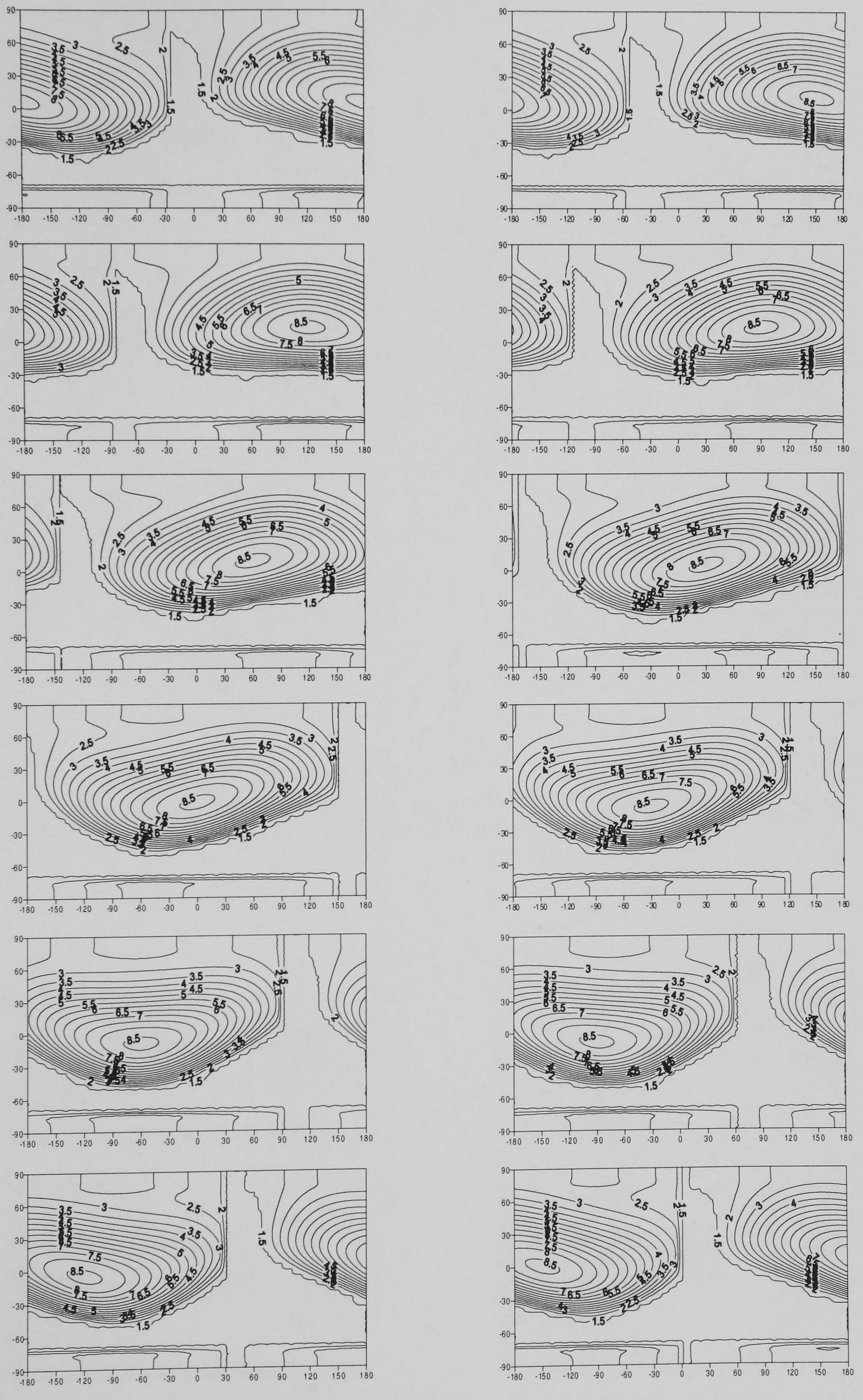

Figure 4.4: Two-hourly snapshots of the Earth's zenithal ionospheric delay in meters for August 10, 2001,as produced using the Klobuchar model with CODE coefficients.

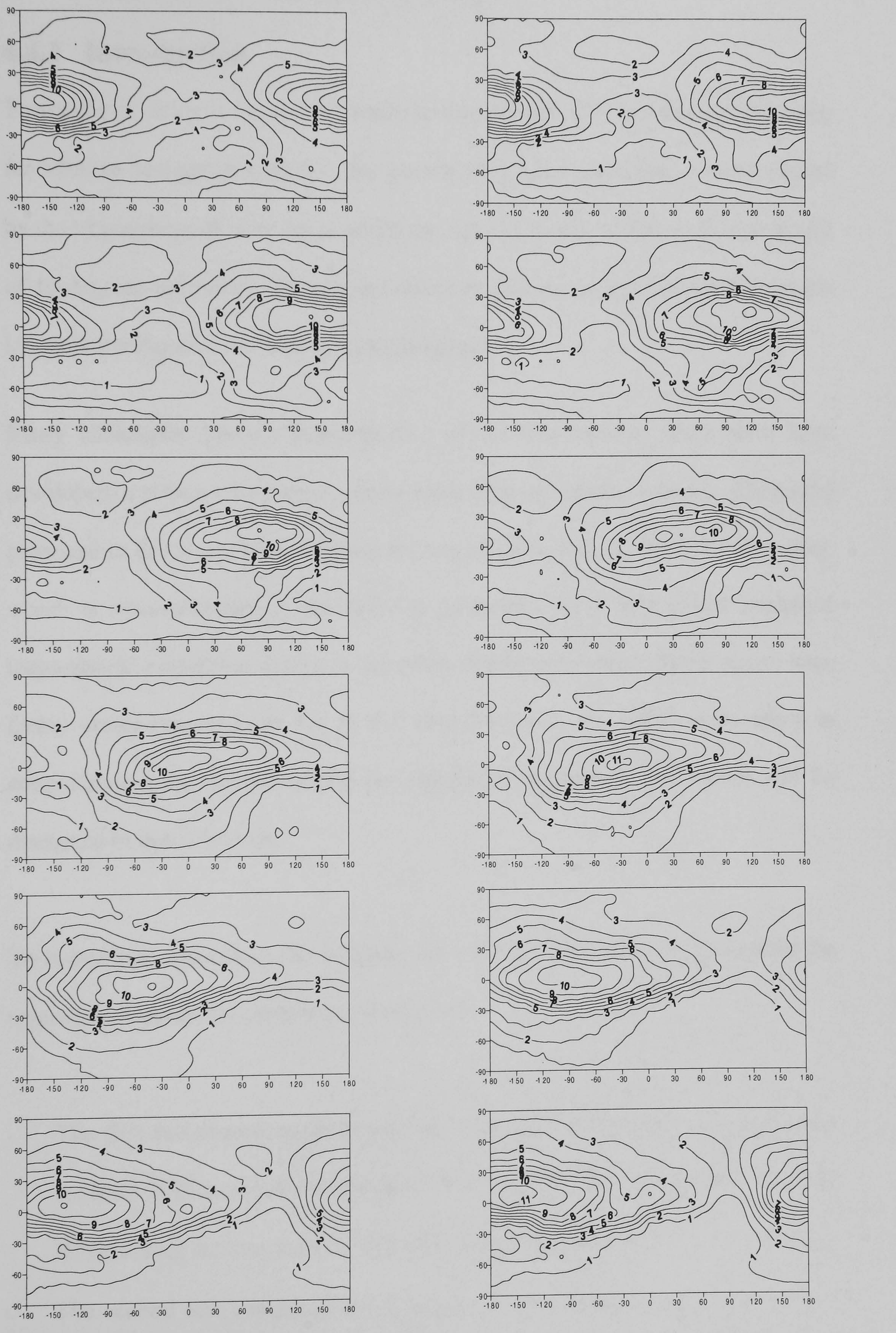

Figure 4.5: Two-hourly snapshots of the Earth's zenithal ionospheric delay in meters for August 10,2001, as produced using the newly developed model based on IGS-GIM's.

4.4 Simulation of Tropospheric Delay

4.4.1 Introduction

Tropospheric delay is the second major source of error after the ionospheric delay for satellite navigation systems. The transmitted signal could face a delay caused by the troposphere of over 2m at zenith and 20m at lower satellite elevation angles of 10 degrees and below. Positioning errors of 10m or greater can result from the inaccurate mitigation of the tropospheric delay.

Many techniques for the determination of the tropospheric delay have been developed, a review of the most widely used models is given in §2.6.5. The model proposed in this study for simulating the tropospheric delay is the EGNOS model, which is recommended by the EGNOS guidelines for it is a global statistical tropospheric model that describes the mean tropospheric delay (RMS zenith trop. Delay errors ranged from 4.0 to 4.7 cm) (Penna et al., 2001) with safety in computation time (recommended for simulation purposes). The model will be discussed in detail later on.

To investigate and assess the adequacy of the EGNOS model for simulating the tropospheric delay, two tests were conducted:

- The first test compares the behaviour of the EGNOS model with the highly accurate IGS-tropospheric products from CODE. This study involves four IGS tracking stations for four non consecutive seasonal weeks over one year.
- The second test compares the behaviour of the EGNOS model with other tropospheric models. These models can be categorized in two types: surface meteorological models and global empirical models. The study involved

three IGS tracking stations for four nonconsecutive seasonal weeks over one year. The IGS tropospheric products were used in this study for reference. The findings of these two studies were presented in Farah (2003c), Farah et al. (2003).

4.4.2 The EGNOS Tropospheric Model Description

The European Geo-stationary Navigation Overlay Service (EGNOS) is the first phase of Europe's contribution to the Global Navigation Satellite System-1 (GNSS-1). The system consists of a number of ground Receiver Integrity Monitors (RIM's) and geo-stationary satellites where the RIM's provide the wide area differential GPS and integrity services for both the GPS and GLONASS systems, the geo-stationary satellites are used to broadcast the integrity and wide area differential corrections to the users as well as providing extra pseudo-range observations. The wide area differential GPS service separates the measurement errors into different components; orbit, satellite clock, ionospheric delay and tropospheric delay. The tropospheric delay correction is not broadcast to the user due to the large variation in tropospheric delay with different weather conditions. Instead an estimate is generated locally by the user, based on a tropospheric model (Penna et al., 2001), which is following the International Civil Aviation Organisation (ICAO) Standards and Recommended Practices (SARPs) for Satellite Based Augmentation Systems (SBAS) (RTCA, 1999).

The recommended EGNOS model provides an estimate of the zenith total tropospheric delay that is dependent on empirical estimates of five meteorological parameters at a receiver - namely, pressure, temperature, water vapour pressure,

temperature lapse rate and water vapour lapse rate. These estimates of the meteorological parameters are dependent on the receiver's height, latitude and day-of-year, and are interpolated from reference values for the yearly averages of the parameters and their associated seasonal variations, derived primarily from North American meteorological data. The same scenario is followed on other satellite-based augmentation systems such as: USA Wide Area Augmentation System (WAAS) and Japanese Multi-functional Transport Satellite, MTSAT-based Satellite Augmentation System (MSAS) (Penna et al., 2001). This is so that the EGNOS model is consistent with the tropospheric model for the WAAS program detailed in (Collins and Langley, 1997) and also discussed in (Collins and Langley, 1998). The EGNOS guidelines then recommend mapping the zenith total tropospheric delay estimate to the appropriate receiver-to-satellite elevation angle using an elevation angle-dependent mapping function.

4.4.3 EGNOS Tropospheric Model Algorithm

The EGNOS model is described in (Penna et al., 2001) and for reference is repeated here. The total tropospheric delay for a receiver-to-satellite range at elevation angle α is modelled using (RTCA, 1999):

$$d_{\alpha} = \left(d_{dry} + d_{wet}\right). MF(\alpha) \tag{4.8}$$

where: d_{dry} is the zenith dry delay,

d_{wet} is the zenith wet delay,

$MF(\alpha)$ is the mapping function to map the zenith total delay to the appropriate receiver-to-satellite elevation angle.

The estimation of the zenith total tropospheric delay is depending on five meteorological parameters: the total pressure, temperature and water vapour pressure at mean sea level, and temperature and water vapour lapse rates, used to scale the pressures and temperatures to the user's height above sea level. These meteorological parameters can be obtained from a table of values (Table 4.1) given at discrete latitudes, with linear interpolation applied as necessary. The seasonal variation of the parameters is modelled via a sinusoidal function of the day-of-year. So, the zenith dry and wet delays are computed using:

$$d_{dry} = z_{dry}\left[1 - \frac{\beta H}{T}\right]^{\frac{g}{R_d \beta}} \tag{4.9}$$

$$d_{wet} = z_{wet}\left[1 - \frac{\beta H}{T}\right]^{\frac{(\lambda+1)g}{R_d \beta} - 1} \tag{4.10}$$

where : g $= 9.80665$ m/s^2,

H is the height of the receiver above mean sea level (m),

T is the temperature at mean sea level (K),

β is the temperature lapse rate (K/m),

R_d = 287.054 J/kg/K,

λ is the water vapour lapse rate (dimensionless),

z_{dry} is the zenith dry delay at mean sea level,

z_{wet} is the zenith wet delay at mean sea level.

The zenith dry and wet delays at mean sea level are given as follows:

$$z_{dry} = \frac{10^{-6} k_1 R_d P}{g_m} \tag{4.11}$$

where : k_1 = 77.604 K/mbar,

P is the pressure at mean sea level (mbar),

g_m = 9.784 m/s^2.

and

$$z_{wet} = \frac{10^{-6} k_2 R_d}{g_m(\lambda + 1) - \beta R_d} \cdot \frac{e}{T} \tag{4.12}$$

where : k_2 = 382000 K^2/mbar,

e is the water vapour pressure at mean sea level (mbar).

Using the average values and seasonal variations for the five meteorological parameters given in Table 4.1, each meteorological parameter value (ξ) may then be computed using the following equation:

$$\xi(\phi, D) = \xi_0(\phi) - \Delta\xi(\phi) \cdot \cos\left[\frac{2\pi (D - D_{\min})}{365.25}\right] \tag{4.13}$$

where: ϕ is the receiver's latitude,

D is the day-of-year (starting with 1 January),

$D_{\min}$ = 28 for northern latitudes,

$D_{\min}$ = 211 for southern latitudes,

ξ_0 and $\Delta\xi$ are the average and seasonal variation respectively for the particular parameter at the receiver's latitude.

Average					
Latitude (°)	P_o (mbar)	T_o (K)	e_o (mbar)	β_0 (K/m)	λ_0
≤ 15	1013.25	299.65	26.31	$6.30e^{-3}$	2.77
30	1017.25	294.15	21.79	$6.05e^{-3}$	3.15
45	1015.75	283.15	11.66	$5.58e^{-3}$	2.57
60	1011.75	272.15	6.78	$5.39e^{-3}$	1.81
≥ 75	1013.00	263.65	4.11	$4.53e^{-3}$	1.55
Seasonal Variation					
Latitude (°)	ΔP_o (mbar)	ΔT_o (K)	Δe_o (mbar)	$\Delta \beta_0$ (K/m)	$\Delta \lambda_0$
≤ 15	0.00	0.00	0.00	$0.00e^{-3}$	0.00
30	-3.75	7.00	8.85	$0.25e^{-3}$	0.33
45	-2.25	11.00	7.24	$0.32e^{-3}$	0.46
60	-1.75	15.00	5.36	$0.81e^{-3}$	0.74
≥ 75	-0.50	14.50	3.39	$0.62e^{-3}$	0.30

Table 4.1: Average values and seasonal variation values of the five meteorological parameters used by the EGNOS model.

The mapping function $MF(\alpha)$ which is not valid for elevation angles of less than 5 degrees (RTCA, 1999) is expressed as:

$$MF(\alpha) = \frac{1.001}{\sqrt{0.002001 + \sin^2 \alpha}}. \tag{4.14}$$

4.4.4 First Test Study

A comparison study was conducted between the EGNOS model and the CODE tropospheric product. CODE produces zenithal tropospheric delay products from about 114 IGS-tracking stations every two hours with a 10 degrees elevation cut-off angle applied and using the Niell (wet) mapping function (Niell, 1993). Four IGS tracking stations, varying in latitude and height, were selected for this study. The selection of the stations was restricted by the availability of IGS-CODE

tropospheric estimates. The tropospheric zenith delay data from four weeks in different seasons were chosen to assess the seasonal variation of the weather conditions. The dates of the data samples are shown in Table 4.2. The geographical positions of the tested IGS stations in the first test using the 4 character IGS-codes (Bor1, Gala, Mac1 and MAS1) and second test study (Bor1, Hers, Bahr) are shown in Figure 4.6 and Table 4.3.

GPS week	1097	1110	1123	1136
Date	14/1/01-20/1/01	15/4/01-21/4/01	15/7/01-21/7/01	14/10/01-20/10/01

Table 4.2: Dates of Data Samples for the First Tropospheric Comparison Test.

With the highly accurate estimation of the total tropospheric delay from the CODE-Tropospheric products, the differences of total zenith delay between the EGNOS model and the CODE-Troposphere estimation will give an indication of the quality of the EGNOS model and assess its adequacy for the GPS-data simulation.

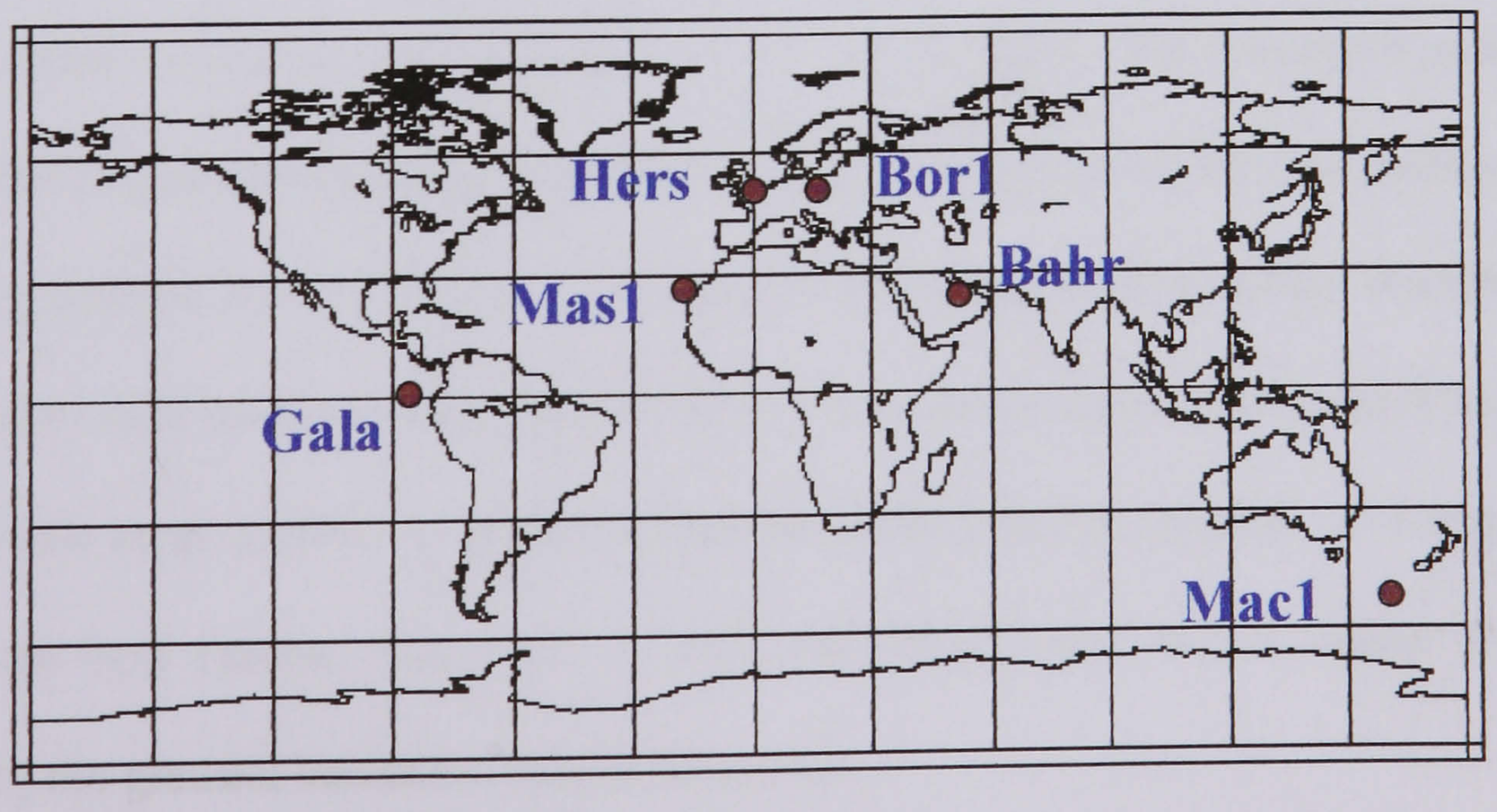

Figure 4.6: The geographical positions of the tested IGS stations.

Station IGS-ID	Latitude (degree)	Longitude (degree)	Height (meter)	City	Country
BOR1	52.276 N	17.073 E	124.358	Borowiec	Poland
GALA	0.742 S	89.696 W	7.441	Galapagos Island	Ecuador
MAC1	54.499 S	158.936 E	-6.763	Macquarie Island	Southern Ocean
MAS1	27.763 N	15.633 W	197.161	Maspalomas	Spain
BAHR	26.209 N	50.608 E	-17.03	Manama	Bahrain
HERS	50.867 N	0.336 E	76.521	Hailsham	United Kingdom

Table 4.3: The detailed geographical positions of the tested IGS tracking stations.

Figures 4.7 to 4.22 show the total tropospheric zenith delay estimates from both the EGNOS model and the CODE-Tropospheric delay estimates for each of the four stations, for each of the four weeks. Table 4.4 shows the total zenith delay differences between the EGNOS model and the CODE-Tropospheric delay estimation. Note that some of the CODE estimations in Figures 4.7 to 4.22 contains null periods due to a lack of data. It can be shown that 67% of the mean differences are within 7 cm, with the largest value being 12 cm. The EGNOS model cannot represent the tropospheric delays due to weather changes because it has no input of meteorological data at the receiver position. The maximum zenith delay difference between the model and CODE estimates over the four weeks at the four stations are 5 to 16 cm respectively. Thus, the EGNOS model describes reasonably well the mean total zenith delay. These results agree with related work by Dodson et al. (1999). It is shown that the BOR1 station (middle of Europe) gives the best results, then GALA, with the MAC1 and MAS1 island sites showing the greatest variations between seasons.

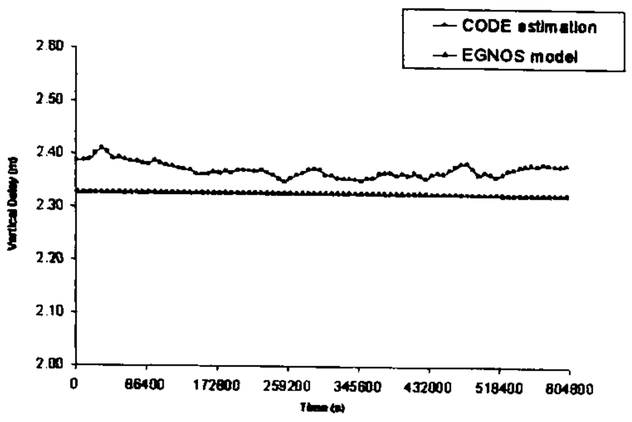

Fig. 4.7: The Total Trop. Zenith Delays in GPS week 1097 [BOR1] station

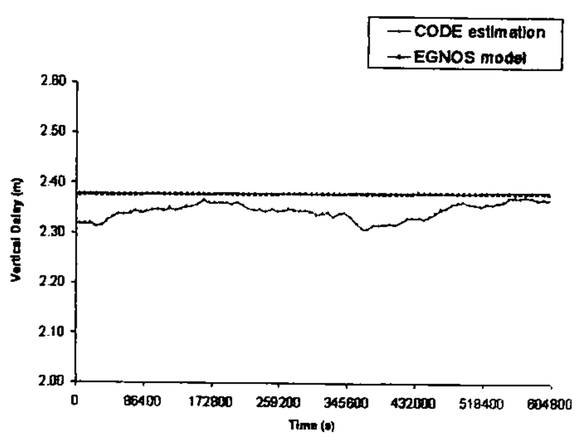

Fig. 4.8: The Total Trop. Zenith Delays in GPS Week 1110 [BOR1] station

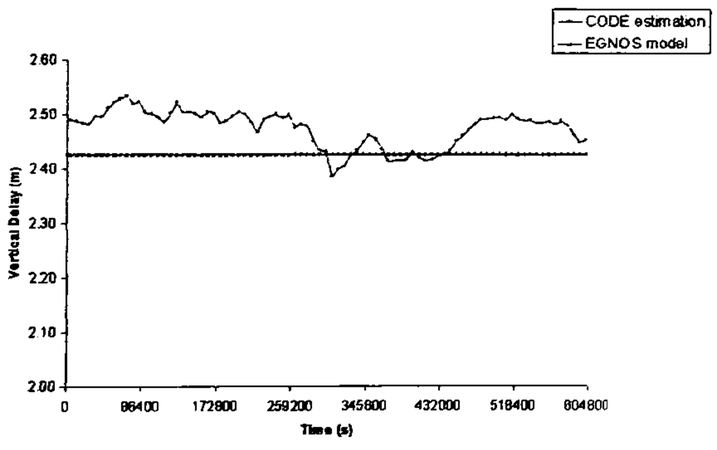

Fig. 4.9: The Total Trop. Zenith Delays in GPS week 1123 [BOR1] station

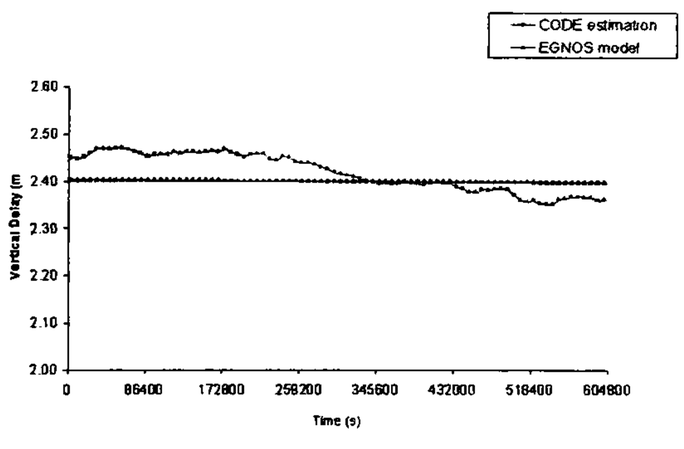

Fig. 4.10: The Total Trop. Zenith Delays in GPS week 1136 [BOR1] station

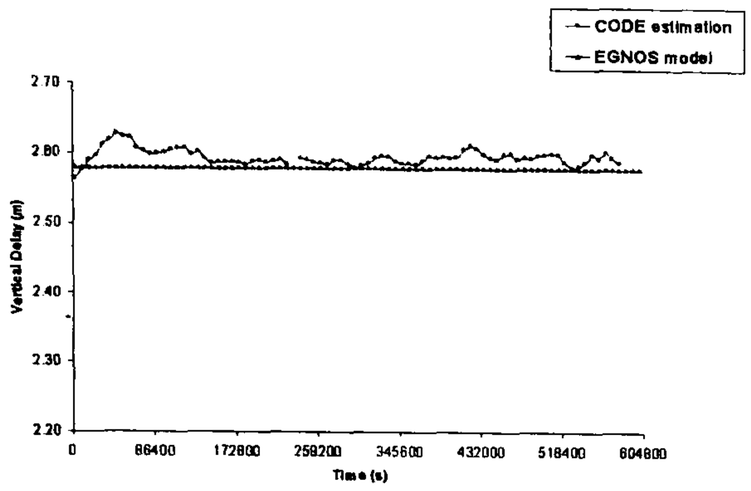

Fig. 4.11: The Total Trop. Zenith Delays in GPS week 1097 [GALA] station

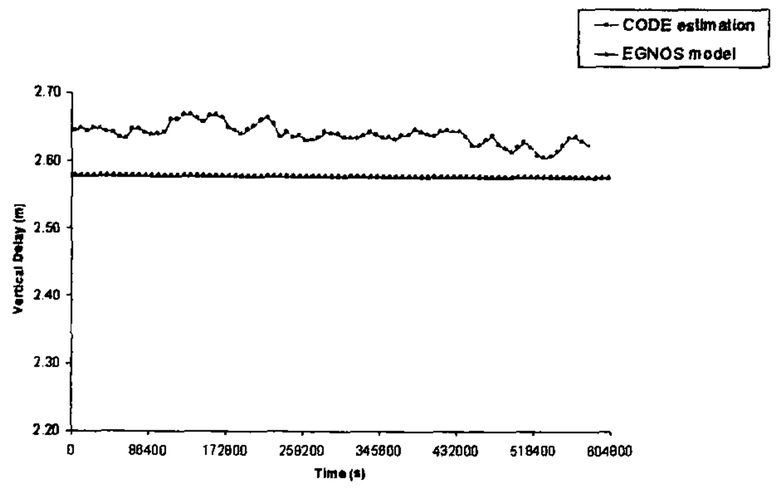

Fig. 4.12: The Total Trop. Zenith Delays in GPS week 1110 [GALA] station

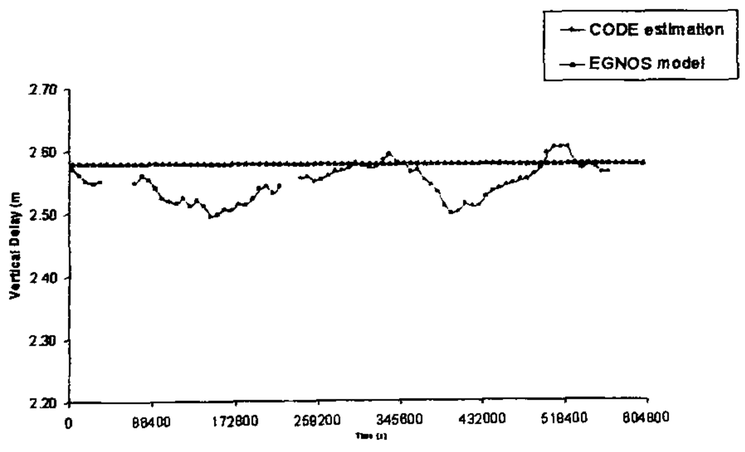

Fig. 4.13: The Total Trop. Zenith Delays in GPS week 1123 [GALA] station

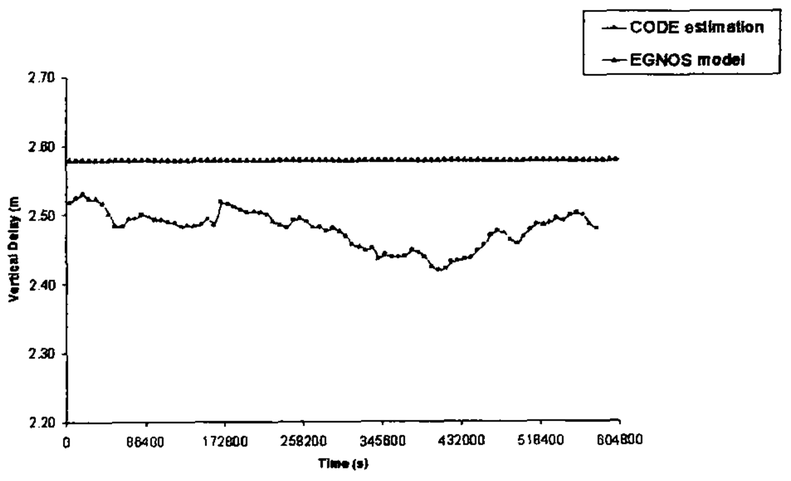

Fig. 4.14: The Total Trop. Zenith Delays in GPS week 1136 [GALA] station

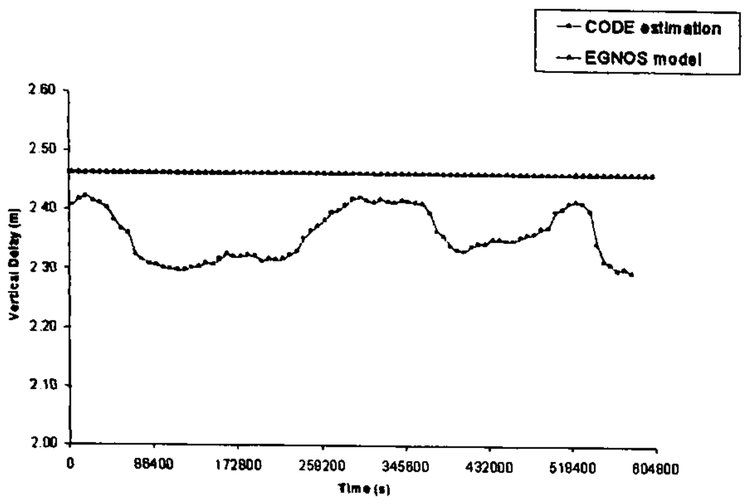

Fig. 4.15: The Total Trop. Zenith Delays in GPS week 1097 [MAC1] station

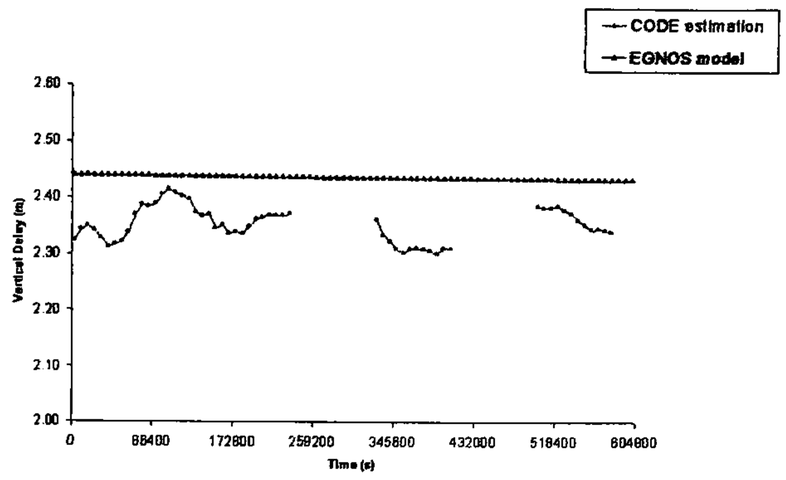

Fig. 4.16: The Total Trop. Zenith Delays in GPS week 1110 [MAC1] station

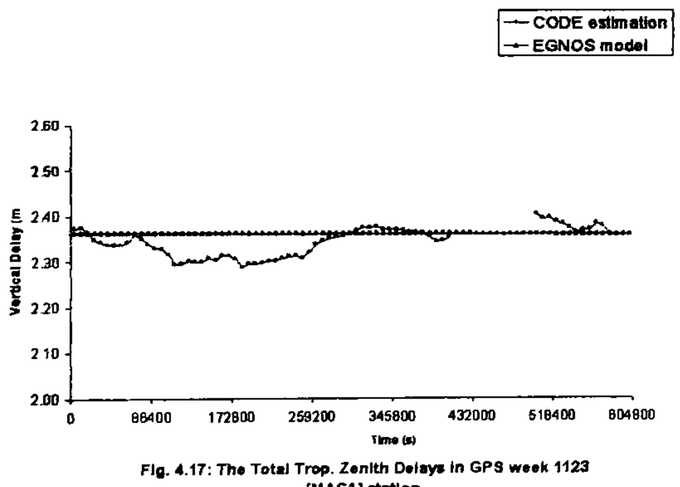

Fig. 4.17: The Total Trop. Zenith Delays in GPS week 1123 [MAC1] station

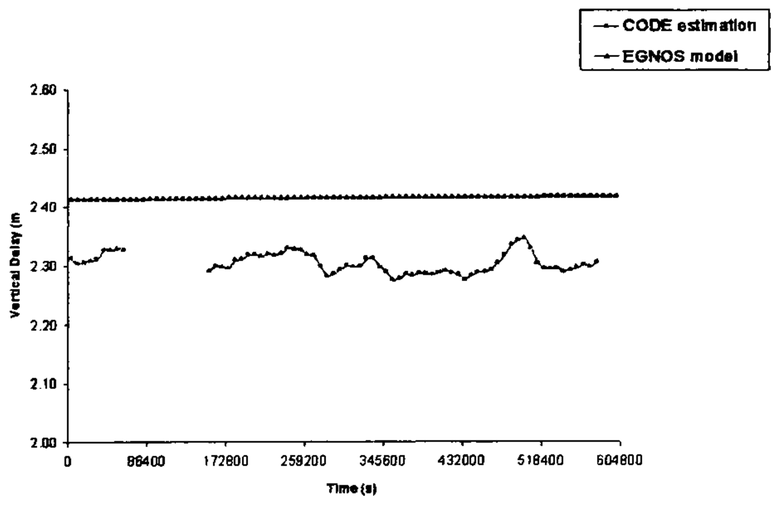

Fig. 4.18: The Total Trop. Zenith Delays in GPS week 1136 [MAC1] station

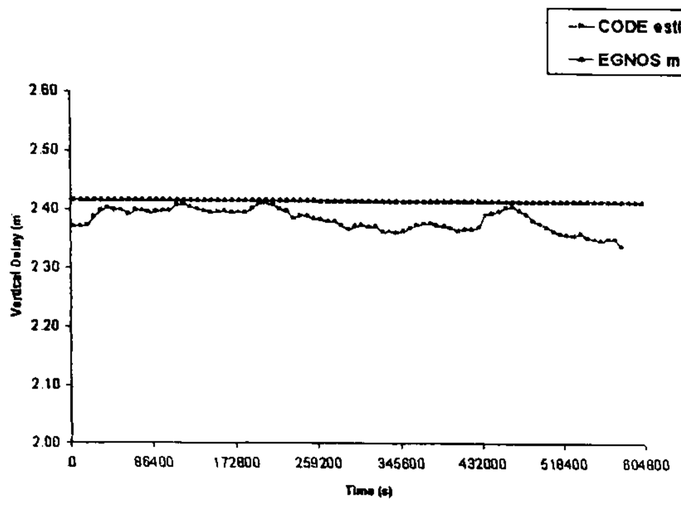

Fig. 4.19: The Total Trop. Zenith Delays in GPS week 1097 [MAS1] station

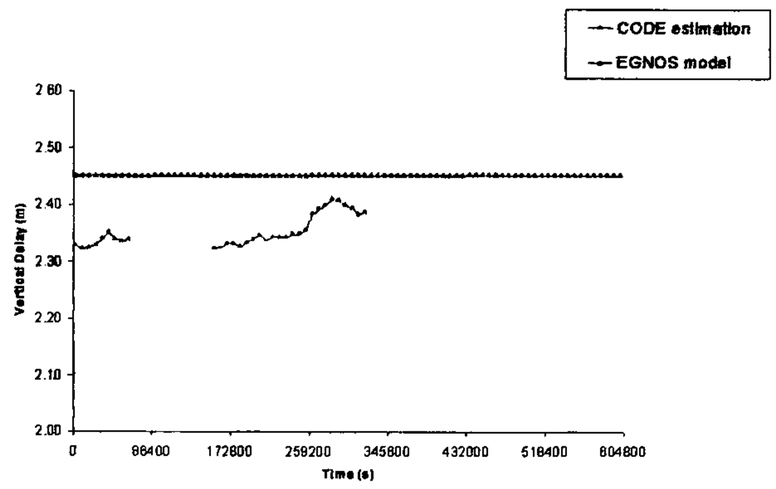

Fig. 4.20: The Total Trop. Zenith Delays in GPS week 1110 [MAS1] station

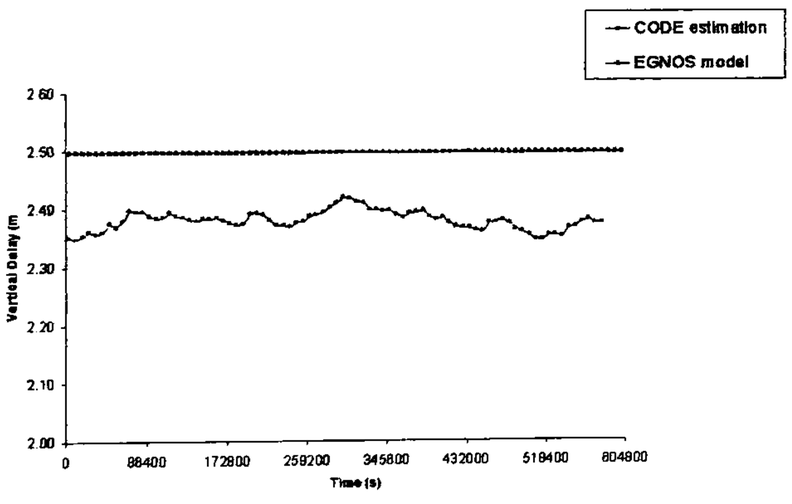

Fig. 4.21: The Total Trop. Zenith Delays in GPS week 1123 [MAS1] station

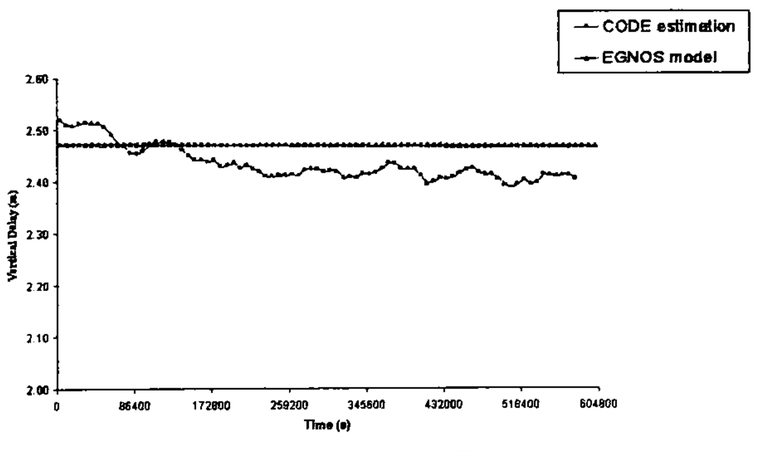

Fig. 4.22: The Total Trop. Zenith Delays in GPS Week 1136 [MAS1] station

Station	GPS week	Mean (cm)	RMS (cm)	Max. (cm)
BOR1	1097	4.4	4.6	8.3
	1110	-3.6	3.9	-7.1
	1123	4.7	5.8	10.9
	1136	1.8	4.2	6.7
GALA	1097	1.4	1.9	4.9
	1110	6.2	6.3	9.1
	1123	-3.0	4.1	-8.4
	1136	-9.9	10.3	-15.9
MAC1	1097	-10.3	11.2	-16.7
	1110	-8.6	9.2	-13.5
	1123	-1.8	3.6	-6.9
	1136	-11.2	11.3	-14.3
MAS1	1097	-3.4	3.8	-7.7
	1110	-10.1	10.5	-12.8
	1123	-11.9	12.1	-15.2
	1136	-3.4	4.8	-7.9

Table 4.4: Total Tropospheric Zenith Delay Difference between EGNOS model and CODE-tropospheric estimation.

4.4.5 Second Test Study

A second comparison study compared the behaviour of the EGNOS tropospheric model with other tropospheric models. These tropospheric models can be categorized in two groups: surface meteorological models such as (Saastamoinen, Hopfield and Marini) and global empirical models such as the Magnet model (see §2.6.5). The IGS-tropospheric estimations (combined tropospheric estimates from all IGS analysis centers) were used in the study as a reference. The surface meteorological models used the IGS meteorological measurements for the tested stations to assure high performance. The study involved three IGS-stations, details of which are given in Table 4.3 and Figure 4.6. Figures 4.23 to 4.34 show the total tropospheric zenith delays resulting from IGS-estimations and the other five models for four non-consecutive weeks over one year (to assess seasonal variations) which dates are shown in Table 4.5.

GPS week	1135	1149	1162	1175
Date	07/10/01-13/10/01	13/1/02-19/1/02	14/4/02-20/4/02	14/7/02-20/7/02

Table 4.5: The Tested Dates for the Second Tropospheric Comparison Test.

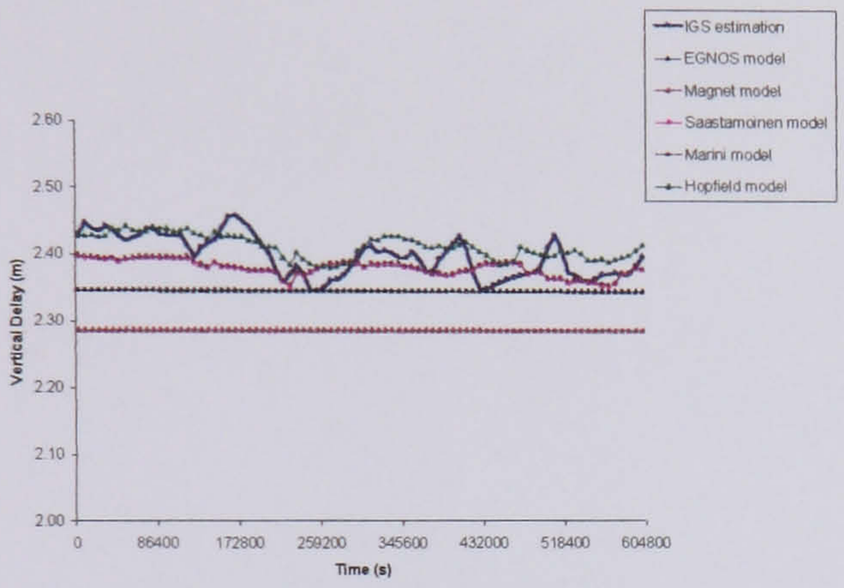

Fig. 4.23: The Total Trop. Zenith Delays in GPS week 1149 [HERS] station

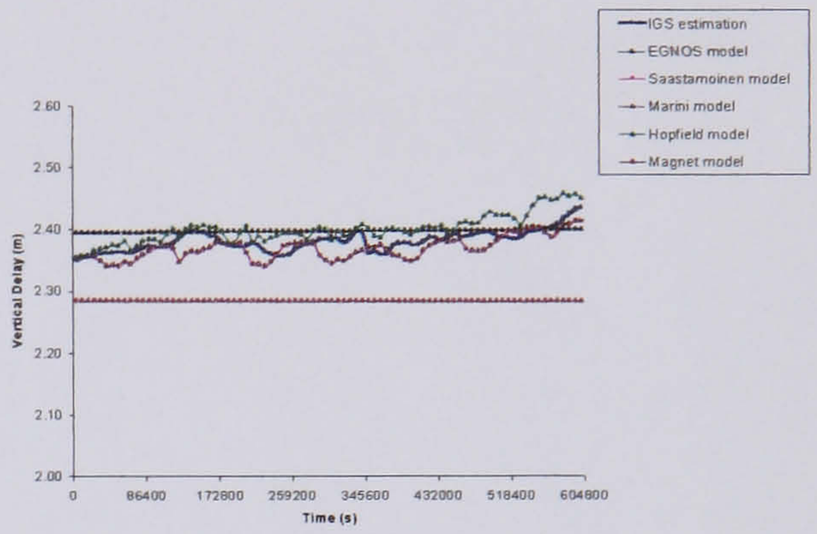

Fig. 4.24: The Total Trop. Zenith Delays in GPS week 1162 [HERS] station

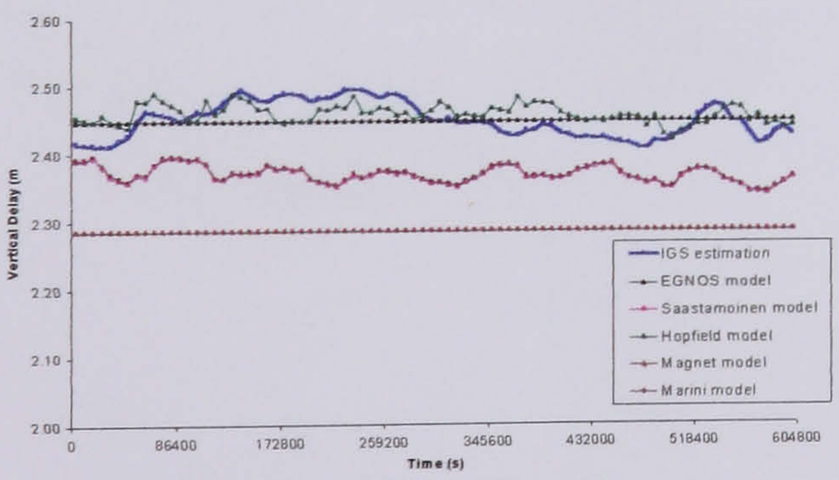

Fig. 4.25: The Total Trop. Zenith Delays in GPS week 1175 [HERS] station

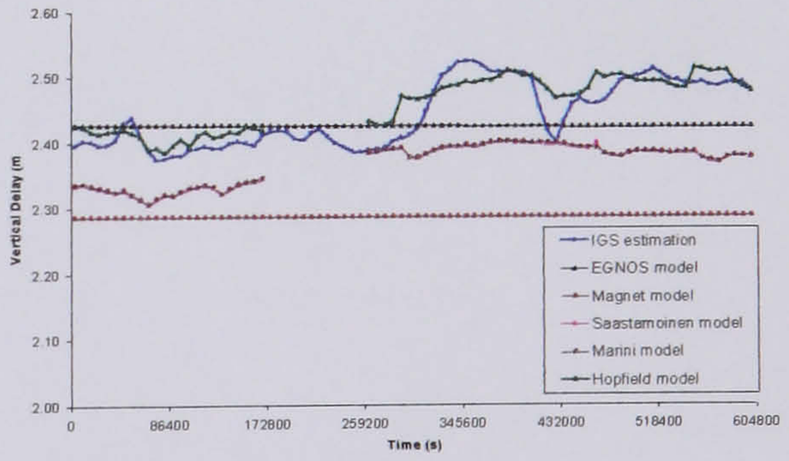

Fig. 4.26: The Total Trop. Zenith Delays in GPS week 1135 [HERS] station

Fig. 4.27: The Total Trop. Zenith Delays in GPS week 1097
[BOR1] station

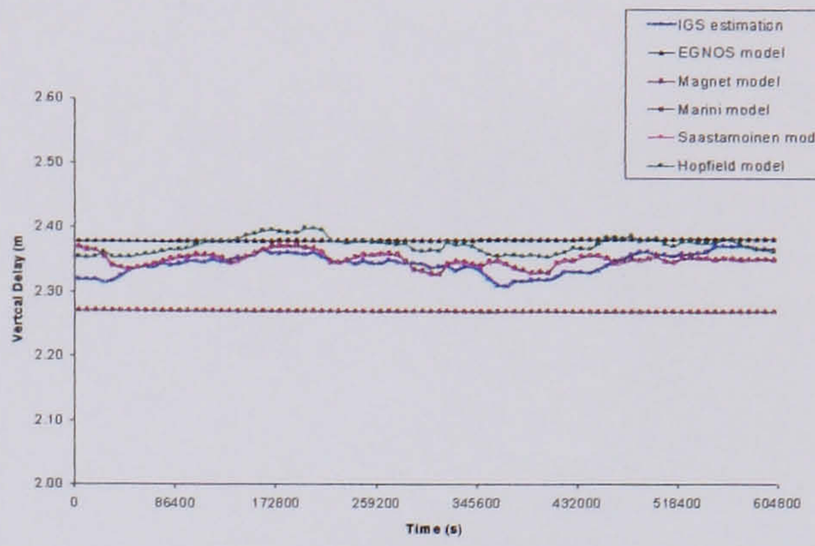

Fig. 4.28: The Total Trop. Zenith Delays in GPS Week 1110
[BOR1] station

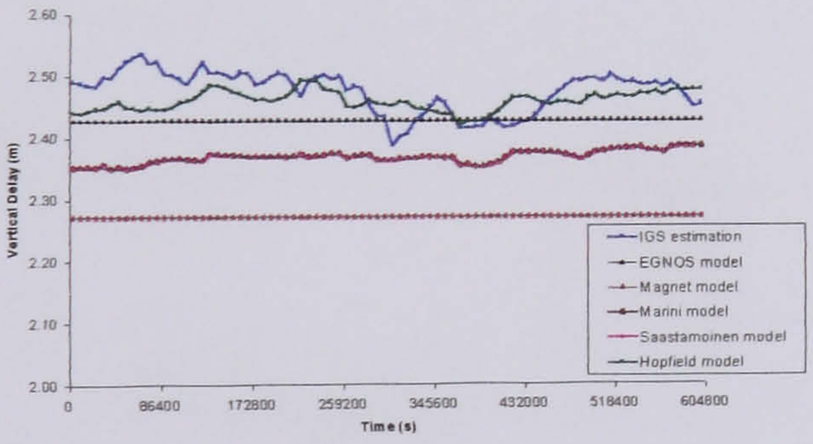

Fig. 4.29: The Total Trop. Zenith Delays in GPS week 1123
[BOR1] station

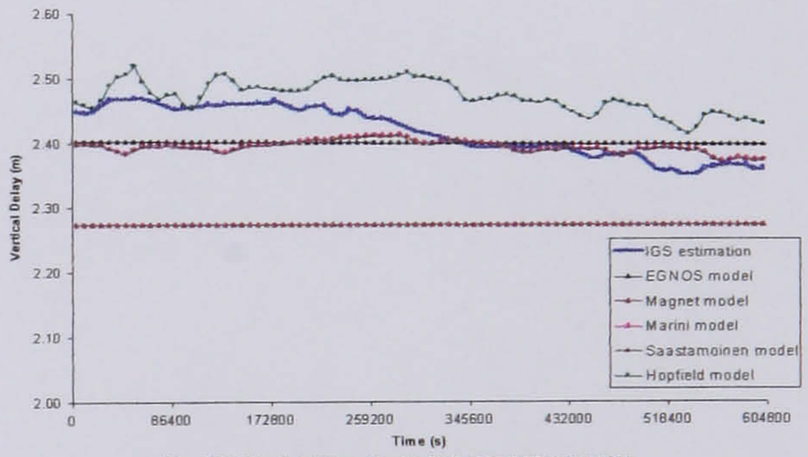

Fig. 4.30: The Total Trop. Zenith Delays in GPS week 1136
[BOR1] station

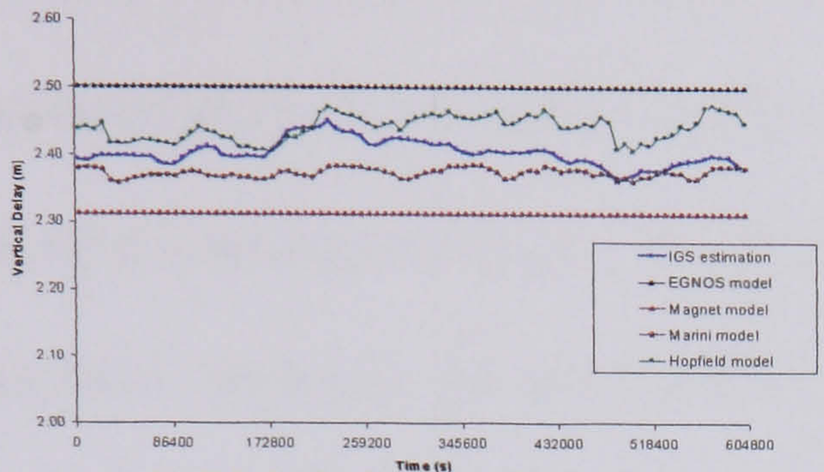

Fig. 4.31: The Total Trop. Zenith Delays in GPS week 1149
[BAHR] station

Fig. 4.32: The Total Trop. Zenith Delays in GPS week 1162
[BAHR] station

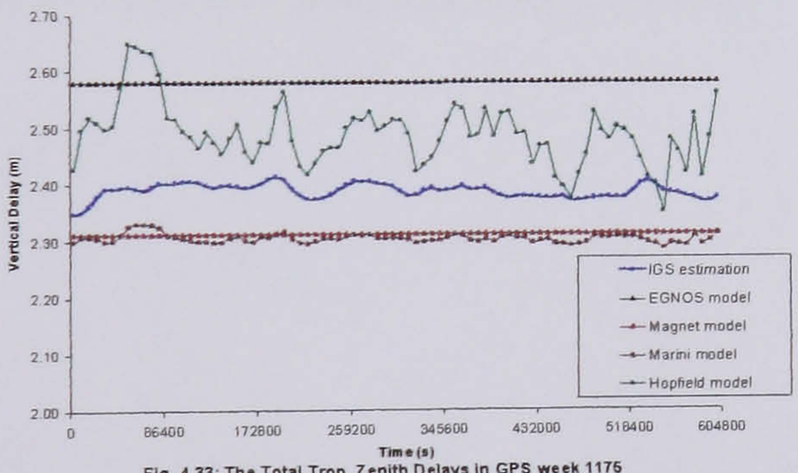

Fig. 4.33: The Total Trop. Zenith Delays in GPS week 1175
[BAHR] station

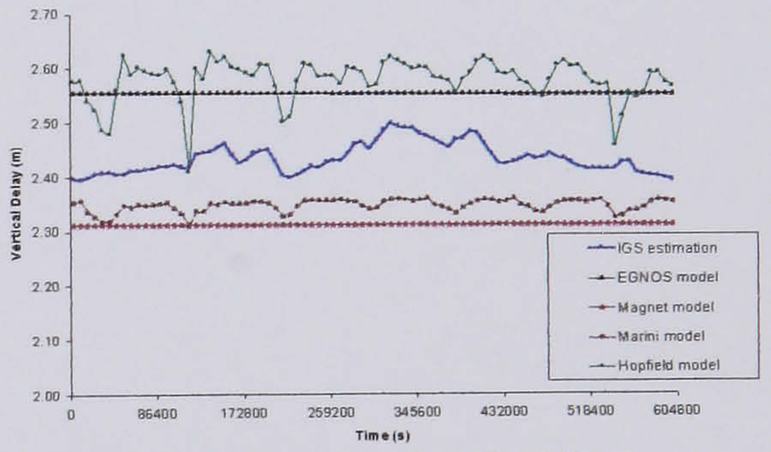

Fig. 4.34: The Total Trop. Zenith Delays in GPS week 1188
[BAHR] station

From Figures 4.23 to 4.34 it can be seen that the EGNOS model follows the IGS tropospheric estimates more closely than the Magnet model. The Magnet model was previously considered as a possible model for tropospheric delay in GPS data simulation process, as it is an empirical global model, which does not require meteorological data as input but it is only account for the hydrostatic delay part of the total tropospheric delay. The EGNOS model fits better for HERS and BOR1 (northern stations) but not for BAHR (southern station), for the fact that the EGNOS model is optimised to fit well in Central Europe region only.

The EGNOS model behaves well comparing with other surface meteorological models, which show more accurate behaviour but the need for surface meteorological data as input data is not ideal for simulation purposes. The behaviour of the Saastamoinen and Marini models is identical, so only one of them is considered in some figures.

4.4.6 Discussion & Conclusion

The EGNOS tropospheric correction model has shown acceptable level of accuracy in describing the average tropospheric delay model as it agrees reasonably well with the CODE-tropospheric products based on GPS measurements. The mean difference in total zenith delay between the EGNOS model and the precise CODE-estimations of the tropospheric delay is about 7 cm with maximum difference of up to 16 cm.

The EGNOS model shows a better level of agreement with the IGS estimates than do other empirical tropospheric models; such as the Magnet model. The EGNOS model also shows a good level of agreement with surface meteorological tropospheric models. However, these need real-time meteorological input data to estimate the tropospheric delay, and so are not ideal for GPS data simulation

The week point about the EGNOS model is its inability to model the temporal and small-scale regional variations of the troposphere as the model does not have the ability to model sub-seasonal variations Penna et al., (2001) and Dodson, (1999) as well as modelling small-scale tropospheric variations. This may be overcome by using other mathematical techniques to add these regional variations over the basic model. This subject will be investigated in the next section of this chapter.

The EGNOS tropospheric model is adequate for GPS-data simulation as it fulfils many requirements;

- Computationally simple.
- Good behaviour in describing the mean tropospheric delay compared with IGS-tropospheric estimations and other established models.
- The model may have the ability of modelling spatial and temporal tropospheric variations through using statistical mathematical theories (see §4.5).

4.5 Improving Chosen Atmospheric Models

4.5.1 Introduction

This section will deal with techniques for improving the two chosen models for simulating the atmospheric error: namely the ionospheric delay model based on IGS-global ionospheric maps and the EGNOS tropospheric model. As it has been shown in previous sections (§4.3) and (§4.4) both models are adequate for simulating errors in GPS- measurements, however both models are unable to simulate the small-scale regional variations in the atmosphere. Improving this aspect of both models will result in models with a high spatial resolution for simulating the ionospheric and tropospheric delays.

It is true that using both models as they are now will yield a high accuracy in positioning computations without adding any ability of simulating any regional variations to them, however from the data-simulation point of view, it will be a powerful tool to have the ability of simulating the real behaviour of both the ionosphere and troposphere and show these regional variations as they appear in the real world.

Using a mathematical technique called "Gaussian Random Fields", it would be possible to add a controlled random surface over the base value of each model, giving the ability to simulate these regional variations. This nature of the used random surface depends on how the ionosphere and troposphere changes regionally. A brief review about the Gaussian random fields will be given in the next section.

4.5.2 Gaussian Random Fields

Studying and analysis of spatial data is a common task for different branches of sciences such as geology, geography, meteorology and geodesy. Given a quantity of interest, z, varies over a domain D in space according to an unknown function $z: D \subset R^d \rightarrow R$. In most cases z is observed only in a small number of locations in D, and inference about z is then based on a proposed mathematical model for the function $z(.)$. The stochastic approach to modelling $z(.)$ is to consider it as a realisation of a random field where the Gaussian random fields roll in this process.

The justification of using the Gaussian model in many applications comes from (Kozintsev, 1999):

- Firstly, many data-sets from the natural sciences display obviously Gaussian characteristics.
- Secondly, Gaussian random fields are well known as well as convenient mathematical objects, defined completely by their mean and covariance functions.

The Gaussian random field is 'stationary' if its distribution is unchanged when the origin of the index set D is translated. If the distribution is also unchanged when the index set is rotated about the origin, the field called 'isotropic'.

In cases where values of the field at several locations are available as observations and the interest is to predict the field only in a few locations, a multivariate Gaussian vector can contain both observed and unobserved values. However when the interest

is in the values of the field everywhere, the multivariate Gaussian vector becomes too long to work with because of storage and computational requirements. In such cases the generation of multivariate normal vectors based on Cholesky decomposition (Cressie, 1993) of the covariance matrix is not valid. A new technique called circular embedding (Kozintsev, 1999) is used instead. Many algorithms were developed for generating stationary Gaussian random fields using the circular embedding technique Dembo et al. (1989), Dietrich and Newsam (1993) and Wood and Chan (1994).

The algorithm considered in this thesis for improving the atmospheric models is the stationary Gaussian random fields algorithm presented by (Chan, 1999) for its computational efficiency. The Fortran programs implementing the simulation algorithm were available through (Chan, 2003), also they are shown in Appendix-A for reference with the defined parameters used for the following test study (Section 4.5.3). These Fortran programs were coded within DATSIM software to add the generated random surface over the base results of each atmospheric model discussed earlier applying scale factors to control the amount of variations expected from the ionosphere and troposphere. The troposphere could face a change of (5 cm to 10 cm) in zenith wet delay for spatial scale of (10 km to 100 km) (Bock, 2001), however the ionosphere's variation depends mainly on the latitude of the tested stations as well as the Sun's geomagnetic activity. A test study revealing the effect of the implemented algorithm is investigated in the following section.

4.5.3 The Test Study

GPS Data was simulated for two adjacent IGS stations in the United Kingdom (HERS, NPLD) with a baseline of about 77km. The details of these two stations are shown in Table 3.6. The amount of variation applied for the zenith tropospheric and ionospheric delays were 10cm, 0.32m respectively. 0.32m variation in zenith ionospheric delay corresponds to 2TECU variation, which is expected for middle latitude stations under quiet ionospheric activity case (Aquino, 2004). The limitation of the test to one baseline could be justified for the limitation in existing short baselines (< 100 km) with available true tropospheric zenith delay estimations as IGS stations offer. The short baseline is crucial for showing the small scale regional and temporal variation which is the scope of this study.

IGS-Station ID	Latitude (degree)	Longitude (degree)	Height (meter)	City	Country
HERS	50.867 N	0.336 E	76.521	Hailsham	United Kingdom
NPLD	51.421 N	0.338 W	72.719	Teddington	United Kingdom

Table 4.6: The Details of the two IGS-stations for the regional variation test.

The total zenithal tropospheric delays were plotted for both stations from the IGS-tropospheric estimations, the EGNOS basic model and the EGNOS modified model. Those plots are shown in Figures 4.35, 4.36. The total tropospheric zenith delays difference between the two stations (HERS, NPLD) is shown in Figure 4.37. Table 4.7 shows the RMS values for plots in Fig. 4.35, 4.36 and 4.37. The zenith ionospheric delay for the two stations from the basic IGS-GIM's model and the

modified model are shown in Figures 4.38, 4.39 with the difference in the zenith ionospheric delay plotted in Figure 4.40.

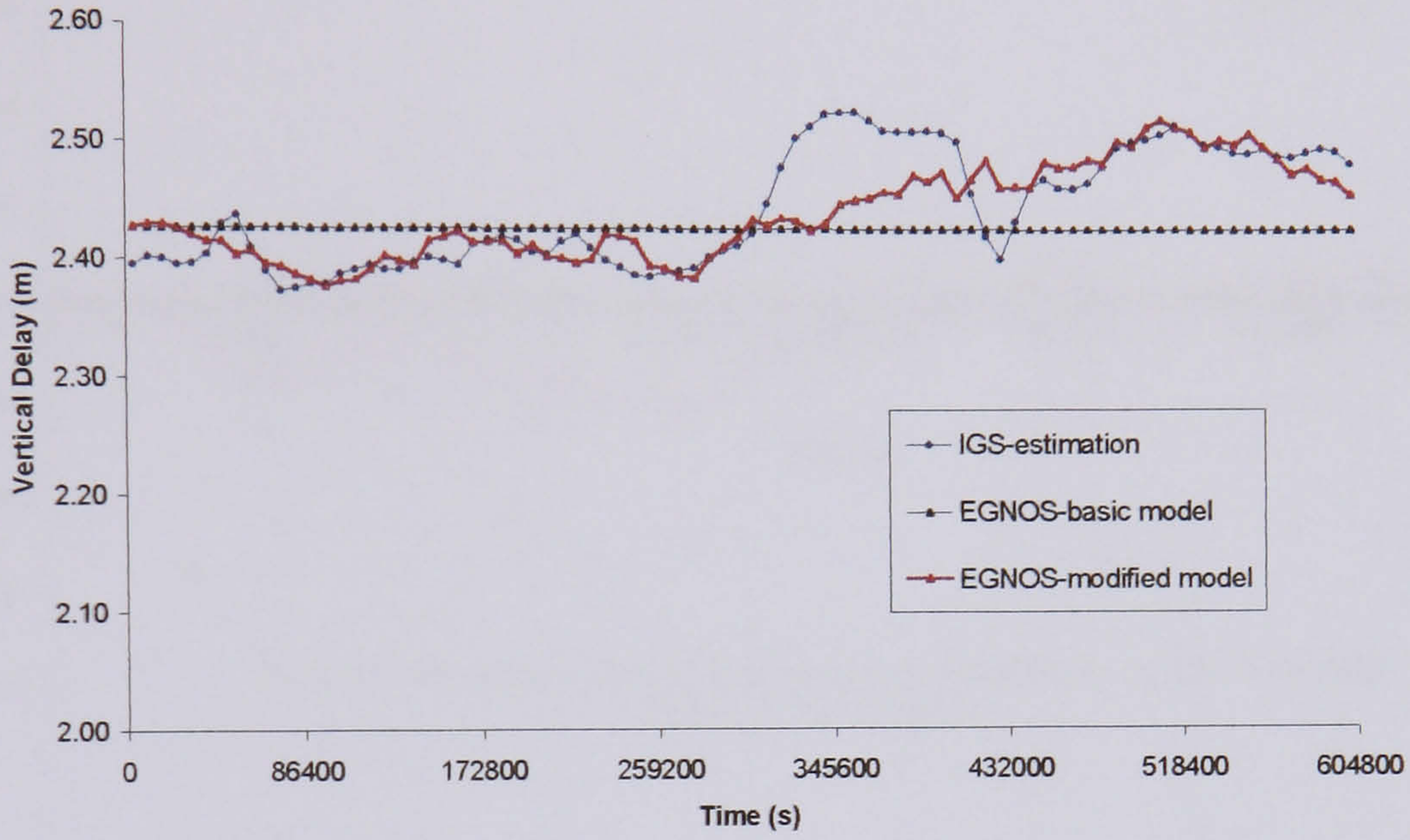

Fig. 4.35: The Total Trop. Zenith Delays in GPS week 1135 [HERS] station

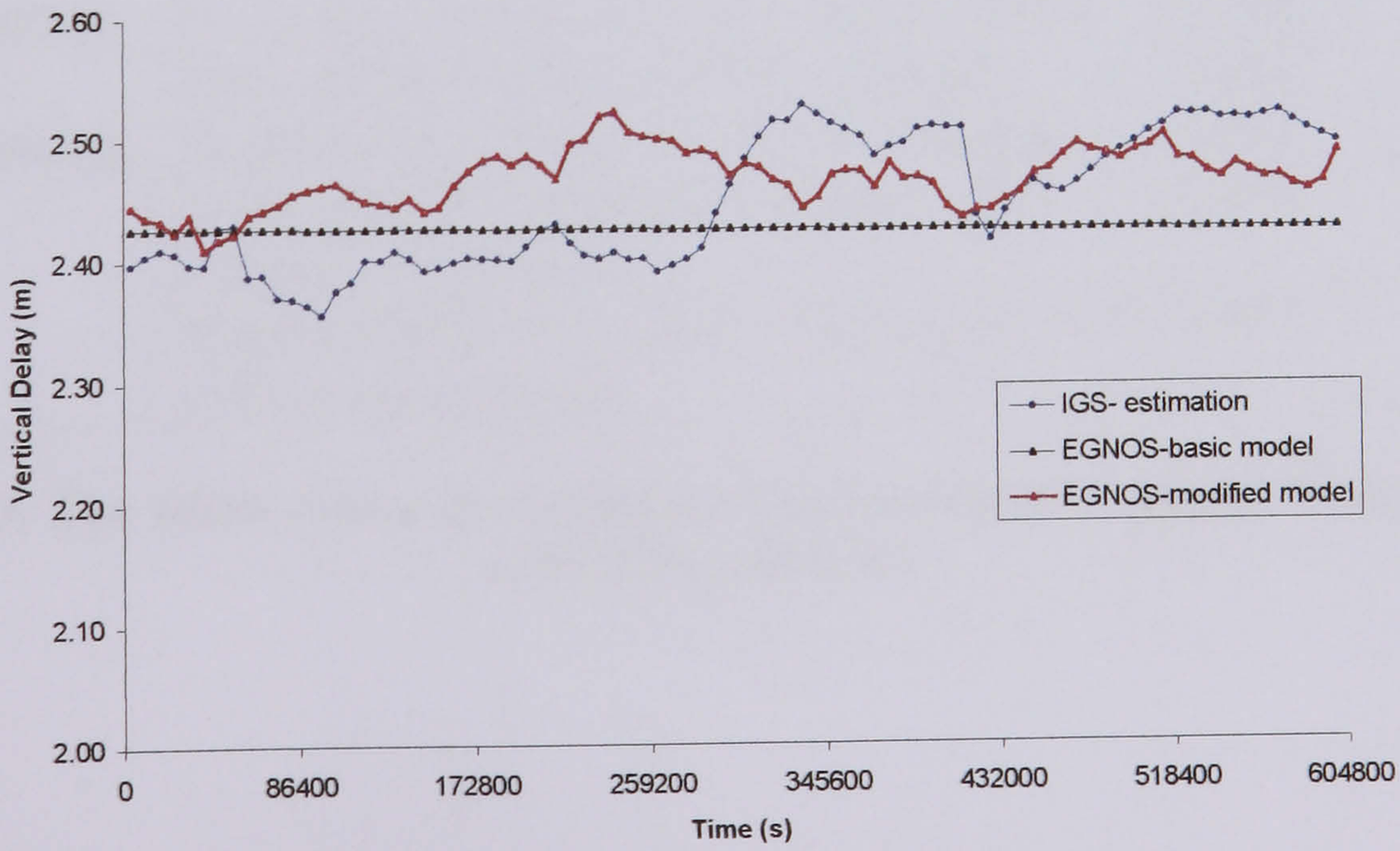

Fig. 4.36: The Total Trop. Zenith Delays in GPS week 1135 [NPLD] station

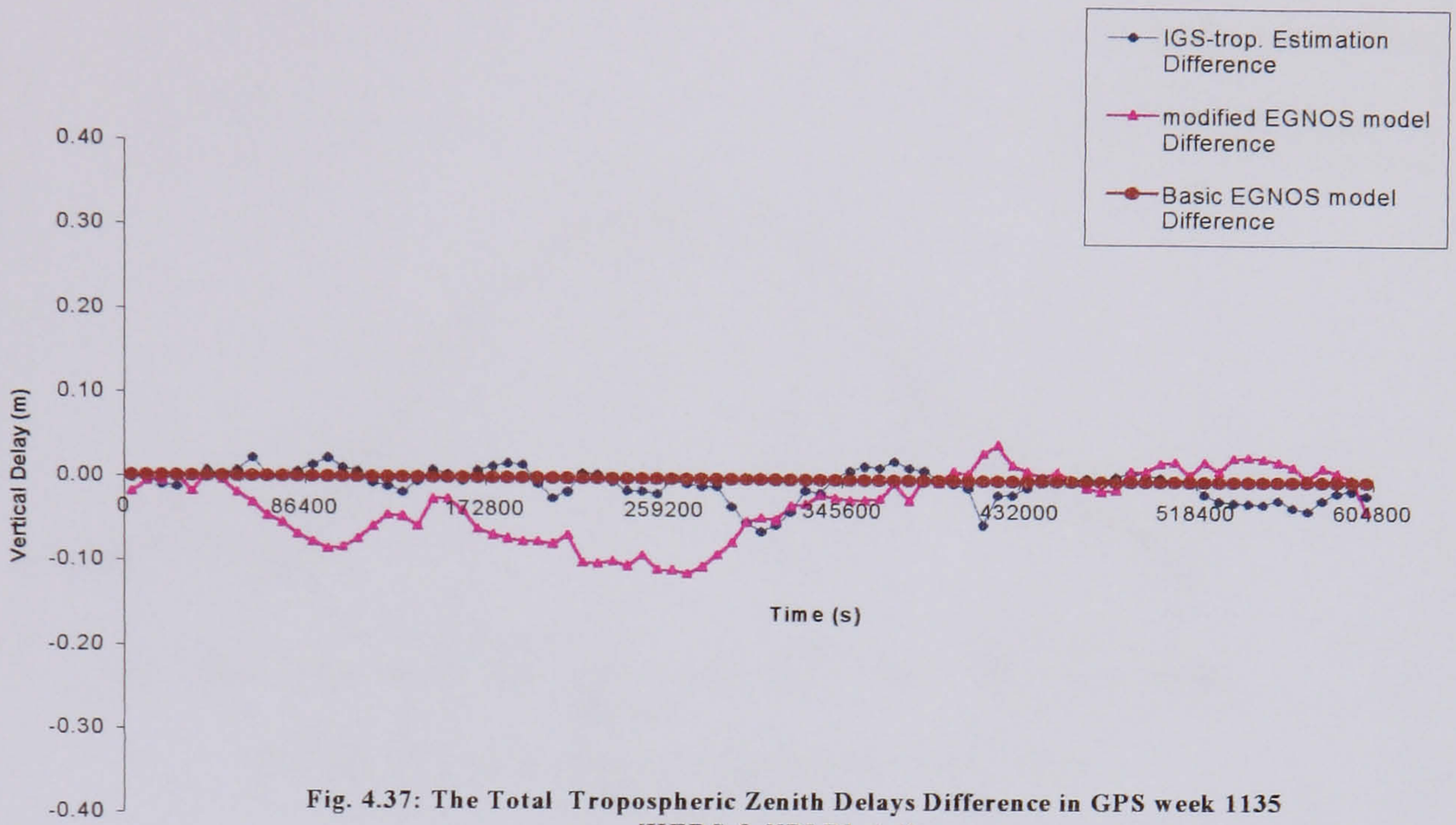

Fig. 4.37: The Total Tropospheric Zenith Delays Difference in GPS week 1135 [HERS & NPLD] stations

Figure	Data Type (Tropospheric estimates)	RMS (m)
4.35 (HERS station)	Basic EGNOS estimates-IGS estimates	0.052
	Modified EGNOS estimates- IGS estimates	0.030
4.36 (NPLD station)	Basic EGNOS estimates-IGS estimates	0.057
	Modified EGNOS estimates- IGS estimates	0.057
4.37	Basic EGNOS Difference estimates- IGS Difference estimates	0.018
	Modified EGNOS Difference estimates- IGS Difference estimates	0.053

Table 4.7: The RMS values for Different Tropospheric estimates from Figures 4.35, 4.36 and 4.37.

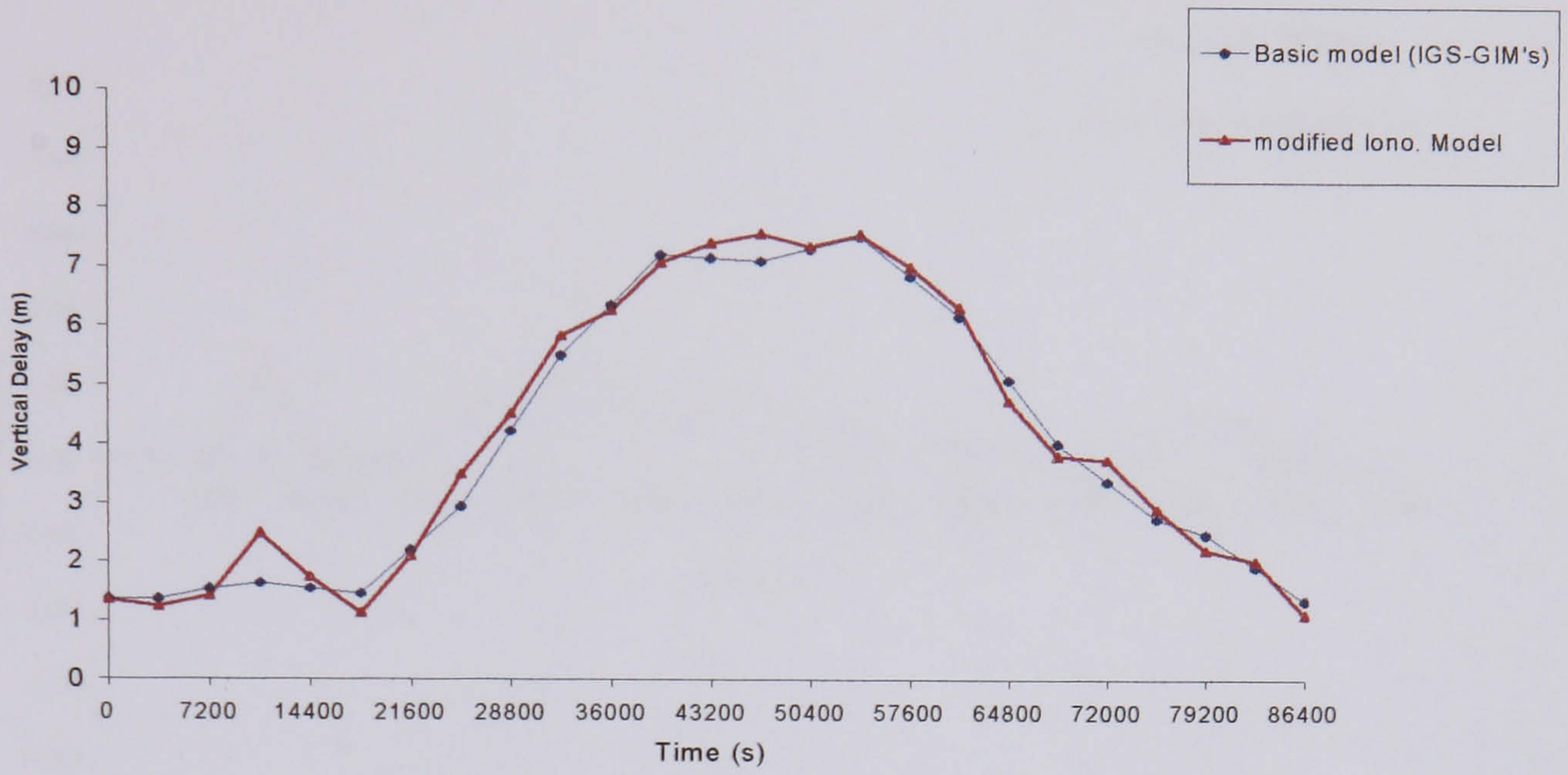

Fig. 4.38: The Total Ionospheric Zenith Delays in GPS day 11350 [HERS] station

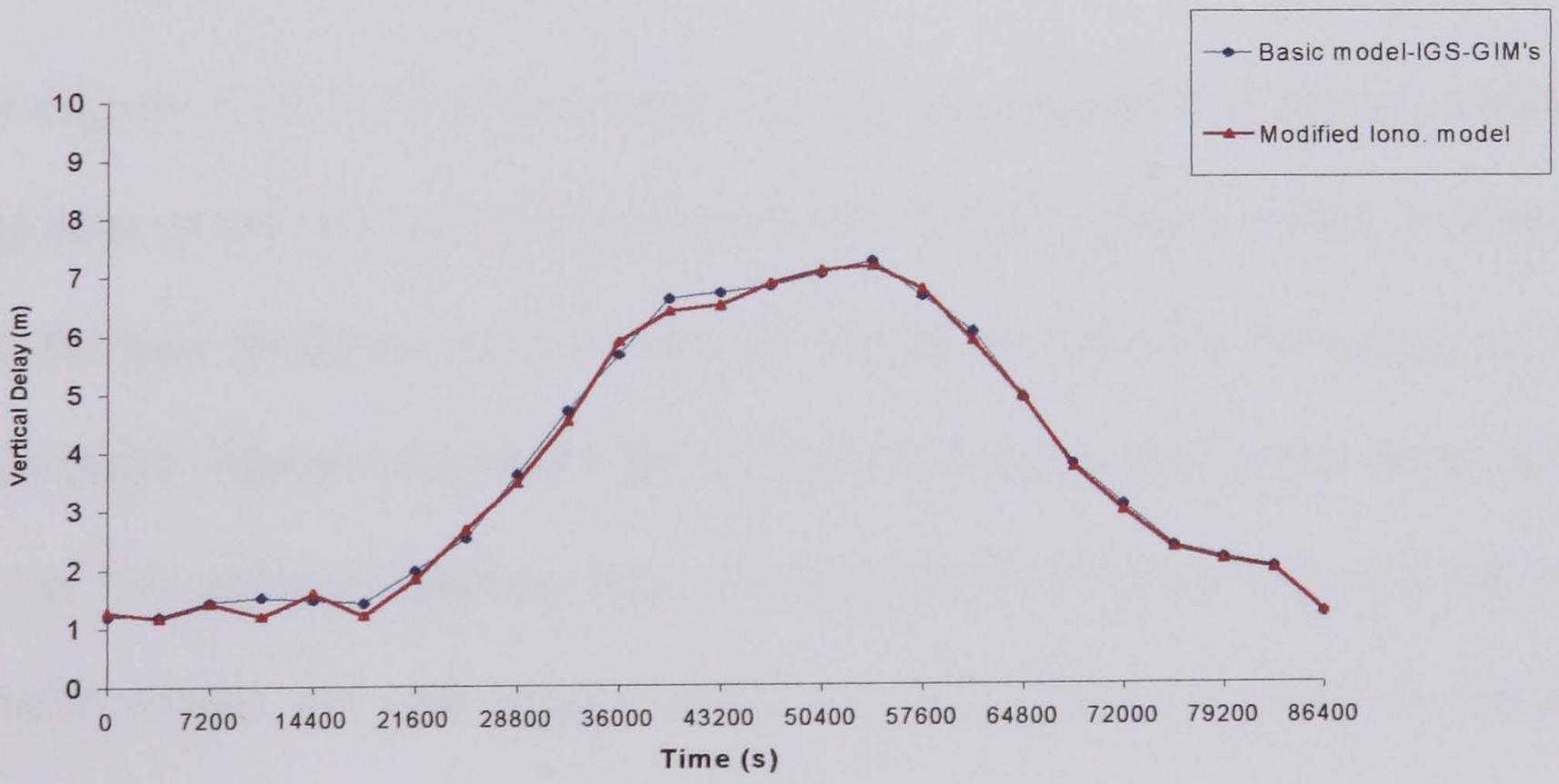

Fig. 4.39: The Total Ionospheric Zenith Delays in GPS day 11350 [NPLD] station

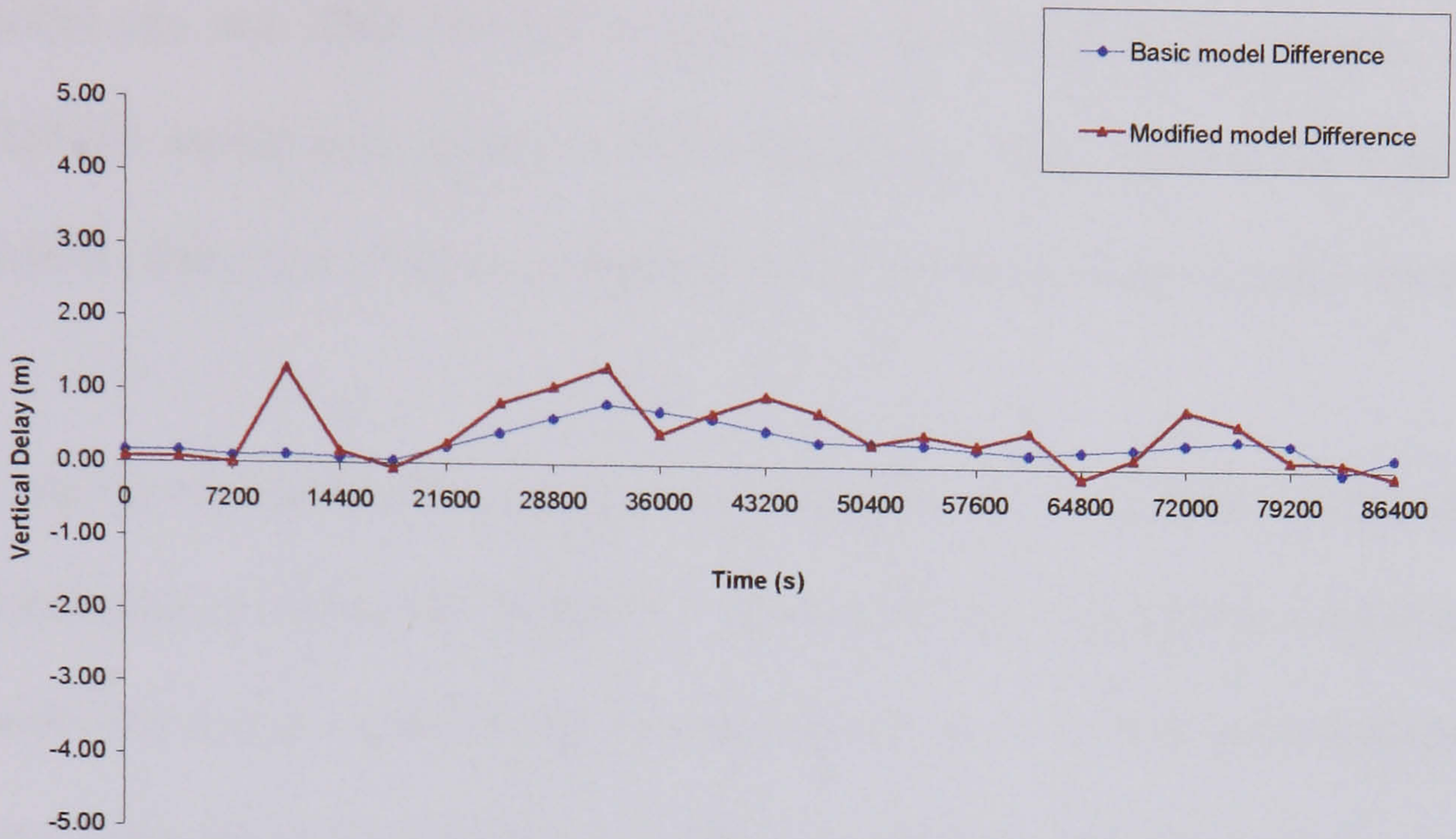

Fig. 4.40: The Total Ionospheric Zenith Delays Difference in GPS Day 11350 [HERS & NPLD] stations

4.5.4 Discussion & Conclusion

The Figures 4.35, 4.36 show clearly the impact of the new Gaussian random fields algorithm on the behaviour of the basic EGNOS tropospheric model, it shows clearly that the new modified model simulates highly accurate the behaviour of the real troposphere. Figure 4.37 shows how is the total tropospheric zenith delays difference for the two stations resulting from IGS-tropospheric estimations and the modified EGNOS model are well agreed where the basic EGNOS model is incapable of delivering this behaviour.

Table 4.7 shows how the RMS value (0.030 m) for the modified EGNOS model is better than the RMS value (0.052 m) for the basic model with respect to IGS trop.

estimates for HERS station. Similar RMS values were obtained for NPLD station noting that the modified model simulates the temporal variations where the basic model can not. This new advantage over-ruled the key disadvantage of the basic EGNOS model and makes the new modified model capable of simulating more realistic behaviour of the troposphere, which makes it a high spatial variation model.

It can be concluded also that the new model for the troposphere delay can simulate amplitudes of regional & temporal variation of the troposphere, however it can not model the actual variations for the troposphere as no surface meteorological data are used. Thus the new tropospheric model is qualitatively accurate but not quantitatively accurate which is adequate for simulation purposes.

The Figures 4.38, 4.39 and 4.40 show the results for the same test with the same scenario for the ionospheric delay basic and modified models. It can be concluded that the modified model keeps the behaviour of the basic IGS-GIM's model, however it gives variations between the ionospheric zenith delays for the two adjacent stations (HERS & NPLD). This follows the real ionosphere behaviour which does not behave as smoothly as the basic model (IGS-GIM's) offer. This modified ionospheric model gives the ability of simulating the regional variations occurred between two adjacent stations or in a regional network of 100 km by 100 km.

In summary, it has been shown that the two basic models for simulating the two major sources of error for GPS signals are adequate for the task (§ 4.3, § 4.4) but their performance can be improved by using the technique described in §4.5. The

technique gives both models a higher spatial resolution and temporal variation, to simulate the real behaviour of the ionosphere and troposphere. No doubt is left that using both these models for simulating the ionosphere and troposphere delays will result in more realistic simulated GPS data.

4.6 Simulation of Multipath

4.6.1 Introduction

Multipath is one of GPS errors which causes serious problems for accurate positioning since it is affected by various factors which are difficult to model or predict. Differential positioning technique allows removing many of GPS errors however multipath can not be removed.

Multipath, as the name explains is the phenomenon whereby a radio signal arrives at a fixed receiver via two or more possible paths (multi-path). This causes problems because these signals have the same time origin at the transmitter (satellite) however they are arriving with a relative phase offset at the receiver. These interfering signals may not be recognisable to the receiver (Tranquilla, 1986).

Many studies tried to enhance the understanding of multipath propagation and its effects in GPS terrestrial applications such as (Hannah, 2001). The Multipath delay is a dominant factor in the GPS error budget (Shaw et al., 2000) as shown in the following table;

Error source	Error Magnitude (meters, 1 s)	
	SA activated	SA deactivated
Selective Availability	24.0	0.0
Ionosphere	7.0	7.0
Troposphere	0.2	0.2
Clock and Ephemeris	2.3	2.3
Receiver Noise	0.6	0.6
Multipath	1.5	1.5
User Equivalent Range Error (UERE)	25.0	7.5
Typical Horizontal DOP (HDOP)	1.5	1.5
Stand-Alone Horizontal Accuracy (95%)	± 75.0	± 22.5

Table 4.8: GPS Error Budget with and without SA (Shaw et al., 2000).

Multipath was and still is the focus of intensive research work, as it is a limiting factor for highly accurate GPS positioning. Many classifications had been defined for Multipath. A short description of these classifications will follow.

Multipath can be classified according to the source of signal reflections into two main types (Shardlow, 1990):

- Satellite Multipath: where the different propagation paths will result from reflection at the transmitting satellite.
- Receiver Multipath: where the different propagation paths result from reflection in the surrounding environment of the receiver's antenna.

From another point of view, Multipath can also be classified as (Baker, 1997):

- Specular Multipath: where the reflected signals are relatively coherent, having undergone both a phase shift and a decrease in signal to noise ratio.
- Diffuse (non-coherent) Multipath: where the reflected signals having an increase in noise levels above the normal receiver noise threshold.

For more details about the Multipath; classifications, models and mitigation methods the reader is referred to Shardlow (1990), Jack (1994), Baker (1997) and Hannah (2001).

4.6.2 Multipath Simulation

The suggested multipath simulation model is based on the Gaussian colored noise theory, as it is a strong tool for simulating the real behaviour of multipath (Meng, 2002). Figure 4.41 shows a typical behaviour of Gaussian colored noise. Gaussian colored noise provides the correlation between different time series of multipath. The real behaviour of raw C/A code multipath is shown in Figure 4.42. The original multipath model that was used within DATSIM before this thesis' effort consists of two parts; the first is Gaussian white noise and the second is single replica model.

The original multipath model gives only single behaviour for any multipath environment. The behaviour of the original multipath model is shown in Figures 4.43 and 4.44. It can be shown that the original multipath model gives unrealistic behaviour when compare to real behaviour of multipath shown in Figure 4.42.

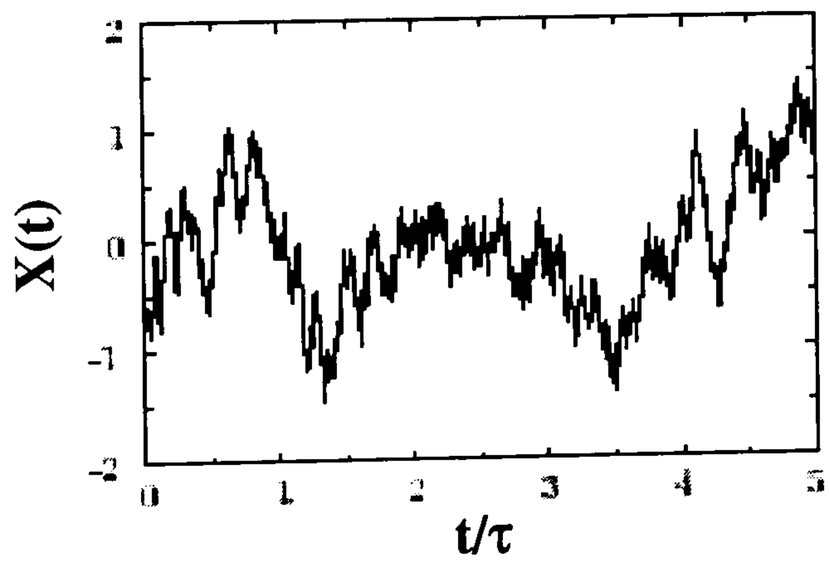

Figure 4.41: Colored Noise Signature as produced by (Bartosch, 2001).

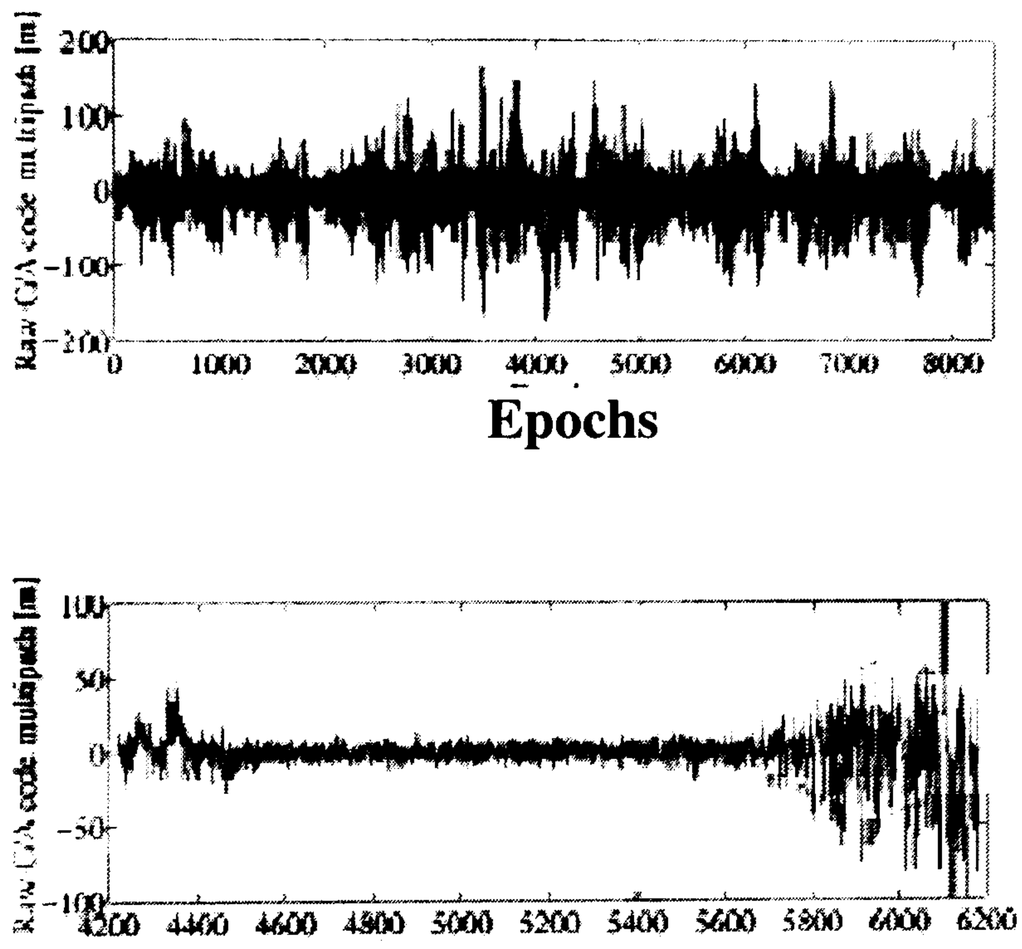

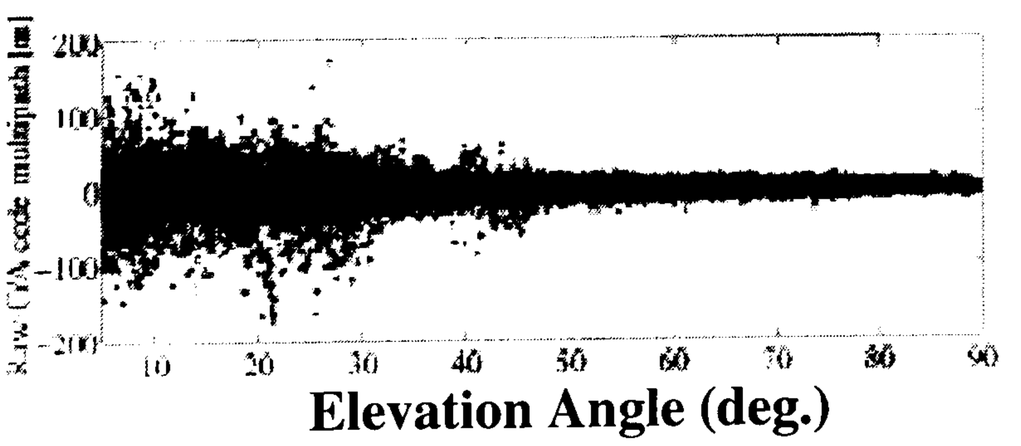

Figure 4.42: Raw C/A Code multipath (Collins et al., 1998).

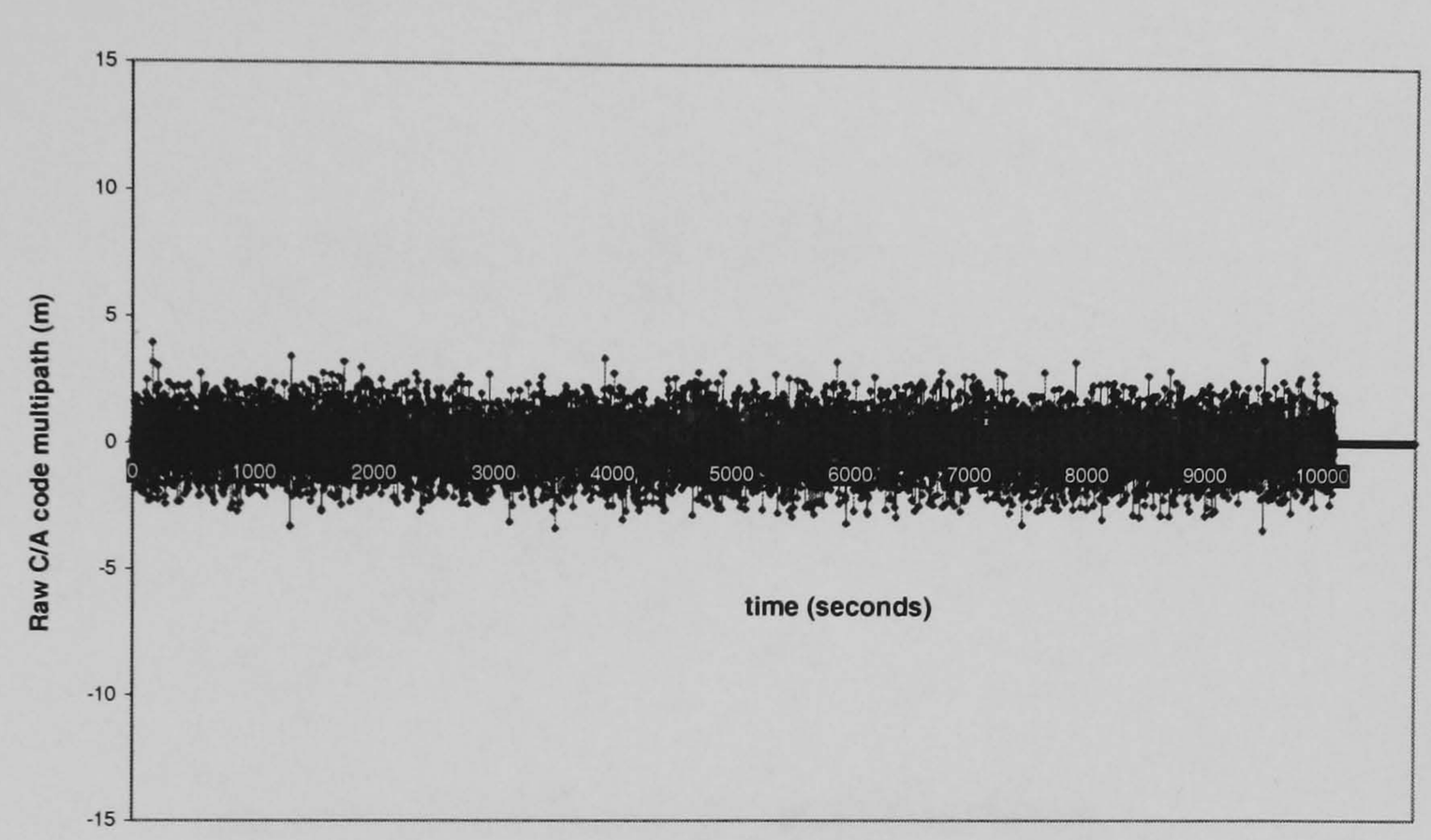

Figure 4.43: Simulated-Raw C/A code multipath (original multipath model) (single multipath environment)

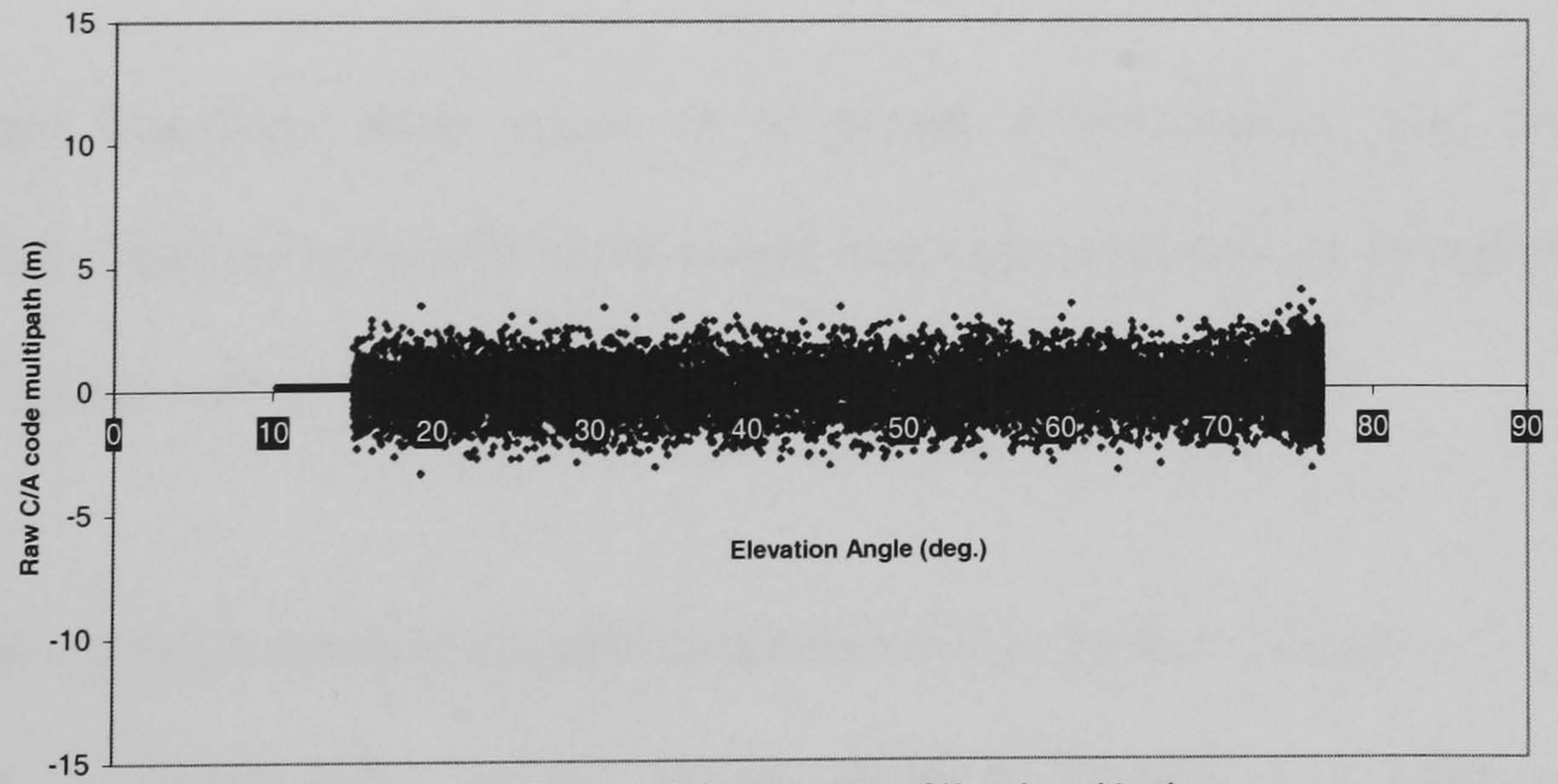

Figure 4.44: Simulated-Raw C/A code multipath (Elevation Angle Dependence) (original multipath model) (single multipath environment)

4.6.2.1 Multipath Simulation Model

A new multipath simulation model was implemented based on the Gaussian colored noise generation algorithm discussed in (Bartosch, 2001) where the following formula is given to generate Gaussian colored noise,

$$X_n = \rho_n X_{n-1} + \sqrt{1-\rho_n^2}\,\sigma Z_n, \tag{4.15}$$

where,

$$\rho_n = e^{-\left|t_n - t_{n-1}\right|/\tau},$$

X_n real correlated Gaussian random numbers,

Z_n independent Gaussian random numbers,

τ correlation time.

The model simulates three cases of multipath environments; low multipath environment, medium multipath environment and high multipath environment based on the following aspects:

- The multipath delay in pseudo-range can be very large (~ 40 m).
- The multipath delay in the carrier phase is limited to a quarter of the wavelength.
- The multipath delay is elevation angle dependent as GPS signals from lower elevation angle-satellites face higher multipath delay.

- The correlation time for multipath delay is elevation angle dependent as well, as for lower elevation angle satellites, the multipath delay has larger correlation time.

The following formula expresses the multipath delay in pseudo-range and carrier phase offered by the new model:

$$dmp(j) = [dmp(j).R + (\sqrt{1-R^2}.p(j)).m].\cos(elevang), \tag{4.16}$$

$$dmc(j) = [dmc(j).R + (\sqrt{1-R^2}.c(j)).m].\cos(elevang), \tag{4.17}$$

where,

$dmp(j)$ the multipath delay in pseudo-range observables (metres),

$dmc(j)$ the multipath delay in carrier phase observables (metres),

$R = e^{-1/\tau}$,

τ the correlation time (seconds),

$p(j)$ white Gaussian random function for pseudo-range observables,

$c(j)$ white Gaussian random function for carrier phase observables,

m multipath environment factor (high, medium, low),

$elevang$ Satellite elevation angle (radians).

The elevation-angle dependency of the model comes from:

- For Satellite elevation angle $\geq 60^0$:

  τ = 1 sec.,

$p(j)$ = random(0.0, 0.1),

$c(j)$ = random(0.0, 0.001),

where,

random (0.0,0.1) : white Gaussian random function of mean 0.0 and variance 0.1.

random (0.0,0.001) : white Gaussian random function of mean 0.0 and variance 0.001.

- For satellite elevation angle $< 60^0$:

τ = 250 sec.,

$p(j)$ = random (0.0, 1.0),

$c(j)$ = random (0.0, 0.01),

where,

random (0.0,1.0) : white Gaussian random function of mean 0.0 and variance 1.0.

random (0.0,0.01) : white Gaussian random function of mean 0.0 and variance 0.01.

The multipath environment factor m could take different values based on the amount of multipath activity for different environments. The behaviour of the new-implemented multipath simulation model is shown in Figure 4.45 to 4.50 with C/A code multipath for the three cases of multipath environments (high, medium and low).

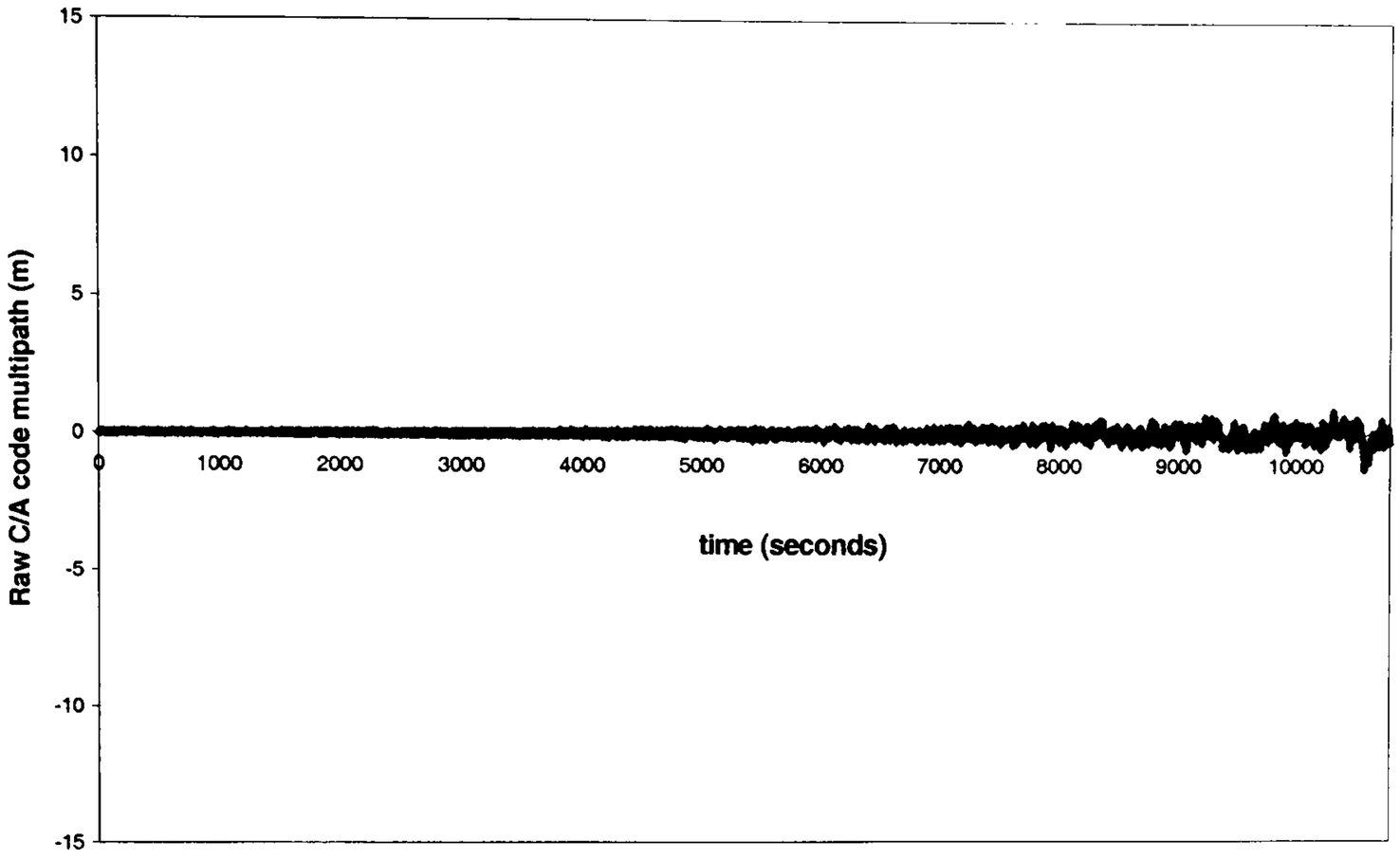

Figure 4.45: Simulated-Raw C/A Code multipath (Low multipath environment)

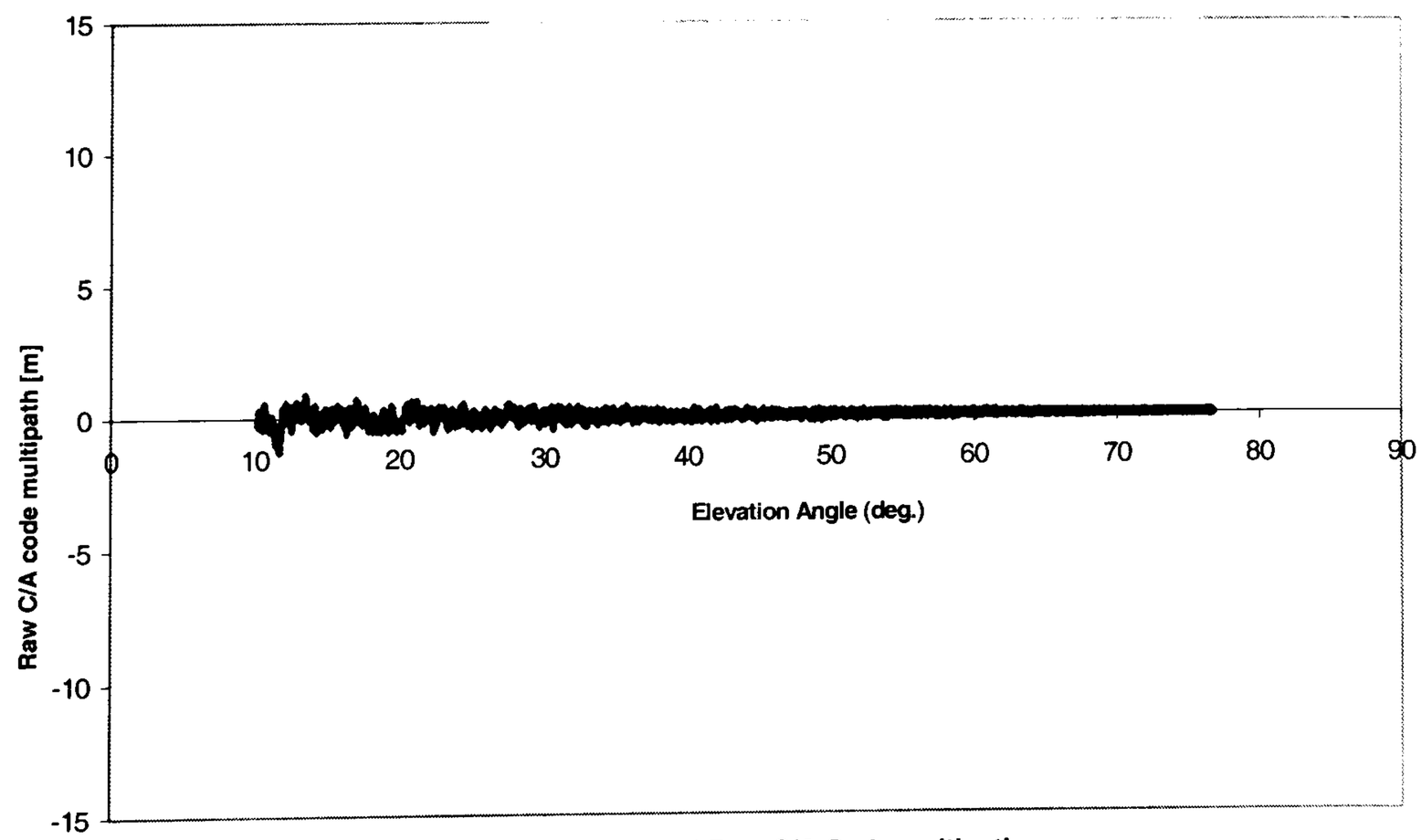

Figure 4.46: Simulated-Raw C/A Code multipath (Elevation Angle Dependence) (Low multipath environment)

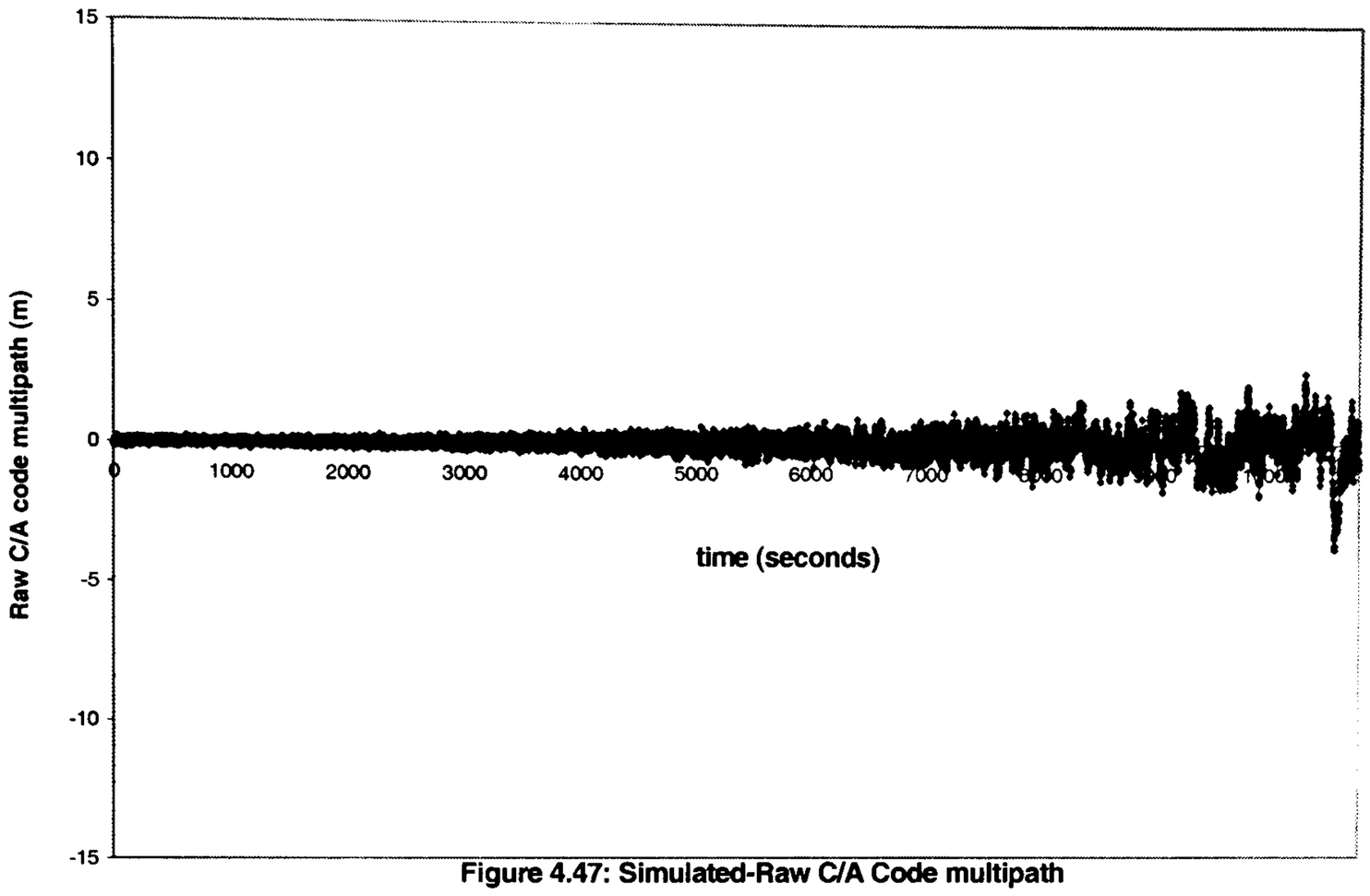

Figure 4.47: Simulated-Raw C/A Code multipath (medium multipath environment)

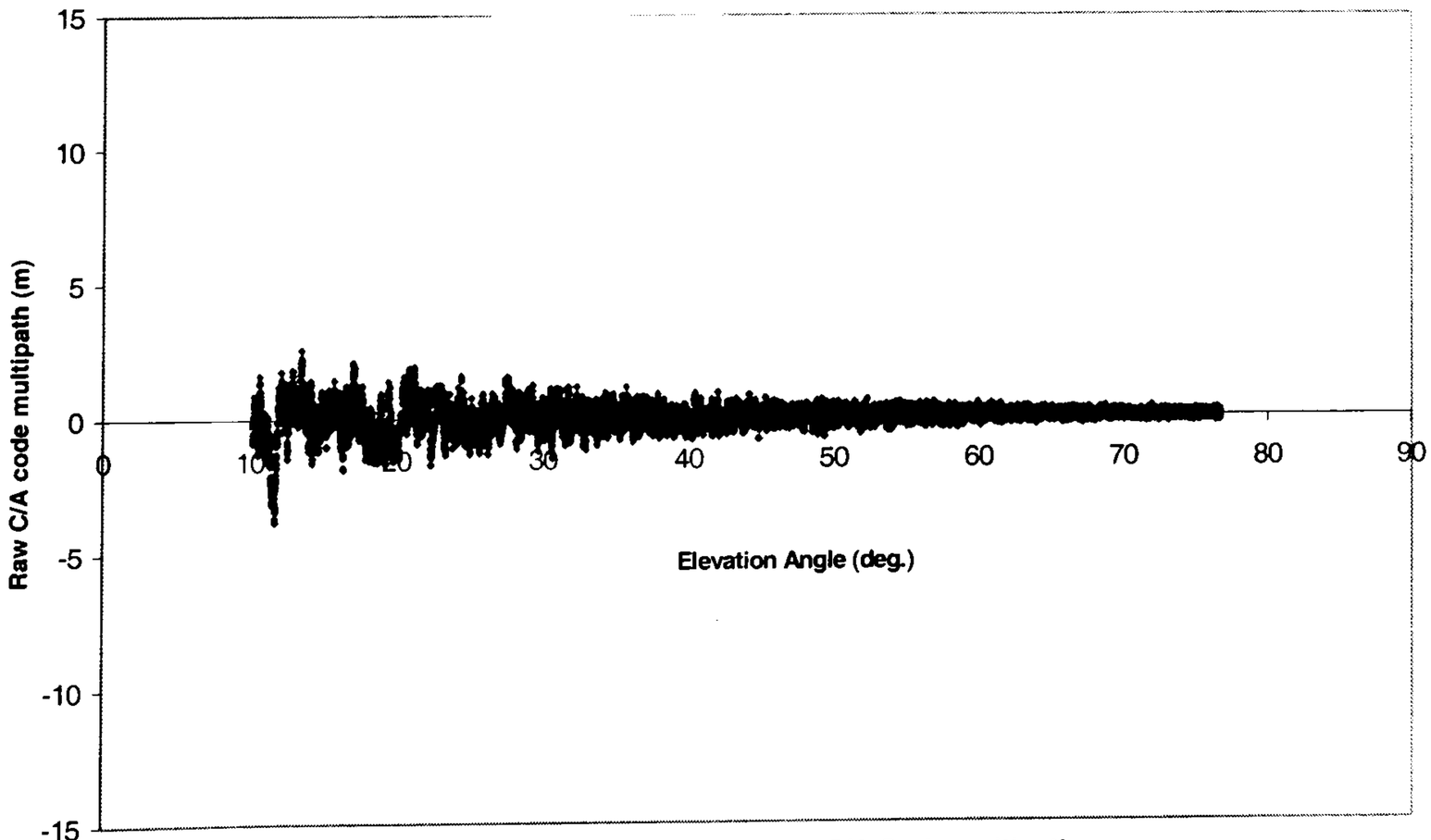

Figure 4.48: Simulated Raw C/A Code multipath (Elevation Angle Dependence) (medium multipath environment)

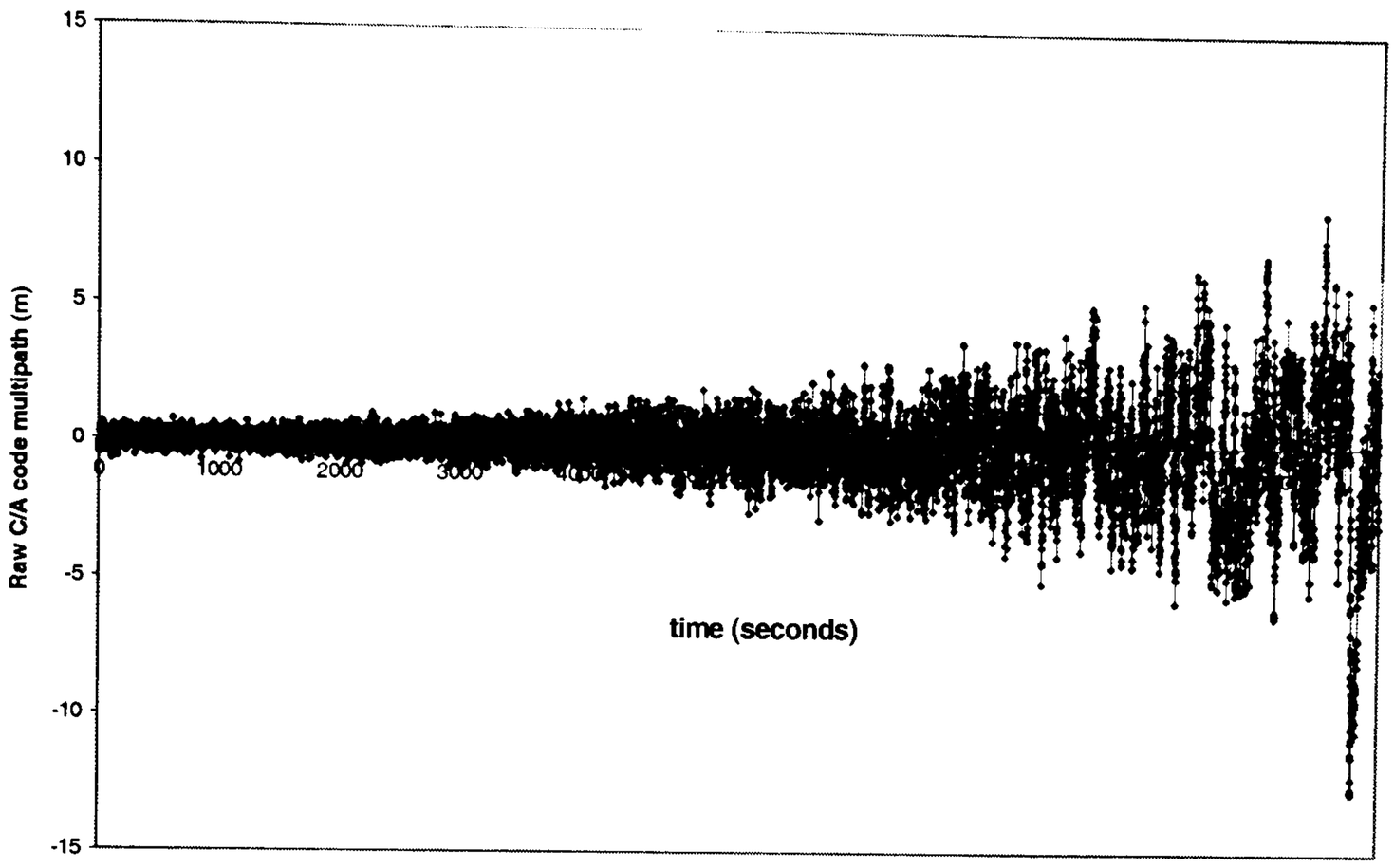

Figure 4.49: Simulated-Raw C/A code multipath (high multipath environment)

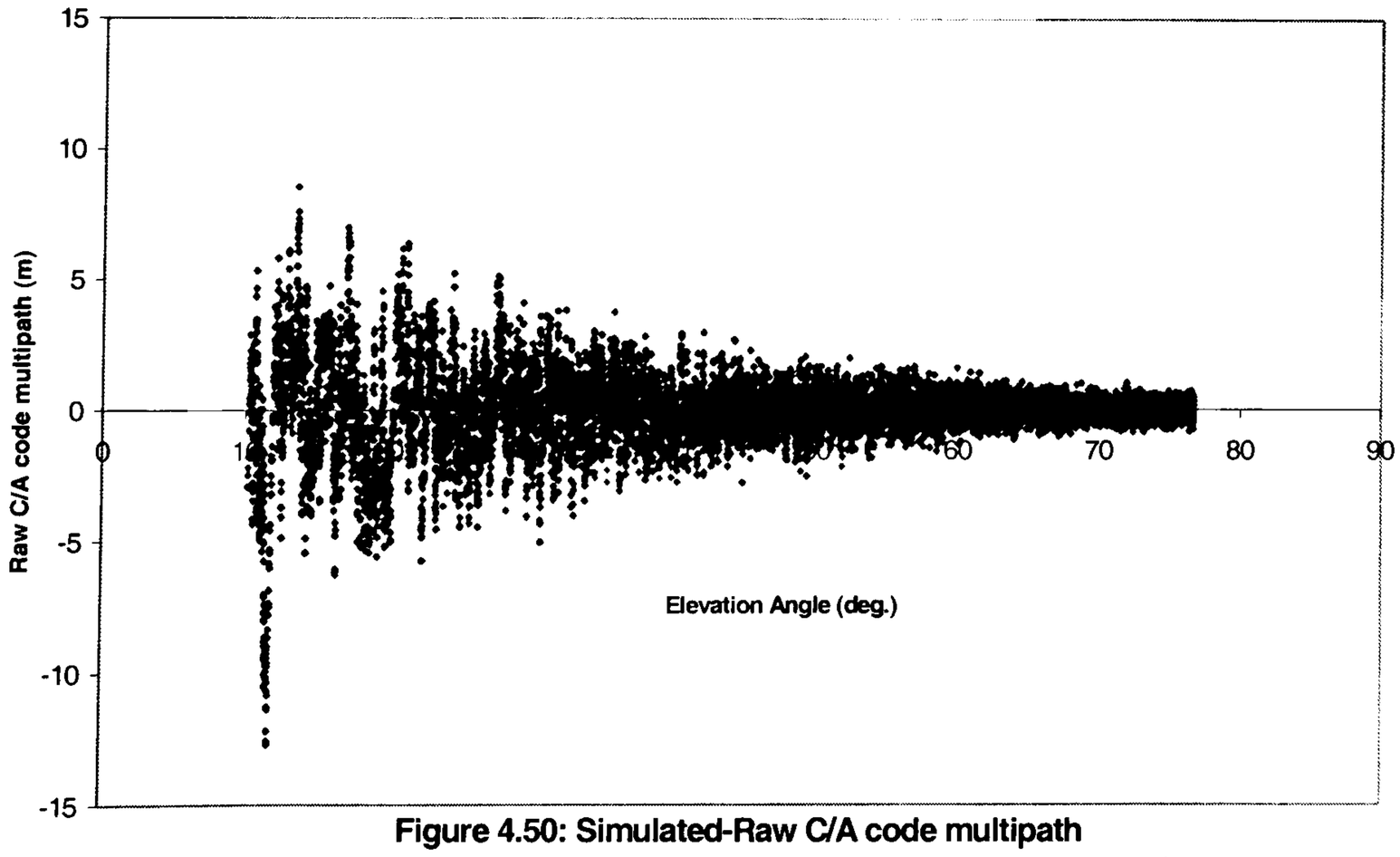

Figure 4.50: Simulated-Raw C/A code multipath (Elevation Angle Dependence) (high multipath environment)

4.6.3 Discussion

The accurate simulation of multipath error for GPS data simulation requires a model that gives realistic behaviour as well as different options for multipath activity corresponding to different multipath-environments.

The original multipath simulation model within DATSIM does not satisfy the previously mentioned criteria because its behaviour is far from realistic multipath behaviour, this can be shown clearly by comparing Figure 4.42 with Figure 4.43 and Figure 4.44. The behaviour of this model did not show any change of multipath behaviour with changing the satellite's elevation angle, which is unrealistic, as the multipath delay increases as the elevation angle decreases. As well as the original model only gives a single behaviour of multipath whatever the environment, which is unrealistic too.

The new implemented model for multipath simulation meets the previously mentioned criteria as it simulates the real multipath behaviour giving the necessary correlation between different multipath time series. The model gives the privilege of simulating three different cases of multipath behaviour for three cases of multipath environment activity. Comparing the behaviour of simulated raw C/A code multipath using the new implemented model shown in Figures 4.45, 4.46, 4.47, 4.48, 4.49 and 4.50 with the real raw multipath C/A code shown in Figure 4.42 proves this findings. It is clearly shown that the simulated multipath behaviour changes with the change in the satellite's elevation angle, which is realistic. The new implemented model has the

advantage of offering three cases of multipath activity and can be modified easily to give as many as required of multipath activity cases.

4.6.4 Conclusion

The new implemented model for multipath simulation based on the Gaussian colored noise gives more realistic behaviour over the original multipath model within DATSIM for the following reasons;

- The original multipath model was implemented based on Gaussian white noise, which assumes no correlation between the time series of multipath delay however this is unrealistic matter.
- The new model was implemented based on the Gaussian colored noise, the behaviour of which is very close to the real multipath behaviour where there's correlation between the time series of multipath delay.
- The new model shows accurately the change of multipath behaviour with the change in the satellite's elevation angle where the original model does not.
- The new model offers the ability of simulating three cases of multipath activity where the original model offers a single behaviour.
- The new model can be modified easily to provide any multipath activity required.

CHAPTER 5

GPS/GALILEO Simulated Data Tests

5.1 GPS Simulated Data

The generation of realistic simulated GPS data requires an accurate modelling of the various GPS errors. The focus of the work in the first part of this thesis was the development and implementation of three new models to model the three major sources of GPS errors, namely the ionosphere, the troposphere and multipath delays. The following table is a brief summary of the predominate GPS errors and the corresponding models used to simulate these errors within DATSIM.

GPS Error	The Simulating Model
Ionospheric Delay	New implemented model based on IGS-GIM's with added temporal and regional variations (resulting from this thesis's work)
Tropospheric Delay	The modified EGNOS model (resulting from this thesis's work)
Satellite Ephemeris & Clock	IGS-final precise ephemeris
Multipath	New implemented model based on colored noise (resulting from this thesis's work)
Receiver Clock	Polynomial function & Gaussian noise
Measurement Noise	Gaussian white noise Model
Cycle Slip	Gaussian white noise Model

Table 5.1: The Predominate GPS-errors and the corresponding models within DATSIM.

The expected outcome of any GPS-data simulation software is the ability to simulate accurately any part of the GPS observation process resulting in realistic simulated data that can be used for any GPS applications such as precise orbit determination of the LEO satellites (the scope of the second part of this thesis). It has been shown that the three new implemented models for the ionosphere, troposphere and multipath delays are capable of accurately simulating these three types of errors. It should therefore follow that the resulting simulated observation data has a much more realistic behaviour.

A comparison study has been performed investigating the positioning accuracy of five types of GPS data: real GPS data, original simulated GPS data (before implementing the three new models), improved ionosphere-simulated GPS data (applying the new implemented ionospheric model §4.3), improved ionosphere + troposphere-simulated GPS data (applying the new implemented ionospheric model §4.3 and tropospheric model §4.4) and new generated simulated GPS data (applying the new implemented ionospheric model §4.3, tropospheric model §4.4 and multipath model §4.5). The models used in the original GPS simulation were the Klobuchar model, the Magnet model and the original multipath model (Gaussian white noise & single replica) for the ionosphere, troposphere and multipath delays respectively. The study focused on the determination of the height coordinate of six stations. The height coordinate was chosen because it contains the largest error (Shardlow, 1994) and its variation clearly evident in the results. The first two tested stations (IESSG, LERW) are stations that are part of the British Isles GPS archive Facility (BIGF) operated by the IESSG and the last four tested stations (ANKR, BAHR, COCO and KOUR) are

IGS-tracking stations. The geographical positions of the tested stations are shown in Figures 5.1. The datasets consisted of 24 hours of data for GPS day 3 of week 1137, (24/10/2001). The different types of data were processed using the IESSG processing software P4 (Pseudo-range and Phase Post Processor) (Hill, 2002) which allows the data to be processed without the application of any models for removing the effect of the ionosphere, troposphere and multipath.. The processing technique was static standalone pseudo-range C/A code without applying any models for all types of data.

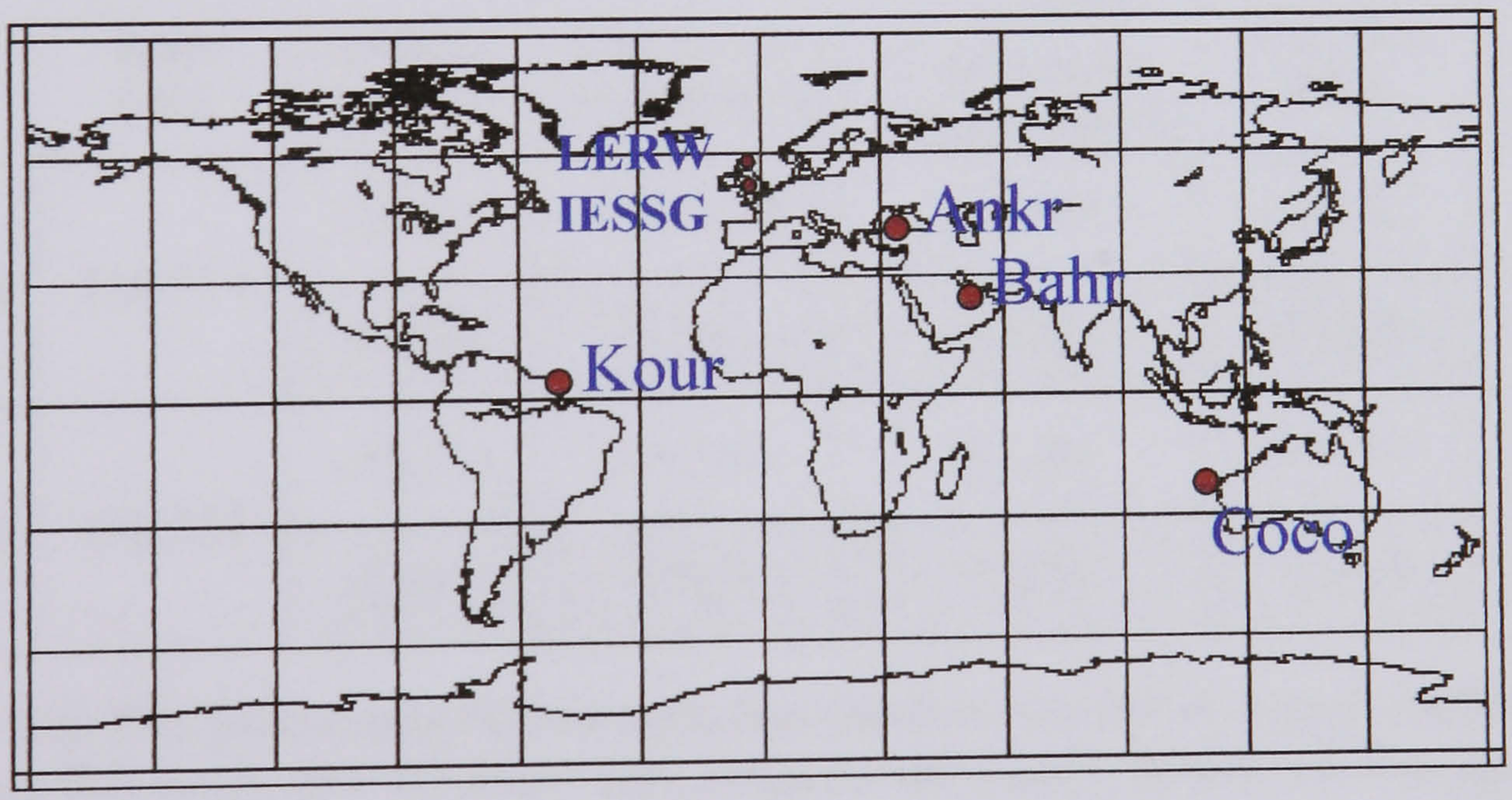

Figure 5.1: The Geographical Positions of the Tested IGS-tracking Stations.

Station ID	Latitude (degree)	Longitude (degree)	True Height (meter)
IESSG	52.940689 N	1.192285 W	98.495
LERW	60.139139 N	1.1849398 W	131.265
ANKR	39.8875 N	32.7586 E	974.800
BAHR	26.2091 N	50.6081 E	-17.030
KOUR	5.2522 N	52.806 W	-25.745
COCO	12.1883 S	96.8339 E	-35.2212

Table 5.2: Details of the involved stations in the real & simulated data test.

Tables 5.3 and 5.4 show the height variations for the different types of data as well as the height difference between these different types of simulated data and real GPS data shown in dashed cells.

Station ID	Data Type				
	Real GPS	**Original sim. GPS**	**Improved Ionosphere**	**Improved Ionosphere +Troposphere**	**New Sim. GPS**
IESSG	116.514	120.746	116.764	117.156	116.552
		4.232	0.250	0.642	0.038
LERW	148.552	145.725	141.948	142.282	147.063
		-2.827	-6.604	-6.270	-1.489

Table 5.3: The height coordinate variation (metres) for BIGF tested stations for one day five types of GPS data (real, original simulated, Improved Ionosphere, Improved Ionosphere + Troposphere, new simulated) processed using P4 (static stand-alone pseudo-range C/A code).

Station ID	Data Type				
	Real GPS	Original sim. GPS	Improved Ionosphere	Improved Ionosphere +Troposphere	New Sim. GPS
ANKR	996.899	998.792	995.449	995.835	996.199
		1.893	-1.450	-1.064	-0.700
BAHR	12.009	15.846	21.557	22.310	19.572
		3.837	9.548	10.301	7.563
COCO	-6.710	-16.195	-12.231	-11.358	-4.310
		-9.485	-5.521	-4.648	2.400
KOUR	2.288	-3.316	3.913	4.864	0.715
		-5.604	1.625	2.576	-1.573

Table 5.4: The height coordinate variation (metres) for IGS tested stations for one day five types of GPS data (real, original simulated, Improved Ionosphere, Improved Ionosphere + Troposphere,new simulated) processed using P4 (static stand-alone pseudo-range C/A code).

Table 5.5 and 5.6 show some statistical analysis of the relation between original simulated GPS data, new generated simulated GPS data and real GPS data where values of the mean difference, difference standard deviation and difference RMS are shown for the height coordinate of the tested stations.

Station ID	Comparison Test	Data Type	
		Original Sim. GPS	New Sim. GPS
IESSG	Mean Difference	4.232	0.038
	Difference Standard Deviation	248.921	3.601
	Difference RMS	248.849	4.523
LERW	Mean Difference	-2.827	-1.489
	Difference Standard Deviation	367.304	5.043
	Difference RMS	367.159	5.709

Table 5.5: Statistical analysis parameters (metres) for the height difference between different types of simulated GPS data with respect to real GPS Data for BIGF tested stations.

Station ID	Comparison Test	Data Type	
		Original Sim. GPS	New Sim. GPS
ANKR	Mean Difference	1.893	-0.700
	Difference Standard Deviation	258.479	3.226
	Difference RMS	258.378	3.878
BAHR	Mean Difference	3.837	7.563
	Difference Standard Deviation	295.632	11.132
	Difference RMS	295.508	11.142
COCO	Mean Difference	-9.485	2.400
	Difference Standard Deviation	241.099	3.969
	Difference RMS	241.192	4.425
KOUR	Mean Difference	-5.604	-1.573
	Difference Standard Deviation	258.747	72.197
	Difference RMS	258.634	72.723

Table 5.6: Statistical analysis parameters (metres) for the height difference between different types of simulated GPS data with respect to real GPS Data for IGS tested stations.

Figures 5.2 and 5.3 show time series of the height coordinate difference between original simulated GPS data, new simulated GPS data and real GPS data for the (IESSG) station as an example.

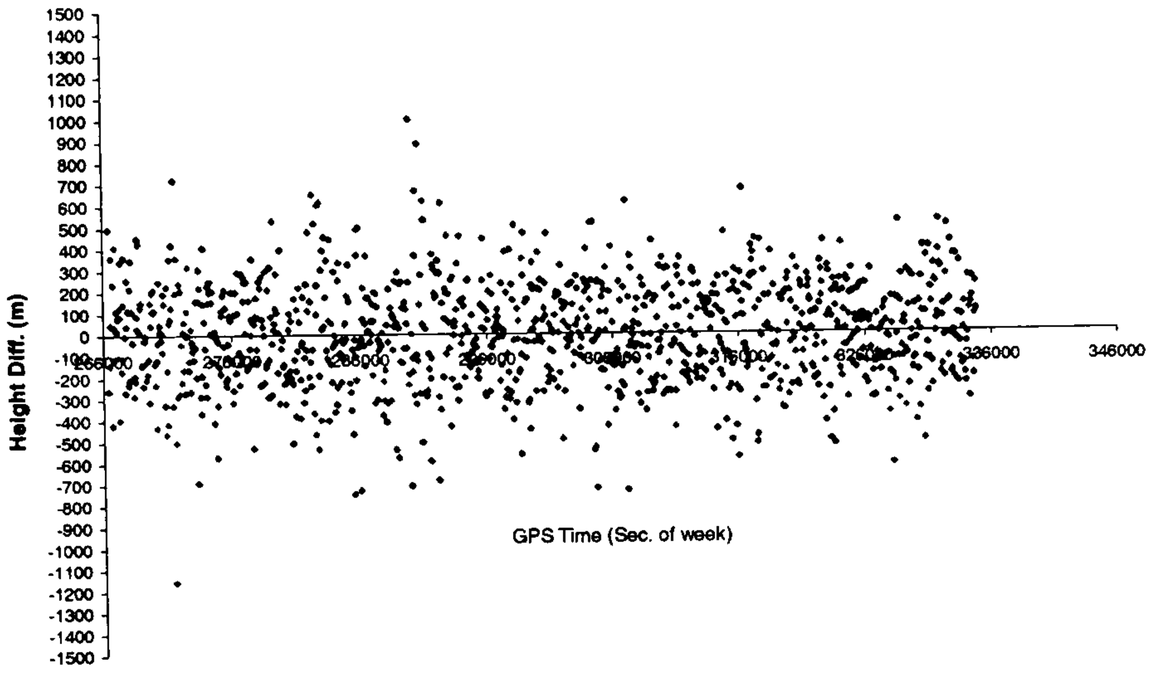

Fig. 5.2: The Height difference between Original Sim. GPS Data and Real GPS data for IESSG station

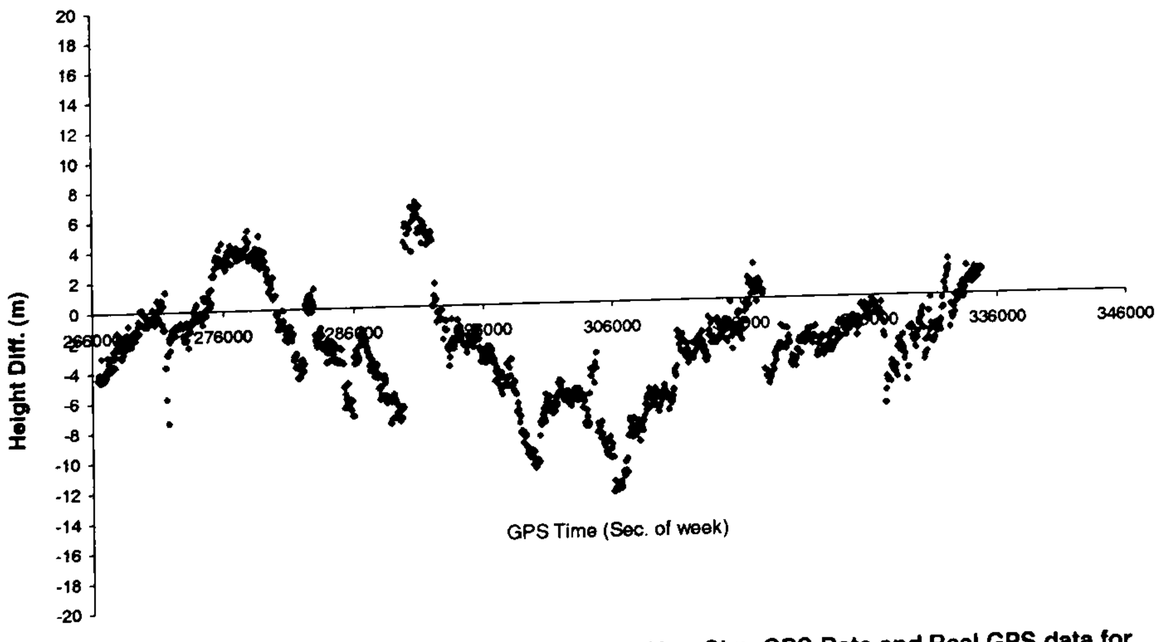

Fig. 5.3: The Height difference between New Sim. GPS Data and Real GPS data for IESSG station

It can be seen that the new simulated GPS data follows the behaviour of the real GPS data more closely than the original simulated GPS data. This is evident from the agreement in the output height coordinate from processed real GPS data and the new simulated GPS data.

It can be concluded that the effect of the new ionospheric model is superior to the effect of the new tropospheric and multipath models as shown from height difference values at Tables 5.3 and 5.4. The combined effect of the three improvements is evident from Tables 5.5 and 5.6, which show that the RMS and standard deviation values for the original data are much higher than those obtained for the new simulated data. This behaviour is further evident from figures 5.2 and 5.3 for the IESSG station.

5.2 GALILEO Simulated Data

As the time is getting closer for the first GALILEO satellite to be launched, which is scheduled for 2005, the need is inevitable for generating GALILEO simulated data to give indications of GALILEO's expected achievements and capabilities. Also, simulated GALILEO data would give researchers a strong tool for exploring the performance of the combined GPS/GALILEO constellation and the effects of having two fully operational systems on the numerous applications, which currently rely on only GPS.

The Author modified the DATSIM software to generate simulated data from the different services offered by GALILEO which are, briefly described in Table 5.7. GALILEO simulated data had been generated from DATSIM. The necessary modifications that were performed to generate GALILEO simulated data within DATSIM software can be stated as follows:

- GALILEO ephemeris file has been prepared based on Walker (27/3/1) Constellation (Walker, 1984) with specifications (GALILEO, 2002):
  - The constellation consists of 27 satellites & 3 spare satellites in three Medium Earth Orbits (MEO),
  - Altitude ~ 23616 km,
  - Semi Major Axis = 29993.707 km,
  - Inclination = 56^{0},
  - Orbital period of 14 hours 4 minutes, ground track repeats about 10 days.
- Modify the DATSIM software to generate GALILEO simulated data from different services offered by GALILEO (Table 5.7) using different ranging accuracies corresponding to different services. The ranging accuracies values for GALILEO services reflect approximately the chip rate relation between GPS and GALILEO frequencies.

A short comparison study between the new simulated GPS data (Pseudo-range C/A code) and simulated GALILEO data (Pseudo-range-E2L1E1 frequency) has been

investigated without applying any processing models to remove the effect of any errors. The output results are shown in Table 5.8.

Frequency	Open Service (OS)	Safety Of Life (SOL)	Commercial Service (CS)	Public Regulated Service (PRS)
E2-L1-E1 (1575.42) MHz	*	*	*	*
E5a-E5b (1192) MHz	*	*	*	
E6 (1278.75) MHz			*	*

Table 5.7: The GALILEO different services & frequencies simulated within DATSIM.

Station ID	True Height	Data Type	Processing Technique
			No models
IESSG	98.495	Sim. GPS	116.552
		Sim. GALILEO	112.452
CAMB	139.567	Sim. GPS	158.570
		Sim. GALILEO	154.507
LERW	131.265	Sim. GPS	147.063
		Sim. GALILEO	144.529
SUNB	65.208	Sim. GPS	83.456
		Sim. GALILEO	79.249
ANKR	974.800	Sim. GPS	996.199
		Sim. GALILEO	993.173
BAHR	-17.030	Sim. GPS	19.572
		Sim. GALILEO	15.537
COCO	-35.221	Sim. GPS	-4.310
		Sim. GALILEO	-1.910
KOUR	-25.745	Sim. GPS	0.715
		Sim. GALILEO	9.684

Table 5.8: The height coordinate variation (metres) for BIGF and IGS tested stations for one day, two types of data (new simulated GPS data (Pseudo-range C/A code) & simulated GALILEO data (Pseudo-range-E2L1E1 frequency)) processed using P4 (static stand-alone).

Tables 5.9 and 5.10 gives some statistical analysis showing values for the mean difference, difference standard deviation and RMS for the height coordinate for new simulated GPS data and GALILEO simulated data with respect to the true height of the tested stations. Figures 5.4 and 5.5 show time series of the height coordinate difference between new simulated GPS data and GALILEO simulated data with respect to the true height for the (IESSG) station as an example

Station ID	**Comparison Test**	**Data Type**	
		New sim. GPS Data	**GALILEO Sim. Data**
IESSG	**Mean Difference**	15.237	13.642
	Difference Standard Deviation	3.759	4.562
	Difference RMS	15.693	14.384
LERW	**Mean Difference**	14.705	12.784
	Difference Standard Deviation	3.926	4.049
	Difference RMS	15.219	13.409

Table 5.9: Statistical analysis parameters (metres) for the height difference of New GPS Simulated Data and GALILEO Simulated Data with respect to the True height for BIGF tested stations.

Station ID	Comparison Test	Data Type	
		New sim. GPS Data	GALILEO Sim. Data
ANKR	Mean Difference	18.608	17.717
	Difference Standard Deviation	5.151	5.516
	Difference RMS	19.307	18.555
BAHR	Mean Difference	31.664	34.558
	Difference Standard Deviation	9.867	11.214
	Difference RMS	33.164	36.331
COCO	Mean Difference	26.852	33.060
	Difference Standard Deviation	26.852	33.060
	Difference RMS	27.852	33.773
KOUR	Mean Difference	31.009	32.544
	Difference Standard Deviation	9.896	11.571
	Difference RMS	32.549	34.537

Table 5.10: Statistical analysis parameters (metres) for the height difference of New GPS Simulated Data and GALILEO Simulated Data with respect to the True height for IGS tested stations.

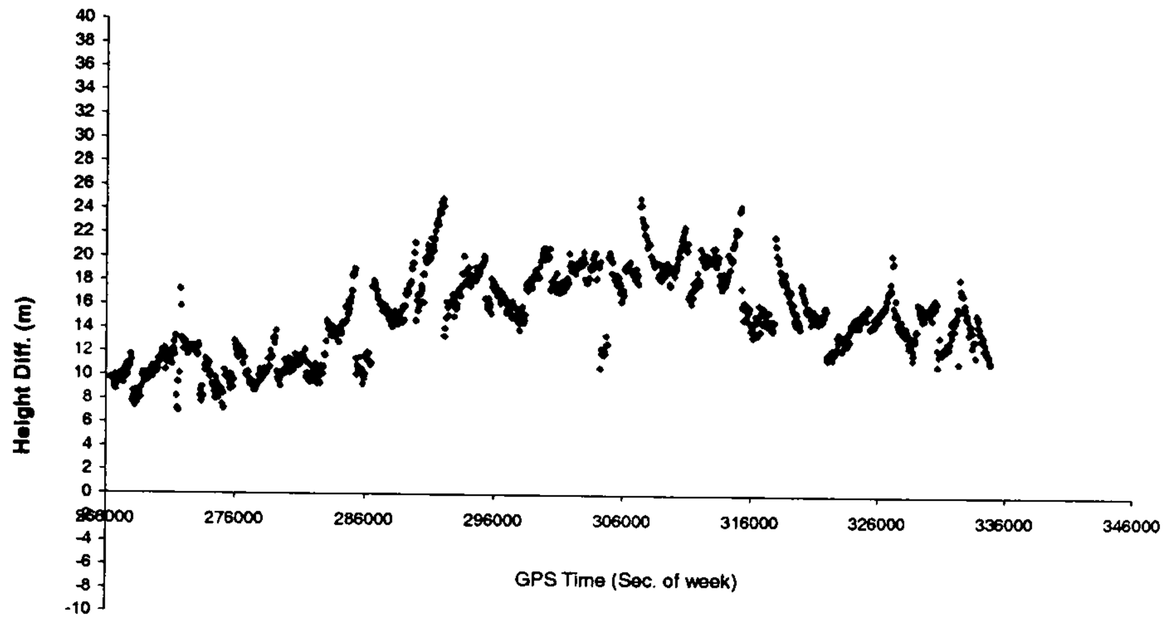

Fig. 5.4: The Height difference between New Sim. GPS Data and True Height for IESSG station

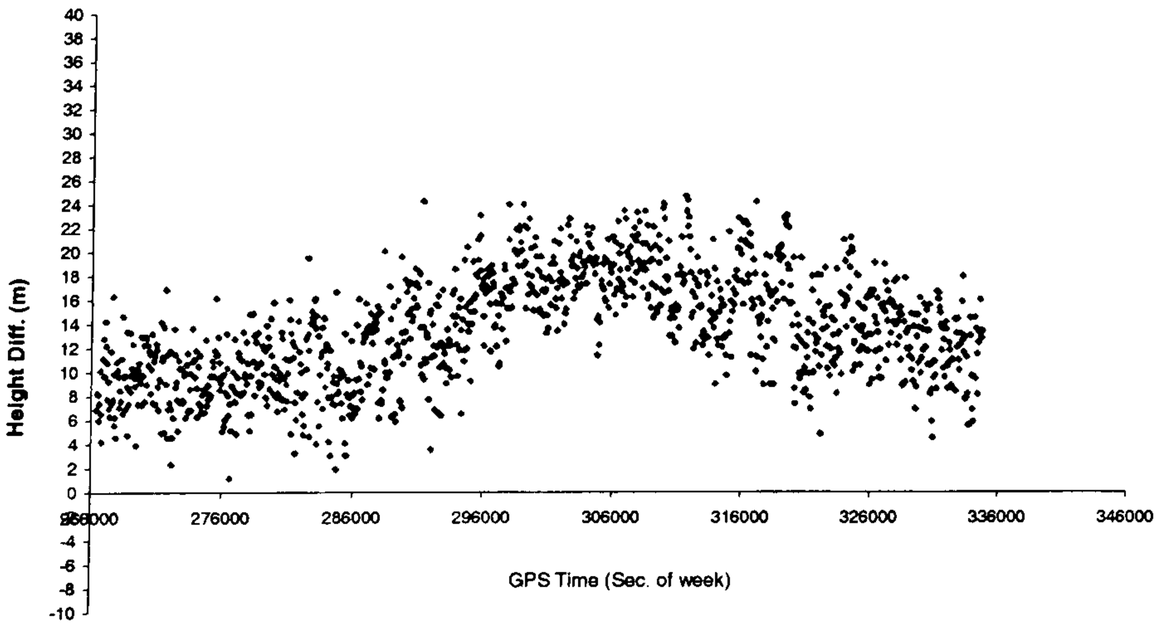

Fig. 5.5: The Height difference between GALILEO Sim. Data and True Height for IESSG station

It is understood that such a study will not allow any definitive statements to be made about the accuracies achievable with the two systems (GPS and GALILEO) but it does enable some form of comparison to be made.

Considering the results given in Table 5.8 it can be seen that, with the exception of COCO and KOUR, the simulated GALILEO results are systematically offset from the simulated GPS results by approximately 3 to 4 m, but the simulated GALILEO results are closer to the true heights. This could be taken as a good sign that the increased number of visible satellites in GALILEO's constellation (see Appendix B) and the improved pseudo-range accuracy for GALILEO observations will have a positive impact on positioning accuracy.

Tables 5.9 and 5.10 shows with the exception of stations BAHR, COCO and KOUR that GALILEO simulated data gives a better height mean difference, nearly the same standard deviation and better RMS values comparing with GPS simulated data with respect to the true height of the tested stations.

To accurately distinguish between the two systems GPS & GALILEO requires comparison of the performance with respect to an area of application that requires high levels of accuracy. Any conclusion from such an exercise, depend to a great extent on the quality of the simulated data. This will be shown in the second part of this thesis, which covers the use of simulated GPS and GALILEO data, both individually and combined in the orbit determination process for the Topex/Poseidon satellite.

5.3 Concluding Remarks

GPS, GALILEO, GLONASS and any other future satellite navigation and positioning system needs a data simulation tool to assess its capabilities, revealing its advantages and disadvantages and explore the future of the system for new applications.

DATSIM is the IESSG's tool for research working with GPS and exploring the future for GPS and GALILEO. The software has been shown to deliver realistic simulated GPS data and has been assessed in high accuracy real GPS-applications (Ashkenazi et al., 1997). The backbone of any data simulation tool is its ability to simulate the different types of errors that face the system to a high degree of accuracy.

Realistic models for simulating the different GPS errors are not easily obtained. The continuing research in this field gives different models with different areas of application. As the atmospheric error (the ionosphere and troposphere) is the major source of error for any satellite-based positioning and navigation system (apart from intentional degradation of the system's accuracy), the research effort in this type of error is enormous compared to the other errors. Using this rich body of research allowed the selection of two highly accurate models for simulating the atmospheric error within DATSIM. The behaviour of these models was assessed and then improved upon giving the ability to simulate the regional variations within the ionosphere and troposphere. The first part of this thesis' effort has resulted in two high resolution spatially varying models for the ionosphere and troposphere as well as a more realistic model for simulating multipath. This has allowed the simulation of

more realistic GPS data. DATSIM has also been modified to simulate GALILEO data using the same models for the environmental delays.

The modified DATSIM software will now be used to assess the performance of GPS and GALILEO with respect to the application of high accuracy orbit determination. The second part of this thesis will handle this subject using simulated GPS data, simulated GALILEO data and combined GPS/GALILEO simulated data in the LEO satellite orbit determination for Topex/Poseidon.

CHAPTER 6

LEO Satellite Orbit Determination Techniques

6.1 Introduction

Since the early 1980s, a new era of developments in the fields of solid Earth, oceanography and atmosphere science applications started with the first launches of Low Earth Orbiting satellites. The goals of those LEO-satellites are varied, however a large number of them depend on the accurate determination of the satellite's position to a high degree of accuracy (10 cm or better for LEO altimetric satellites (Nouel et al., 1994)). The best example for this is the use of LEO-satellites in measuring the precise height of the sea surface for studying the dynamics of the circulation of the world's oceans. Two significant missions in this field are Topex/Poseidon (1992-present) and Jason-1 (2001-present) (NASA, 2003).

The orbits of LEO-satellite can be determined using different tracking systems such as Satellite Laser Ranging (SLR) (Hill, 1989), the Doppler Orbitography and Radio-positioning Integrated by Satellites (DORIS) (Willis et al., 1989), the Precise Range And Range Rate Equipment (PRARE) (Lechner and Wilmes, 1989) and GNSS (Yunck and Wu, 1986). LEO satellite missions usually use different tracking systems; DORIS, SLR, GNSS such as Topex/Poseidon (1992-present) and Jason-1 (2001-

present) missions (Haines et al., 2002), (NASA, 2003). GNSS as a LEO-tracking system has many advantages over the other systems (Ashkenazi et al., 1994), which can be summarized as follows:

- Low cost.
- Global coverage.
- GNSS is a full three-dimensional positioning system, other systems needs three ground stations at least.
- GNSS can provide real-time orbit determination (other systems not).

The GPS tracking system has demonstrated that it can provide high precision precise orbit determination products through the GPS flight experiment on Topex/Poseidon Melbourne et al. (1994), Bertiger et al. (1994). The precise orbits computed from the GPS tracking data are estimated to have a radial orbit accuracy comparable to or better than the precise orbit ephemerides computed from the combined use of SLR and DORIS tracking data, Yunk et al. (1994), Christensen et al. (1994), Schutz et al. (1994) and Tapley et al. (1994).

For LEO satellites, there are many orbit determination techniques: dynamic technique, kinematic technique and reduced-dynamic technique. These techniques will be discussed in detail in this Chapter, however, briefly, the dynamic technique depends on accurate modelling of the forces acting on the satellite and then evaluating the acceleration of the satellite and numerically integrating it to get the position and velocity. The kinematic technique determines the satellite positions using data from the GPS receiver onboard the satellite, processed in either a stand-

alone or differential mode. The reduced–dynamic technique combines both the above techniques using an accurate force model along with the GPS data.

This Chapter starts with providing the reader with the basics of dynamic orbit determination for GNSS satellites (§ 6.2, 6.3 and 6.4) which are applied for LEO satellites as well. The various components of the force model with the numerical integration are discussed in sections (§ 6.3) and (§ 6.4) respectively. (§ 6.5) gives a detailed description for the different techniques available for LEO satellite orbit determination. The reduced dynamic technique for LEO satellite orbit determination adopted for this research is described in (§ 6.5.3)

6.2 Coordinate Reference Frames

The orbit determination process involves using more than one coordinate system. As the numerical integration must be performed in an Inertial (non-rotating) reference Frame (IF). Meanwhile, the coordinates of the tracking stations and other components of the force model are given in an Earth-Fixed (EF) frame. A brief description for the different coordinate reference frames and the transformations between them are given in this section, further details can be found in (Agrotis, 1984), (Moore, 1986).

6.2.1 Earth Fixed Reference Frame

The origin of the conventional terrestrial system is at the earth's centre of mass, with the X- axis directed towards the Bureau International de l'Heure (BIH) zero meridian. The Z-axis passes through the Conventional International Origin (CIO) pole and the

Y- axis completes the right-handed coordinate system. The IERS Reference Pole and Reference Meridian are consistent with the corresponding directions in the BIH directions within +/- 0.005". The coordinates of the tracking stations are given in an earth fixed geocentric reference frame and the gravitational potential coefficients are provided in an earth fixed spherical reference frame (Whalley, 1990). The geodetic community uses different reference frames, however for GPS, WGS84, which based on the conventional terrestrial system, has been used since 1987. For more details about WGS84, the reader is referred to (NIMA, 2002).

6.2.2 Inertial Reference Frame

FK5, is the fundamental astronomical reference frame adopted by the International Astronomical Union (IAU) in 1976 which describes the apparent positions of over 500 stars and extragalactic radio sources at the epoch of January 1.5, year 2000.

The inertial reference system used in this thesis is a geocentric cartesian system based upon the FK5 frame. The origin is at the earth's centre with the X-axis of the system is directed towards the mean equinox of J2000 and the Z-axis is normal to the mean equatorial plane of J2000. The Y-axis is perpendicular to both the X and Z-axes so as to form a right handed system. A lunar and planetary ephemeris, known as the Development Ephemeris Number DE200/LE200 was produced by the Jet Propulsion Laboratory which describes the planetary ephemeris.

The inertial reference frame is used for the satellite's ephemeris computation, mean while the tracking stations coordinates and geopotential models are given in earth

fixed reference frame. The position of a point must be subjected to a number of rotations in order to be transformed from any of the two systems to the other and this is given by,

$$\underset{\sim}{R} = P\,E\,N\,Q\,\underset{\sim}{r} \tag{6.1}$$

where $\underset{\sim}{R}$: inertial frame coordinates

$\underset{\sim}{r}$: earth fixed frame coordinates at UTC time

P : rotation matrix for polar motion (see § 6.2.7)

E : rotation matrix for earth rotation (see § 6.2.6)

N : rotation matrix for nutation (see § 6.2.5)

Q : rotation matrix for precession (see § 6.2.4)

The reverse transformation is given using the transpose of the rotation matrices as follows,

$$\underset{\sim}{r} = Q^T\,N^T\,E^T\,P^T\,\underset{\sim}{R} \tag{6.2}$$

The following sections give a short description for the used time scales and various rotation matrices. For more details the reader is referred to (Agrotis, 1984), (Moore, 1986).

6.2.3 Time Scales

This section gives a brief description of the various time scales used during the orbit determination process, and the relationships between these time scales.

6.2.3.1 Sidereal Time Scale

Two main types of sidereal times will be defined, that is the Greenwich Apparent Sidereal Time (GAST) and the Local Apparent Sidereal Time (LAST). (GAST) is the hour angle measured in units of time between the Greenwich Meridian and the true equinox of date, meanwhile, (LAST) is the hour angle between the meridian which includes the point of observation (the local meridian) and the true equinox of date. The relationship between (GAST) and (LAST) is given by (Agrotis, 1984),

$$LAST = GAST + \lambda \tag{6.3}$$

where λ : astronomical longitude in units of time of the local meridian from the Greenwich meridian (measured positive eastwards).

Another type of sidereal time is Greenwich Mean Sidereal time (GMST) which is the hour angle between the Greenwich meridian and the mean equinox of date, as the true equinox of date differs from the mean equinox of date due to nutation effects. Also, the mean equinox of date is obtained from the mean equinox at the reference epoch (J2000) by correcting for the precession effects.

6.2.3.2 Universal Time Scales

The IERS produced number of time scales, which are known as Universal Time (UT) resulting from global observations of the transits of stars. There are four universal time scales referred to as, UT0, UT1, UT2 and UTC. Following is a brief description of each one of them and other time scales,

* UT0: The time from the determination of (LAST) has periodic and irregular variations due to polar motion and varying earth's rate of rotation,

* UT1 : The time scale produced after the correction of UT0 for polar motion effects,

* UT2 : The time scale produced after the correction of UT1 for predicted values of the seasonal variations in the earth's rotation rate,

* TAI : International Atomic Time, the time scale produced from the weighted mean of the readings of various global atomic clocks, changes in the rate of rotation of the earth,

* UTC : Coordinated Universal Time, the time scale based on the International System (SI) second and cope with any changes in the rate of earth's rotation. Differs from TAI by leap seconds.

IERS is maintaining both the TAI and UTC. The differences from UTC, (UT1-UTC) and (UT1-TAI) are published monthly in the IERS Bulletin B and yearly in the IERS annual report.

6.2.3.3 GPS-Time Scale

The GPS time is an atomic time scale which has the same unit (seconds) as the UTC. GPS time was coincident with UTC on January 6, 1980. The relationship between UTC and GPS time is available in time bulletins of the USNO (United State Naval Observatory) and the BIPM (International Bureau of Weights and Measures) as well as the GPS satellite message (Seeber, 1993).

6.2.3.4 Barycentric Dynamical Time & Terrestrial Dynamical Time

Barycentric Dynamical Time (TDB) is the time scale for the equations of motion relative to the solar system's barycentre where, Terrestrial Dynamical Time (TDT) is the time scale for an apparent geocentric ephemeris and replaces ephemeris time. TDB differs from TDT by periodic relativistic terms, as given by (Moore, 1986),

$$TDB = TDT + 0.001658 \sin(g + 0.0167 \sin g) \tag{6.4}$$

Where, g : mean anomaly of the earth in its orbit

$$g = (357.528^0 + 35999.05^0 T) . \frac{2\pi}{360} \tag{6.5}$$

T : the interval in Julian centuries of TDB, between J2000 and the epoch.

$$T = \frac{(J - 2451545)}{36525} \tag{6.6}$$

J : the TDB Julian date of the epoch.

6.2.4 Precession

The attraction of the moon and sun on the earth equatorial bulge causes the celestial pole to rotate in a westerly motion around the pole of the ecliptic, with a period of about 25800 years and an amplitude (the obliquity of the ecliptic) of about 23.5^{o}, this is what so called 'luni-solar precession'. Meanwhile, the motion of the ecliptic plane due to the action from the varying configuration-planets is known as 'planetary precession' and causes an eastward motion of the equinox of about $12^{``}$ per century and $47^{``}$ decrease in the obliquity. The general precession is the combined effect of the luni-solar precession and planetary precession, which described by three angles called the equatorial precession parameters, ζ_A, Z_A and θ_A. The precession rotation matrix Q is given by,

$$Q = R_3(-Z_A)R_2(\theta_A)R_3(-\zeta_A) \tag{6.7}$$

The rotation matrices R_2 and R_3 are defined in Appendix C.

6.2.5 Nutation

Moreover the general precession, the moon causes two periodic motions; long period and short period nutation. The long period nutation has a period of 18.6 years, with amplitude of about 9 seconds. The short period nutation has a period of two weeks, with amplitude of less than 0.5 seconds.

Nutation is described in terms of two angles, the nutation in longitude $\Delta\Psi$ and the nutation in obliquity $\Delta\varepsilon$. The nutation rotation matrix N is given by,

$$N = R_1(-\varepsilon - \Delta\varepsilon)R_3(-\Delta\Psi)R_1(\varepsilon) \tag{6.8}$$

The values of $\Delta\Psi$ and $\Delta\varepsilon$ are given by the summation of a 106 term series. The rotation matrix R_1 is defined in Appendix C.

6.2.6 Earth Rotation

The non-constant irregular and seasonal varying rotation of the earth causes the coordinates transformation from a space fixed reference system to an earth fixed system must be done through the rotation of the true equinox-of-date to the Greenwich meridian through an angle equivalent to the Greenwich Apparent Sidereal Time (GAST). The transformation between the true-of-date and the instantaneous-terrestrial coordinates is given by,

$$\underset{\sim I}{R} = E\,\underset{\sim T}{r} \tag{6.9}$$

where E , the earth rotation matrix is given by,

$$E = R_3(GAST) \tag{6.10}$$

where $\underset{\sim T}{r}$: true-of-date coordinates

$\underset{\sim I}{R}$: instantaneous-terrestrial coordinates

R_3 : rotation matrix (Appendix C)

6.2.7 Polar Motion

The instantaneous terrestrial system's pole is not fixed with respect to the earth but in a state of constant motion. This polar motion is caused by a number of factors with the main factor is the no-parallelism of the earth's axis of rotation with that of maximum inertia (Chandler Wobble) and meteorological effects (Argotis, 1984). The movement of the true pole is governed by means of two angles, x_p, y_p relative to the mean axis known as Conventional International Origin (CIO). The values of x_p and y_p are published by the BIH in their circular D. The polar motion matrix is given by,

$$P = R_2(-x_p)R_1(-y_p) \tag{6.11}$$

where R_1, R_2 : rotation matrices about the X and Y axis respectively (see Appendix C)

6.3 Force Model Components

6.3.1 Introduction

The dynamic orbit determination of a satellite using numerical integration requires accurate modelling of the forces acting on the satellite. These forces vary in its strength and behaviour depending on the altitude of the satellite.

The principal forces acting on the satellite can be divided into two main categories, gravitational forces and surface forces. The Earth's gravitational force is the major component of the force model but also the attraction from the moon, sun and other planets are accounted for. The model of the gravitational field must be corrected for the tidal effect of the moon and sun on the Earth. The surface forces depend on the cross sectional area, mass, shape and altitude of the satellite. These forces include the effects of solar radiation pressure and atmospheric drag.

6.3.2 Gravitational Attraction of the Earth

The attraction of the gravitational field of the Earth is the principal component of the total force acting on an Earth satellite. The gravitational field U_e is described by a geopotential expansion in terms of spherical harmonics (Agrotis, 1984),

$$U_e = \frac{GM}{R}\left[1+\sum_{n=2}^{\infty}\sum_{m=0}^{n}\left(\frac{a}{R}\right)^n P_n^m(\sin\phi)\left[C_{n,m}\cos(m\lambda)+S_{n,m}\sin(m\lambda)\right]\right] \qquad (6.12)$$

where ,

G : the universal gravitational constant,

M : the mass of earth,

a	:	the earth's equatorial radius,
R, ϕ, λ	:	the spherical polar coordinates of the point,
n, m	:	the degree and order of spherical harmonic expansion,
P_n^m	:	the associated Legendre polynomial of degree n and order m,
$C_{n,m}, S_{n,m}$	:	the spherical harmonic coefficients.

The series of the spherical harmonic expression of the gravitational potential is infinite but it is truncated depending on the accuracy required for practical purposes.

The acceleration of the satellite $\ddot{r}_e$ is then given by the gradient of the potential field at the satellite,

$$\ddot{r}_e = \nabla U_e \tag{6.13}$$

The accuracy of the models of the Earth's gravity field has shown a great improvement over the last 20 years. A major effort to improve the existing gravity models was initiated in 1983 as a joint effort between the NASA Goddard Space Flight Center Space Geodesy Branch (GSFC) and the University of Texas Center for Space Research (CSR). This effort consisted of an iterative reprocessing of historical tracking data from a number of satellites covering a range of orbit configurations in combination with new data from the Satellite Laser Ranging (SLR) and Doppler Orbitography and Radio positioning Integrated by Satellites (DORIS) tracking networks. The result of this effort led to the Goddard Earth Model (GEM)-Tn and University of Texas Earth gravitational model (TEG)-n series of fields detailed by Marsh et al. (1988,1990) and (Tapley et al., 1989). In addition a group at the Ohio

state university continued to expand and improve the surface gravity database (Pavlis and Rapp, 1990). The individual gravity model efforts were combined to develop the pre-launch gravity model for the Topex/Poseidon mission, the Joint Gravity Model JGM-1 (Nerem et al., 1994), which predicted a radial orbital error of 6 cm RMS. Further analysis using only the SLR and DORIS data collected by Topex/Poseidon during a portion of the initial 6-months calibration period led to the post launch improved model JGM-2 (Nerem et al., 1994) giving a radial orbital error of 3 to 4 cm. Subsequently the JGM-3 model (Tapley et al., 1996) was developed which improved slightly on JGM-2. The model used in this study is the JGM-2 model. There have been many modern development gravity models in the last few years such as EGM-96, GRIM4-S4, GRIM4-C4 and TEG-4 model. A summary of modern gravity models is shown in Table 6.1. Using one of the modern gravity models in the study will not affect the orbit solutions much as the reduced dynamic technique applied absorb the errors in the force model.

Model	**Description**
JGM3 (70x70; 1994)	Tuned with TOPEX/GPS Tracking data
EGM96 (70x70; 360x360; 1996)	New tracking data, surface data & altimetry
GRIM5C1 (120x120)	GRGS/GFZ: Pre-champ combination model
DGME04 (70x70) (~1997)	DEOS: EGM96-Tuned with ERS crossovers
EIGEN1S (115x115) (Dec., 2001)	CHAMP (~88 days) + other satellites
EIGEN2 (140x140) (2003)	CHAMP-only, ~ six months
EIGEN3p (140x140) (Oct., 2003)	CHAMP-only, ~ three years
GGM01S (120x120) (July, 2003)	CSR: GRACE-only, ~111 days of Grace data
GGM01C (200x200) (July, 2003)	GGM01S combination model
EIGEN-GRACE01S, (140x140) (Fall, 2003)	GFZ: ~39-days of GRACE data
GRACE-EIGEN02, 66 days, (120x120) (Dec. 2003)	GFZ:~ 66 days of GRACE data ; (aug2002+aug2003)
GRACE-EIGEN02, 111 days, (150x150) (Feb. 2004)	GFZ:~111 days of GRACE data ; (aug2002-aug2003)
GRACE-JPL-MEAN, APR-Nov.2003 (120x120) (Jan. 2004)	JPL:~191 days of GRACE data: (apr 2003 – nov 2003)
PGS7772P24 (99X99) (April 2003)	GSFC: CHAMP-only (~87 days)
PGS7777B (110x110) (Oct., 2003)	GSFC:CHAMP + other satellites (e.g., GFO, Envisat, Topex, Jason)
PGS7779E (110x110) (Dec., 2003)	GSFC: PGS7777B + 3days GRACE

Table 6.1: Summary of Modern Gravity Models (Lemoine et al., 2004).

6.3.3 Moon, Sun and Planetary Attraction

The moon, the sun and other planets ('third body') also exert gravitational attractions on the satellite, which results in an acceleration vector of the satellite towards the 'third body' and is given as,

$$\ddot{r}_d = \nabla U_d \tag{6.14}$$

where the potential U_d at the satellite due to the third body is given as,

$$U_d = \frac{GM_j}{|r - r_j|} \tag{6.15}$$

where, M_j : the mass of the third body,

r : the satellite position vector,

r_j : the position vector of the third body.

The position and mass of the moon, the sun and the other planets must be known to evaluate this acceleration. The planetary and lunar ephemeris adopted in this study is the DE200/LE200, which gives the positions of the moon and planets in the J2000.0 inertial frame at 0.0 hrs TDB of each day, together with the masses of the planets and the constants associated with the ephemeris.

6.3.4 Solid Earth and Ocean Tides

6.3.4.1 Solid Earth Tides

As the Earth is not entirely rigid, the attraction of the moon and the sun will cause the solid Earth and the ocean to deform. These are usually referred to as solid Earth tides and ocean tides respectively. These deformations will yield extra accelerations on the satellite. At any point P on the surface of the Earth, the potential due to either the moon or the sun is given as,

$$U = \frac{GM_j}{|r_p - r_j|} \tag{6.16}$$

where, M_j : the mass of the sun or the moon,

r_p : the position vector of a point P on the Earth surface.

This potential causes the solid Earth to deform as shown in Figure (6.1). For the solid tide, the deformation leads to an additional potential U_t due to the tidal bulge as given by (Ashkenazi et al., 1994),

$$U_t = k_2 \frac{GM_j a^5}{r^3 r_j^3} P_2 COS\, z \tag{6.17}$$

where

k_2 : the Love number,

r : the satellite position vector,

a : the earth's equatorial radius,

and $$COS\, z = \frac{r.r_j}{r\, r_j}. \tag{6.18}$$

The body tide Love number k_2 which gives the change of potential of the Earth due to the tidal potential varies slightly according to the period of various tides. However, in practice, k_2 is treated as nominally constant with a value of 0.3. In this study, the frequency dependent tidal effect is also accounted for in a two-stage procedure. A frequency independent Love number (k_2=0.3) is used during the first stage to evaluate the acceleration of the satellite. The effect of the frequency dependent love number is accounted for by computing the corrections to the normalised spherical harmonic coefficients during the second stage.

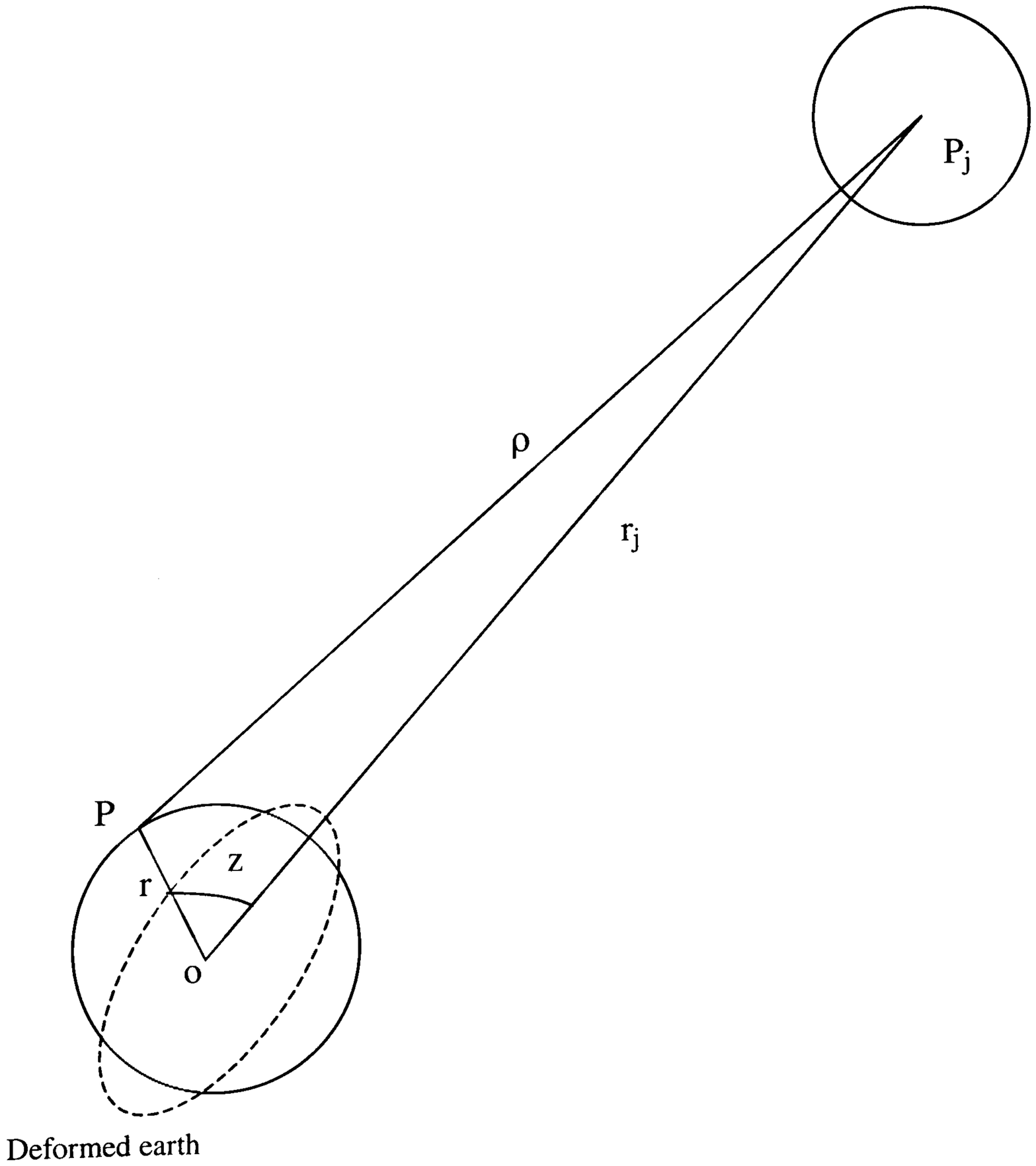

Figure 6.1: The Earth Tide Caused by The "Third Body".

6.3.4.2 Ocean Tides

As the surface of the ocean is an equipotential surface, this tide raising potential causes the level of the oceans to fluctuate with time. This also affects the potential field at the satellite. The effect of the ocean tides is most efficiently implemented as corrections to the normalised spherical harmonic coefficients to the geopotential mode. In this study, the GEM-T1 ocean tide model (Marsh et al., 1988) is used to evaluate the ocean tide effect.

6.3.5 Solar Radiation Pressure

The intensity of solar radiation emitted by the sun varies inversely with distance away from the sun. The radiation pressure acting on the satellite orbiting the Earth is given as,

$$P = \frac{I_o}{c}\left(\frac{A_u}{r - r_j}\right)^2, \tag{6.19}$$

where, A_u : the astronomical unit (1.4959787×10^{11}m),

r : the position vector of the satellite,

r_j : the position vector of the sun,

I_o : the intensity of solar radiation (w/m^2),

c : the speed of light (m/s)

This solar radiation pressure results in an acceleration of the satellite in a direction away from the sun, which is given as,

$$\ddot{r} = C_R P \frac{A}{m} \frac{r - r_j}{|r - r_j|} \tag{6.20}$$

where C_R : the radiation reflectance coefficient,

P : the solar pressure defined in equation (6.19),

A : the cross section area of the satellite,

m : the mass of the satellite.

The precise modelling of the solar radiation pressure is a complex process. Many factors should be taken into account, including the reflectivity of the satellite surface, the geometric relationship between the satellite and the sun, the moon and the Earth, the solar activity, and the shape of the satellite.

To account for the uncertainty in the model, introduced by these various effects, a correction to the reflectance coefficient C_R is determined as an unknown in the least squares solution to absorb some of the model errors.

6.3.6 Atmospheric Drag

The Effect of atmospheric drag on the satellite depends on its altitude, thus for LEO satellites the acceleration due to air drag is significant and should be taken into account. The acceleration due to air drag can be expressed as,

$$\ddot{r}_a = -\frac{1}{2} C_D \left(\frac{A}{m}\right) \rho_a \, v_r \, v_r \tag{6.21}$$

where, C_D : the satellite drag coefficient,

ρ_a : the air density at satellite altitude,

v_r : the velocity of the satellite with respect to the atmosphere.

In this study, a correction to the drag coefficient C_D is also included as an unknown in the least squares solution.

6.4 Equations of Motion & Numerical Integration

6.4.1 Equations of Motion

The motion of the satellite is governed by the following equation;

$$\ddot{r} = f(t, r, \dot{r}), \tag{6.22}$$

where,

$\ddot{r}$ = acceleration vector,

$\dot{r}$ = velocity vector,

r = position vector,

t = time.

The integration of the satellite equation of motion (6.22) with respect to time from an initial velocity vector $\dot{r}_0$ will give the velocity of the satellite at a given time t, as shown in the following equation (6.23),

$$\dot{r}(t) = \dot{r}_o + \int_{t_o}^{t} \ddot{r}\, dt \tag{6.23}$$

Following the same rule, the position of the satellite at any time t will be produced from the integration of the satellite velocity equation (6.23) with respect to time from an initial position vector r_0 as shown in the following equation,

$$r(t) = r_o + \int_{t_o}^{t} \dot{r}\, dt \tag{6.24}$$

The integration process to produce both the velocity and position equations of the satellite should be implemented in an inertial (non-rotating) reference frame, also it can be applied using analytical or numerical techniques. The numerical integration technique is more adequate for the quantitative high precision orbit determination while the analytical techniques are more suitable for qualitative orbit analysis (Whalley, 1990).

6.4.2 Numerical Integration

The numerical integration basically fits a polynomial through a series of consecutive points, in order to create extra points through extrapolation of the polynomial. The coefficients of the polynomial are derived from the given points and their partial derivatives, based on the equation of motion. There are two methods generally used, namely single-step and multi-step methods. The single-step methods employ only the value from the last integration step to predict the following point, such as the Runge-

Kutta method. Conversely, the multi-step methods termed predictor-corrector methods, such as the Adams-Bashforth predictor-corrector method, predict the value at the following epoch and then correct the value in an iterative approach. The predicted value X_{n+1} is obtained from X_n, and then evaluated using the previous n values. If the differences between the predicted and corrected values exceed the specified criteria, the process is iterated by applying the corrected value until the requirements are satisfied.

The multi-step methods produce better results than single-step methods in the same integration step length, but require information of the previous n values and are more time consuming. The choice of the integration step length depends on the compromise of two-error sources, the round-off and truncation errors. Round-off errors are characteristic of the computer hardware or the algorithms used. The recent developments in computer hardware are such that round-off errors are now usually due to the algorithms used. These effects of round-off errors can be minimised by using large step lengths in the process. The truncation error, which arise due to the higher terms of approximation polynomial are cut off, can be reduced by using a rather small step length, as a contrast with the round-off errors (Chao, 1996).

In this study the orbit integration program, applies a 4^{th} order Runge-Kutta single-step integrator, to provide sufficient integration steps for a more precise 8^{th} order Adams-Bashforth multi-step predictor-corrector integrator to take over. The step length of 10 seconds for the Runge-Kutta scheme and 60 seconds for Adams-Bashforth scheme is employed (Ashkenazi et al., 1996).

6.5 LEO Satellite Orbit Determination Techniques

Various orbit determination techniques can be used for LEO satellites with onboard GPS measurements, these techniques can be separated into kinematic, dynamic and reduced-dynamic orbit determination. Detailed description will follow for each technique.

6.5.1 Kinematic Orbit Determination

This technique is based on a conventional GPS navigation solution using a GPS receiver onboard the LEO satellite. The receiver can measure four or more independent pseudo-ranges from a number of different GPS satellites, so the three-dimensional position of the satellite and the receiver clock error could be easily determined. The position at each epoch is dependent only on GPS-observations at the specific epoch without any influence from GPS observations at the previous or next epochs. Stand-alone and differential solutions could be used varying the resultant accuracy. The orbit solution using the kinematic technique is referenced to the phase centre of the onboard GPS antenna instead of the satellite's centre of mass. The kinematic solution is sensitive to geometrical factors, such as the direction of the GPS satellites and the GPS orbit accuracy.

(Yunck and Wu, 1986) proposed a geometric method that uses the continuos record of satellite position changes obtained from the GPS carrier phase to smooth the position measurements made with pseudo-range. (Byun, 1998) developed a kinematic

orbit determination algorithm using double and triple-difference GPS carrier phase measurements.

The kinematic technique is the simplest way of determining the LEO-satellite's position and allows a real-time solution however it gives the least achievable accuracy (Ashkenazi et al., 1994).

6.5.2 Dynamic Orbit Determination Technique

The Dynamic Orbit Determination technique (Tapley, 1973) is based on the fact that an accurate knowledge of the forces acting on a satellite and the satellite's mass gives the acceleration vector of the satellite which can be integrated twice from an initial position and velocity vectors to get the position vector of the satellite. The accuracy of the integrated orbit depending only on the accuracies of the force models and the initial conditions of the satellite (position & velocity).

Figure 6.2 illustrates the principle steps of the dynamic orbit determination technique. Starting with an initial state vector at an initial epoch, the orbit integration program numerically integrates the total acceleration acting on the satellite once to get the satellite velocity and twice to get the satellite position. This process generates the partials of the velocity and position of the satellite with respect to the initial starting elements. The next step is to use a least-squares solution with all the available observations to produce an improved initial state vector containing the force model parameters. Then a more accurate integrated orbit can be obtained using the new

initial state vector with the improved force model parameters. This iteration process continues until the target accuracy is achieved.

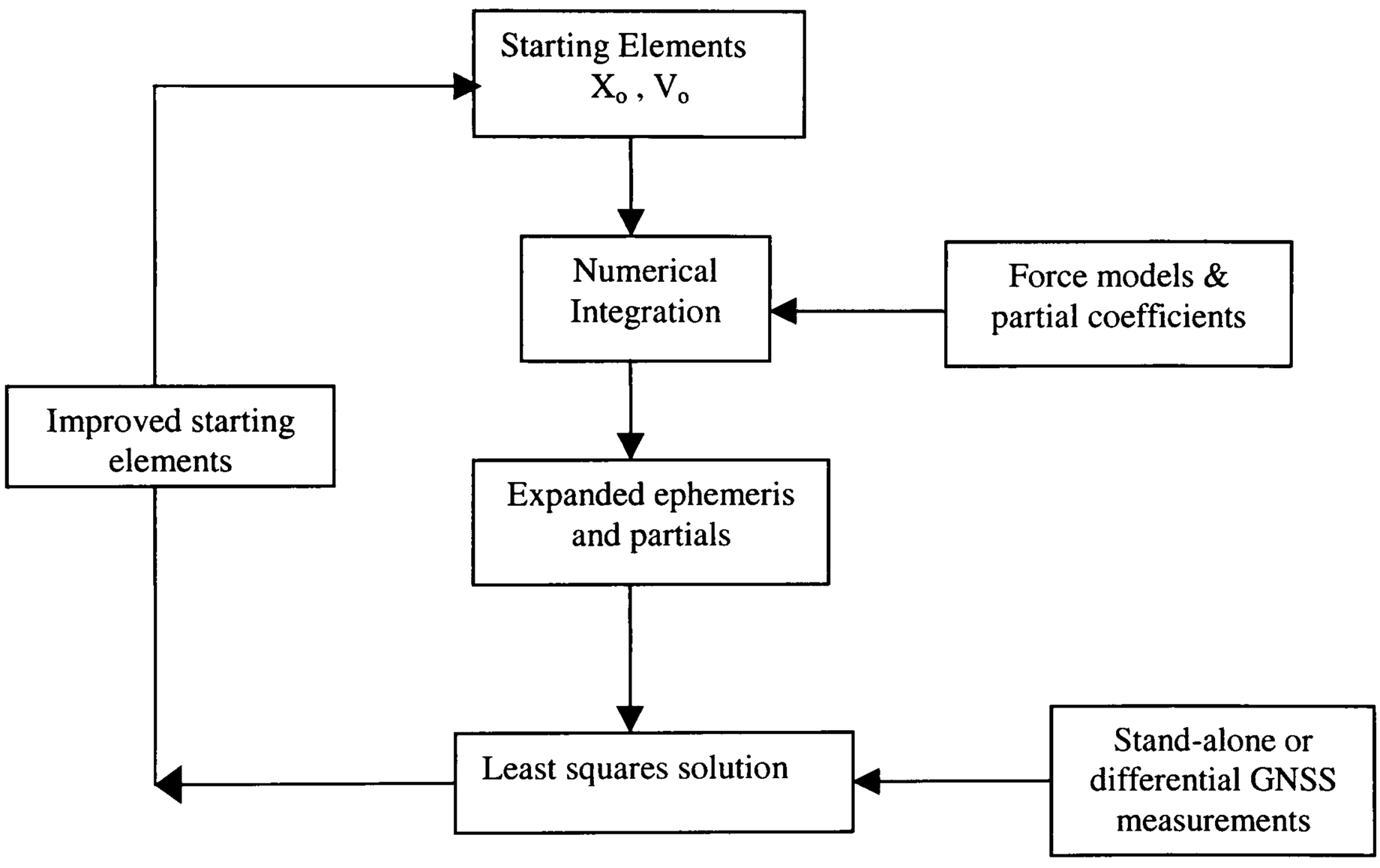

Figure 6.2: Flow Chart of Dynamic Orbit Determination Technique.

This technique is normally used as a post-processing method, which requires all the measurements from a chosen observation period. The real-time implementation of the dynamic orbit determination method is "the sequential least square method" which overcomes the difficulty of waiting for all the measurements from the chosen period to become available by calculating an improved initial state vector of every epoch using all measurements up to this epoch. An improved position and velocity at the

current epoch can then be obtained by mapping forward the improved initial position and velocity using the corresponding partial derivatives (Ashkenazi et al., 1994).

6.5.3 Reduced Dynamic Orbit Determination Technique

The Reduced Dynamic Technique, Melbourne et al. (1986), Wu et al. (1991) for the LEO satellite orbit determination is made available with GPS observations. This technique involves satellite-state-transition information obtained from both the dynamic model and continuous GPS observations, which is optimally combined to improve the orbit determination accuracy.

The Reduced Dynamic technique tries to benefit from the advantages of both the previously mentioned techniques (kinematic technique & dynamic technique) and avoid their disadvantages. As previously mentioned, the dynamic orbit determination technique produces the orbit of the satellite using numerical integration, adjusting the initial starting elements (position & velocity) and some force model parameters to obtain the best fit with the tracking measurements. Obviously, the main errors that will affect the orbit accuracy will be the force model errors and the accuracy of the starting elements.

(Wu et al., 1991) have compared qualitatively the dynamic, kinematic and reduced-dynamic techniques. They showed that the dynamic solution adjusts the fewest parameters, preserving maximum data strength and yielding the lowest formal error however, it can suffer large systematic errors due to mismodelled dynamics. The

kinematic solution eliminates modelling errors but the orbit transition is determined entirely from the observations so the data strength is depleted and the formal error can grow large. The reduced-dynamic solution optimally combines the two techniques to achieve the lowest overall error (Wu et al., 1991).

The reduced dynamic technique tries to minimise the unmodelled force errors by introducing a modelling noise n_p (Ashkenazi et al., 1994) where,

$$F + n_p = m\,a \tag{6.25}$$

Where, F is the resultant acting force on the satellite,

m mass of the satellite,

a acceleration of the satellite.

The orbit solution is weighted between the dynamic model and the observation model through a Kalman filter process by varying the variance of the dynamic modelling noise. Applying a minimum value for the dynamic modelling noise will result in an orbit purely determined by the dynamic model however applying a maximum value for the dynamic modelling noise will produce an orbit purely determined by the observation model. Hence this technique depends on the proper selection of the force modelling and measurements noises.

The main task when using the reduced dynamic technique is to select the appropriate modelling noise, which represents the actual accuracy of the dynamic model. It is not

easy to determine the accuracy of the dynamic model because the modelling errors are dependent on the dynamics of the satellite and may change with time. Two methods could deal with this problem: simulation method will be appropriate if the satellite dynamics are quite smooth and the noise variance can be considered constant. However if the satellite motion is dynamically unpredictable such as a space station or space shuttle then an adaptive filter method must be used to determine the dynamic modelling noise (Ashkenazi et al., 1994). Due to the recursive nature of the filtering algorithm, the satellite position is updated epoch by epoch, making it ideally suited for real-time orbit determination. Figure 6.3 shows flow chart of the reduced dynamic orbit determination technique. For more detailed information about the reduced dynamic orbit determination technique and the Kalman filter, the reader is referred to Appendix D and Appendix E respectively.

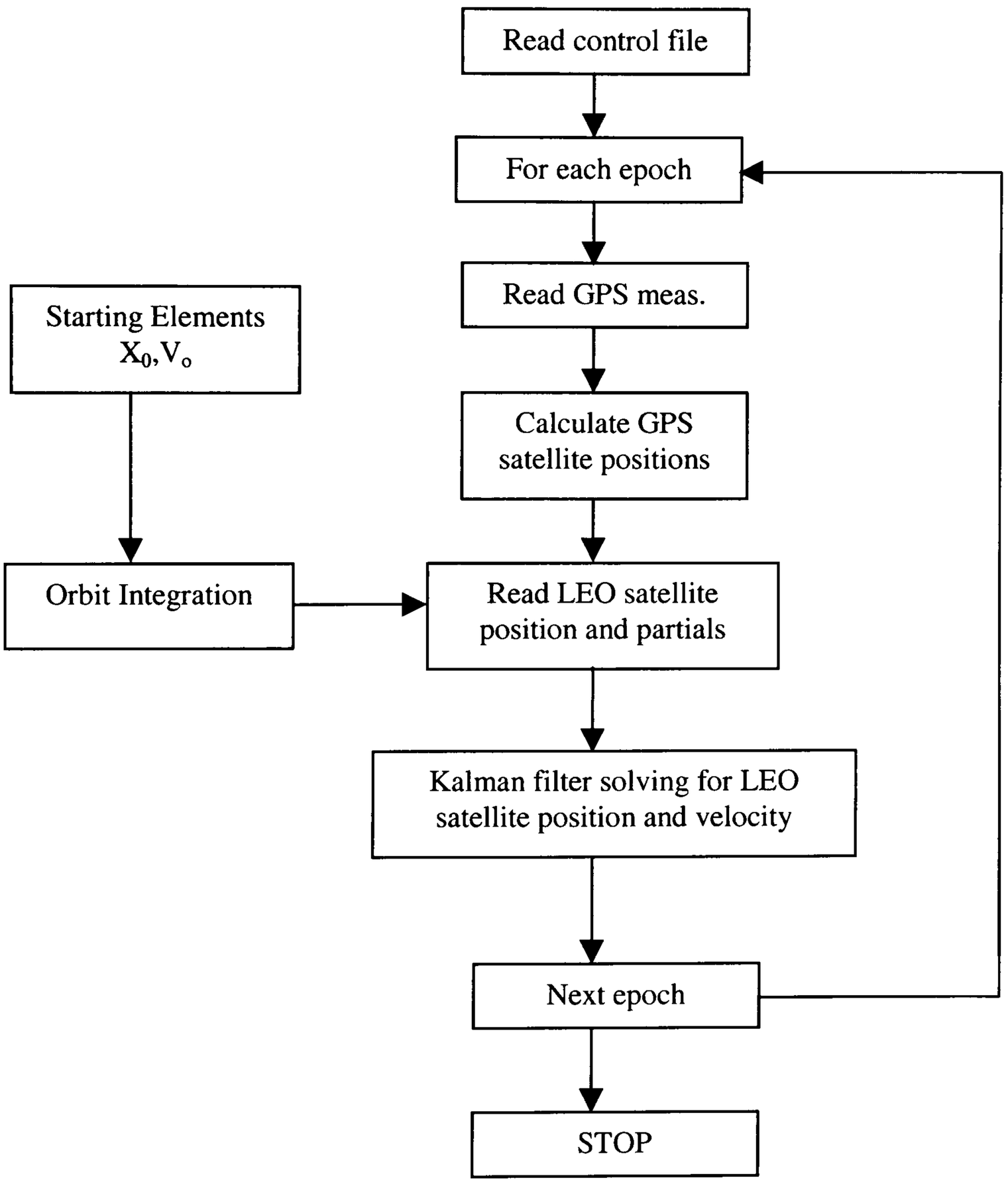

Figure 6.3: Flow Chart of the Reduced Dynamic Orbit Determination Technique (Ashkenazi et al., 1996).

CHAPTER 7

Topex/Poseidon Reduced Dynamic Orbit Determination Tests

7.1 Introduction

The reduced dynamic technique for orbit determination is the most efficient technique among those mentioned in the previous chapter because it combines the other two methods, allowing the weighing of each method to obtain the most accurate orbits for the desired satellite. (Ashkenazi et al., 1994) have demonstrated the quality of such technique by using it to determine the orbits of the Topex/Poseidon satellite using GPS measurements. Achieving maximum benefit from the altimetric data collected by the T/P satellite requires a radial orbit accuracy of 10 cm or better (Nouel et al., 1994).

This chapter will investigate the Topex/Poseidon orbit determination using the reduced dynamic technique for three different types of simulated measurements: GPS measurements, GALILEO measurements and combined GPS/GALILEO measurements. Three different types of GNSS solutions will be used for each type of

measurements: stand-alone solution; differential pseudo-range solution and differential carrier phase solution.

The Stand-alone solution from any measurement type requires generation of simulated measurements from a receiver onboard the T/P satellite, which requires an accurate satellite trajectory. The satellite trajectory was provided from the AVISO service (Archiving, Validation and Interpretation of Satellites Oceanographic data), (AVISO, 2002) using their Topex/Poseidon (POE) product which is generated using DORIS and SLR data and has an accuracy at the centimeter level (Nouel et al., 1994). The quality of all the output T/P ephemeris through this research was assessed by comparing it with the high accuracy AVISO ephemeris. The error sources which are accounted for in the T/P GNSS data are the receiver and satellite clocks, ephemeris errors and measurement noise. The atmospheric error is ignored due to the altitude of the satellite (about 1300 km above the earth).

The differential solution requires generating measurements for a number of ground stations for the different types of constellations (GPS, GALILEO and GPS/GALILEO). The error sources which are accounted for in the ground station data are the receiver and satellite clocks, ephemeris errors, atmospheric error (ionosphere and troposphere) and measurement noise. The simulated ground data from GPS includes dual frequency measurements using L1 (1575.42 MHz) and L2 (1227.60 MHz) frequencies while the simulated ground data from GALILEO includes dual frequency measurements using the open service frequencies E2L1E1 (1575.42 MHz) and E5AB (1192 MHz).

The measurement noise considered for the T/P onboard GPS receiver pseudo-range and carrier phase measurements was 50 cm and 1 cm respectively (Ashkenazi et al., 1996). The GPS Ground data from GPS had measurement noise of 20 cm and 1 mm for pseudo-range and carrier phase respectively to reflect the performance of a typical GPS receiver. The measurement noise for GALILEO ground data using E2L1E1 frequency was 13.333 cm and 0.7000 mm for pseudo-range and carrier phase respectively while the measurement noise for GALILEO ground data using E5AB frequency was 6.667 cm and 0.3000 mm for pseudo-range and carrier phase respectively. These chosen values reflect approximately the chip rate relation between GPS and GALILEO frequencies (Hein et al., 2002), (Tiberius et al., 2002). The IGS-final orbits were used to generate all types of simulated GPS data due to its high accuracy (< 5cm/0.1ns) as well as high quality GALILEO ephemeris file for generating GALILEO data without any ephemeris error (Section 5.2).

The following softwares have been used in this study:

- "ORBIT" program, the IESSG's in-house developed program used for dynamic orbit determination. "ORBIT" contains the various force model components expressed in (§ 6.3) and follows the flow chart for dynamic orbit determination shown in Figure 6.2.
- "SOLORB" LEO Satellites orbit solution program, the IESSG's in-house developed program was used for the reduced dynamic orbit determination. SOLORB follows the flow chart of reduced dynamic orbit determination technique shown in Figure 6.3.

Section (7.2) will show some tests to assess the effect of the GPS satellite ephemeris errors as well as the accuracy of the initial predicted orbit on the quality of the reduced dynamic final orbits.

Section (7.3) will show the validation of the simulation studies by comparing the behavior of the T/P GPS real data with the T/P GPS simulated data from GPS constellation only. Obviously this study couldn't be expanded to involve GALILEO and combined GPS/GALILEO for the lack of GALILEO real data.

Section (7.4) will show the output results from simulated data-reduced dynamic orbit determination technique from three different types of constellations GPS, GALILEO, and combined GPS/GALILEO. This section will end with an orbit overlap study for stand-alone reduced dynamic solution using combined GPS/GALILEO simulated data.

Finally Section (7.5) shows a comparison of Topex/Poseidon reduced dynamic orbits using GPS simulated data from this study with other studies using the same technique. For the importance of the radial orbital error in the LEO satellite orbit determination for oceanography applications (this research's focus), re-plot for the radial orbital error of all the tests shown in this chapter is shown in Appendix G.

7.2 Behaviour Tests

7.2.1 Effect of GPS Satellite Ephemeris Errors

To assess the effect of GPS satellite ephemeris errors on the quality of the final reduced dynamic orbits, four different categories of tests had been investigated. Each one of them uses a different type of the IGS-GPS ephemeris products to process the measurements in the reduced dynamic process while the IGS final orbits are used to generate the data as mentioned before. Stand-alone solution was adopted through these different tests. The error sources which are accounted for in the T/P GPS simulated data are the receiver and satellite clocks, ephemeris errors and measurement noise. The results shown here were presented by (Farah et al., 2004).

The IGS offers four different types of GPS ephemeris:

- The Final orbits
- The Rapid orbits
- The predicted (UltraRapid) orbits
- The Broadcast orbits (sent through GPS navigation message)

Table 7.1 explains the features of each type of these orbits. GPS broadcast ephemeris accuracy statistics are presented in Appendix F compared with other IGS-GPS ephemeris (GPS Lab, 2004).

IGS GPS Ephermeis Product	**Accuracy**	**Latency**	**Updates**	**Sample Interval**
Broadcast	~260 cm/~7 ns	Real time	----	Daily
Predicted (Ultra-Rapid)	(Pred.) ~10cm/~5ns	Real time	Twice daily	15 min/15 min
	(Obs.) ~5cm/~0.2ns			
	(Total) ~25cm/~5ns			
Rapid	5 cm/0.2 ns	17 hours	Daily	15 min/5 min
Final	< 5 cm/ 0.1 ns	~ 13 days	weekly	15 min/5 min

Table 7.1: The features of IGS-GPS Ephemeris Products (IGS, 2003).

7.2.1.1 The Effect of GPS Broadcast Ephemeris

As the broadcast GPS ephemeris offers the lowest accuracy comparing with other IGS-GPS Ephemeris products, then it should be expected to give lower accuracy for the reduced dynamic final orbits and this is assured from Table 8.2 which shows the RMS errors for the T/P reduced dynamic orbit processed with GPS broadcast ephemeris. This behaviour is shown in Figures 7.1 and 7.2 that show the reduced dynamic orbital errors for a one-day arc and a two-day arc respectively.

RMS Errors (m)	One-day arc	Two-day arc
Radial	0.059	0.129
Along-track	0.408	0.697
Across-track	0.771	0.406
Total	0.874	0.817

Table 7.2: The LEO Satellite Reduced dynamic Orbit RMS Errors processed with GPS Broadcast Ephemeris.

It can be shown that the reduced dynamic orbit has different behaviour for one-day and two-day arc which due to different modelling noise adopted for the dynamic model as the accuracy of GPS broadcast ephemeris degraded in the second day with approximately 1.00 m RMS with respect to IGS-final GPS orbits (Appendix F).

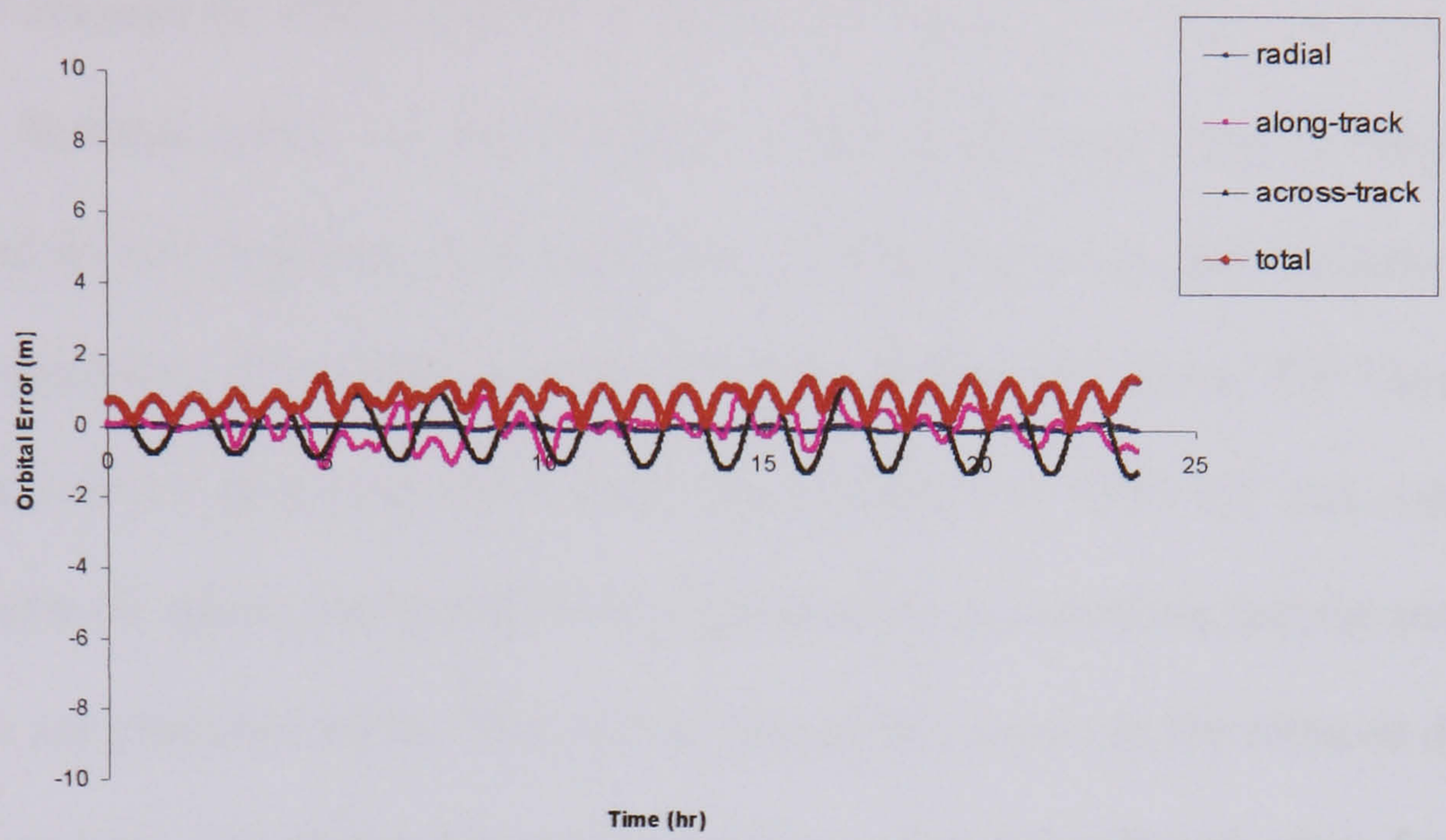

Figure 7.1: Reduced Dynamic Solution for stand-alone simulated GPS receiver (GPS Broadcast Ephemeris) (one-day arc)

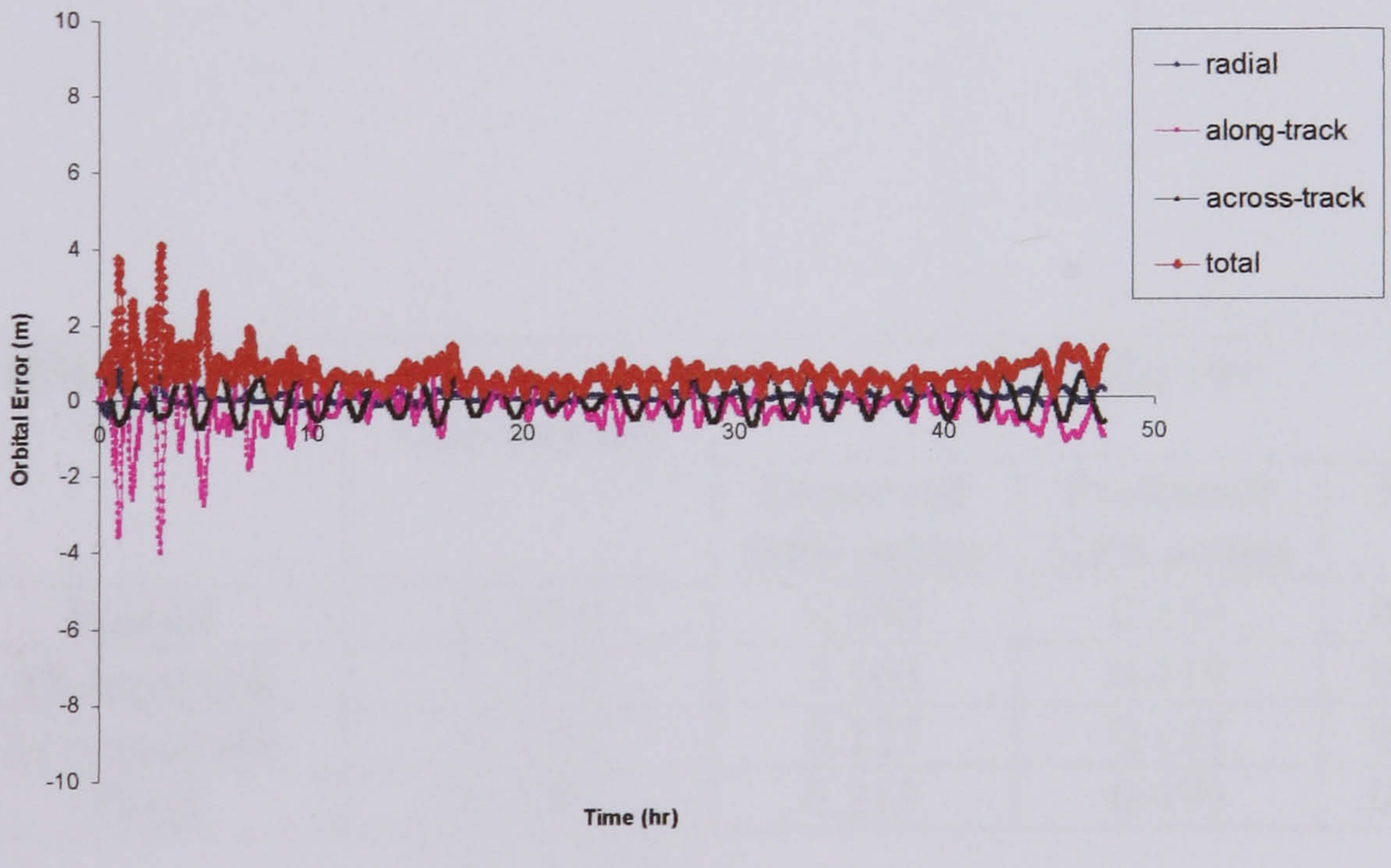

Figure 7.2: Reduced Dynamic Solution for Stand-alone simulated GPS receiver (GPS Broadcast Ephemeris) (two-day arc)

7.2.1.2 The Effect of IGS Ultra-Rapid GPS Orbit

This test assesses the effect of using the IGS Ultra-Rapid GPS orbits on the quality of reduced dynamic orbits. As the accuracy of the Ultra-Rapid orbits is much better compared to the broadcast ephemeris, this should also affect the accuracy of the reduced dynamic orbits produced using the Ultra-Rapid GPS orbits. The Ultra-Rapid combinations are generated twice each day at 0300 and 1500 UT and contain 48 hours worth of orbits; the first 27 hours are based on observations and the remaining 21 hours are predicted orbits. This feature should be evident in the reduced dynamic solution as well. The reduced dynamic solutions using Ultra-Rapid orbits for a one-day arc and a two-day arc are shown in Figures 7.3 and 7.4. Table 7.3 shows the RMS errors for the one-day arc as well as the observed 27 hours, predicted 21 hours of the two-day arc. The RMS errors for the total two-day arc are also shown in Table 7.3.

RMS Errors (m)	One-day arc	Two-day arc		
		Observed GPS orbits	Predicted GPS orbits	Total
Radial	0.056	0.050	0.153	0.115
Along-track	0.103	0.163	0.419	0.316
Across-track	0.084	0.127	0.222	0.146
Total	0.145	0.213	0.499	0.367

Table 7.3: The LEO Satellite Reduced dynamic Orbit RMS Errors using IGS Ultra-Rapid Orbits.

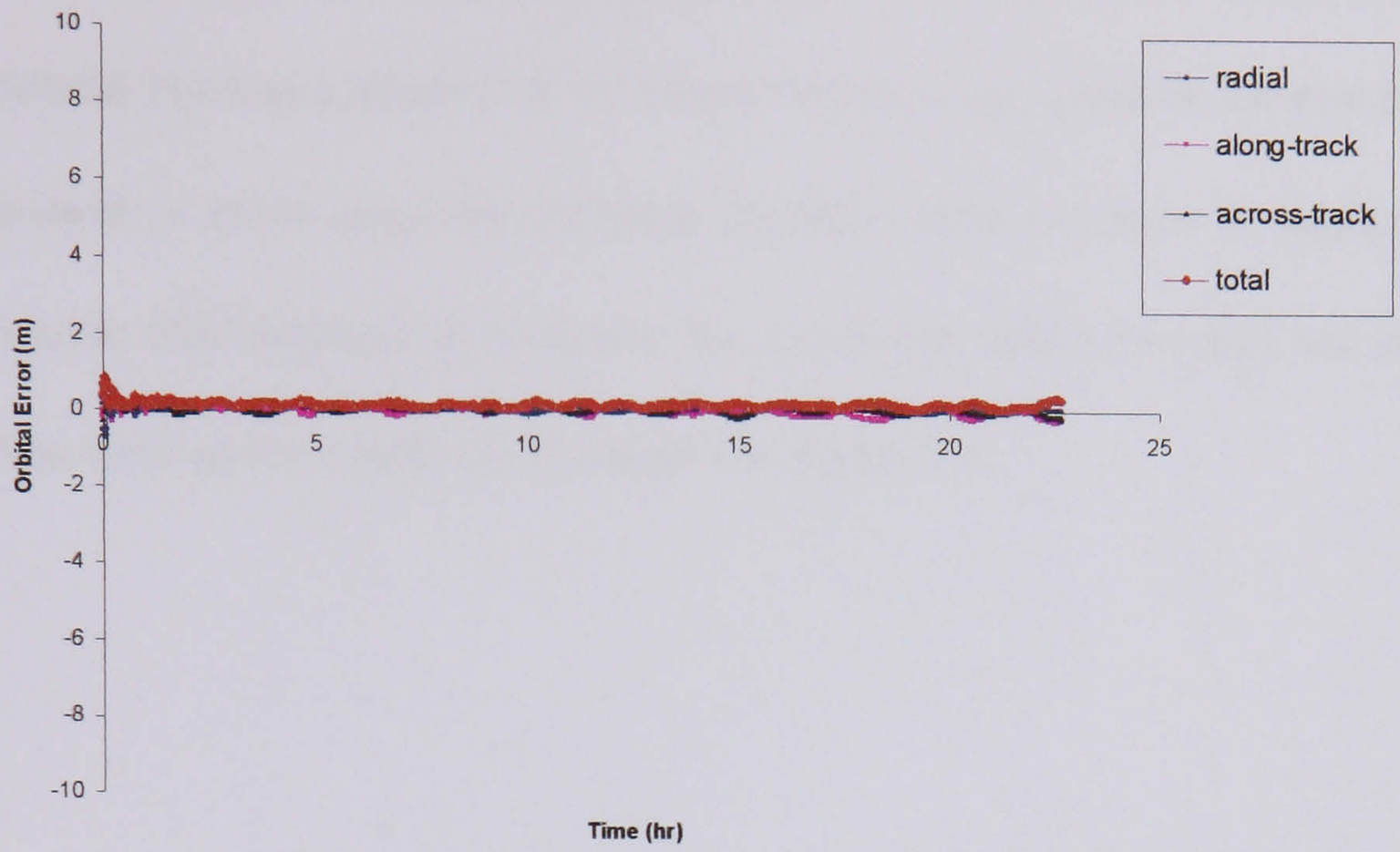

Figure 7.3: Reduced Dynamic Solution for stand-alone simulated GPS receiver (IGS UltraRapid GPS Orbits) (one-day arc)

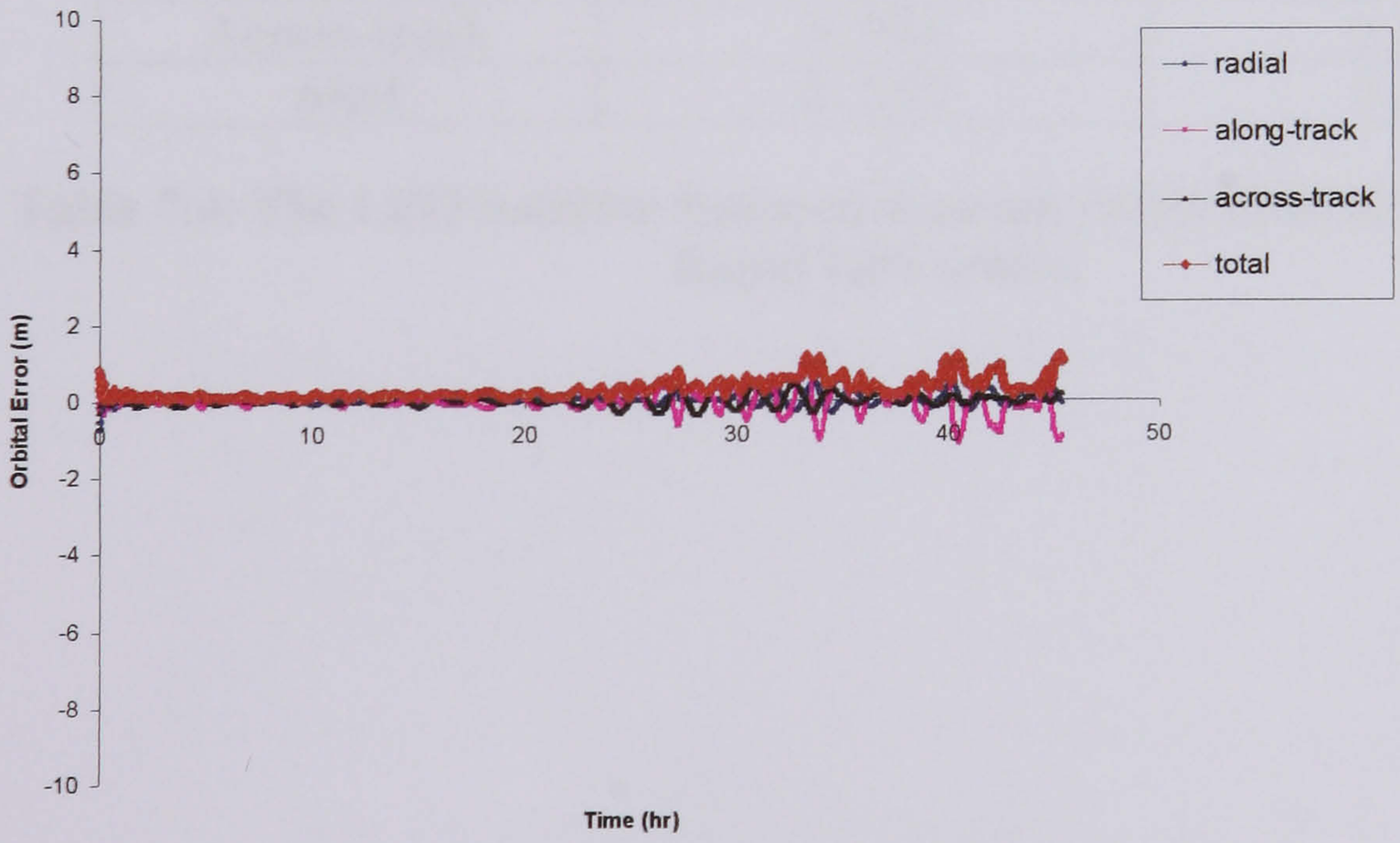

Figure 7.4: Reduced Dynamic Solution for Stand-alone simulated GPS receiver (IGS UltraRapid GPS Orbits) (two-days arc)

7.2.1.3 The Effect of IGS Rapid GPS Orbit

The IGS Rapid GPS orbit is much more accurate than the broadcast & Ultra-Rapid products but has a latency of 17 hours which is not suitable for real time applications. However a more accurate reduced dynamic orbit solution is expected. The reduced dynamic orbit behaviour is shown for a one-day and a two-day arc in Figures 7.5 and 7.6 as well as the RMS errors shown in Table 7.4.

RMS Errors (m)	One-day arc	Two-day arc
Radial	0.083	0.067
Along-track	0.096	0.109
Across-track	0.085	0.161
total	0.152	0.206

Table 7.4: The LEO Satellite Reduced dynamic Orbit RMS Errors using IGS Rapid GPS orbits.

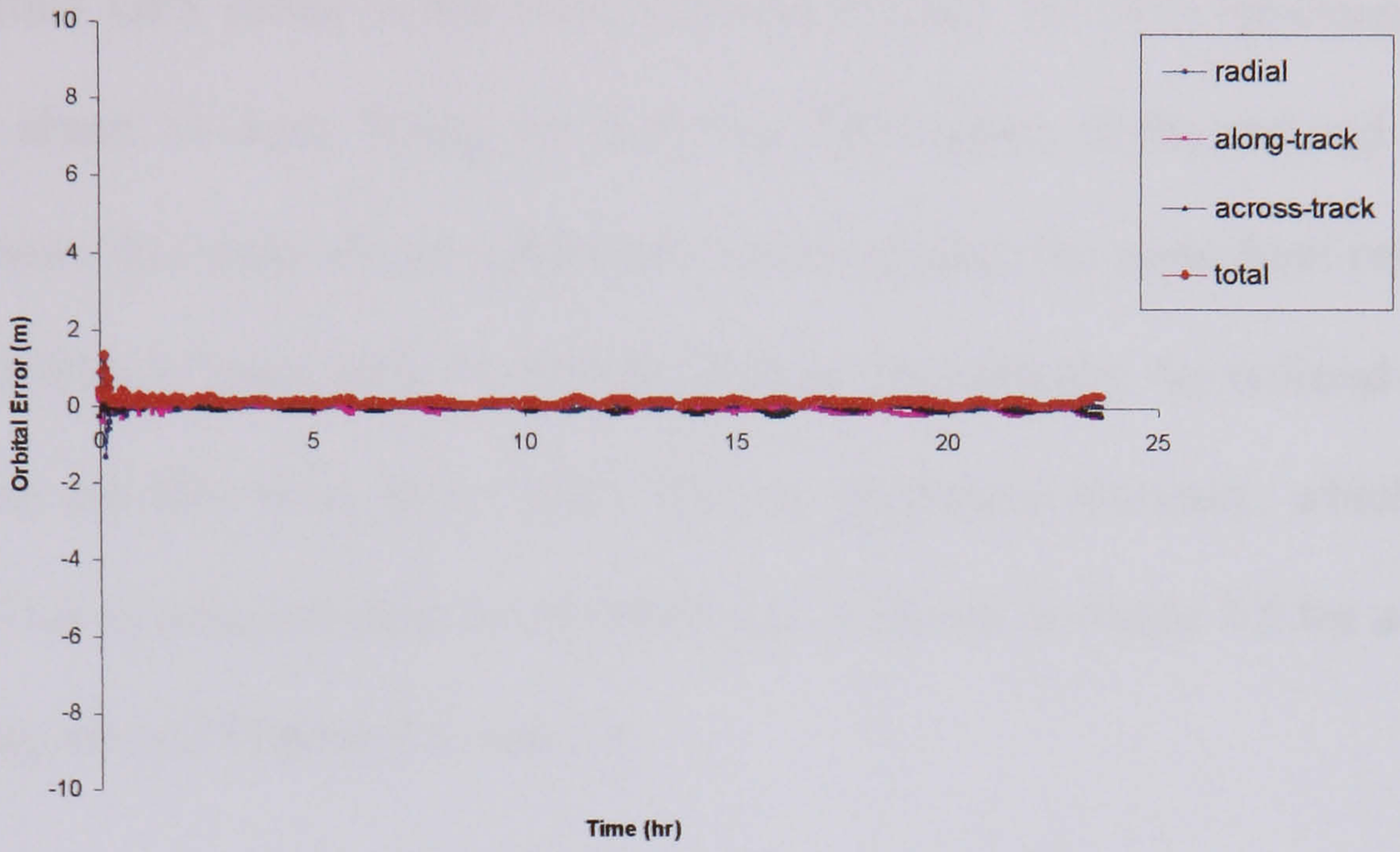

Figure 7.5: Reduced Dynamic Solution for stand-alone simulated GPS receiver (IGS Rapid GPS Orbits) (0ne-day arc)

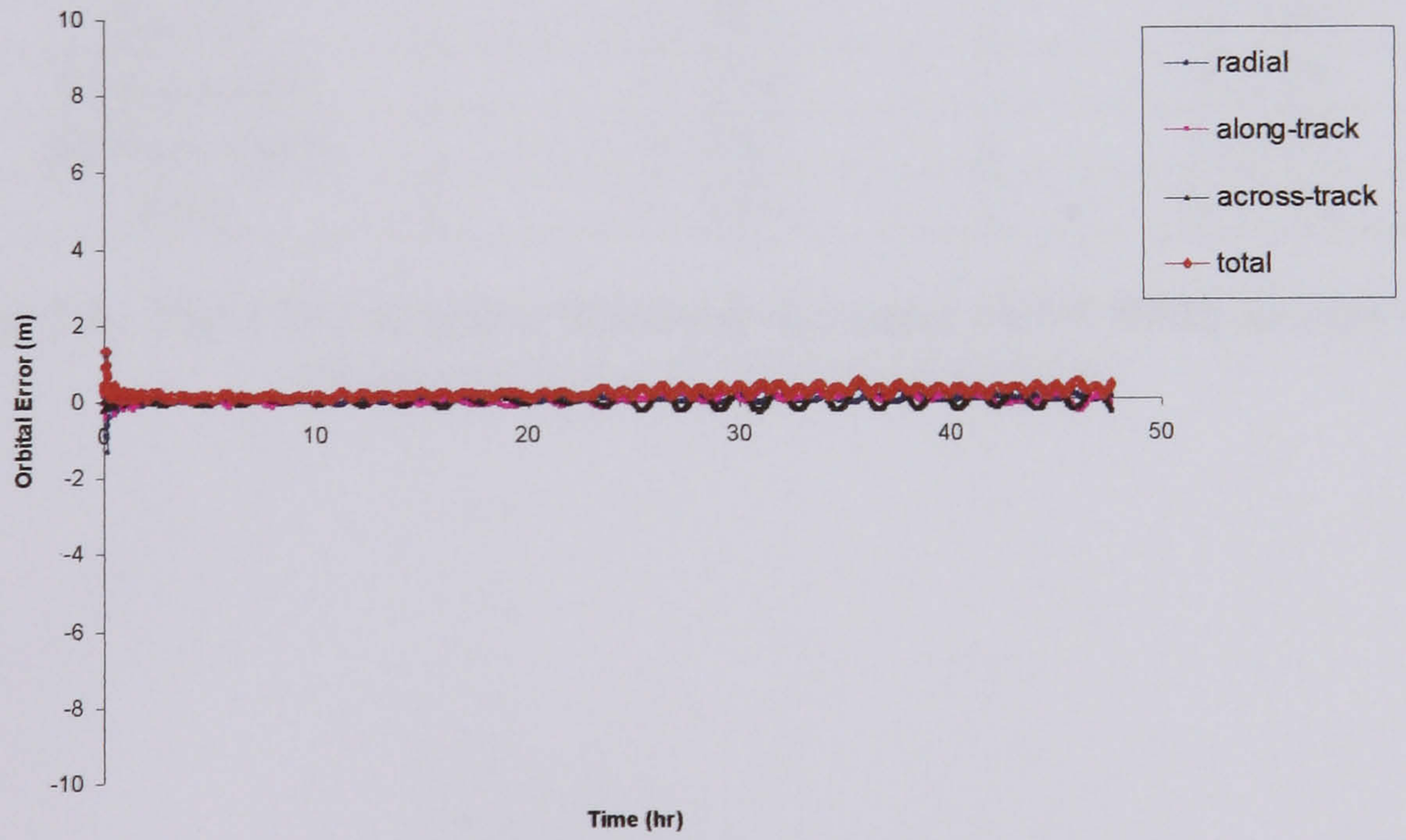

Figure 7.6: Reduced Dynamic Solution for Stand-alone simulated GPS receiver (IGS Rapid GPS Orbits) (two-day arc)

7.2.1.4 The Effect of IGS Final GPS Orbit

The IGS final GPS orbits is the most accurate product for GPS ephemeris with a latency of about 13 days. Using the IGS final GPS orbits in the reduced dynamic process means that there are no ephemeris errors because the same final orbits were used as the truth in generating the simulated data. Accordingly, the reduced dynamic orbits using the IGS final orbits will offer the maximum accuracy, which can be obtained. This is demonstrated by the RMS errors shown in Table 7.5 for a one-day and two-day arc and Figures 7.7 and 7.8.

RMS Errors (m)	One-day arc	Two-day arc
Radial	0.081	0.066
Along-track	0.096	0.108
Across-track	0.082	0.157
total	0.149	0.202

Table 7.5: The LEO Satellite Reduced dynamic Orbit RMS Errors using Precise ephemeris (IGS final Orbits).

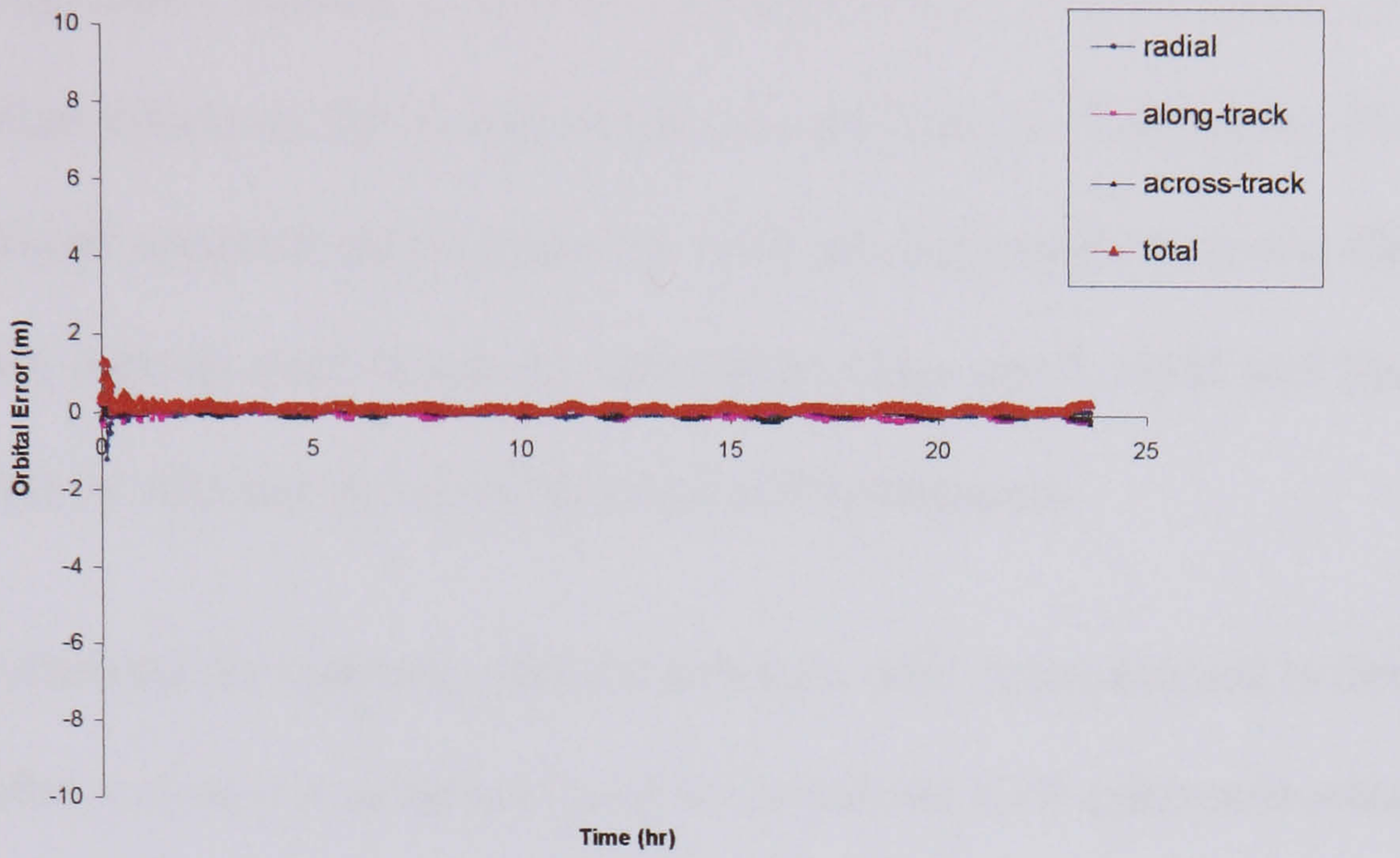

Figure 7.7: Reduced Dynamic Solution for stand-alone simulated GPS receiver (Precise Ephemeris)(IGS Final Orbits) (one-day arc)

Figure 7.8: Reduced Dynamic Solution for Stand-alone simulated GPS receiver (Precise Ephemeris) (IGS Final Orbits) (two-day arc)

7.2.1.5 Discussion

From the above studies, it can be concluded that the GPS ephemeris errors have significant effects on the quality of the reduced dynamic final orbits. The accuracy of the reduced dynamic orbits improves with the improvement in the GPS ephemeris accuracy starting with broadcast ephemeris, Ultra-rapid, rapid and finally with the true orbit, in this case given by IGS final GPS ephemeris.

The limitations for real-time reduced dynamic orbit determination is demonstrated as the lowest accuracy is achieved using the broadcast GPS ephemeris which is the only data available in real time. The UltraRapid orbits give a better performance if it can be used in real time. The improvement is high in the reduced dynamic orbits using the UltraRapid ephemeris over the broadcast ephemeris which is explained by referring to the accuracy of the both types of ephemeris shown in Table 7.1.

Figure 7.4 shows that, the accuracy is better within the first 27 hours of using the ultra-rapid ephemeris and then degrades for the next 21. Table 7.3 shows clearly how is the reduced dynamic solution affected with different accuracies of ultra-rapid GPS ephemeris. For two-day arc, the first 27 hours of ephemeris based on observations (Accuracy ~5cm/~0.2ns (IGS, 2003)) gives a better reduced dynamic solution rather than last 21 hours of ephemeris which based on predicted orbits (Accuracy ~10cm/~5ns (IGS, 2003)). The improvement is 0.10m, 0.22m, 0.10m, 0.24m for radial, along-track, across-track and total orbital error. The improvement is relatively small between the use of the rapid orbits and the final ones, as they had similar accuracies.

7.2.2 Effect of The Accuracy of The Initial Predicted Orbit

The reduced dynamic orbit determination technique is combining two solution methods: a dynamic model and measurements model. The accuracy of the reduced dynamic orbit is therefore dependent on the accuracy of those two models and the degree of weighting given to each of them. In the previous section (7.2.1) the effect of the measurements model accuracy on the quality of the reduced dynamic orbit was assessed where the accuracy of the GPS satellite ephemeris represented the accuracy of the measurements model. This section deals with the effect of the dynamic model accuracy on the quality of the reduced dynamic orbit.

The accuracy of the dynamic model determined by the accuracy of the initial predicted orbit (which mainly depends on the accuracy of the starting elements of position and velocity for the numerical integration of the force model) as well as the errors in various force models. Many of these force model errors can be estimated during the dynamic orbit determination process. Thus the main factor in the accuracy of the predicted orbit will be the accuracy of the starting elements.

A study of the sensitivity of the predicted orbit to the change in the starting elements carried out through this research showed that any change of over 10 cm in the starting elements position coordinates will result in degrading the accuracy of the predicted orbit. Also any slight change over 0.001 m/sec in the starting elements velocity vector will highly degrade the accuracy of the predicted orbit. The effect increases as the change increases which could be justified in the view of the approximate velocity of Topex/Poseidon LEO satellite is 6 km/sec (AVISO, 2003). Table 7.6 shows some of this study's results.

Position change (m)	RMS total error (m)	Velocity change (m/sec)	RMS total error (m)
0	3.00	0	3.00
0.01	6.50	0.0001	44.00
0.10	40.00	0.001	410.00
0.50	190.00	0.01	4000.00
1.00	380.00	1.00	400000.00

Table 7.6: The RMS total errors for the accuracy of the predicted orbit resulting from changes in the starting elements (two-day arc).

The reduced dynamic orbits shouldn't depend on the accuracy of the predicted orbit, so it should be expected to have similar accuarcies for different accuracies of the predicted orbits however this is not true generally and there are some limitations. These limitations came from the other factor affecting the quality of the reduced dynamic orbit, which is the measurements model.

As it can be concluded that the accuracy of the measurements model is mainly dependent on the accuracy of the ephemeris data (in the absence of any other errors). The effect of The GPS ephemeris errors on the quality of the reduced dynamic orbits was investigated in Section 7.2.1.

Following this study, another study was concluded to assess to what extent the accuracy of the reduced dynamic orbits did not depend on the accuracy of the initial predicted orbit using both GPS broadcast ephemeris (real time application)

and GPS precise ephemeris (IGS final orbits) (an indication of future better quality GPS orbits).

It can be concluded that using GPS broadcast ephemeris, the reduced dynamic orbits was largely unaffected by the accuracy of the predicted orbit up to a 20 cm change in the starting elements position coordinates. Using better quality GPS ephemeris such as the IGS final orbits improves this behaviour with the reduced dynamic orbit accuracy. Mainly unaffected by changes of up to 2 m in the starting elements position coordinates. Table 7.7 shows a part of the results of this study.

RMS Errors (m)	GPS Broadcast Ephemeris		GPS Precise Ephemeris	
	Position Change		Position change	
	0	20 cm	0	2 m
Radial	0.126	0.231	0.066	0.134
Along-track	0.693	0.771	0.108	0.116
Across-track	0.400	0.353	0.157	0.157
Total	0.810	0.879	0.202	0.237

Table 7.7: The LEO Satellite Reduced dynamic Orbit RMS Errors (Different GPS ephemeris) (Different initial orbits).

7.3 Validating The Simulation Studies

7.3.1 Introduction

Generally the major advantage of the simulation studies is that it makes it possible to test the behaviour of systems that do not exist yet such as GALILEO.

The simulation studies must include a validation study, which involve comparing the behaviour of the simulation studies with available real studies for existing systems (GPS). The agreement between the simulation studies outputs with the real studies gives the trust in the simulation studies outputs for non-existing future systems (GALILEO).

In our particular case, the validation study will require the comparison of the behaviour of the reduced dynamic technique using simulated GPS data with the behaviour using real GPS data. The real GPS data from the Topex/Poseidon onboard GPS receiver is available through JPL (Jet Propulsion Laboratory). A dataset of four months was under investigation (July to October 2002). Despite the low quality of the data (many epochs contains only 2 or 3 visible satellites, which cannot give a solution), the validation study had been investigated.

The validation study involved determining the reduced dynamic solution for a stand alone receiver from real GPS data for different spans of time (3 hours, 5 hours, 10 hours and 24 hours) of one day and then repeating the same scenario using simulated GPS data for the T/P receiver. The simulated data had a measurement noise of 50 cm

for pseudo-range and have the same visible satellites in each epoch as the real data (the gaps of data is similar in both types of data). The error sources which are accounted for in the T/P simulated GPS data are the receiver and satellite clocks, ephemeris errors and measurement noise. The test day for all types of data was 21/7/2002. The following results were presented by (Farah et al., 2004).

7.3.2 Comparison of Simulated GPS Data and Real GPS Data

The RMS errors for the reduced dynamic solution from simulated GPS data and real GPS data for different spans of time are shown in Table 7.8. The behaviour of the reduced dynamic solution using real GPS data and simulated GPS data for 24 hours is shown in Figures 7.9 and 7.10 respectively.

RMS Errors (m)	Simulated GPS Data				
	3 hours	5 hours	10 hours	15 hours	0ne day
Radial	0.197	0.158	0.042	0.100	0.102
Along-track	1.987	1.695	0.471	1.230	1.007
Across-track	0.510	0.506	0.582	0.577	0.614
Total	2.061	1.776	0.750	1.363	1.184
RMS Errors (m)	Real GPS Data				
	3 hours	5 hours	10 hours	15 hours	0ne day
Radial	0.134	0.037	0.046	0.057	0.059
Along-track	1.964	1.265	0.923	1.056	1.000
Across-track	0.501	0.516	0.591	0.634	0.752
Total	2.031	1.367	1.097	1.234	1.253

Table 7.8: Comparison of The Reduced Dynamic RMS errors using Simulated GPS Data and Real GPS Data.

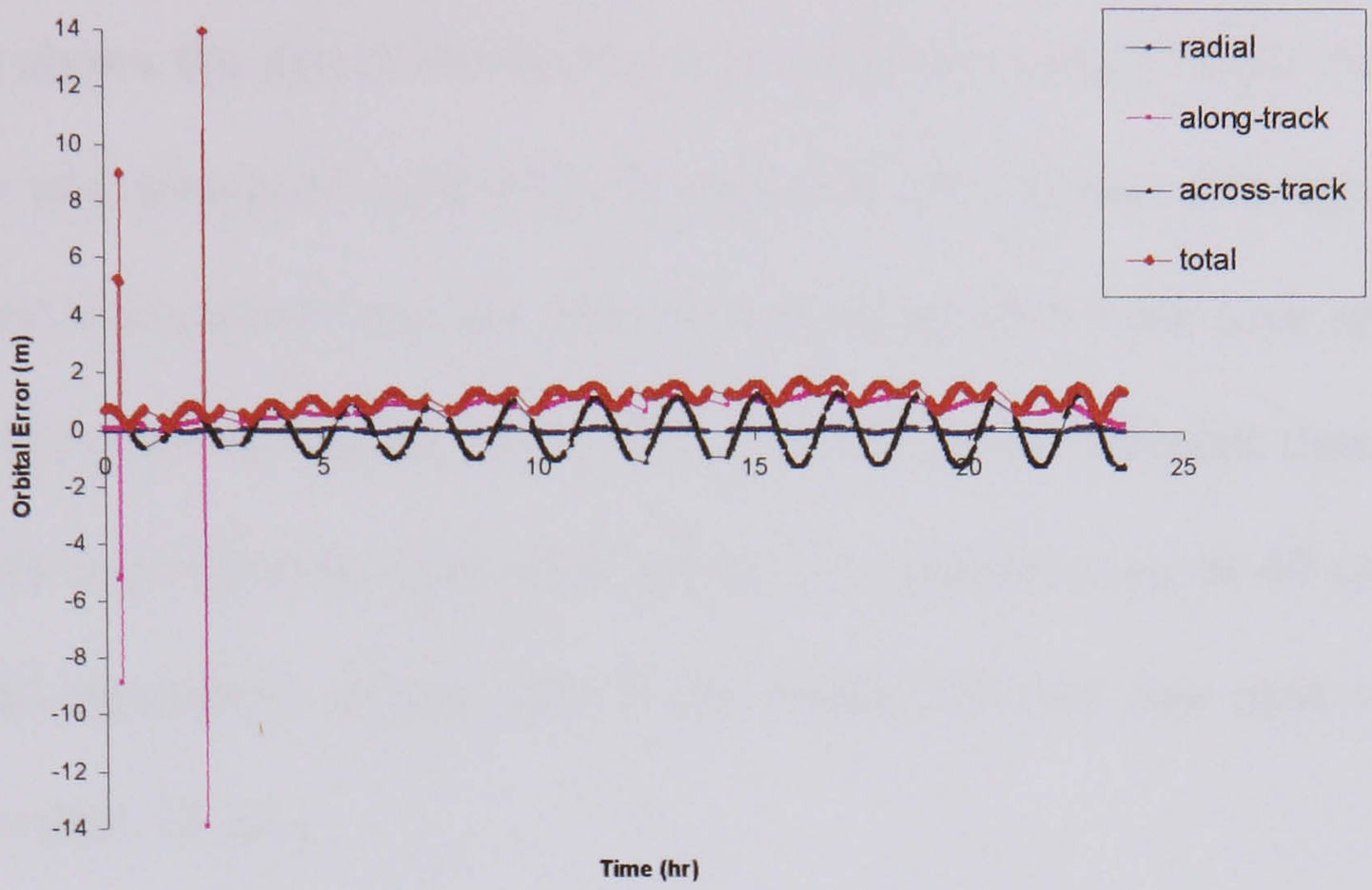

Figure 7.9: Reduced Dynamic Solution for stand-alone GPS receiver (Real Data) (one-day arc)

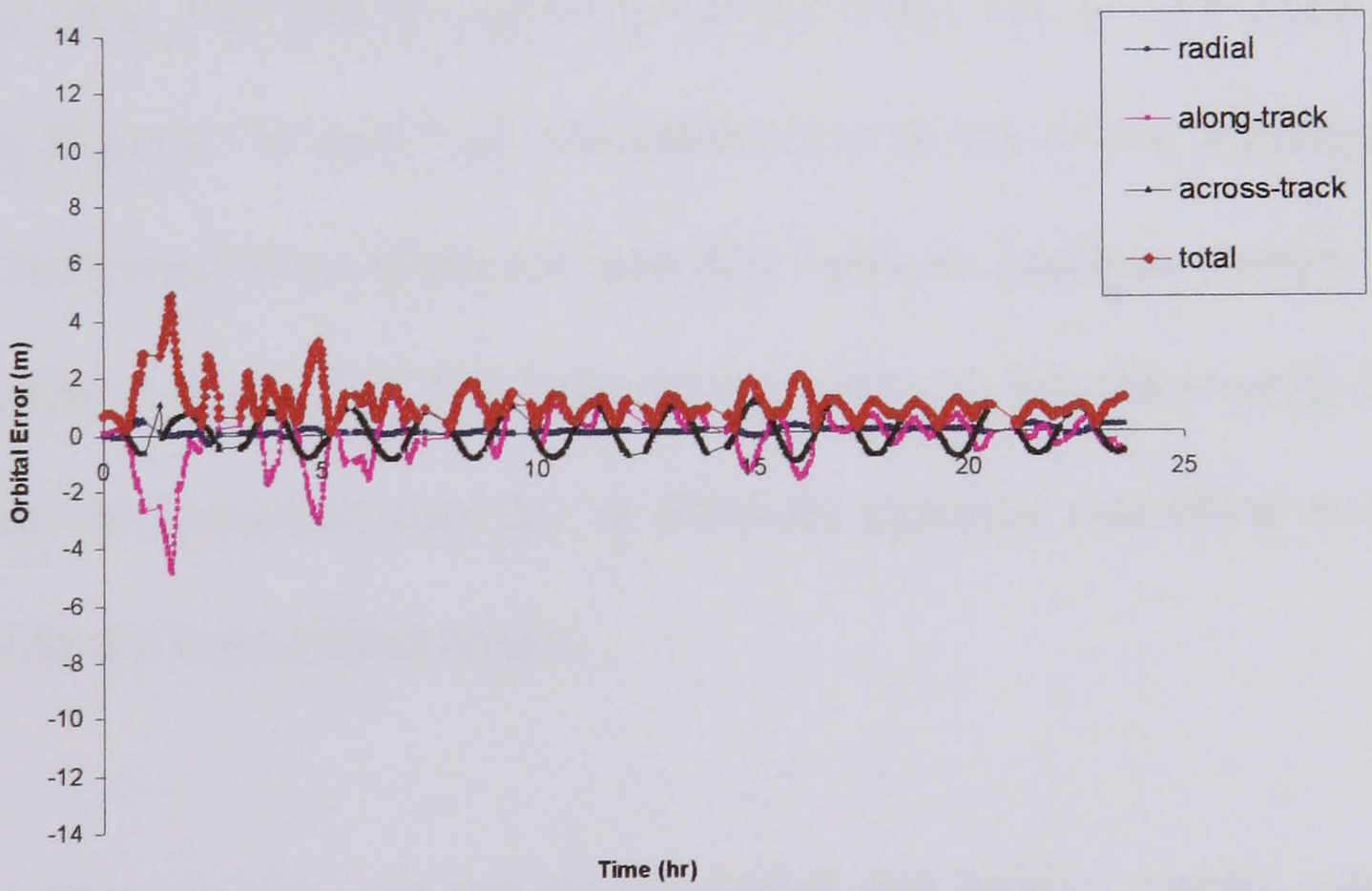

Figure 7.10: Reduced Dynamic Solution for stand-alone GPS receiver (Simulated Data) (one-day arc)

7.3.3 Discussion

Table 7.8 shows the agreement between the reduced dynamic RMS errors from real GPS data and simulated GPS data for different time spans. The agreement in the RMS radial component was less than 10 cm except in 5 hour time span, the along track RMS component agrees within less than 20 cm for different time spans except for 5 hours and 10 hours time spans where the agreement up to 40 cm. The across track RMS agreement is less than 5 cm except for one day time span where it becomes within 14 cm.

Focusing on the shortest (3 hours) and longest time spans (one day) the agreement is highly obvious and it proves the ability of the simulated GPS data to give realistic behaviour even with a short period of simulated GPS data as well as with longer periods of data. The relative agreement in the behaviour of both types of GPS data is shown in Figures 7.9 and 7.10 and proves the ability of the simulated data to give realistic behaviour even when the real data behaves badly as shown in the first few epochs under 5 hour time. The total error appears to worsen slightly in the real data rather than the simulated data due to different dynamic modelling noise applied that end up with the least orbital errors.

From the above analysis, it can be concluded that similar results could be obtained using both simulated and real GPS data for the reduced dynamic technique from GPS constellation and that therefore the simulation studies were realistic compared with the real situations. This gives confidence in the future reduced dynamic results from the GALILEO and combined GPS/GALILEO constellations analysis.

7.4 Simulated Data Reduced-Dynamic Orbit Determination

7.4.1 Introduction

This section will investigate the resulting reduced dynamic orbits obtained using simulated data from the constellations GPS, GALILEO and combined GPS/GALILEO. Each constellation will involve three types of solutions;

- Stand-alone solution: based on measurements from T/P onboard receiver
- Differential Pseudo-range solution: based on differential measurements from selective ground stations using pseudo-range observations.
- Differential Carrier-phase solution: based on differential measurements from selective ground stations using Carrier-phase observations

The positions for the ground stations were the same for the three constellations. (Bertiger et al., 1994) suggested a 13 ground stations to gain an accurate orbits from differential solutions. This research uses 12 ground stations for differential solutions. The choice of their number and positions was made to guarantee the differential solutions at each epoch (so a common number of satellites is visible by the T/P onboard receiver as well as one or more of the ground stations) with a high number (12-22) of common satellites. This choice was crucial for getting a high quality solution from the measurement model in the reduced dynamic technique. The geographical positions for the chosen ground stations for differential solutions are shown in Figure 7.11. The following results were presented by (Farah et al., 2004).

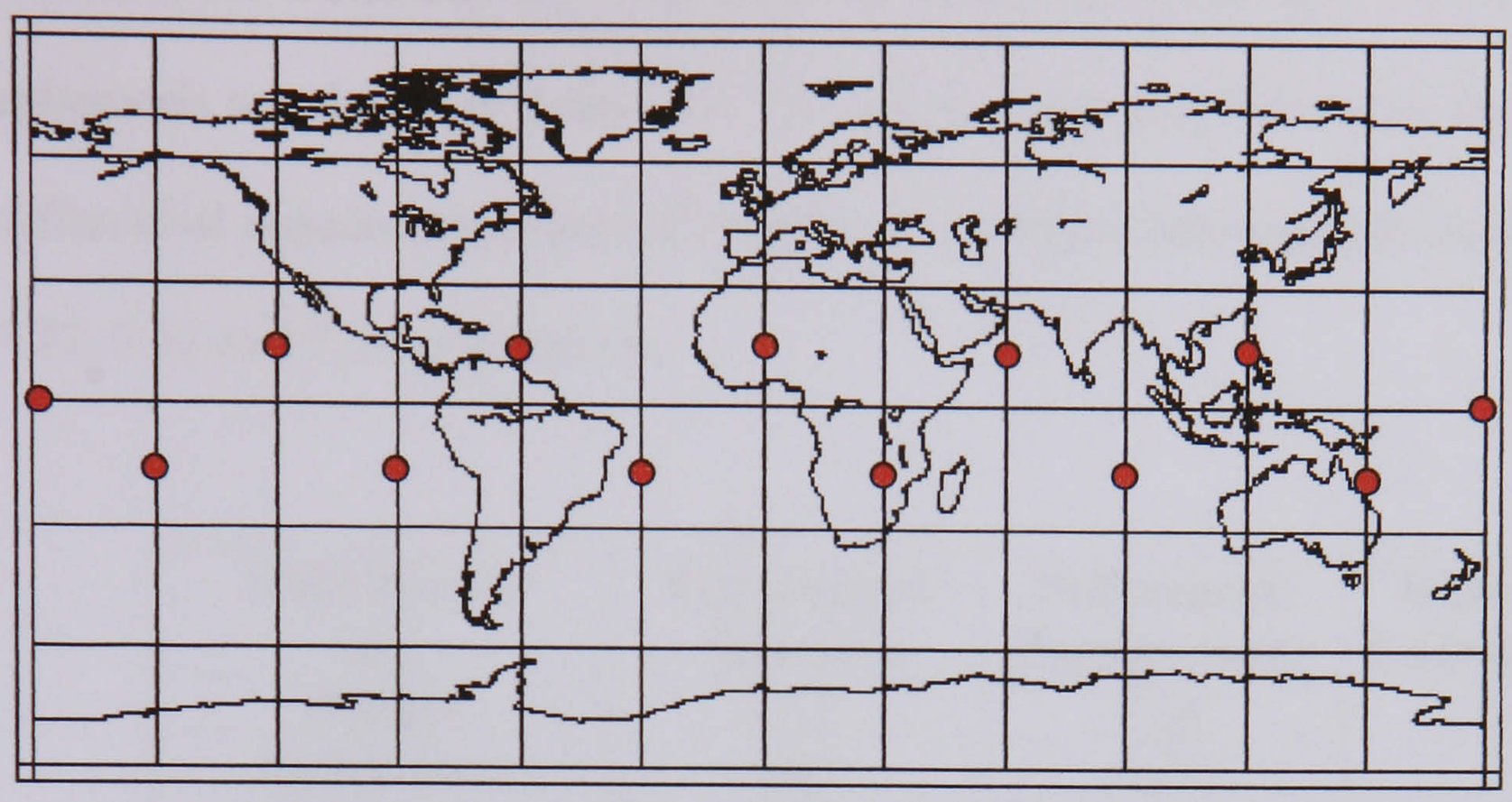

Figure 7.11: The Geographical Positions for the Ground Stations used for Differential Solutions From three Constellations; GPS, GALILEO and Combined GPS/GALILEO.

7.4.2 GPS Based Topex/Poseidon Ephemeris

The simulated GPS data from T/P onboard receiver was generated using AVISO ephemeris as a trajectory with IGS final GPS orbits. The simulated errors for T/P GPS receiver were the receiver and satellite clocks, ephemeris errors and measurement noise. The atmospheric error is ignored due to the altitude of the satellite (about 1300 km above the earth). The simulated errors in the ground stations data are the receiver and satellite clocks, ephemeris errors, atmospheric error (ionosphere and troposphere) and measurement noise. The chosen parameters for the measurement noise are revealed in (§ 7.1). The Broadcast GPS ephemeris was used in the reduced dynamic processing for different types of solutions to follow real time applications requirements. The testing days were the 21st and 22nd of July 2002, for which the real GPS data from T/P onboard receiver are giving acceptable solutions (§ 7.3). The reduced dynamic solutions were produced for three different types of

solutions for a two-day arc. The RMS errors for different types of GPS based T/P ephemeris are shown in Table 7.9. The reduced dynamic behaviour for stand-alone, differential pseudo-range and differential carrier-phase solutions are shown in Figures 7.12, 7.13 and 7.14 respectively.

RMS Errors (m)	Stand-alone Solution	Differential Pseudo-range	Differential Carrier-phase
Radial	0.12	0.14	0.10
Along-track	0.68	0.25	0.21
Across-track	0.40	0.14	0.15
Total	0.80	0.32	0.28

Table 7.9: The RMS errors for Topex/Poseidon reduced dynamic orbits from different types of solution for GPS constellation.

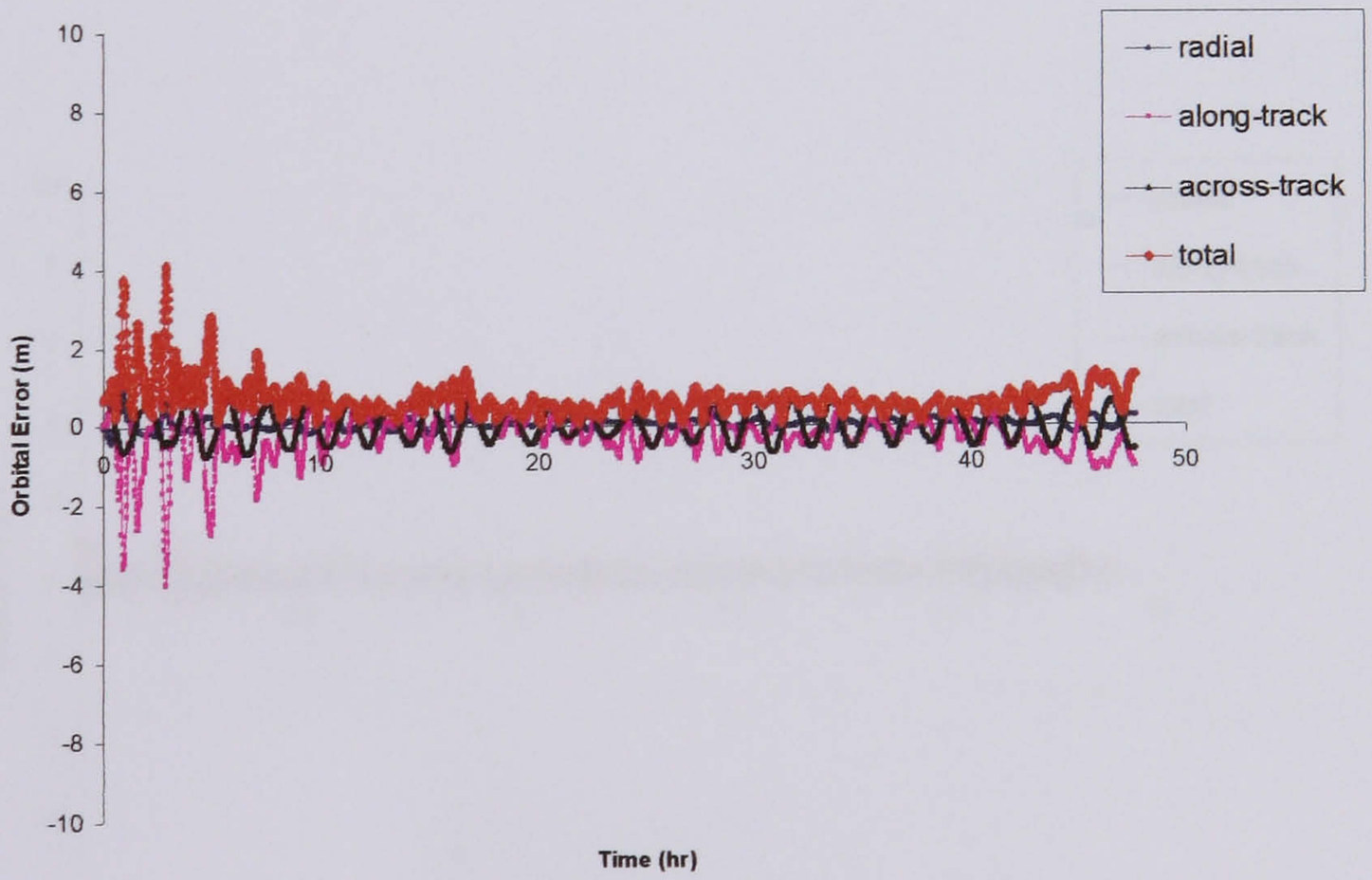

Figure 7.12: Reduced Dynamic Stand-alone Solution for simulated GPS receiver

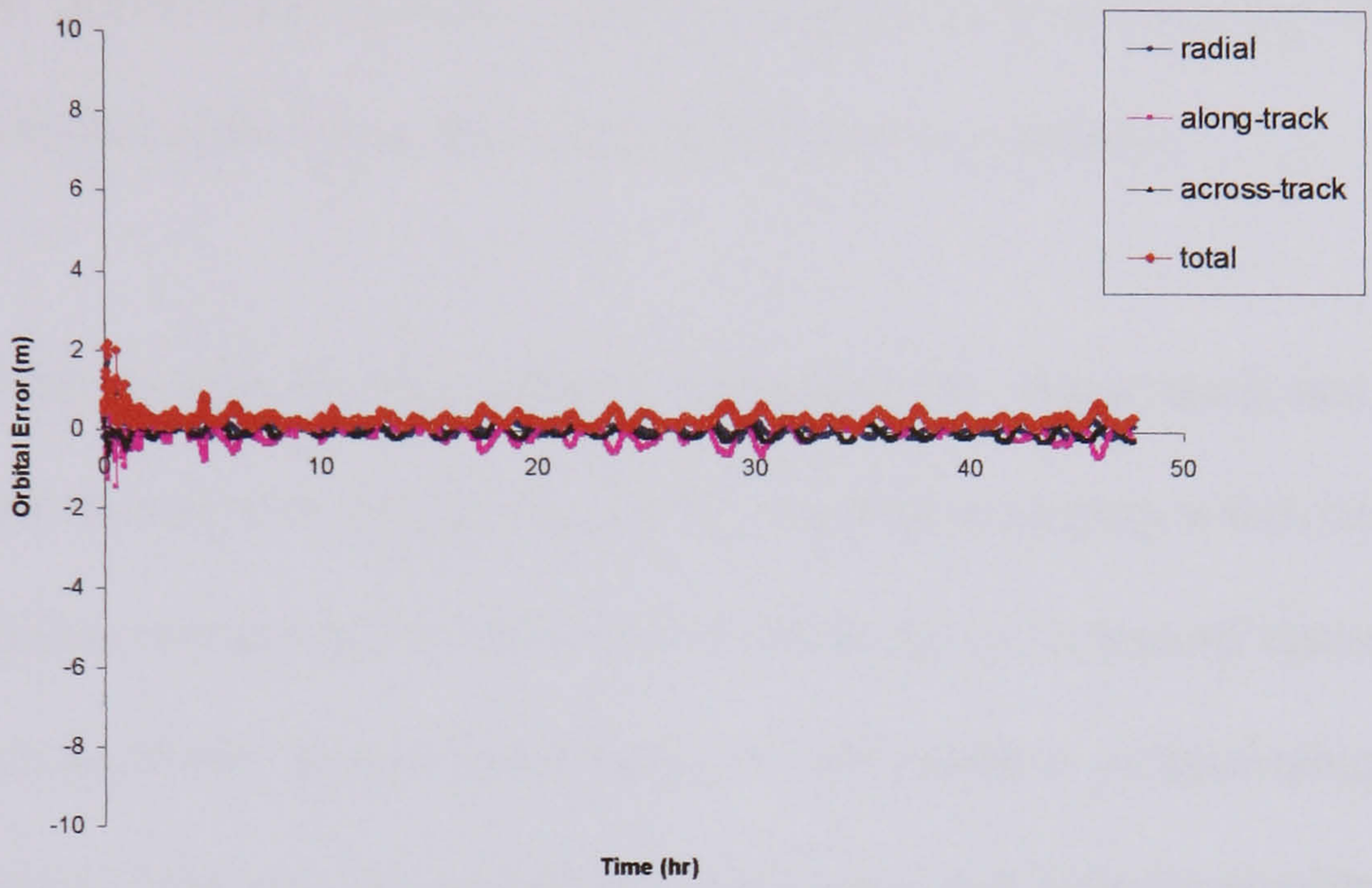

Figure 7.13: Reduced Dynamic Differential Pseudo-range Solution for simulated GPS receiver

Figure 7.14: Reduced Dynamic Differential Carrier-phase Solution for simulated GPS receiver

It can be concluded that the stand-alone solution gives the lowest accuracy because of the low accuracy of GPS broadcast ephemeris which has significant effects on the reduced dynamic stand-alone solution as shown in Section 7.2.1. The differential solution in general gives a more accurate solution as it removes the GPS ephemeris error which affects the along track and across track components.

The differential pseudo-range solution improves the along track and across track components however it degrades the radial component slightly which could be due to the increase in measurements noise as a result of using 12 ground stations. However, because of the better measurement noise in carrier phase measurements, the carrier phase solution improves the radial and along track components resulting in the best accuracy for total error.

The different types of solutions also affects the time needed for the kalman filter to settle and give accurate results. The filter needs about 10 hours of data until it settles with the stand-alone solution, however this settling time is decreased to less than 5 hours with the differential pseudo-range solution. The minimum settling time for the filter happens with the differential carrier phase solution when it becomes about 2 hours. Reasonably, the shorter the settling time, the more efficient the filtering process and the better behaviour for real time applications.

7.4.2 GALILEO-Based Topex/Poseidon Ephemeris

The simulated data for the T/P onboard receiver with the GALILEO constellation was generated using the AVISO ephemeris as a trajectory with high quality GALILEO ephemeris file, without any ephemeris error. The same types of error were simulated as in the GPS case however better measurement noise was simulated for ground stations (§ 7.1). The reduced dynamic solutions were processed using a different GALILEO ephemeris file with RMS ephemeris error of 65 cm (Lucas et al., 2000), (Provenzano et al., 2000) to simulate the perspective future behaviour of the GALILEO constellation. The RMS errors for different types of GALILEO based T/P orbit solution are shown in Table 7.10. The reduced dynamic behaviour for stand-alone, differential pseudo-range and differential carrier-phase solutions are shown in Figures 7.15, 7.16 and 7.17 respectively.

RMS Errors (m)	Stand-alone Solution	Differential Pseudo-range	Differential Carrier-phase
Radial	0.08	0.10	0.05
Along-track	0.19	0.17	0.10
Across-track	0.11	0.12	0.09
Total	0.24	0.23	0.15

Table 7.10: The RMS errors for Topex/Poseidon reduced dynamic orbits from different types of solution for GALILEO constellation.

Figure 7.15: Reduced Dynamic Stand-alone Solution for simulated GALILEO receiver

Figure 7.16: Reduced Dynamic Differential Pseudo-range Solution
for simulated GALILEO receiver

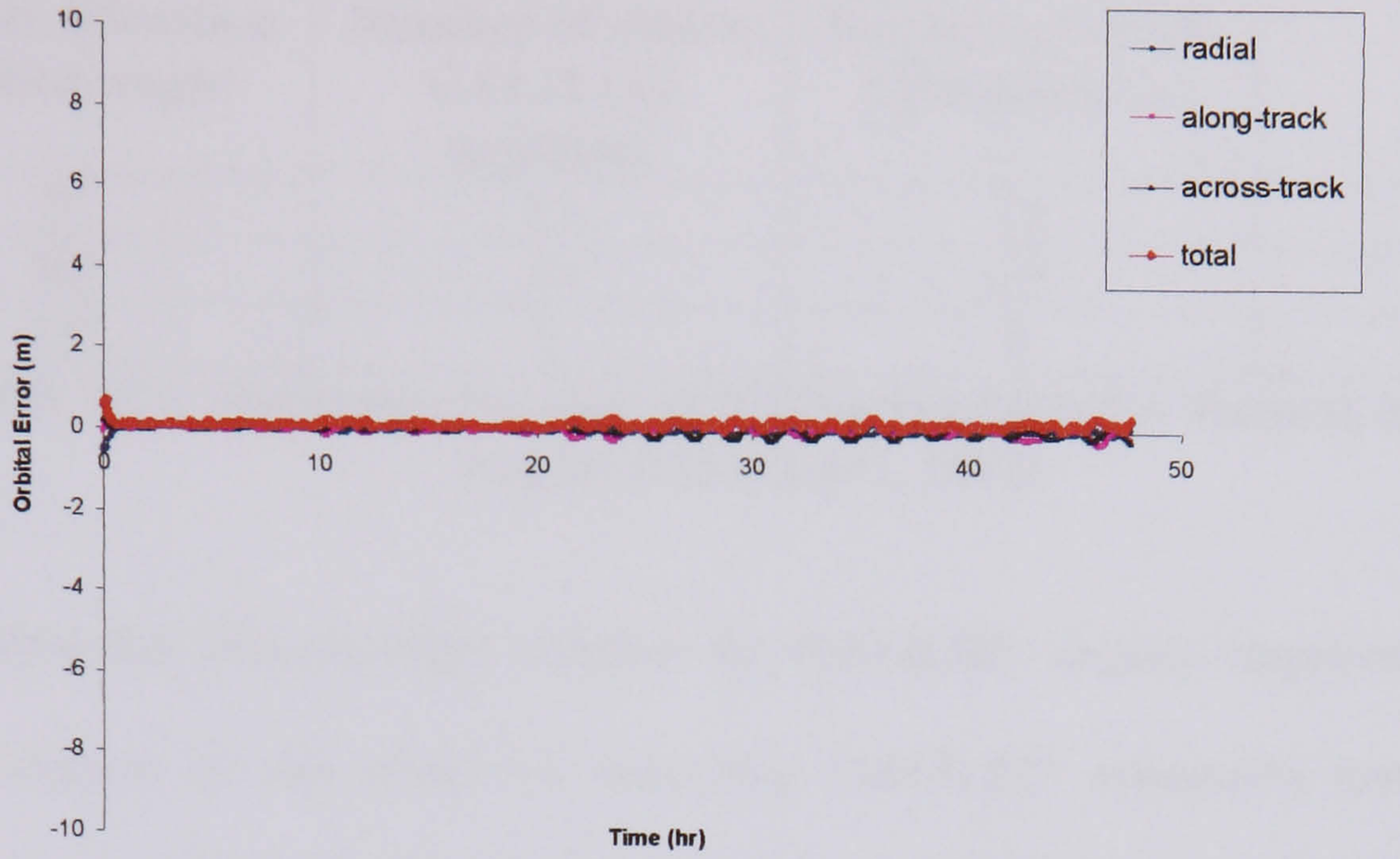

Figure 7.17: Reduced Dynamic Differential Carrier-phase Solution for simulated GALILEO receiver

It can be concluded that GALILEO in general gives more accurate solutions for reduced dynamic orbit determination, this effect must be due to the better geometry for GALILEO over GPS, the matter that end up with more number of visible GALILEO satellites rather than GPS according to Table 7.11 and Appendix B. As well as the high quality GALILEO ephemeris over GPS broadcast ephemeris and the better ranging accuracy (less measurement noise) for GALILEO compared with GPS.

The stand-alone GALILEO solution results shows the impact of better ephemeris for GALILEO on the accuracy of both the along-track and across-track orbital components, as the improvement compared with GPS reaches up to 0.49 m and 0.29 m for both of them respectively.

Receiver Elevation masking angle	Number of visible GALILEO satellites	Number of visible GPS satellites	Total
5°	13	12	25
10°	11	10	21
15°	9	8	17

Table 7.11: Maximum Number of Visible Satellites for Various Masking Angles (GALILEO, 2002).

The differential Pseudo-range solution for GALILEO slightly improves the stand-alone solution as the effect of removing GALILEO ephemeris error with the differential solution is small due to high quality GALILEO ephemeris (RMS 65 cm). Comparing with low quality GPS broadcast ephemeris where the improvement for the differential solution compared with the stand-alone solution is strongly visible.

The GALILEO differential carrier phase solution is much better than the differential pseudo-range solution due to the carrier phase measurements had less measurement noise over the pseudo-range measurements. As the measurement noise for GALILEO ground data using E2L1E1 frequency was 13.333 cm and 0.7000 mm for pseudo-range and carrier-phase respectively while the measurement noise for GALILEO ground data using E5AB frequency was 6.667 cm and 0.3000 mm for pseudo-range and carrier-phase respectively.

The settling time for kalman filter is improved as well with GALILEO solutions as it becomes less than 2 hours for stand-alone and differential pseudo-range solutions and even less than one hour for differential carrier phase solution.

7.4.4 GPS/GALILEO-Based Topex/Poseidon Ephemeris

This section tries to discover the future of GPS and GALILEO working together and whether there will be improvement over the T/P reduced dynamic orbit determination from each constellation individually.

The results in this section reflect the behaviour of present GPS with the behaviour of just implementing GALILEO. So, basically, the specifications that were followed in the past two Sections 7.4.2 and 7.4.3 are followed in this section too. It should be expected to see the effect of having more visible satellites from combined constellation, the combined effect of less measurements noise from GALILEO satellites with higher measurements noise from GPS satellites and the combined effect of high quality ephemeris from GALILEO with lower quality ephemeris from GPS. Those three effects are shown in the RMS errors for reduce dynamic different solutions from combined GPS/GALILEO constellation shown in Table 7.12. The behaviour of each solution is shown in Figures 7.18, 7.19 and 7.20.

RMS Errors (m)	Stand-alone Solution	Differential Pseudo-range	Differential Carrier-phase
Radial	0.12	0.12	0.07
Along-track	0.45	0.17	0.14
Across-track	0.30	0.07	0.07
Total	0.56	0.22	0.17

Table 7.12: The RMS errors for Topex/Poseidon reduced dynamic orbits from different types of solution for Combined GPS/GALILEO constellation.

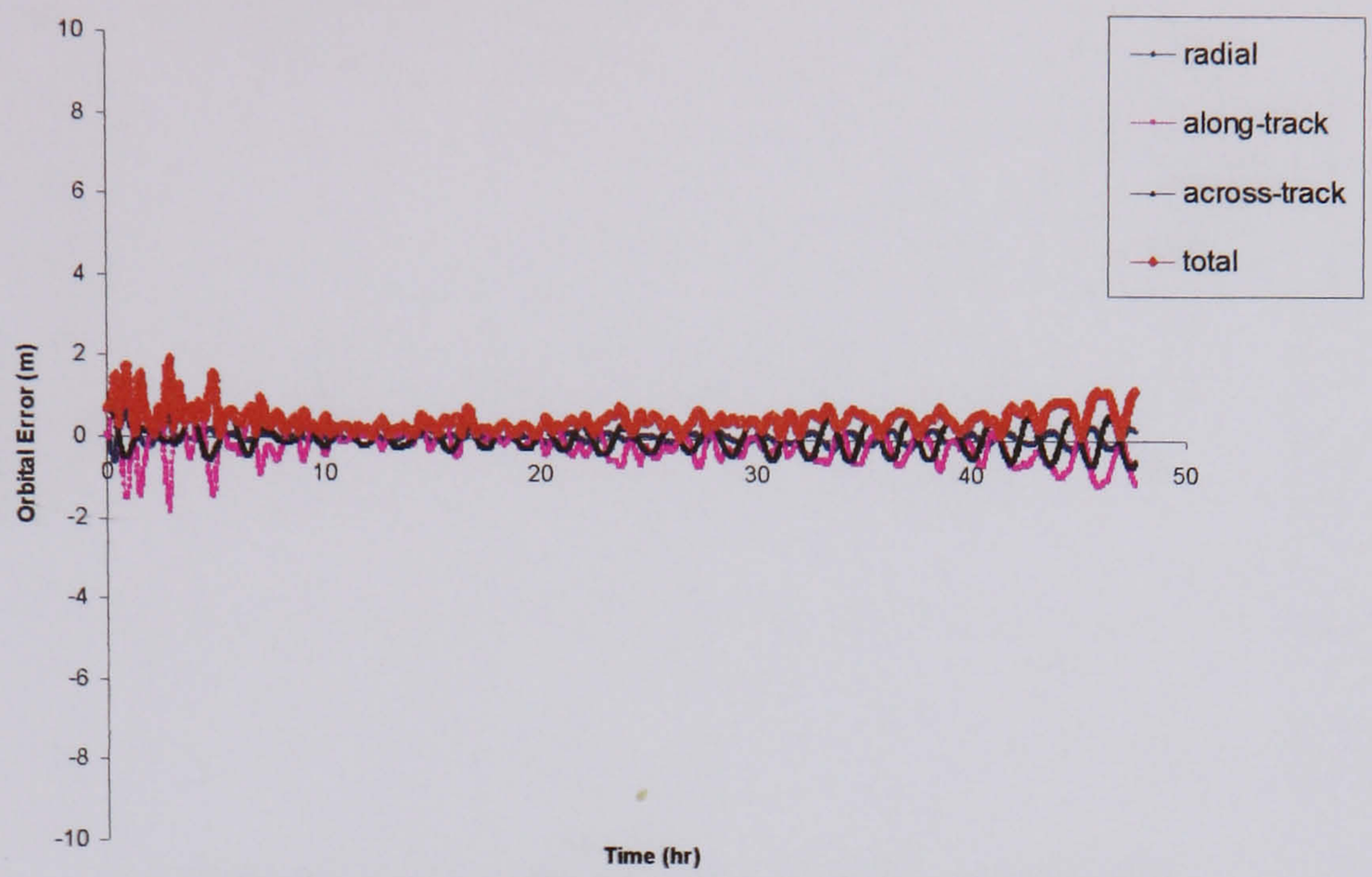

Figure 7.18: Reduced Dynamic Stand-alone Solution for simulated Combined GPS/GALILEO receiver

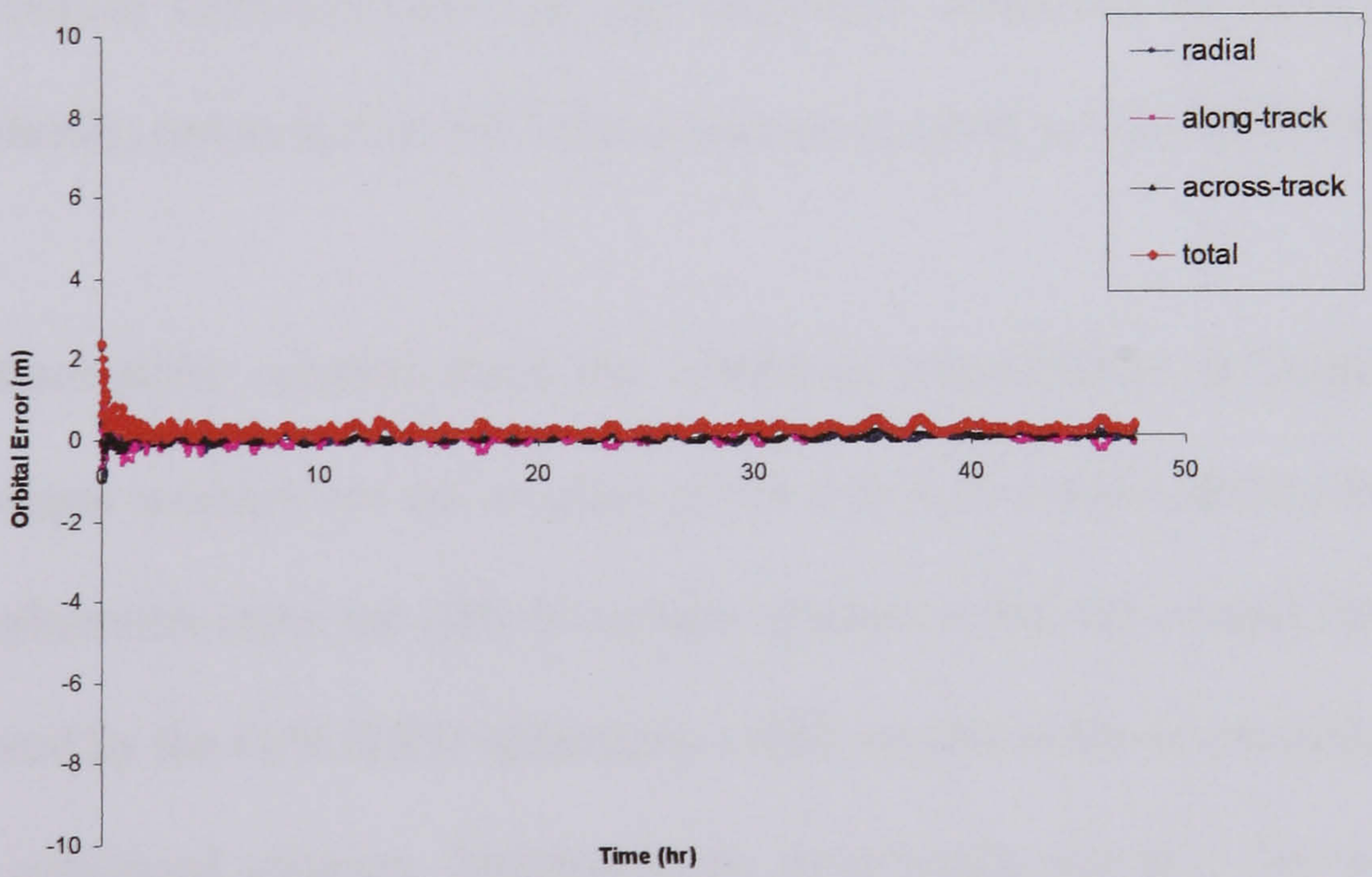

Figure 7.19: Reduced Dynamic Differential Pseudo-range Solution for simulated Combined GPS/GALILEO receiver

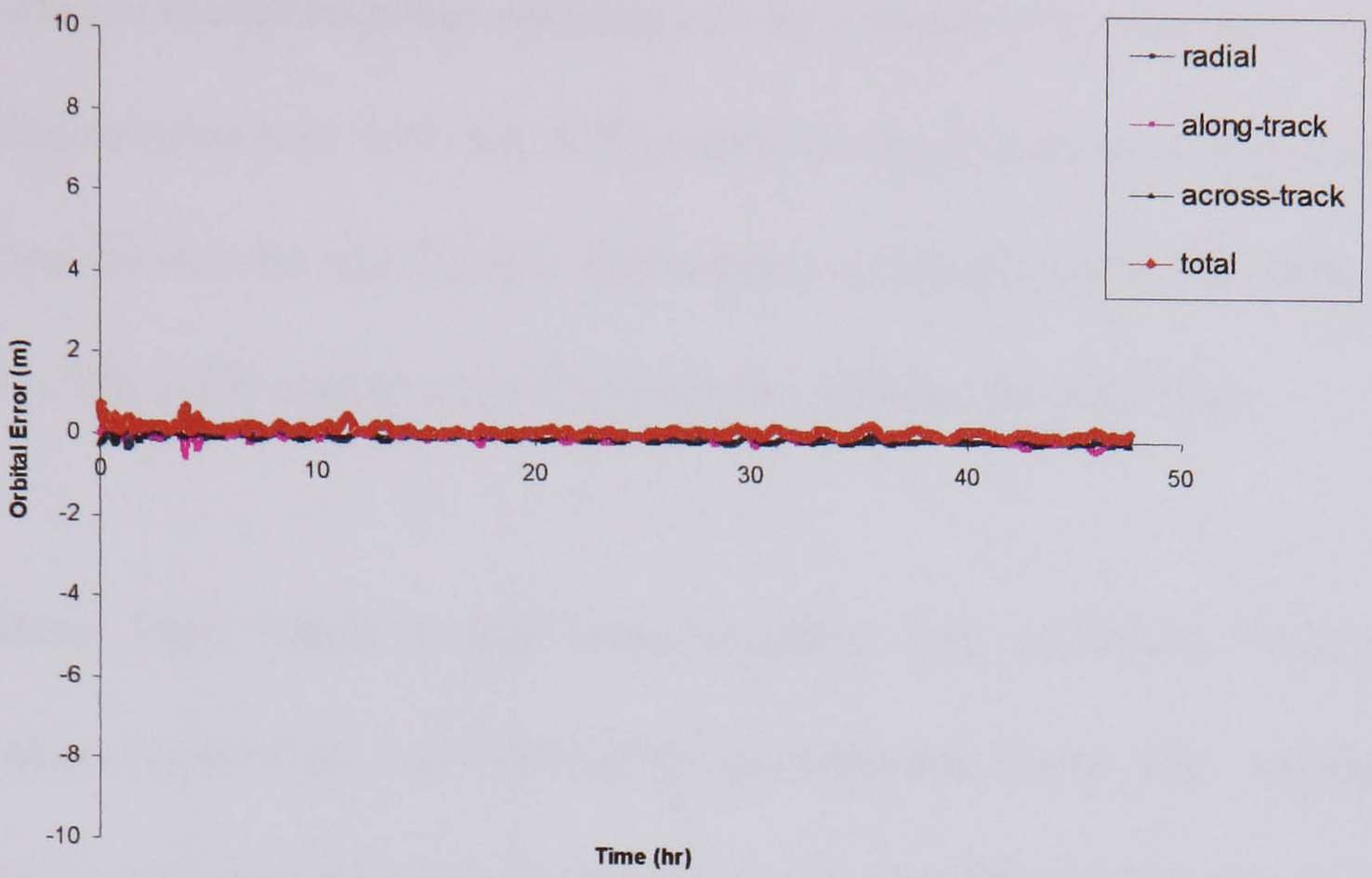

Figure 7.20: Reduced Dynamic Differential Carrier phase Solution for simulated Combined GPS/GALILEO receiver

As it was expected the behaviour of the reduced dynamic orbits from the combined constellation GPS/GALILEO is the combined behaviour of GPS and GALILEO individually, not as bad as GPS alone and not as good as GALILEO alone.

The stand-alone solution from the combined constellation is better than the GPS stand-alone solution but not as good as the GALILEO stand-alone solution due to the high ephemeris error for GPS broadcast ephemeris but the overall ephemeris error is improved by the GALILEO ephemeris which results in the improvement in the stand-alone combined solution. Improvements in accuracy are also due to better ranging accuracy for GALILEO compared with GPS and a greater number of visible satellites from the combined constellation (see Table 7.11 and Appendix B).

The results for the differential solution can be explained in the same way as the stand-alone solution however with the differential solution from the combined constellation similar results for the GALILEO differential solutions could be obtained due to the removal of the GPS ephemeris error with the differential technique.

The kalman filter needs longer time to settle with solutions from the combined constellation rather than the GALILEO constellation alone. The settling time for the stand-alone combined solution is about 8 hours, the differential pseudo-range solution needs around 3 hours to settle where as the differential carrier phase solution requires only one hour to settle.

It can be concluded as well that with the expected modernisation of GPS with improvements in the quality of GPS ephemeris data, it would be expected to have an improved behaviour from the combined GPS/GALILEO reduced dynamic solutions. This expectation is investigated in the next section.

7.4.5 GPS-modernised/GALILEO-Based Topex/Poseidon Ephemeris

This section looks at the far future of the reduced dynamic behaviour with the combined constellation of modernised-GPS/GALILEO. It is well understood that the plans for GPS modernisation involve improving the behaviour of the GPS constellation in many aspects, however for the sake of this study, only the improvements in the GPS broadcast ephemeris are considered.

A future GPS ephemeris file was prepared to have an RMS error of 5 cm to simulate the future GPS ephemeris quality as the GPS modernisation process for improving the quality of the broadcast ephemeris not expected before 2012 (Shaw et al., 2000). This new ephemeris file was used to process GPS measurements within the reduced dynamic combined solutions from combined constellations. The expectation was to see an improved behaviour from the reduced dynamic solutions for the combined constellations when compared with those discussed in Section 7.4.4.

The RMS errors of the reduced dynamic solutions from the future combined GPS/GALILEO constellation are shown in Table 7.13. The behaviour of the reduced dynamic solutions are shown in Figures 7.21, 7.22 and 7.23.

RMS Errors (m)	Stand-alone Solution	Differential Pseudo-range	Differential Carrier-phase
Radial	0.06	0.10	0.04
Along-track	0.13	0.15	0.10
Across-track	0.12	0.12	0.10
Total	0.19	0.22	0.15

Table 7.13: The RMS errors for Topex/Poseidon reduced dynamic orbits from different types of solution for GPS-modernised/GALILEO constellation.

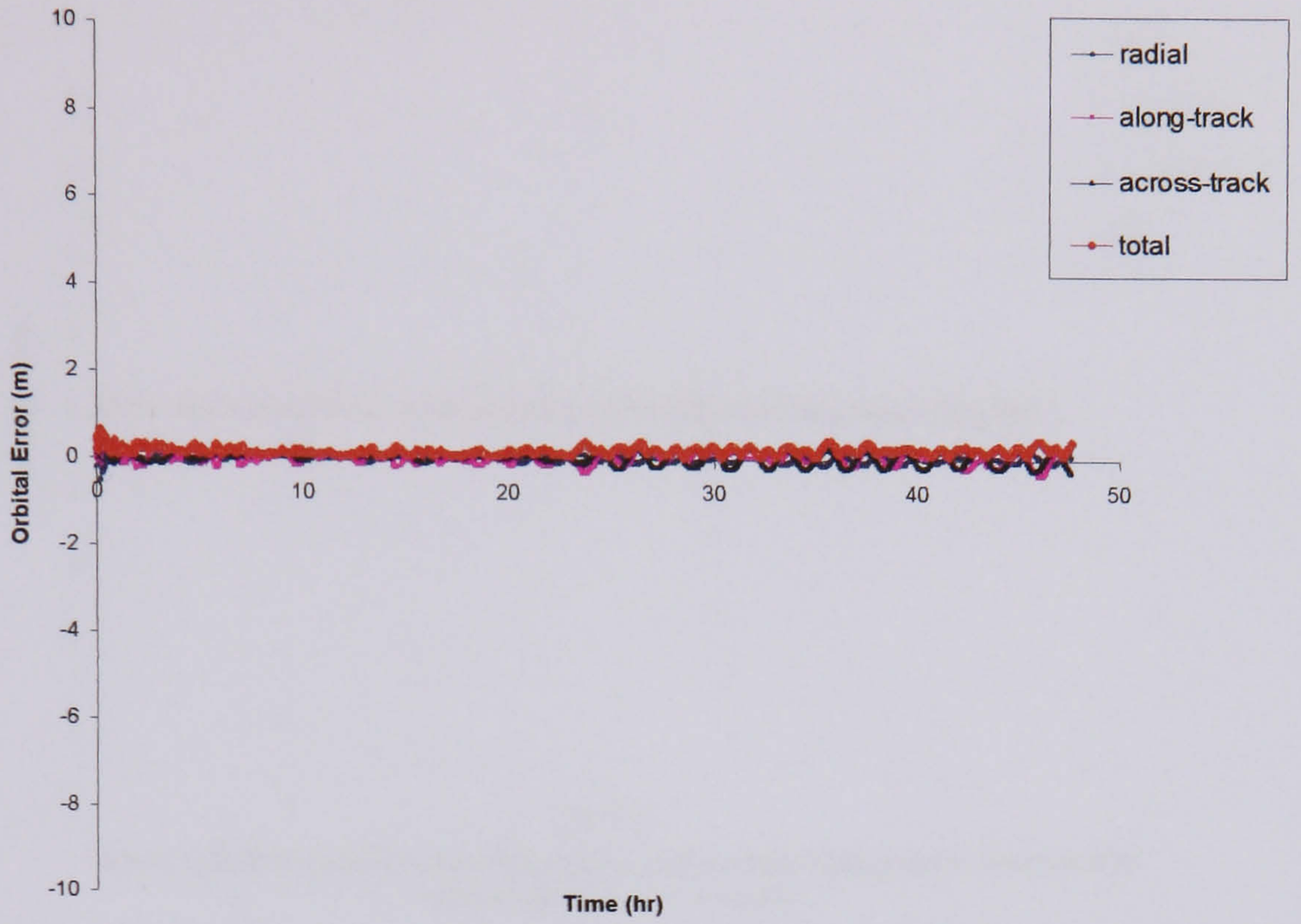

Figure 7.21: Reduced Dynamic Stand-alone Solution for simulated GPS-modernised/GALILEO receiver

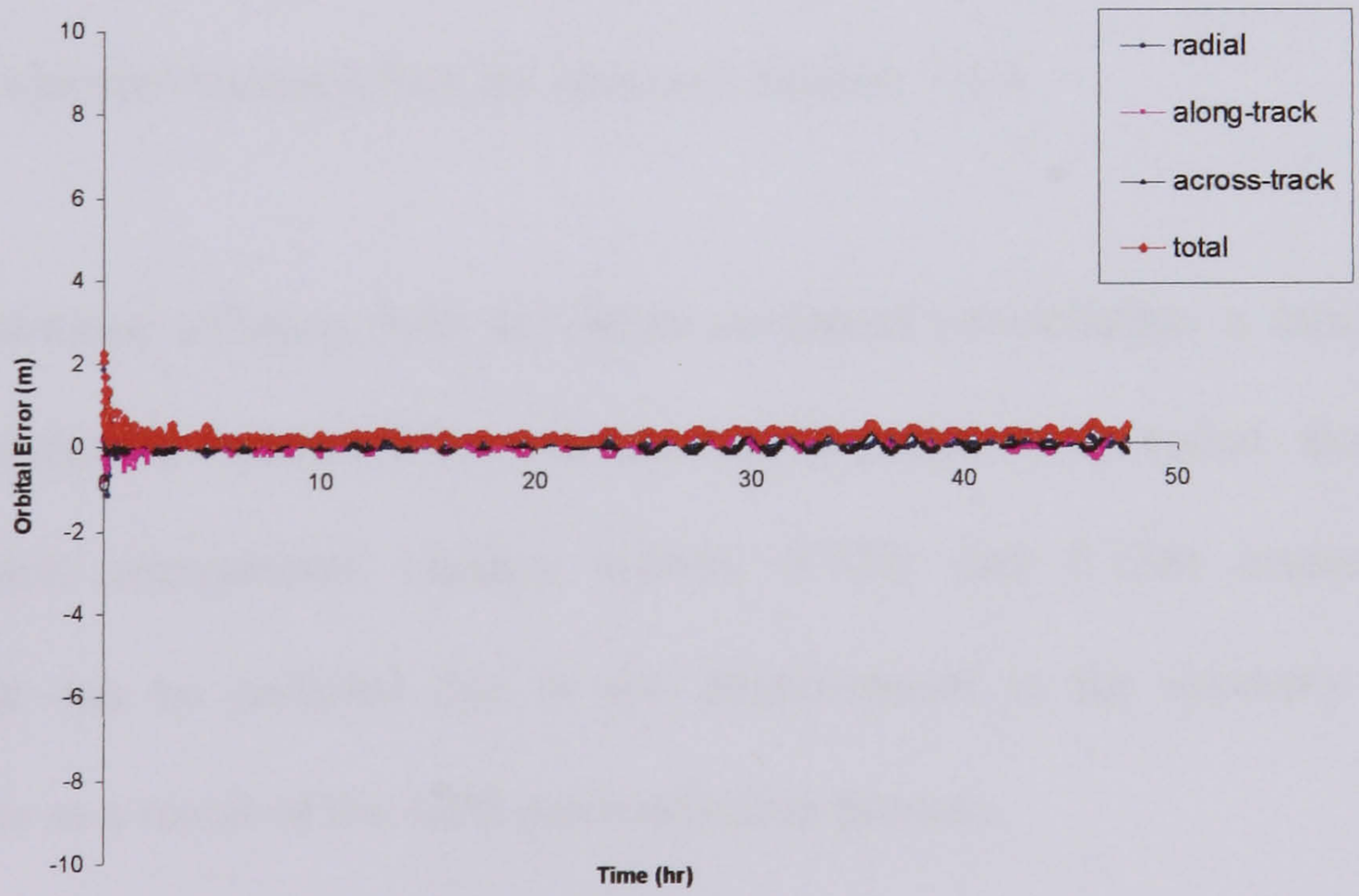

Figure 7.22: Reduced Dynamic Differential Pseudo-range Solution for simulated GPS-modernised/GALILEO receiver

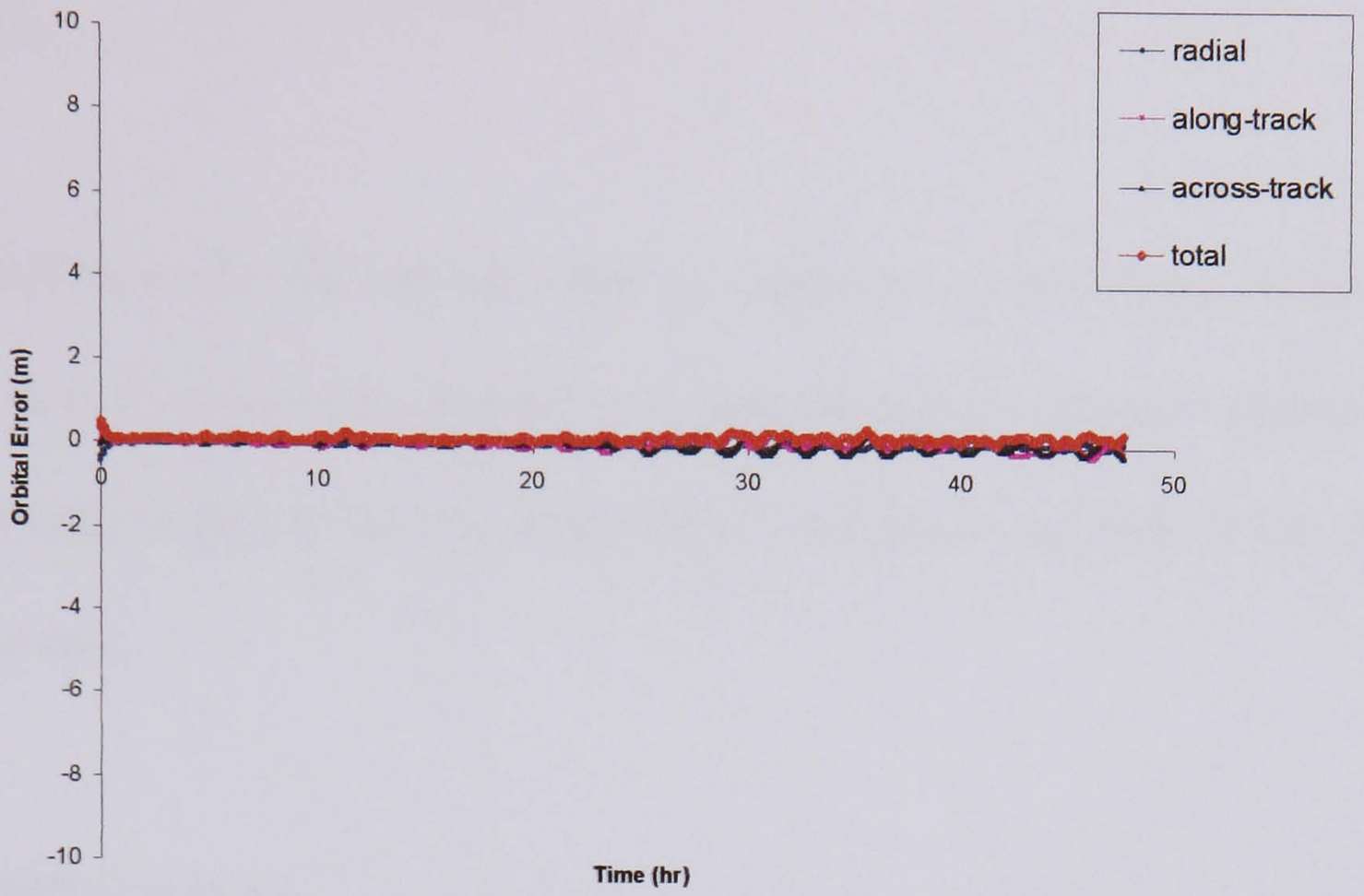

Figure 7.23: Reduced Dynamic Differential Carrier phase Solution for simulated GPS-modernised/GALILEO receiver

The behaviour of the reduced dynamic solution from the future combined constellation satisfies the expectations as in general the results shown in this section give a better performance than the previous Section 7.4.4.

The stand-alone solution from the future combined constellation is much better than its counterpart in Section 7.4.4 with the improvement in the radial, along-track and across-track components reaches 0.06m, 0.12m and 0.18m respectively. This behaviour can be justified due to the improvement in the accuracy of the GPS ephemeris as a result of the GPS modernisation process.

The differential solutions improved slightly over its counterparts in Section 7.4.4 due to the fact that the differential solution removes the effect of the errors in the high

quality GPS ephemeris (5cm RMS), so the improvement in the GPS ephemeris will not affect it.

The settling time for the kalman filter is improved as well over its counterpart in Section 7.4.4, as it becomes around one hour for the stand-alone combined solution compared with 8 hours for the stand-alone solution in Section 7.4.4 (before GPS modernisation).

7.4.6 Orbit Overlap

This section looks at the reduced dynamic orbit overlap, which is the ability of the reduced dynamic technique to produce similar results from different sets of measurements where the GPS and GALILEO constellations repeat themselves. The GPS constellation repeats itself on daily (just short of 24 hours) basis (orbital period of 11 hours, 58 min.) whereas the GALILEO constellation repeats approximately every three days (orbital period of 14 hours, 4 min.). In this test the reduced dynamic stand-alone solution for the combined GPS/GALILEO constellation for a two-day arc was produced from overlapping three groups of two day measurements (with a one-day overlap), optimising the software to put more weight towards the observations to maximise the effect of the observations model which mainly affected with the status of GPS and GALILEO constellations. The test three groups of measurements were (21/7/2002-22/7/2002), (22/7/2002-23/7/2002) and (23/7/2002-24/7/2002). The RMS errors for this test's results are shown in Table 7.14. The behaviour of the reduced dynamic stand-alone solutions for each type of data set are shown in Figures 7.24, 7.25 and 7.26.

RMS Errors (m)	(21/7/2002-22/7/2002)	(22/7/2002-23/7/2002)	(23/7/2002-24/7/2002)
Radial	0.58	0.64	0.50
Along-track	0.69	0.74	0.80
Across-track	0.36	0.36	0.52
Total	0.98	1.05	1.08

Table 7.14: The RMS errors for Topex/Poseidon reduced dynamic orbits from stand- alone solution for Combined GPS/GALILEO constellation for three different data sets (weight towards observations).

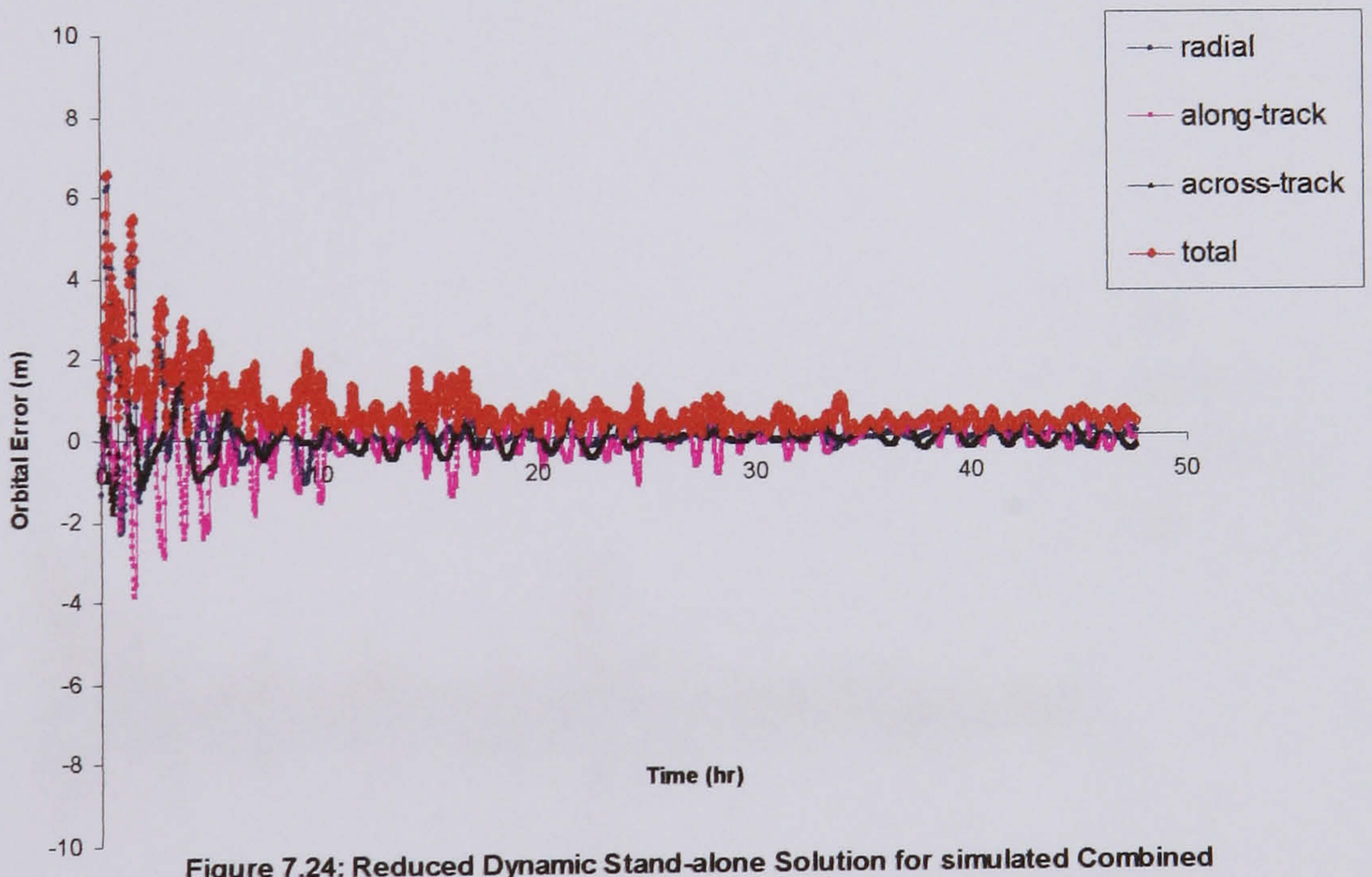

Figure 7.24: Reduced Dynamic Stand-alone Solution for simulated Combined GPS/GALILEO receiver (21/7/2002-22/7/2002) (Weight towards Observations)

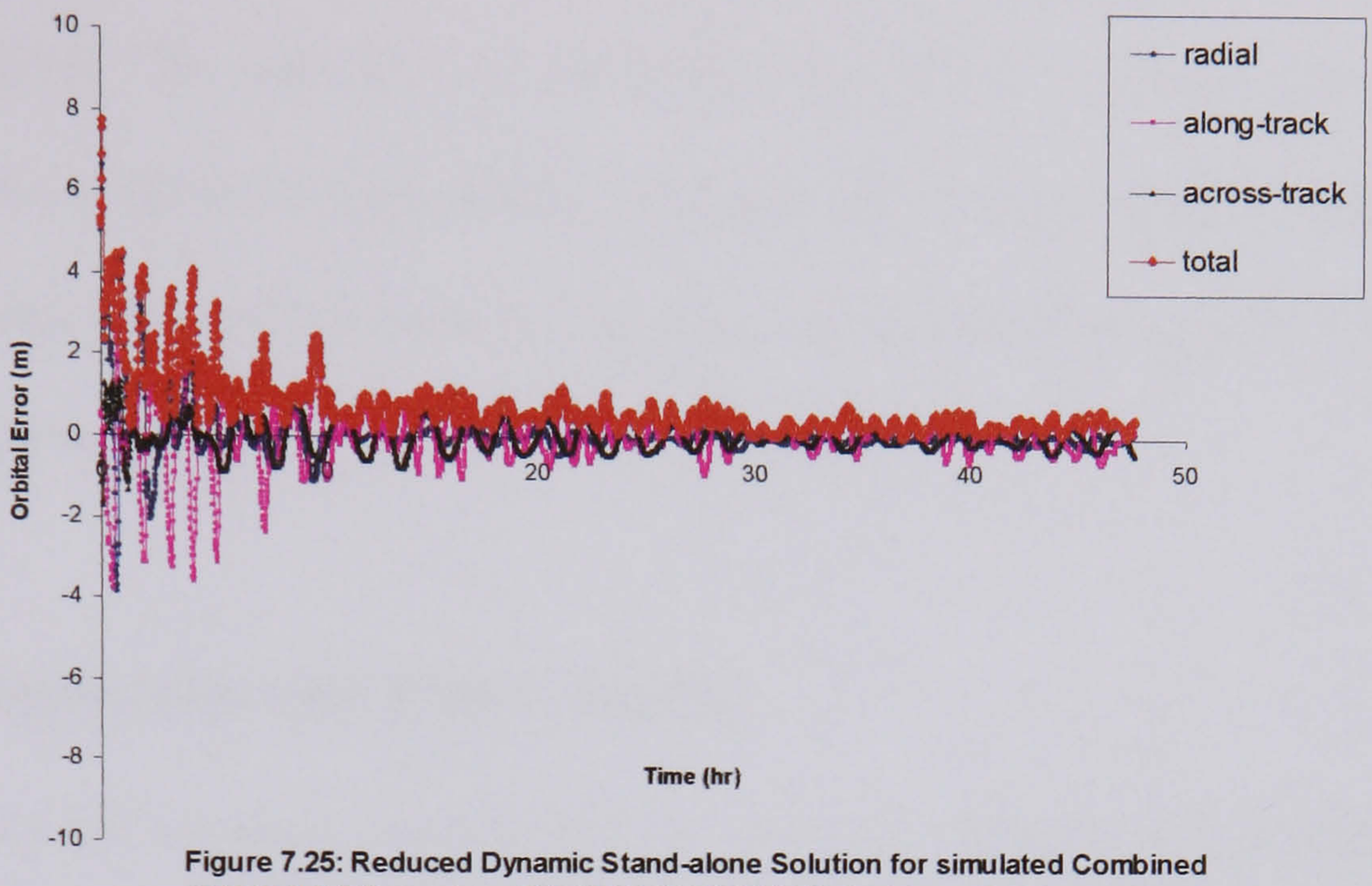

Figure 7.25: Reduced Dynamic Stand-alone Solution for simulated Combined GPS/GALILEO receiver (22/7/2002-23/7/2002) (Weight towards Observations)

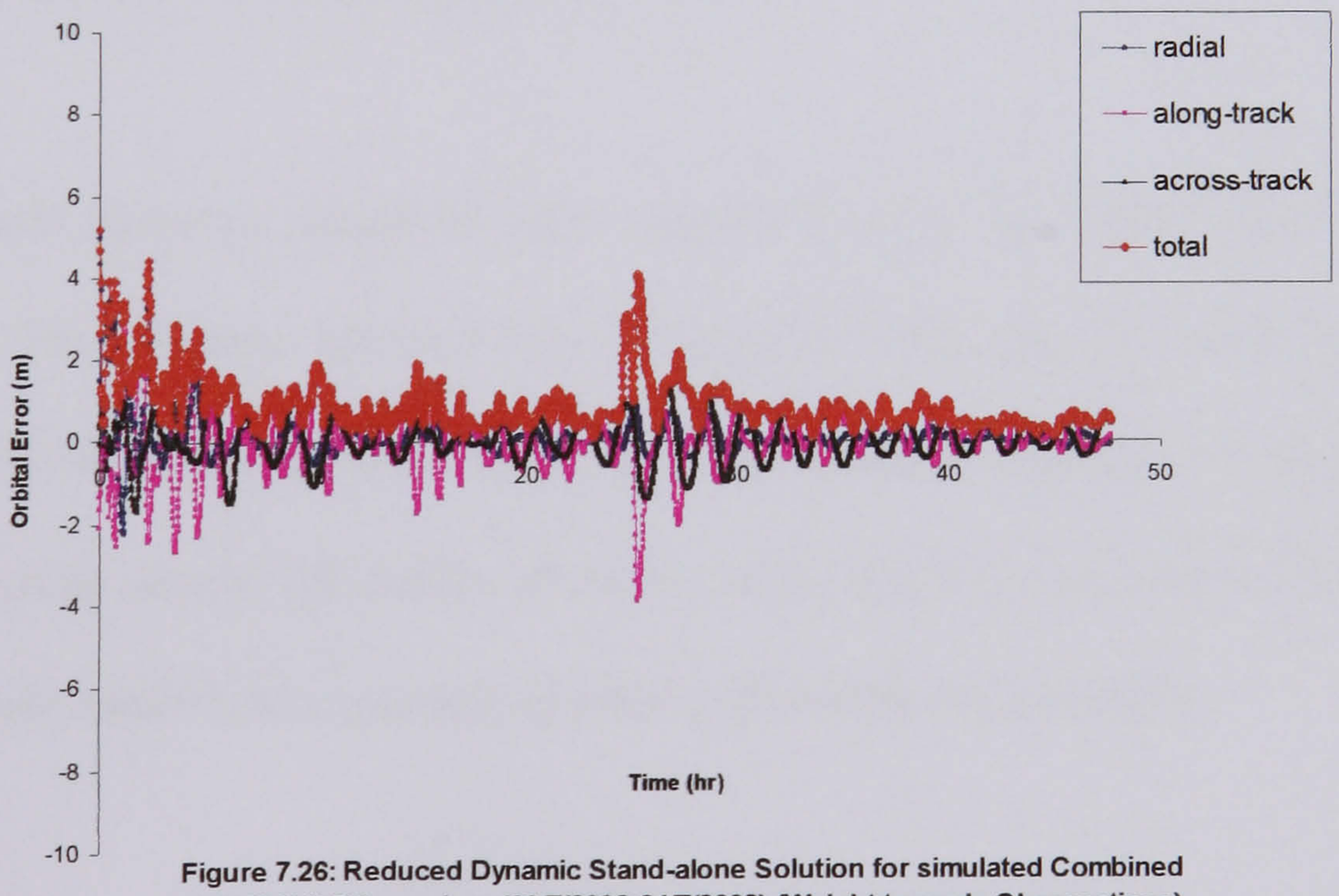

Figure 7.26: Reduced Dynamic Stand-alone Solution for simulated Combined GPS/GALILEO receiver (23/7/2002-24/7/2002) (Weight towards Observations)

It can be concluded that the reduced dynamic technique is capable of providing similar consistent results whatever the positions of the GPS and GALILEO constellations. The agreement in the RMS total error for the three sets of data was around 10 cm taking in mind that the weight of the reduced dynamic was towards the observations which means that the accuracy of the agreement should improved with the optimal weight.

7.5 Comparison with Other Studies

A similar work has been investigating the ability of using the reduced dynamic orbit determination technique in GPS precise tracking of Topex/Poseidon satellite. This work was come out by the Jet Propulsion Laboratory (JPL), the Centre for Space Research (CSR) of the university of Texas at Austin and the Institut Geographique National (IGN) in Paris (Bertiger et al., 1994).

The reduced dynamic solutions were computed using the GIPS-OASIS II analysis software. The solution adopted was differential GPS solution using data from 13 ground stations. Data from all receivers were brought together and processed in a grand solution where T/P orbits, all GPS orbits, receiver and satellite clock offsets, carrier phase biases and a number of other parameters are estimated.

A corresponding solution from this thesis had been investigated for the sake of comparison using differential carrier phase solution applying the IGS final GPS orbits to process the reduced dynamic orbits. For more information about their processing

technique, the reader is referred to (Bertiger et al., 1994). Table 7.15 shows the RMS errors comparison study for JPL solution and this research's solution against the precise SLR/DORIS orbits.

RMS Errors (cm)	JPL	This study
Radial	3.33	4.00
Along-track	12.00	12.00
Across-track	8.00	10.00
Total	14.80	16.70

Table 7.15: Comparison with Other Studies.

The agreement is strongly achieved as it less than 1 cm in the radial component and about 2 cm in the total orbital error, which gives another evidence in the accuracy and reliability of this thesis's findings.

7.6 Concluding Remarks and Recommendations

7.6.1 Concluding Remarks

In the previous sections of this chapter, a full detailed study of the behaviour of the reduced dynamic technique for orbit determination was conducted. In this section, a concise discussion will be presented based on these findings.

It has been shown that the reduced dynamic technique is an effective tool for determining LEO satellites orbits with the ability of working in real-time. By comparing results from simulated datasets with those using real GPS data, confidence in the simulated results for future systems was gained.

The reduced dynamic orbit solutions are seen to be mainly affected by the quality of the ephemeris data. The ephemeris errors greatly affect the accuracy of the observations model which is used to reduce the dynamic model errors within the reduced dynamic process. The reduced dynamic orbits depend more or less on the accuracy of the predicted orbit based on the accuracy of the observations model which is governed by the accuracy of the ephemeris data. Modernisation of GPS will increase the accuracy of the reduced dynamic orbits as the quality of the GPS ephemeris will be improved.

The GALILEO based reduced dynamic orbit solution is much more accurate than the GPS based orbits, especially in the stand-alone case as the GALILEO ephemeris has a better accuracy (65 cm RMS error) (Lucas et al., 2000; Provenzano et al., 2000)

compared with the GPS ephemeris (5~10 m RMS error) (David Jefferson and Yoaz Bar-Sever, 2000). The GALILEO based differential solution is also more accurate than the corresponding GPS based solution because of the better measurements noise used for GALILEO compared with GPS and more visible GALILEO satellites compared with GPS due to GALILEO better geometry (Table 7.11 and Appendix B).

The choice of the ground stations positions is vital for the accuracy of differential reduced dynamic solution to ensure differential solution available at each epoch with high number of common visible satellites between the LEO satellite and the ground stations. Therefore the best choice for the ground stations is around the equator to have the maximum visibility of any constellation.

The differential solutions reduced dynamic orbits are much more accurate than the stand-alone due to the removal of the ephemeris error, which is vital in GPS case due to the low quality GPS broadcast ephemris.

The GALILEO reduced dynamic orbits solutions show a better performance than the reduced dynamic orbits from the GPS and the combined GPS/GALILEO constellations (with the present accuracy for GPS ephemeris). As the modernisation process for GPS goes on and the quality of the GPS ephemeris is improved, it should expected to have more accurate reduced dynamic solutions from both constellations rather than each constellation individually.

A comparison study was conducted between this thesis' differential carrier phase solution using GPS constellation and previous work (Bertiger et al., 1994) using the same technique for T/P satellite. This study proved the strong agreement between the findings of this research and the results of the other group's work which is evidence for the reliability of this thesis's outputs for LEO satellite reduced dynamic orbit determination

As it has been shown before, one of the key advantages of the reduced dynamic orbit determination technique for LEO satellites is the ability of working as a real-time application (Ashkenazi et al., 1996). Some recommendations should be followed during this real-time operation which will be expressed in the following section.

7.7 Recommendations for Real-time Application

For real time application, a test study has been conducted producing a stand-alone reduced dynamic solution for the combined GPS/GALILEO constellation for the following three consecutive sets of data:

1- Predicted orbit produced for two day arc (21/7/2002-22/7/2002) using some good quality starting elements followed by reduced dynamic stand-alone solution produced for the same two days (21/7/2002-22/7/2002).

2- Predicted orbit produced for two day arc (22/7/2002-23/7/2002) using starting elements from the previous produced predicted orbit (step 1) followed by reduced dynamic stand-alone solution produced for the same two days (22/7/2002-23/7/2002).

3- Predicted orbit produced for two day arc (23/7/2002-24/7/2002) using starting elements from the previous produced predicted orbit (step 2) followed by reduced dynamic stand-alone solution produced for the same two days (23/7/202-24/7/2002)

The reduced dynamic solutions for each data set are shown in Figures 7.27, .28 and 7.29.

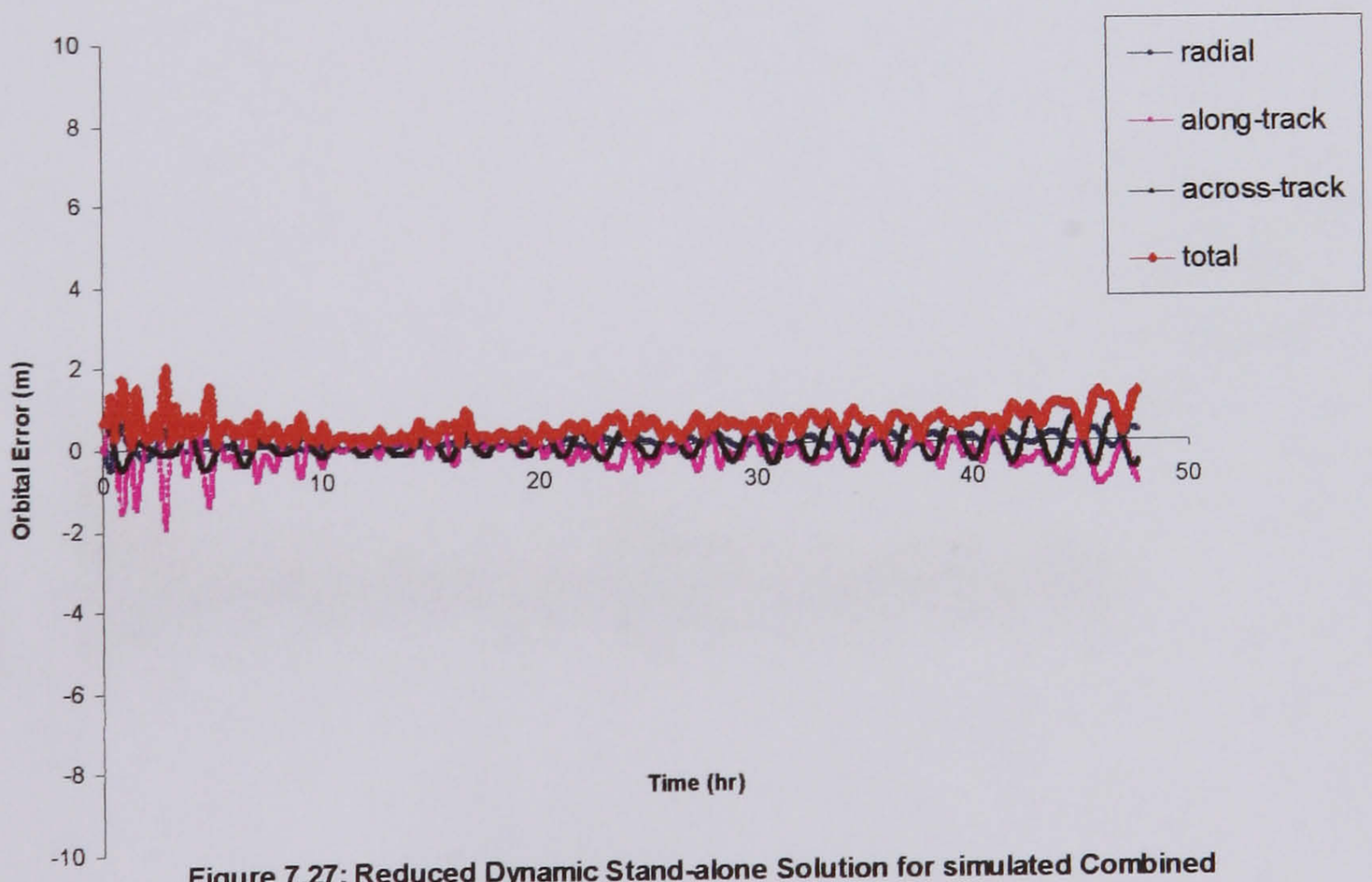

Figure 7.27: Reduced Dynamic Stand-alone Solution for simulated Combined GPS/GALILEO receiver (21/7/2002-22/7/2002)

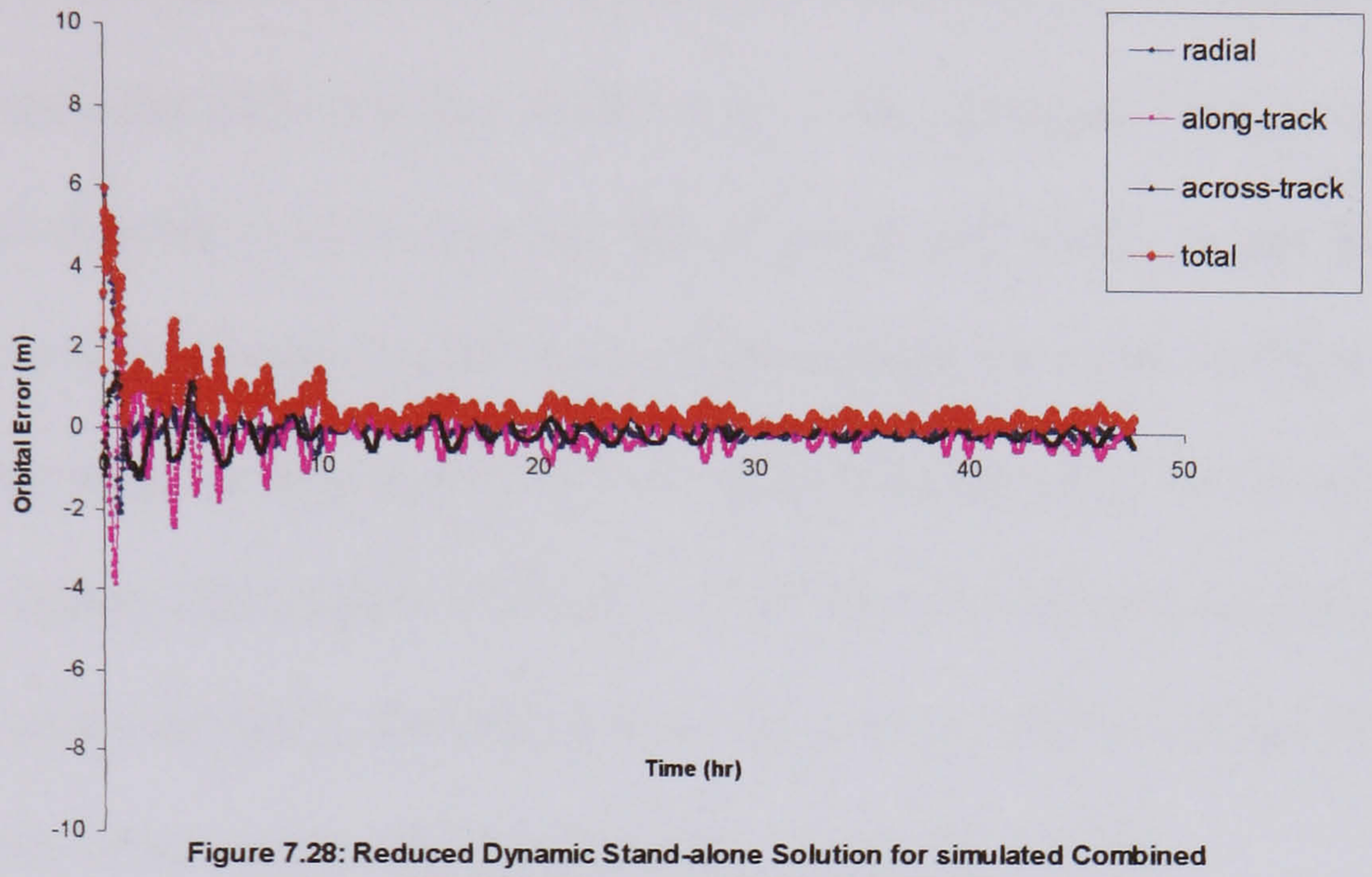

Figure 7.28: Reduced Dynamic Stand-alone Solution for simulated Combined GPS/GALILEO receiver (22/7/2002-23/7/2002)

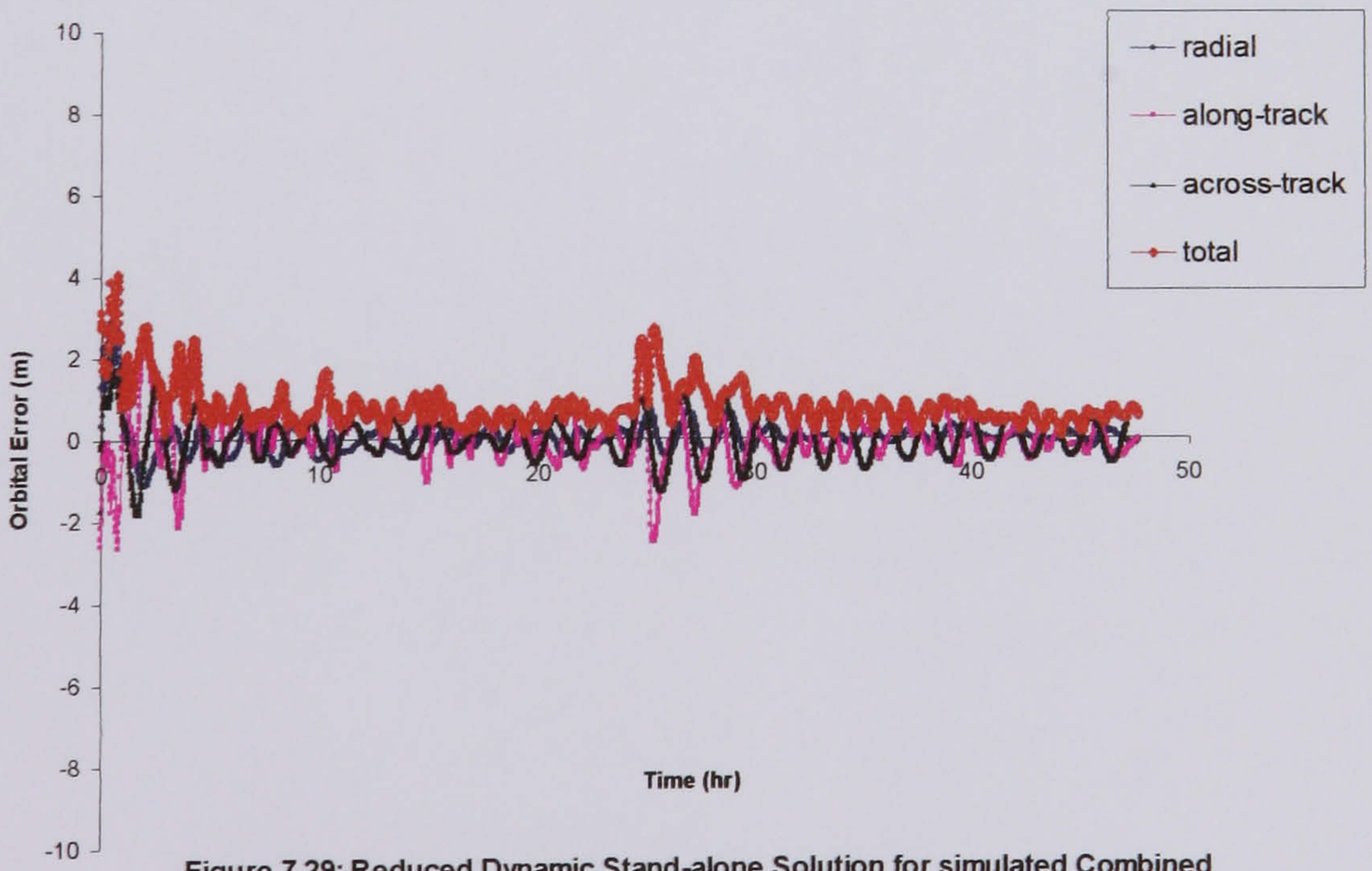

Figure 7.29: Reduced Dynamic Stand-alone Solution for simulated Combined GPS/GALILEO receiver (23/7/2002-24/7/2002)

It can be concluded from the resulting figures that the reduced dynamic kalman filter needs more than 10 hours to settle before it can deliver accurate reduced dynamic orbits. Following the previous scenario of extracting the starting elements from the predicted orbit after one day of the start of the predicted orbit as well as using the reduced dynamic orbits after one day of processing which means give the filter 24 hours to settle (longer period than actually needed for more confident in the reduced dynamic results). So from Figure 7.27 the reduced dynamic orbits will be valid for 24 hours during (22/7/2002). For Figure 7.28 the reduced dynamic orbits will be valid for 24 hours during (23/7/2002). Following the same rule, for Figure 8.29 the reduced dynamic orbits will be valid for 24 hours during (24/7/2002).

CHAPTER 8

CONCLUSIONS & SUGGESTIONS FOR FUTURE WORK

8.1 Conclusions

The following is a summary of the main conclusions resulting from the research presented in this thesis.

GPS/GALILEO Simulation

The GNSS data simulation is a strong research tool in GNSS fields as most of the applications of GNSS depend on the quality of the measurements. Thus an accurate simulation of GNSS measurements requires an accurate simulation of the environmental biases, which is the main emphasis of the work shown in the first part of this thesis.

The ionospheric delay modelling required more attention as it is the current major challenge faced when processing GNSS data. A detailed study investigated the

available options for modelling this type of delay, resulting in an ionospheric simulation model based on the IGS-GIM's which gives a high realistic behaviour in determining the ionospheric delay and the best description and visualisation of the ionosphere's behaviour with a reasonable computation time (Section 4.3).

The modelling of the tropospheric delay was also part of the focus of this thesis. The tropospheric delay is the second major challenge faced by users of GNSS measurements. An investigation study compared the performance of a statistical tropospheric model (EGNOS model) with the performance of surface tropospheric models (Hopfield model, Saastamonien model, Marini model) along with an empirical model (Magnet model). This demonstrated the adequacy of the EGNOS model for modelling the tropospheric delay, as it provides good behaviour in describing the mean tropospheric delay (7cm RMS difference with IGS-estimates) without the need for surface meteorological data, with a reasonable computation time (Section 4.4).

The need for simulating the regional and temporal variations in the ionosphere and troposphere which is not provided by the two chosen models meant it was important to develop an algorithm that gave them this ability. This was satisfied through using a statistical theory (Gaussian random fields) which transformed the chosen models into more realistic high spatial variation models, capable of simulating small-scale regional and temporal variations within the ionosphere and troposphere, the success of which was demonstrated through the study shown in Section 4.5.

Gaussian Colored noise is a powerful tool for more realistic modelling of the multipath delay, as it provides the correlation between different time series of multipath delay, where Gaussian white noise can not. A new model for the multipath delay was implemented based on Gaussian colored noise. The model has three main features: various multipath activity cases, correlation-time dependence and elevation-angle dependence. Thus more realistic modelling of the multipath is achieved and presented (Section 4.6).

The behaviour of the simulated GPS data from the modified DATSIM software (using IGS GIM's for ionospheric delay simulation, modified EGNOS model for tropospheric delay simulation and a coloured noise multipath model) is highly realistic when compared with the behaviour of real GPS data. A test study using P4 software showed an acceptable agreement in the determination of the height coordinate for eight stations between the new simulated GPS data and real GPS data. This was not achievable with the original simulated GPS data (Section 5.1).

GALILEO simulated data were generated through the modification of the DATSIM software to allow for the different services offered by GALILEO and the implementation of an ephemeris data file for the GALILEO constellation based on a Walker (27/3/1) constellation (§ 5.2). The positioning accuracy of the new simulated GPS data with the GALILEO simulated data was investigated using P4 software (Section 5.2). It showed that the GALILEO constellation may offer better performance due to better ranging accuracies, better quality ephemeris data and more visible satellites (see Table 7.11 and Appendix B).

LEO-Satellite Orbit Determination

The accuracy of the ephemeris data for any GNSS constellation has a strong effect on the performance of the reduced-dynamic solutions for LEO satellites, as it highly affects the accuracy of the observation model, which has the job of reducing the effect of the dynamic model on the final reduced dynamic solution. A detailed study revealed the effect of different types of GPS ephemeris data on the reduced dynamic solutions for the T/P satellite (Section 7.2.1). The limitations are shown for real-time reduced dynamic solutions using GPS, due to the low quality of the GPS broadcast ephemeris data.

A validating study was carried out which found an agreement between the reduced dynamic solutions for T/P satellite provided by simulated GPS data and real GPS data (JPL) (Section 7.3). This agreement means that trust can be placed in the reduced dynamic solutions for GALILEO and combined GPS/GALILEO constellations.

The stand-alone reduced dynamic solution gives the lowest accuracy for GPS constellation due to low quality GPS broadcast ephemeris data. Thus the differential solution gives better performance due to the elimination of the ephemeris errors. The best reduced dynamic solution from the GPS constellation is achieved using a differential carrier phase solution. (Section 7.4.2)

The GALILEO constellation will offer better performance for LEO-satellite reduced dynamic solutions due to better quality GALILEO ephemeris data, better ranging

accuracies and more visible satellites (see Table 7.11 and Appendix B) compared with the GPS constellation (Section 7.4.3).

The combined GPS/GALILEO constellation will give better performance for LEO satellites reduced dynamic solutions compared with the GPS constellation. However the performance of the combined constellation will still be affected by the low quality GPS broadcast ephemeris. The GPS modernisation process is therefore vital for improved reduced dynamic solutions from the combined constellation (Section 7.4.4).

The performance of the combined GPS-modernised/GALILEO constellation is the best compared to the performance of the GPS constellation or the GALILEO constellation alone, due to the better quality of the combined ephemeris data and more visible satellites from both constellations (Section 7.4.5).

Certain criteria were suggested for real-time LEO-satellites reduced dynamic applications to work with satisfying flexibility and accuracy (Section 7.4.6).

8.2 Suggestions for Future Work

The following contains some suggestions for future work:

The modelling of the tropospheric delay within DATSIM software needs further work. The currently available options are surface meteorological models (not recommended for simulation purposes) or global models (recommended for simulation purposes) such as the EGNOS model, which was the scope of this study.

However the EGNOS model still needed a statistical theory algorithm (Gaussian random fields) to have the ability of simulating regional variations of the troposphere. The regional tropospheric maps provided by regional dense GPS network such as the German GASP-Project (GASP, 2003), could play a strong part in this research providing high accuracy tropospheric delay estimation with the ability of simulating regional and temporal variations of the troposphere. Clearly this scenario can not be expanded globally as the water vapour distribution has a high local fluctuation which limits the availability and usefulness of global tropospheric maps.

The generation of more realistic GPS simulated data and GALILEO simulated data creates the possibility of studying the performance of the two constellations in LEO satellite orbit determination (this study) and also in many other applications. The simulation data will be useful for many other GNSS applications.

The accuracy of the GPS broadcast ephemeris is a limiting factor in the achievable accuracy of the reduced dynamic technique for LEO satellites orbit determination as shown in this thesis (Section 7.2.1). It is highly recommended that a study should be carried out to investigate the possible options by which the effect of the broadcast errors could be minimised, either by estimating GPS orbits together with the LEO satellite orbits or using the IGS Ultra-Rapid GPS orbits optimised to suit real-time applications.

The carrier phase solution is the most precise GNSS solution and offers the best accuracy in LEO satellites reduced dynamic orbit determination. The main challenge

faced when computing this type of solution is the resolution of the initial integer ambiguity. The reduced dynamic simulated studies in this thesis depended on pre-known initial integer ambiguities, so a future study could investigate the implementation of reliable methods for the resolution of these ambiguities. Also, the importance of correct ambiguity resolution for real–time carrier phase solutions should be investigated.

The tests and results presented in this thesis are limited to a single satellite altitude (T/P). Since the characteristics of the LEO satellite force models vary depending on the altitude of the satellite, further tests are required to assess the accuracy of the reduced dynamic technique discussed in this thesis for different mission scenarios.

The strength of the reduced dynamic orbit determination technique is its ability to absorb errors in the force model used for orbit integration of LEO satellites. The orbit integration software used in this thesis applied a very detailed force model, using accurate models for each affecting force on the LEO satellite, it is likely that this complex force model could be significantly simplified. Thus a study is recommended to assess the effect of the different force model components on LEO orbit determination accuracy with the reduced dynamic method.

The differential solution gives more accurate reduced dynamic orbits than the stand-alone solution, which is currently the only available option for real-time applications. A future study is recommended from the practical point of view to study the necessary requirements for developing differential solution as a real-time application

for LEO missions. This will include studying the availability of the ground data and uploading it to the LEO satellite to have the orbits solutions in real-time.

REFERENCES

Agrotis, L. G. (1984). Determination of Satellite Orbits and the Global Positioning System. Ph.D. Thesis, Nottingham University.

Aquino, M., (marcio.aquino@nottingham.ac.uk)(2004). Ionosphere TEC Variations. Email to: Ashraf Farah (isxamaf@nottingham.ac.uk).

Ashkenazi, V. and Summerfield,P. J. (1989). Rapid Static and Kinematic GPS Surveying: With or Without Cycle Slips. 2nd International Seminar on the Global Positioning System, IESSG, University of Nottingham.

Ashkenazi, V., Moore, T., Hill, C. J. and Chen, W. (1994). Precise Orbits for LEO Spacecraft using GPS. Final Report, IESSG, University of Nottingham.

Ashkenazi, V., Moore, T., Hill, C. J. and Chen, W. (1996). GPS for LEO Real-Time Operations. Final Report, IESSG, University of Nottingham.

Ashkenazi, V., W. Chen,C J. Hill, T. Moore, D. Stanton and D. Fortune (1997). GPS for Real-Time Autonomous Orbit Determination of LEO Satellites, Proceeding GNSS '97, First European Symposium on Global Navigation Satellite Systems, pp 657 – 665, Munich.

AVISO (2002). Archiving, Validation and Interpretation of Satellites Oceanographic data, CNES, Toulouse, France. Http://www.jason.oceanobs.com.

AVISO (2003). Archiving, Validation and Interpretation of Satellites Oceanographic data. Document accessed on (20/12/2003). http://www-aviso.cls.fr/html/missions/tp/orbite_uk.html.

Baker D. F. (1997). Multipath Modelling for The GPS. MSc dissertation. IESSG, Nottingham University, UK.

Baker, H. C. (1998). GPS Water Vapour Estimation for Meteorological Applications. Ph.D. Thesis, University of Nottingham.

Barry, R. G. and R. J. Chorley (1986). Atmosphere, Weather and Climate (4th edition). Methuen Publishers (London and New York).

Bartosch L. (2001). Generation of Colored Noise. International Journal of Modern Physics C., Vol. 12, No. 6, pp. 851-855.

Baur, F., K. Hartman and E. Lightsey (1998). Spaceborne GPS Current Status and Future Visions. Proceeding of ION GPS-98, The 11th International Meeting of the Satellite Division of The American Institute of Navigation. Nashville, Tennessee, USA. September (15-18).

Bertiger, W. I., Y. E. Bar-Sever, E. J. Christensen, E. S. Davis, J. R. Guinn, B. J. Haines, R. W. Ibanez-Meier, J. R. Jee, S. M. Lichten, W. G. Melbourne, R. J. Mullerschoen, T. N. Munson, Y. Vigue, S. C. Wu, T. P. Yunck, R. e. Schutz, P. A. M. Abusali, H. J. Rim, M. M. Watkins and P. Willis (1994). GPS Precise

Tracking of TOPEX/POSEIDON: Results and Implications. Journal of Geophysical Research, 99, C12, pp 24449-24464.

Bierman, G. F. (1977). Factorization Methods for Discrete Sequential Estimation. Academic Press New York.

Bilitza, D. (1990). NSSDC 90-22, World Data Centre A Rockets & Satellites, Greenbelt, USA.

Bilitza, D. (2001). International Reference Ionosphere 2000. Journal of Radio Science, Vol. 36, No. 2, pp. 261-275.

Bilitza, D., Rawer, K., Bossy, L. and Gulyaeva, T. (1993). International Reference Ionosphere-Past, Presesnt and Future: I Electron Density. Journal of Advanced Space Research, Vol. 13, No. 3, pp. (3)3-(3)13.

Black, H. D. (1978). An Easily Implemented Algorithm for the Tropospheric Range Correction. Journal of Geophysical Research, Vol. 83, No. B4.

Bock, O. and E. Doerflinger (2001). Atmospheric Modeling in GPS Data Analysis for High Accuracy Positioning. Phys. Chem. Earth (A), Vol. 26, No. 6-8, pp. 373-383.

Bomford, G. (1975). Geodesy (3rd edition). Oxford at Clarendon Press.

Brunner, F. K. (1992). Refraction, Refractive Index and Dispersion: Some Relevant History. Proceeding Refraction Transatmospheric Signals in Geodesy. Netherlands Geodetic Commission. No. 36, edited by DeMunck and Spoelstra.

Byun, S. H. (1998). Satellite Orbit Determination Using GPS Carrier Phase in Pure Kinematic Mode. Dissertation, Department of Aerospace Engineering and Engineering Mechanics. The University of Texas at Austin.

Chan, G. (1999). An Effective Method for Simulating Gaussian Random Fields. American Statistical Association, 1999 Proceedings of The Statistical Computing Section, pp. 133-138.

Chan, G. (2003). Fortran programs for two-dimensional Gaussian Random Fields. http://www.stat.uiowa.edu/~grchan/programs/statprog.html. Accessed 20/4/2003.

Chao, chih hung Jason (1996). Improved Modelling of High Precision Wide Area Differential GPS. Ph.D. Thesis, Nottingham University.

Christensen, E. J., B. J. Haines, K. C. McColl, and R. S. Nerem (1994). Observations of Geographically Correlated Orbits Errors for TOPEX/Poseidon Using the Global Positioning System. Geophys. Res. Lett., 21(19), pp. 2175-2178.

Cole, A. E., A. Court, and A. J. Cantor (1965). Model atmospheres in Handbook of Geophysics and Space Environments. McGraw-Hill, New York, edited by S. L. Valley, pp. (2-1)- (2-22).

Collins P., Stewart P. and Langely R. (1998). Multipath and Atmospheric Propagation Errors in Offshore Aviation DGPS Positioning. 2nd Workshop on Offshore Aviation. Research Centre for Cold Ocean Resources Engineering, Memorial University of Newfoundland, St. John's, Nfld.

Collins, J.P. and Langely, R.B. (1997). A Tropospheric Delay Model for the User of the Wide Area Augmentation System. Final contract report prepared for Nav. Canada, Department of Geodesy and Geomatics Engineering Technical Report No. 187, University of New Brunswick, Federiction, N.B., Canada.

Collins, J.P. and Langely, R.B. (1998). The residual tropospheric propagation delay: How bad can it get? Proceeding of ION GPS-98, The 11th International Meeting of the Satellite Division of the Institute of Navigation, Nashville, Tenn., September 15-18, pp. 729-738.

Cressie, N. A. C. (1993). Statistics for Spatial Data. Wiley, New York.

Cross, P. A. (1982). Advanced Least Squares Applied to Position-fixing. Working paper No. 6, Department of Land Survey, North East London Polytechnic.

Curley, R. A. (1988). The Use of TI4100 GPS Receivers and MAGNET Software to Determine Height Differences. M.Sc. Thesis, University of Nottingham.

David C. Jefferson and Yoaz E. Bar-Sever (2000). Accuracy and Consistency of Broadcast GPS Ephemeris Data. ION GPS 2000, 19-22 September, Salt Lake, UT.

Davis, J. L., T. A. Herring, I. I. Shapiro, A. E. E. Rogers, and G. Elgered (1985). Geodesy by Radio interferometry: effects of atmospheric modeling errors on estimates of baseline length. Radio Science, Vol. 20, No. 6, pp. 1593-1607.

Davis, K. (1989). Ionospheric Radio. IEE Electromagnetic Waves series 31, Peter Peregrinus Ltd., London, UK.

De Jong, J. C. (1991). GPS-Satellite Orbits and Atmospheric Effects. Publication from Delft University of Technology.

Dembo, A., C. L. Mallows and L. A. Shepp (1989). Embedding nonnegative definite Toeplitz matrices in nonnegative definite circulant matrices, with applications to covariance estimation. IEEE Transactions on Information Theory, 35, pp. 1206-1212.

Dietrich, C. and Newsam, G. (1993). A Fast and Exact Method for Multidimensional Gaussian Stochastic Simulations. Water Resources Research, 29, pp. 2861-2869.

Dodson, A. H. (1986). Refraction and Propagation Delays in Space Geodesy. International Journal of Remote Sensing, Vol.7, No.4, pp. 515-524.

Dodson, A. H. (1988). The Effects of Atmospheric Refraction on GPS Measurements. Seminar on the Global Positioning System, Nottingham university.

Dodson, A. H., Hill, C. J. and Shardlow, P. J. (1992). The Effects of Propagation Errors on GPS Measurements. 5th Seminar on the Global Positioning System, University of Nottingham.

Dodson, A.H., Chen, W., Baker, H. C., Penna, N. T., Roberts, G. W., Westbrook, J. and Jeans, R. (1999). Assessment of EGNOS Tropospheric Correction Model. Proceeding of ION GPS-99, The 12th International Meeting of the Satellite Division of The Institute of Navigation, Nashville, Sept. 14-17, pp.1401-1407.

Engler, E., (Evelin.Engler@dlr.de) (2004). Re: GPS/GALILEO Satellite Availability. Email to: Ashraf Farah (isxamaf@nottingham.ac.uk).

Engler, E., T. Noack, S. Schluter et. al. (2001). First Impressions of GALILEO Positioning Performance derived with the Simulation Tool NavSim. GNSS-2001 conference. 5th GNSS International Symposium (GNSS 2001), 8-11 May, Spain.

Farah, A., (2002a). Ionospheric-Delay Simulation Study for GPS Single-Frequency Users. The 2002 International Symposium on GPS/GNSS. Wuhan, China, November 6 - 8.

Farah, A., (2002b). The Ionospheric Delay Effort for GPS Single-frequency Users-Analysis Study for Simulation Purposes. Proceeding of ION GPS-02, The 15th International Meeting of the Satellite Division of The American Institute of Navigation. Portland, Oregon, USA. September (24-27).

Farah, A., (2003a). A Light on: GPS/GALILEO Data Simulation. The 2003 International Symposium on GPS/GNSS. Tokyo, Japan, November 15 - 18.

Farah, A., (2003b). A New Ionospheric Delay model for GPS Single-Frequency Data Simulation. 1st International Conference of Civil Engineering Science ICCES1, Assiut University, Assiut, EGYPT.

Farah, A., (2003c). EGNOS Tropospheric Model For GPS-Data Simulation. The 2003 International Symposium on GPS/GNSS. Tokyo, Japan, November 15 - 18.

Farah, A., Moore, T. and Hill, C. (2003). High Spatial Variation Tropospheric Model for GPS-Data Simulation. Proceeding of ION GPS-03, The 16th International Meeting of the Satellite Division of The American Institute of Navigation. Portland, Oregon, USA. September (9-12).

Farah, A., Moore, T. and Hill, C. (2004). LEO Orbit Determination by GNSS. Proceeding of GNSS-04, The 8th GNSS International Symposium. Rotterdam, Netherlands. May (17-19).

Feltens, J., and Schaer, S., (1998). IGS Products for the Ionosphere, in Proceeding of the IGS Analysis Centre Workshop, edited by J. M. Dow et al., pp. 225-232, ESA/ESOC, Darmstadt, Germany, Februray 9-11.

Galileo (2002). (frequently updating web page)

(http://europa.eu.int/comm/dgs/energy_transport/galileo/documents/index_en.htm)

GASP (2003). GPS Atmosphere Sounding Project. http://www.gfz-potsdam.de/pb1/GASP/. Document accessed on (12/12/2003).

GPS Lab (2004). The accuracy of the GPS Broadcast Ephemeris and the WAAS-corrected Orbit. http://gge.unb.ca/gauss/htdocs/grads/orbit/. Accessed on 10/3/2004. University of New Brunswick. Department of Geodesy and Geomatics Engineering. Canada.

GPS-SPS (2001). Global Positioning System Standard Positioning Service Performance Standards. Assistance Secretary of defence for command, control, communications and intelligence. October 2001.

Haines B., W. Bertiger, S. Desai, D. Kuang, T. Munson, L. Young and P. Willis (2002). Initial Orbit Determination Results for Jason-1: Towards a 1-cm Orbit. Proceeding of ION GPS-02, The 15th International Meeting of the Satellite Division of The American Institute of Navigation. Portland, Oregon, USA. September (24-27).

Hannah B. (2001). Modelling and Simulation of GPS Multipath Propagation. Ph.D. dissertation. Queensland University of Technology, Australia.

Hargreaves, J. K. (1992). The Solar-Terrestrial Environment. Cambridge Atmospheric and Space Sciences Series, Cambridge University Press, UK.

Hein, G. W. (1990). Kinematic Differential GPS Positioning: Applications in

Airborn Photogrammetry and Gravimetry. In : Crosilla F, Mussio L (eds) : II Sistema di Posizionamento Globale Satellite GPS. International Centre for Mechanical Science (CISM), Collana di Geodesica e Cartografia, Udine, Italy.

Hein, G. W., Jeremie Godet, Jean-Luc Issler, Jean-Christophe Martin, Phillippe Erhard, Rafael Lucas-Rodriguez, and Tony Pratt (2002). Status of Galileo Frequency and Signal Design. Proceeding of ION GPS-02, The 15th International Meeting of the Satellite Division of The American Institute of Navigation. Portland, Oregon, USA. September (24-27).

Herring, T. A. (1992). Modeling atmospheric delays in the analysis of space geodetic data. Proceeding of the Symposium on Refraction of Transatmospheric Signals in Geodesy. EDS. J. C. De Munck and T. A. Th. Spoelstra, Netherlands Geodetic Commission, Publications in Geodesy, No. 36, pp. 157-164.

Hill, C. J. (1989). Satellite Laser Ranging and Some Geophysical Applications. Ph.D. Thesis, University of Nottingham.

Hill, C. J. (2002). P4 (Pseudorange & Phase Post Processor) User Guide. Version (2.0.0). Nottingham University.

Hoffmann-Wellenhof, B., Lichtenegger, H. And Collins, J. (2000). Global Positioning System Theory and Practice. Fifth, Revised Edition. Springer-Verlag, Wien, New York.

Hopfield, H. S. (1971). Tropospheric Effect of Electromagnetically Measured Range: Prediction from Surface Weather Data. Journal of Radio Science, Vol. 6, No.3, pp. 357-367.

Hopfield, H. S. (1977). Tropospheric Correction of Electromagnetic Ranging Signals to a Satellite: Study of Parameters. In: Proceeding Of the International Symposium on Electromagnetic Distance Measurement and the Influence of Atmospheric Refraction, Wageningen, The Netherlands, pp. 205-213.

Hugentobler, U., S. Schaer and P. Fridez (2001). Bernese GPS Software Version 4.2. Astronomical Institute, University of Berne. Switzerland.

Ifadis, I. I. (1986). The atmospheric delay of radio waves: modeling the elevation dependence on a global scale. Technical Report 38L, Chalmers, University of Technology, Goteborg, Sweden.

IGS (2003). http://igscb.jpl.nasa.gov/components/prods.html

Jack O. T. J. (1994). Multipath Effects on GPS Observations. MSc dissertation. IESSG, Nottingham University, UK.

Janes, H. W., Langely, R. B. and Newby, S. P. (1989). A Comparison of Several Models for the Prediction of Tropospheric Propagation Delay. Proceeding Fifth International Symposium on Satellite Positioning, Vol. II, Corbett Centre, March 13-17, Las Cruces, New Mexico, pp. 777-788.

Javier Benedicto, Daniël Ludwig (2001). GALILEO System Architecture and Services. Seventh International Workshop on Digital Signal Processing Techniques for Space Communications, Sesimbra, Portugal, 1-3 October.

Jursa, A. S. (1985). Handbook of Geophysics and The Space Environment. Air Force Geophysics Lab, Hanscom AFB, MA., USA.

Kaplan D. (1996). Understanding GPS, Principals and Applications. Artech House Publishers.

Kelly, M. C. (1989). The Earth's Ionosphere: Plasma Physics and Electrodynamics. Academic Press.

Klobuchar, J. A. (1982). Ionospheric Corrections for the Single Frequency User of the Global Positioning System. National Telesystems Conference, NTC'82. Systems for the Eighties. Galveston, Texas, USA (New York: IEEE, 1982).

Klobuchar, J. A. (1987). Ionospheric Time-Delay Algorithm for Single-Frequency GPS Users. IEEE Transactions on Aerospace ad Electronic Systems. Vol. AES-23, No. 3, pp. 325-331.

Komjathy, A. (1997). Global Ionospheric Total Electron Content Mapping Using The Global Positioning System. Ph.D. Thesis, New Brunswick University, Canada.

Kozintsev, B. (1999). Computations with Gaussian Random Fields. Ph.D. Thesis. University of Maryland, USA.

Kunches, J. M. and Klobuchar, J. A. (2001). Eye on The Ionosphere: GPS after SA. GPS Solutions 4(3), PP. 52-54.

Lanyi, G. (1984). Tropospheric delay effects in radio interferometry. Telecommunications and Data Acquisition Progress, JPL Technical Report 42-78, Jet Propulsion Laboratory, Pasadena, CA, pp. 152-159.

Lechner, W. and H. Wilmes (1989). The Precise Range and Range-Rate Equipment (PRARE) on a GPS Satellite-Simulation about the Capability for Orbit Determination and Positioning. Proceeding of 5th International Geodetic Symposium on Satellite Positioning.

Lemoine, F. G. , S. B. Luthcke, N. P. Zelensky and R. Govind (2004). Gravity Model Comparisons and Orbit Determination Analysis with Doris Data. Presentation file (http://lareg.ensg.ign.fr/IDS/events/2004_files/f1.pdf). accessed on (8/7/2004).

Llewellyn, S. K. and Bent, R. B. (1973). Documentation and Description of the Bent Ionospheric Model. IAFCRL-TR-73-0657, July 1973, AD772733.

Lucas, R., Hahn, J., Dinwiddy, S., Lugert, M., Gatti, G. and Benedicto, J. (2000). Galileo Space and Ground Segment Definition: System and Performance.

ION GPS 2000, 19-22 September 2000,Salt Lake City, USA.

Luo, N. (2000). Precise Relative Positioning of Multiple Moving Platforms Using GPS Carrier Phase Observables. PhD Thesis, UCGE Report Number 20147, Department of Geomatics Engineering, The University of Calgary, Canada.

Marini, J. W. (1972). Correction of Satellite Tracking Data for an Arbitrary Tropospheric Profile. Radio Science, Vol. 7, No. 2, pp. 223-231.

Marsh, J. G., Lerch F.J., Putney B.H., Felsentreger T.L., Sanchez B.V. (1990). The GEM-T2 Gravitational Model. Journal of Geophysical Research, 95(B13), pp. 22043-22071.

Marsh, J. G., Lerch, F.J., Putney, B.H., (1988). A New Gravitational Model for the Earth from Satellite Tracking Data: GEM-T1. Journal of Geophysical Research, 93(B6), pp. 6169-6215.

Melbourne, W. G., E. S. Davis, T. P. Yunck, and B. D. Tapley (1994). The GPS Flight Experiment on TOPEX/Poseidon. Geophysical Research Letters, 21(19), pp. 2171-2174.

Melbourne, W. G., T. P. Yunck and S. C. Wu (1986). GPS-Based Precision Positioning of Earth Orbiting Remote Sensing Systems. Paper AAS-86-398, AAS 33RD Annual Meeting–Aerospace: Century XXI, Boulder, Colorado, USA.

Mendes, V. B. and R. B. Langley (1994). A Comprehensive Analysis of Mapping Functions Used in Modeling Tropospheric Propagation Delay in Space Geodetic Data. International Symposium on Kinematic Systems in Geodesy, Geomatics and Navigation. Banff, Canada. August 30- September 2.

Meng, X. (2002). Real-time Deformation Monitoring od Bridges Using GPS/Accelerometers. Ph.D. Thesis. The university of Nottingham.

Moore, T. (1986). Satellite Laser Ranging and the Determination of Earth Rotation Parameters, Ph.D. Thesis, University of Nottingham.

NASA (2003). Ocean Surface Topography from Space. http://sealevel.jpl.nasa.gov/. Accessed on (20/12/2003).

NAVSTAR (1996). NAVSTAR GPS User Equipment Introduction, Public Release Version, September 1996 (document accessed on 10 September, 2001) http://www.spacecom.af.mil/usspace/gps_support/documents/gpsuser.pdf

Nerem, R. S., F. J. Lerch, J. A. Marshall, E. C. Pavlis, B. H. Putney, B. D. Tapley, R. j. Eanes, J. C. Ries, B. E. Schutz, C. K. Shum, M. M. Watkins, S. M. Klosko, J. C. Chan, S. B. Luthcke, G. B. Patel, N. K. Pavlis, R. G. Williamson, R. H. Rapp, R. Biancle, and F. Nouel (1994). Gravity Model Development for TOPEX/POSEIDON: Joint Gravity Models 1 and 2. Journal of Geophysical Research, 99, C12, pp. 24421-24447.

Newby, S. P. , Langely, R. B. and Janes, H. W. (1990). Ionospheric Modelling for Single Frequency Users of the Global Positioning System: A Status Report. In Proceeding of the 2nd International Symposium on Precise Positioning with GPS. Ottawa, Canada.

Newby, S. P. and Langely, R. B. (1992). Three Alternative Empirical Ionospheric Models- Are They Better Than The GPS Broadcast Model? In: Proceeding of The 6th International Symposium on Satellite Positioning. Columbus, Ohio.

Niell, A. E. (1993). Improved global atmospheric mapping functions for VLBI and GPS. URSI/IAU Symposium on VLBI Technology. Progress and Future Observational Possibilities, Kyoto, Japan, 6-10 September.

Niell, A.E. (1996). Global Mapping Functions for the Atmospheric Delay at Radio Wavelengths, Journal of Geophysical Research, Vol 101, No B2, pp. 3227-3246, 10 February 1996.

NIMA (2002). National Imagery and Mapping Agency Technical Report. "Department of Defense World Geodetic System 1984 Its Definition and Relationships with Local Geodetic Systems". NIMA TR8350.2. January 2000.

Nouel F., J. P. Berthias, M. Deleuze, A. Guitart, P. Laudet, A. Piuzzi, D. Pardines, C. Valorge, C. Dejoie, M. F. Susini, and D. Taburiau (1994). Precise Centre National d'Etudes Spatiales Orbits for TOPEX/POSIEDON: Is reaching 2

cm still a challenge. Journal of Geophysical Research, Vol. 99, No. C12, pp. 24405-24419.

Pavlis, N. K. and R. H. Rapp (1990). The Development of an Isostatic Gravitational Model to degree 360 and Its Use in Global Gravity Modeling. Geophys. J. Int., 100, pp. 369-378.

Penna, N., A. Dodson, and W. Chen (2001). Assessment of EGNOS Tropospheric Correction Model. Journal of Navigation, Vol.54, Issue 1, pp. 37-55.

Pidgeon, A., M. Fruhauf, P. Fritzen, M. Begin, B. Davis, P. Bellucci, X. Cyril, V. Ashkenazi, M. Dumville, and J. Llorente (2000). GalileoSat System Simulation Facility A systems Engineering Solution. Proceeding of ION GPS-2000, The 13th International Meeting of the Satellite Division of The Institute of Navigation, Salt Lake city, UT, September 19-22.

Provenzano, J. P., A. Masson, S. Journo, C. Laramas, J. I. Damidaux, and F. Zwolska. (2000). Implementation of a European infrastructure for satellite navigation: from system design to advanced technology evaluation. International Journal of Satellite Communications. Vol. 18, pp. 223-242.

Rawer, K. (1981). International Reference Ionosphere- IRI 79, Rep. UAG-82, Edited by J. V. Lincoln and R. Conkright, World Data Centre A for Sol.-Terr. Phys., Boulder, Colorado, USA.

Rockwell International Corporation (1993). Interface Control Document (ICD-GPS200): NAVSTAR GPS Space Segment /Navigation User Interfaces, October 10, 1993.

RTCA (1999). Minimum operational performance standards for Global Positioning System/ Wide Area Augmentation System airborne equipment. RTCA DO-229B, Issue 10 June 1999.

Saastamoinen, J. (1973). Contributions to the Theory of Atmospheric Refraction. Part II Refraction Corrections in Satellite Geodesy. Bulletin Geodesique, pp13-34.

Santerre, R. (1987). Modification to the GOAD & Goodman tropospheric refraction model. Report of the departement of Surveying Engineering, University of New Brunswick, Fredericton, N. B., Canada.

SATNAV (1998). User's Guide of Satellite Navigation Toolbox. GPSoft LLC.

Schaer S., Gurtner W. and Feltens J. (1998c). IONEX: The IONosphere Map EXchange Format Version 1. Proceeding of the IGS AC Workshop, Darmstadt, Germany, February 9-11.

Schaer, S. (2001). Generating Klobuchar-Style Ionospheric Coefficients for Single-Frequency Real-Time and Post-Processing Users. Astronomical Institute, University of Berne, Switzerland. August 21,2001.

Schaer, S., (1998a). CODE's Global Ionospheric Maps (GIMs), http://www.aiub.unibe.ch/ionosphere.html, automatically updated web site.

Schaer, S., (1998b). Towards an IGS Combined Ionosphere Product, in IGS 1997 Annual Report, pp. 28-29, IGS Central Bureau, JPL, Pasadena, California, USA.

Schaer, S., (1999). Mapping and Predicting the Earth's Ionosphere Using the Global Positioning System. Ph.D. Thesis. Astronomical Institute, University of Berne, Switzerland.

Schutz, B. E., B. D. Tapley, P. A. M. Abusali, and H. J. Rim (1994). Dynamic Orbit Determination Using GPS Measurements from TOPEX/Poseidon. Geophysical Research Letters, 21(19), pp 2179-2182.

SEC (2003). Space Environment Centre. National Oceanic and Atmospheric Administration. http://www.sel.noaa.gov/Education/. Accessed on (23/12/2003).

Seeber, G. (1993). Satellite Geodesy, Foundations, Methods and Applications, Walter de Gruyter, New York, 1993.

Shardlow P. J. (1990). Multipath: an Investigation. MSc dissertation. Nottingham University, UK.

Shardlow, P. J. (1994). Propagation Effects on Precise GPS Heighting. Ph.D. Thesis, University of Nottingham.

Shaw M., Sandhoo K. and Turner D. (2000). Modernization of the Global Positioning System. GPS World, 11(9), pp. 36-44.

Smith, E. K. and Weintraub, S. (1953). The Constants in the Equation for The Atmospheric Refractive Index at Radio Frequencies. In: Proceeding of the Inst. Of Radio Engineers, 41, pp 1035-1057.

Stewart, M. P., Ffoulkes-Jones, G. H., Ochieng, W. Y. O., Chen, W., Shardlow, P. J., Penna, N. T. and Bingley, R.M. (2002). GAS: GPS Analysis Software User Manual. Version 2.4. Publication IESSG, University of Nottingham.

Tapley, B. D. (1973). Statistical Orbit Determination Theory. Advances in Dynamical Astronomy, pp. 396-425.

Tapley, B. D., C. K. Shum, D. N. Yuan, J. C. Ries, and B. E. Schutz (1989). An Improved Model for the Earth's Gravity Field. Determination of the Earth's Gravity Field, Rep. 397, pp. 8-11, Department of Geodetic Science Surveying, Ohio State University, Columbus.

Tapley, B. D., J. C. Ries, G. W. Davis, R. J. Eanes, B. E. Schutz, C. K. Shum, M. M. Watkins, J. A. Marshall, R. S. Nerem, B. H . Putney, S. M. Klosko, S. B. Luthcke, D. Pavlis, R. G. Williamson, and N. P. Zelensky (1994). Precision Orbit Determination for TOPEX/POSEIDON. Journal of Geophysical Research, 99, pp. 24383-24404.

Tapley, B. D., M. M. Watkins, J. C. Ries, G. W. Davis, R. J. Eanes, S. Poole, H. J. Rim, B. E. Schutz, C. K. Shum, R. S. Nerem, F. J. Lerch, E. C. Pavlis, S. M. Klosko, N. K. Pavlis, and R. G. Williamson (1996). The Joint Gravity Model 3. Journal of Geophysical Research, 101, B12, pp. 28029-28049.

Taylor (1961). Elementary Meteorology. 5th edition. Prentice-Hall Inc.

Teuissen, P. J. G. (1995). The Least-squares ambiguity decorrelation adjustment: a method for fast GPS integer ambiguity estimation. Journal of Geodesy, Vol. 70, No. 1-2, pp. 65-82.

Thompson, R. and J. M. Kunches (2002). Solar Cycle Number 23- a progress report. GPS Solutions, Vol. 6, No. 1-2, pp. 121-123.

Tiberius, C., T. Pany, B. Eissfeller, K. de Jong, P. Joosten and S. Verhagen. (2002). Integral GPS-Galileo ambiguity resolution. Proceeding, GNSS-2002, Copenhagen, Denmark.

Urban, T., Shum, C., Kruizinga, G., Tapley, B., Bilitza, D. and Yuan, D. (1997). Comparison of Ionospheric Models for Single-Frequency Radar Altimeters. Journal of Advanced Space Research. Vol. 20,No. 9, pp 1769- 1772.

Volpe (2001). Vulnerability Assessment of The Transportation Infrastructure Relying on The Global Positioning System. Final Report prepared by John A. Volpe National Transportation Systems Centre for Office of The Assistance

Secretary for Transportation Policy. U.S Department of Transportation. 29August.

Walker, J. G. (1984). Satellite Constellations. Journal of British Interplanetary Society. Vol. 37, pp. 559-571.

Walsh, D. (1994). Kinematic GPS Ambiguity Resolution. Ph.D. Thesis, University of Nottingham.

Werner W., Zink T., Lohnert E. and Pielmeier J. (2001). GALILEO Integrity Performance Assessment (GIPA). Proceeding of the ION GPS 2001, Salt Lake City, UT, USA, 11-14 September.

Whalley, S. (1990). Precise Orbit Determination for GPS Satellites. Ph.D. Thesis, University of Nottingham.

Willis, P., Boucher, C., Kasser, M., Biancale, R., Cazenave, A. Dorrer, M. and F. Nouel (1989). The Doris Satellite Radio Tracking System: Status and plans. IAG general meeting, Edinburgh, UK.

Wood, A. T. A. and Chan, G. (1994). Simulation of Stationary Gaussian Processes in $[0,1]^d$. Journal of Computational and Graphics Statistics. Vol. 3, pp. 409-432.

Wu, S. C., T. P. Yunck and C. Thornton (1991). Reduced Dynamic Techniques for Precise Orbit Determination of Low Earth Satellites. Journal of Guidance, Control and Dynamics, No. 1, Vol. 14. PP. 24-30.

Yunck, T. P. and S. C. Wu (1986). Non-Dynamic Decimeter Tracking of Earth Satellites Using the Global Positioning System. Paper AIAA-86-0404, AIAA 24th Aerospace Sciences Meeting, Reno, Nevada, USA.

Yunk, T. P., W. I. Bertiger, S .C. Wu, Y. E. Bar-Server, E. J. Christensen, B. J. Haines, S. M. Lichten, R. J. Muellerschoen, Y. Vigue, and P. Willis (1994). First Assessment of GPS-based Reduced Dynamic Orbit Determination on TOPEX/Poseidon. Geophysical Research Letters, 21(7), pp 541-544.

APPENDIX A

Gaussian Random Fields Algorithm

The Fortran programs for two-dimensional Gaussian Random Fields are presented below after (Chan, 2003). The used variables for ionosphere and troposphere algorithms were as follows:

N1	=	100
N2	=	100
EVEN	=	'YES'
G1	=	8
G2	=	8
MAXG1	=	10
MAXG2	=	10

A different scale factor was applied in each case to reflect the amount of variations in the troposphere and the ionosphere. The values of these scale factors for the test study in Section 3.5 were as followed:

Ionosphere scale factor	=	0.25
Troposphere scale factor	=	0.02

```
C       File name: example2.f

C       This program was last modified on Tuesday 1 June, 1999.

C       Example program to simulate 2 dimensional Gaussian process,
C       which has covariance function
C                   exp{-c(t_1^2 + t_2^2)^(alpha/2)}
C       where c = 100 and alpha = 1.9 as defined in a DOUBLE PRECISION
C     FUNCTION COV2, using the two subroutines, EIGEN2
C       and SIMSGF2.

C       Set upper bound for m_1 and m_2 to be 2^10 = 1024
        INTEGER MAXSIZE, MMAXSIZE
        PARAMETER (MAXSIZE = 1024, MMAXSIZE = MAXSIZE*MAXSIZE)
        EXTERNAL EIGEN2, SIMSGF2, COV2
        DOUBLE PRECISION COV2
```

```
      DOUBLE PRECISION X(MMAXSIZE), LAM(MMAXSIZE), RHO, SIGMA,EIG(3)
      INTEGER N(2), M(2), G(2), MAXG(2), ICORR, IFAULT, ICOUNT
      CHARACTER EVEN, ANS
C     Timing parameters
      DOUBLE PRECISION TIMEARRAY(2), TIMEDIFF

      WRITE(*,*) 'SIMULATE ONE 2-DIMENSIONAL GAUSSIAN PROCESS'
      WRITE(*,*) 'PLEASE ENTER THE REQUIRED DIMENSION LENGTHS:'
      READ(*,*) N(1), N(2)
      WRITE(*,*) 'IS THE COVARIANCE FUNCTION EVEN? (Y/N)'
      READ(*,*) EVEN
    IF ((EVEN .EQ. 'Y') .OR. (EVEN .EQ. 'y')) THEN
RHO = DLOG(2D0*DBLE(N(1) - 1))/DLOG(2D0)
      G(1) = IDINT(RHO)
      IF (DBLE(G(1)) .LT. RHO) THEN
       G(1) = G(1) + 1
      ENDIF
RHO = DLOG(2D0*DBLE(N(2) - 1))/DLOG(2D0)
      G(2) = IDINT(RHO)
      IF (DBLE(G(2)) .LT. RHO) THEN
       G(2) = G(2) + 1
      ENDIF
      WRITE(*,*) 'THE DEFAULT INITIAL VALUES OF G ARE', G, '.'
      WRITE(*,*) 'DO YOU WANT TO SET HIGHER INITIAL VALUES? (Y/N)'
READ(*,*) ANS
IF ((ANS .EQ. 'Y') .OR. (ANS .EQ. 'y')) THEN
       WRITE(*,*) 'PLEASE ENTER THE NEW INTEGER INITIAL VALUES:'
 READ(*,*) G(1), G(2)
 ENDIF
      WRITE(*,*) 'THE DEFAULT MAXIMUM VALUES OF G1 AND G2 ARE 10.'
      WRITE(*,*) 'DO YOU WANT TO SET LOWER MAXIMUM VALUES? (Y/N)'
      READ(*,*) ANS
      IF ((ANS .EQ. 'Y') .OR. (ANS .EQ. 'y')) THEN
       WRITE(*,*) 'PLEASE ENTER THE NEW INTEGER MAXIMUM VALUES:'
       READ(*,*) MAXG(1), MAXG(2)
      ELSE
       MAXG(1) = 10
       MAXG(2) = 10
      ENDIF
    ELSE
RHO = DLOG(2D0*DBLE(N(1) - 1))/DLOG(3D0)
      G(1) = IDINT(RHO)
      IF (DBLE(G(1)) .LT. RHO) THEN
       G(1) = G(1) + 1
      ENDIF
RHO = DLOG(2D0*DBLE(N(2) - 1))/DLOG(3D0)
      G(2) = IDINT(RHO)
      IF (DBLE(G(2)) .LT. RHO) THEN
       G(2) = G(2) + 1
      ENDIF
      WRITE(*,*) 'THE DEFAULT INITIAL VALUES OF G ARE', G, '.'
      WRITE(*,*) 'DO YOU WANT TO SET HIGHER INITIAL VALUES? (Y/N)'
READ(*,*) ANS
IF ((ANS .EQ. 'Y') .OR. (ANS .EQ. 'y')) THEN
       WRITE(*,*) 'PLEASE ENTER THE NEW INTEGER INITIAL VALUES:'
 READ(*,*) G(1), G(2)
```

```
ENDIF
    WRITE(*,*) 'THE DEFAULT MAXIMUM VALUES OF G1 AND G2 ARE 6.'
    WRITE(*,*) 'DO YOU WANT TO SET LOWER MAXIMUM VALUES? (Y/N)'
    READ(*,*) ANS
    IF ((ANS .EQ. 'Y') .OR. (ANS .EQ. 'y')) THEN
     WRITE(*,*) 'PLEASE ENTER THE NEW INTEGER MAXIMUM VALUES:'
     READ(*,*) MAXG(1), MAXG(2)
    ELSE
     MAXG(1) = 6
     MAXG(2) = 6
    ENDIF
   ENDIF
  ENDIF
  TIMEDIFF = DTIME(TIMEARRAY)
  CALL EIGEN2(LAM, COV2, N, M, G, MAXG, EVEN, ICORR, RHO, SIGMA,
&       EIG, ICOUNT, IFAULT)
  TIMEDIFF = DTIME(TIMEARRAY)
  WRITE(*,9) TIMEDIFF
  TIMEDIFF = DTIME(TIMEARRAY)
  CALL SIMSGF2(X, N, M, LAM, RHO)
  TIMEDIFF = DTIME(TIMEARRAY)
  WRITE(*,9) TIMEDIFF
c     WRITE(*,9) ((X(I+J*M(1)), I = 1, N(1)), J = 0, N(2) - 1)
 WRITE(*,99) G, RHO, SIGMA, EIG, ICOUNT, IFAULT
9     FORMAT(F20.10, 2X)
99   FORMAT(2I3,1X,5(F20.15,2X),2I6)
     END

C    Example of an even covariance function
     DOUBLE PRECISION FUNCTION COV2(T1, T2)
     DOUBLE PRECISION C, ALPHA, T1, T2, DUMMY

     C = 1D2
     ALPHA = 1.9D0
     IF ((DABS(T1) .LE. 0D0) .AND. (DABS(T2) .LE. 0D0)) THEN
      COV2 = 1D0
     ELSE
      IF (DABS(T1) .LE. 0D0) THEN
       DUMMY = C*DEXP(ALPHA*DLOG(T2))
      ELSEIF (DABS(T2) .LE. 0D0) THEN
       DUMMY = C*DEXP(ALPHA*DLOG(T1))
      ELSE
       DUMMY = C*(DEXP(ALPHA*DLOG(DSQRT(DEXP(2D0*DLOG(T1))
&        + DEXP(2D0*DLOG(T2))))))
      ENDIF
      IF (DUMMY .LE. 7D2) THEN
       COV2 = DEXP(-DUMMY)
      ELSE
       COV2 = 0D0
      ENDIF
     ENDIF
     RETURN
     END

C    File name: eigen2.f
```

```
C       This program was last modified on Tuesday 1 June, 1999.

C       Find g_1 and g_2 to satisfy all constraints in the preliminary
C       step and return eigenvalues and other information to simulate
C       the required Gaussian field

C       Auxiliary Algorithms
C       (i)  Call EVEN2 if EVEN = 'Y' or 'y'
C       (ii) Call UNEVEN2 otherwise

C       Auxiliary Algorithms called by both EVEN2 and UNEVEN2
C       (i)   COV2, user supplies covariance function
C       (ii)  UPDATE to compute the next few possible g_1 and g_2
C       (iii) Need to link with NAG library:
C           C06FJF - Computes the two-dimensional discrete Fourier
C                    transform of a two-dimensional array of complex data
C            values.

      SUBROUTINE EIGEN2(LAM, COV2,N,M,G,MAXG,EVEN,ICORR, RHO, SIGMA,
     &           EIG, ICOUNT, IFAULT)
      INTEGER MAXSIZE, MMAXSIZE
      PARAMETER (MAXSIZE = 1024, MMAXSIZE = MAXSIZE*MAXSIZE)
      DOUBLE PRECISION COV2
      EXTERNAL COV2
      DOUBLE PRECISION LAM(MMAXSIZE), RHO
      INTEGER M(2), N(2), G(2), MAXG(2), IFAULT
C     Parameters used only if IFAULT = 1
      DOUBLE PRECISION SIGMA, EIG(3)
      INTEGER ICORR, ICOUNT
      CHARACTER EVEN

      IF ((EVEN .EQ. 'Y') .OR. (EVEN .EQ. 'y')) THEN
       CALL EVEN2(LAM, COV2, N, M, G, MAXG, ICORR, RHO, SIGMA,
     &      EIG, ICOUNT, IFAULT)
      ELSE
       CALL UNEVEN2(LAM, COV2, N, M, G, MAXG, ICORR, RHO, SIGMA,
     &       EIG, ICOUNT, IFAULT)
      ENDIF
      RETURN
      END

      SUBROUTINE EVEN2(LAM, COV2, N, M, G, MAXG, ICORR, RHO, SIGMA,
     &        EIG, ICOUNT, IFAULT)
      INTEGER MAXSIZE, MMAXSIZE
      PARAMETER (MAXSIZE = 1024, MMAXSIZE = MAXSIZE*MAXSIZE)
      DOUBLE PRECISION COV2
      EXTERNAL COV2, UPDATE
      DOUBLE PRECISION LAM(MMAXSIZE), RHO, SUM, Y(MMAXSIZE)
      INTEGER M(2), N(2), G(2), MAXG(2), IFAULT
      INTEGER MHALF(2), MBAR, MAXSUM
      INTEGER I, J, K, IAGAIN, INDEX
C     Parameters needed in subroutine UPDATE
      INTEGER GINIT(2), GTEMP(20,2), GSUM, NEW
      COMMON /A/ GINIT, GTEMP, GSUM, NEW
C     Subroutine from NAG library
```

```
      EXTERNAL C06FJF
C     Parameters used only in calling subroutine from NAG library
      DOUBLE PRECISION WORK(3*MAXSIZE)
      INTEGER LWORK, IFAIL
C     Parameters used only if IFAULT = 1
      DOUBLE PRECISION SIGMA, EIG(3)
      INTEGER ICORR, ICOUNT

C     If there are no initial values for g_1 and g_2, they are set
C     to be the smallest g_1 and g_2 such that 2^{g_i} >= 2(n_i -
C     1), i = 1, 2. If there are no maximum values for g_1 and g_2, C     they are set to be 10.

      DO 1 I = 1, 2
       IF (G(I) .EQ. 0) THEN
        RHO = DLOG(2D0*DBLE(N(I) - 1))/DLOG(2D0)
        GINIT(I) = IDINT(RHO)
        IF (DBLE(GINIT(I)) .LT. RHO) THEN
         GINIT(I) = GINIT(I) + 1
        ENDIF
       ELSE
        GINIT(I) = G(I)
       ENDIF
       GTEMP(1,I) = GINIT(I)
       IF (MAXG(I) .EQ. 0) THEN
        MAXG(I) = 10
       ENDIF
1     CONTINUE

C     Check GINIT before starting the loop
      IF ((GINIT(1) .GT. MAXG(1)) .OR.
     &    (GINIT(2) .GT. MAXG(2))) THEN
        IFAULT = 2
        GOTO 9
      ENDIF
      IAGAIN = 1
      IFAULT = 0
      ICOUNT = 0
      RHO = 1D0
      DO 2 I = 1, 3
       EIG(I) = 0D0
2     CONTINUE
      MAXSUM = MAXG(1) + MAXG(2)
      GSUM = GINIT(1) + GINIT(2)
      NEW = 1
C     Start the loop with the initial g_1 and g_2
      DO 3 WHILE ((IAGAIN .EQ. 1) .AND. (GSUM .LE. MAXSUM))
       DO 4 INDEX = 1, NEW
        SUM = 0D0
        DO 5 I = 1, 2
         M(I) = IDNINT(DEXP(DBLE(GTEMP(INDEX,I))*DLOG(DBLE(2))))
         MHALF(I) = IDINT(DBLE(M(I))/2D0)
5       CONTINUE
        MBAR = M(1)*M(2)
        LWORK = 3*MAX0(M(1), M(2))
C     Compute the eigenvalues of C, i.e. the discrete Fourier
C     transform of the first row of the embedding matrix
```

```
      DO 6 J = 0, M(2) - 1
       DO 7 I = 0, M(1) - 1
        K = I + 1
        IF ((I .LE. MHALF(1)) .AND. (J .LE. MHALF(2))) THEN
         LAM(K+J*M(1)) = COV2(DBLE(I)/DBLE(N(1)),
     &                        DBLE(J)/DBLE(N(2)))
        ELSEIF (J .LE. MHALF(2)) THEN
         LAM(K+J*M(1)) = LAM(M(1)-I+1+J*M(1))
        ELSE
         LAM(K+J*M(1)) = LAM(K+(M(2)-J)*M(1))
        ENDIF
        Y(K+J*M(1)) = 0D0
 7     CONTINUE
 6    CONTINUE
 C    Call subroutine C06FJF from NAG library to compute the DFT
      CALL C06FJF(2, M, MBAR, LAM, Y, WORK, LWORK, IFAIL)
 C    Check if all eigenvalues are non-negative
      DO 8 I = 1, MBAR
       SUM = SUM + LAM(I)
       IF (LAM(I) .LT. 0D0) THEN
        IF (GSUM .LT. MAXSUM) THEN
         IF (INDEX .LT. NEW) THEN
          GOTO 4
         ELSE
          CALL UPDATE(MAXG)
          GOTO 3
         ENDIF
        ELSE
         IF (LAM(I) .LT. EIG(1)) THEN
          EIG(1) = LAM(I)
         ENDIF
         EIG(2) = EIG(2) + DEXP(2D0*DLOG(-LAM(I)))
         EIG(3) = EIG(3) - LAM(I)
         ICOUNT = ICOUNT + 1
         LAM(I) = 0D0
         IFAULT = 1
        ENDIF
       ELSE
        LAM(I) = DSQRT(DBLE(MBAR))*LAM(I)
       ENDIF
 8    CONTINUE
      IAGAIN = 0
      G(1) = GTEMP(INDEX,1)
      G(2) = GTEMP(INDEX,2)
      GOTO 9
 4   CONTINUE
 3   ENDDO
 C   Warning messages which can be commented out.
 9   IF (IFAULT .EQ. 1) THEN
 C    Approximation takes place
      EIG(2) = DSQRT(EIG(2))
      IF (ICORR .EQ. 0) THEN
       RHO = SUM/(SUM + EIG(3))
      ELSEIF (ICORR .EQ. 1) THEN
       RHO = DSQRT(SUM/(SUM + EIG(3)))
      ENDIF
```

```
        SIGMA = DSQRT((DEXP(2D0*DLOG(1 - RHO))*SUM +
&          DEXP(2D0*DLOG(RHO))*EIG(3))/DBLE(MBAR))
       ELSEIF (IFAULT .EQ. 2) THEN
         STOP
       ENDIF
     M(1) = IDNINT(DEXP(DBLE(G(1))*DLOG(DBLE(2))))
     M(2) = IDNINT(DEXP(DBLE(G(2))*DLOG(DBLE(2))))
       RETURN
       END

       SUBROUTINE UNEVEN2(LAM,COV2, N, M, G, MAXG, ICORR, RHO, SIGMA,
&                EIG, ICOUNT, IFAULT)
       INTEGER MAXSIZE, MMAXSIZE
       PARAMETER (MAXSIZE = 1024, MMAXSIZE = MAXSIZE*MAXSIZE)
       DOUBLE PRECISION COV2
       EXTERNAL COV2, UPDATE
       DOUBLE PRECISION LAM(MMAXSIZE), RHO, SUM, Y(MMAXSIZE)
       INTEGER M(2), N(2), G(2), MAXG(2), IFAULT
       INTEGER MHALF(2), MBAR, MAXSUM
       INTEGER I, J, K, IAGAIN, INDEX
C      Parameters needed in subroutine UPDATE
       INTEGER GINIT(2), GTEMP(20,2), GSUM, NEW
       COMMON /A/ GINIT, GTEMP, GSUM, NEW
C      Subroutine from NAG library
       EXTERNAL C06FJF
C      Parameters used only in calling subroutine from NAG library
       DOUBLE PRECISION WORK(3*MAXSIZE)
       INTEGER LWORK, IFAIL
C      Parameters used only if IFAULT = 1
       DOUBLE PRECISION SIGMA, EIG(3)
       INTEGER ICORR, ICOUNT

C      If there are no initial values for g_1 and g_2, they are set
C      to be the smallest g_1 and g_2 such that 3^{g_i} >= 2(n_i –
C      1), i = 1, 2. If there are no maximum values for g_1 and g_2,  C      they are set to be 6.
     DO 1 I = 1, 2
      IF (G(I) .EQ. 0) THEN
          RHO = DLOG(2D0*DBLE(N(I) - 1))/DLOG(3D0)
       GINIT(I) = IDINT(RHO)
          IF (DBLE(GINIT(I)) .LT. RHO) THEN
           GINIT(I) = GINIT(I) + 1
          ENDIF
      ELSE
       GINIT(I) = G(I)
      ENDIF
      GTEMP(1,I) = GINIT(I)
      IF (MAXG(I) .EQ. 0) THEN
       MAXG(I) = 6
      ENDIF
1     CONTINUE

C     Check GINIT before starting the loop
     IF ((GINIT(1) .GT. MAXG(1)) .OR.
&       (GINIT(2) .GT. MAXG(2))) THEN
      IFAULT = 2
      GOTO 9
```

```
      ENDIF
          IAGAIN = 1
          IFAULT = 0
          ICOUNT = 0
          RHO = 1D0
          DO 2 I = 1, 3
            EIG(I) = 0D0
2         CONTINUE
          MAXSUM = MAXG(1) + MAXG(2)
          GSUM = GINIT(1) + GINIT(2)
          NEW = 1
C         Start the loop with the initial g_1 and g_2
          DO 3 WHILE ((IAGAIN .EQ. 1) .AND. (GSUM .LE. MAXSUM))
           DO 4 INDEX = 1, NEW
            SUM = 0D0
            DO 5 I = 1, 2
             M(I) = IDNINT(DEXP(DBLE(GTEMP(INDEX,I))*DLOG(DBLE(3))))
             MHALF(I) = IDINT(DBLE(M(I))/2D0)
5           CONTINUE
            MBAR = M(1)*M(2)
            LWORK = 3*MAX0(M(1), M(2))
C     Compute the eigenvalues of C, i.e. the discrete Fourier
C     transform of the first row of the embedding matrix
            DO 6 J = 0, M(2) - 1
             DO 7 I = 0, M(1) - 1
              K = I + 1
              IF (J .EQ. 0) THEN
             IF (I .LE. MHALF(1)) THEN
              LAM(K) = COV2(DBLE(I)/DBLE(N(1)), 0)
             ELSE
              LAM(K) = LAM(M(1)-I+1)
             ENDIF
            ELSEIF (J .LE. MHALF(2)) THEN
             IF (I .EQ. 0) THEN
                 LAM(1+J*M(1)) = COV2(0, DBLE(J)/DBLE(N(2)))
             ELSEIF (I .LE. MHALF(1)) THEN
              LAM(K+J*M(1)) = COV2(DBLE(I)/DBLE(N(1)),
&                    DBLE(J)/DBLE(N(2)))
             ELSE
              LAM(K+J*M(1)) = COV2(DBLE(I-M(1))/DBLE(N(1)),
&                    DBLE(J)/DBLE(N(2)))
             ENDIF
               ELSEIF (I .EQ. 0) THEN
             LAM(1+J*M(1)) = LAM(1+(M(2)-J)*M(1))
            ELSE
             LAM(K+J*M(1)) = LAM(M(1)-I+1+(M(2)-J)*M(1))
            ENDIF
               Y(K+J*M(1)) = 0D0
7           CONTINUE
6           CONTINUE
C           Call subroutine C06FJF from NAG library to compute the DFT
            CALL C06FJF(2, M, MBAR, LAM, Y, WORK, LWORK, IFAIL)
C           Check if all eigenvalues are non-negative
           DO 8 I = 1, MBAR
            SUM = SUM + LAM(I)
            IF (LAM(I) .LT. 0D0) THEN
```

```
      IF (GSUM .LT. MAXSUM) THEN
       IF (INDEX .LT. NEW) THEN
        GOTO 4
       ELSE
        CALL UPDATE(MAXG)
        GOTO 3
       ENDIF
      ELSE
       IF (LAM(I) .LT. EIG(1)) THEN
        EIG(1) = LAM(I)
       ENDIF
            ENDIF
            EIG(2) = EIG(2) + DEXP(2D0*DLOG(-LAM(I)))
            EIG(3) = EIG(3) - LAM(I)
            ICOUNT = ICOUNT + 1
            LAM(I) = 0D0
            IFAULT = 1
           ENDIF
              ELSE
               LAM(I) = DSQRT(DBLE(MBAR))*LAM(I)
          ENDIF
8        CONTINUE
        IAGAIN = 0
            G(1) = GTEMP(INDEX,1)
            G(2) = GTEMP(INDEX,2)
            GOTO 9
4      CONTINUE
3     ENDDO
C     Warning messages which can be commented out.
9        IF (IFAULT .EQ. 1) THEN
C         Approximation takes place
         EIG(2) = DSQRT(EIG(2))
         IF (ICORR .EQ. 0) THEN
          RHO = SUM/(SUM + EIG(3))
         ELSEIF (ICORR .EQ. 1) THEN
          RHO = DSQRT(SUM/(SUM + EIG(3)))
         ENDIF
         SIGMA = (DEXP(2D0*DLOG(1 - RHO))*SUM +
     &           DEXP(2D0*DLOG(RHO))*EIG(3))/DBLE(MBAR)
        ELSEIF (IFAULT .EQ. 2) THEN
          STOP
           ENDIF
        M(1) = IDNINT(DEXP(DBLE(G(1))*DLOG(DBLE(3))))
        M(2) = IDNINT(DEXP(DBLE(G(2))*DLOG(DBLE(3))))
            RETURN
            END

            SUBROUTINE UPDATE(MAXG)
      INTEGER MAXG(2), GINIT(2), GTEMP(20,2), GSUM
      INTEGER NEW, INC, DUMMY(2), I
      COMMON /A/ GINIT, GTEMP, GSUM, NEW

      NEW = 0
      GSUM = GSUM + 1
      INC = GSUM - GINIT(1) - GINIT(2)

      DO 1 I = 0, INC
```

```
          DUMMY(2) = GINIT(2) + I
          DUMMY(1) = GSUM - DUMMY(2)
          IF ((DUMMY(1) .LE. MAXG(1)) .AND. (DUMMY(2) .LE. MAXG(2))) THEN
           NEW = NEW + 1
           GTEMP(NEW,1) = DUMMY(1)
           GTEMP(NEW,2) = DUMMY(2)
          ENDIF
1         CONTINUE

          RETURN
          END


C         File name: simsgf2.f

C         This program was last modified on Tuesday 1 June, 1999.

C         Simulate the required 2 dimension Gaussian field.

C         Auxiliary Algorithms
C         Need to link with NAG library:
C         C06FJF - Computes the two-dimensional discrete Fourier
C         transform of a two-dimensional array of complex data values
C         G05CCF - Initialises random number generating routines to give
C                  non-repeatable sequence
C         G05FDF - Generates a vector of random numbers from a Normal
C                  distribution

          SUBROUTINE SIMSGF2(X, N, M, LAM, RHO)
          INTEGER MAXSIZE, MMAXSIZE
          PARAMETER (MAXSIZE = 1024, MMAXSIZE = MAXSIZE*MAXSIZE)

          DOUBLE PRECISION X(MMAXSIZE), LAM(MMAXSIZE), RHO, U(MMAXSIZE)
          DOUBLE PRECISION ARE(MMAXSIZE), AIM(MMAXSIZE), HALF(2), ADJUST
          INTEGER N(2), M(2), MHALF(2), MBAR
          INTEGER I, J, INDEX(2), INDEXU
C         Subroutine from NAG library
          EXTERNAL G05CCF, G05FDF, C06FJF
C         Parameters used only in calling subroutine from NAG library
          DOUBLE PRECISION WORK(3*MAXSIZE)
          INTEGER LWORK, IFAIL

          IFAIL = 0
          MBAR = M(1)*M(2)
          LWORK = 3*MAX0(M(1), M(2))
          ADJUST = DEXP(-DLOG(DBLE(2*MBAR))/2D0)
          DO 1 I = 1, 2
           HALF(I) = DBLE(M(I))/2D0
           MHALF(I) = IDINT(HALF(I))
1         CONTINUE
          INDEXU = 1
          CALL G05CCF
          CALL G05FDF(0D0, 1D0, MBAR, U)
          DO 2 J = 0, MHALF(2)
           DO 3 I = 0, MHALF(1)
            IF ((I .GT. 0) .AND. (I .LT. HALF(1)) .AND. (J .GT. 0)
```

```
     &        .AND. (J .LT. HALF(2))) THEN
                INDEX(1) = M(1) - I + 1 + (M(2) - J)*M(1)
                INDEX(2) = I + 1 + J*M(1)
                ARE(INDEX(1)) = DSQRT(LAM(INDEX(1)))*U(INDEXU)*ADJUST
                AIM(INDEX(1)) = DSQRT(LAM(INDEX(1)))*U(INDEXU+1)*ADJUST
                ARE(INDEX(2)) = DSQRT(LAM(INDEX(2)))*U(INDEXU)*ADJUST
                AIM(INDEX(2)) = -DSQRT(LAM(INDEX(2)))*U(INDEXU+1)*ADJUST
                INDEXU = INDEXU + 2
                INDEX(1) = M(1) - I + 1 + J*M(1)
                INDEX(2) = I + 1 + (M(2) - J)*M(1)
                ARE(INDEX(1)) = DSQRT(LAM(INDEX(1)))*U(INDEXU)*ADJUST
                AIM(INDEX(1)) = DSQRT(LAM(INDEX(1)))*U(INDEXU+1)*ADJUST
                ARE(INDEX(2)) = DSQRT(LAM(INDEX(2)))*U(INDEXU)*ADJUST
                AIM(INDEX(2)) = -DSQRT(LAM(INDEX(2)))*U(INDEXU+1)*ADJUST
                INDEXU = INDEXU + 2
              ELSEIF ((I .GT. 0) .AND. (I .LT. HALF(1))) THEN
                INDEX(1) = M(1) - I + 1 + J*M(1)
                INDEX(2) = I + 1 + J*M(1)
                ARE(INDEX(1)) = DSQRT(LAM(INDEX(1)))*U(INDEXU)*ADJUST
                AIM(INDEX(1)) = DSQRT(LAM(INDEX(1)))*U(INDEXU+1)*ADJUST
                ARE(INDEX(2)) = DSQRT(LAM(INDEX(2)))*U(INDEXU)*ADJUST
                AIM(INDEX(2)) = -DSQRT(LAM(INDEX(2)))*U(INDEXU+1)*ADJUST
                INDEXU = INDEXU + 2
              ELSEIF ((J .GT. 0) .AND. (J .LT. HALF(2))) THEN
                INDEX(1) = I + 1 + (M(2) - J)*M(1)
                INDEX(2) = I + 1 + J*M(1)
                ARE(INDEX(1)) = DSQRT(LAM(INDEX(1)))*U(INDEXU)*ADJUST
                AIM(INDEX(1)) = DSQRT(LAM(INDEX(1)))*U(INDEXU+1)*ADJUST
                ARE(INDEX(2)) = DSQRT(LAM(INDEX(2)))*U(INDEXU)*ADJUST
                AIM(INDEX(2)) = -DSQRT(LAM(INDEX(2)))*U(INDEXU+1)*ADJUST
                INDEXU = INDEXU + 2
              ELSE
                ARE(I+1+J*M(1)) = DSQRT(LAM(I+1+J*M(1)))*U(INDEXU)*ADJUST
                AIM(I+1+J*M(1)) = 0D0
                INDEXU = INDEXU + 1
              ENDIF
     3       CONTINUE
     2     CONTINUE
           CALL C06FJF(2, M, MBAR, ARE, AIM, WORK, LWORK, IFAIL)
           DO 4 J = 0, N(2) - 1
            DO 5 I = 1, N(1)
             X(I+J*M(1)) = RHO*DSQRT(DBLE(MBAR))*ARE(I+J*M(1))
     5      CONTINUE
     4     CONTINUE
           RETURN
           END
```

APPENDIX B

GPS/GALILEO Satellites Availability

The following Figures gives a comparison between the number of available satellites for GALILEO (E2L1E1 frequency) and GPS (L1 frequency) as an evidence for the assumption that GALILEO will offer more visible satellites globally compared with GPS.

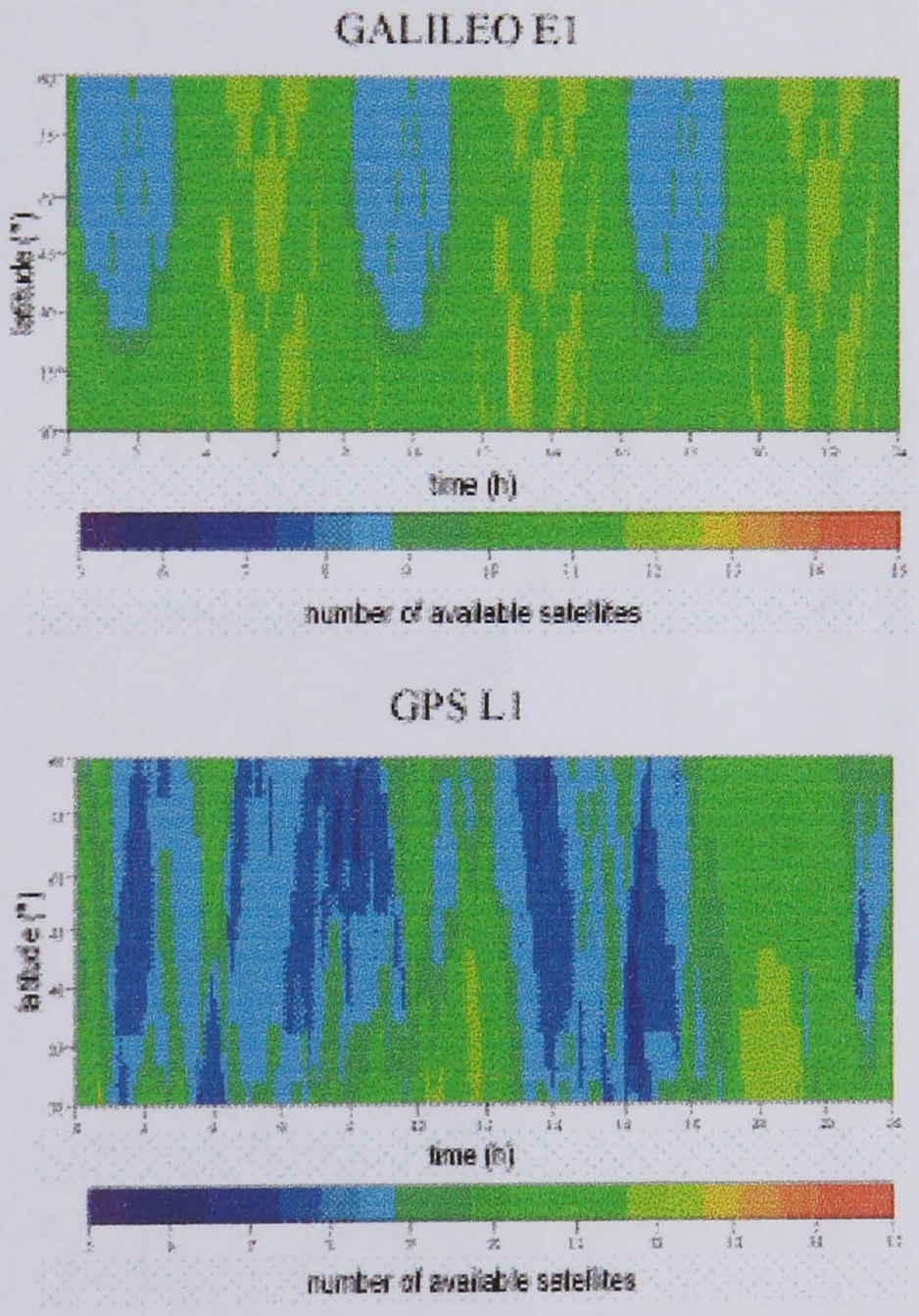

Latitude (30° min., 60° max., 5° step)
Time (0hr min., 24hr max., 2hr step)
Number of available satellites (5 sat. min., 15 sat. max., 1 sat. step)

Figure B.1: Comparison between the number of available satellites for GALILEO and GPS in middle Europe at 11th May 2001, elevation mask 5 degrees (Engler et al., 2001).

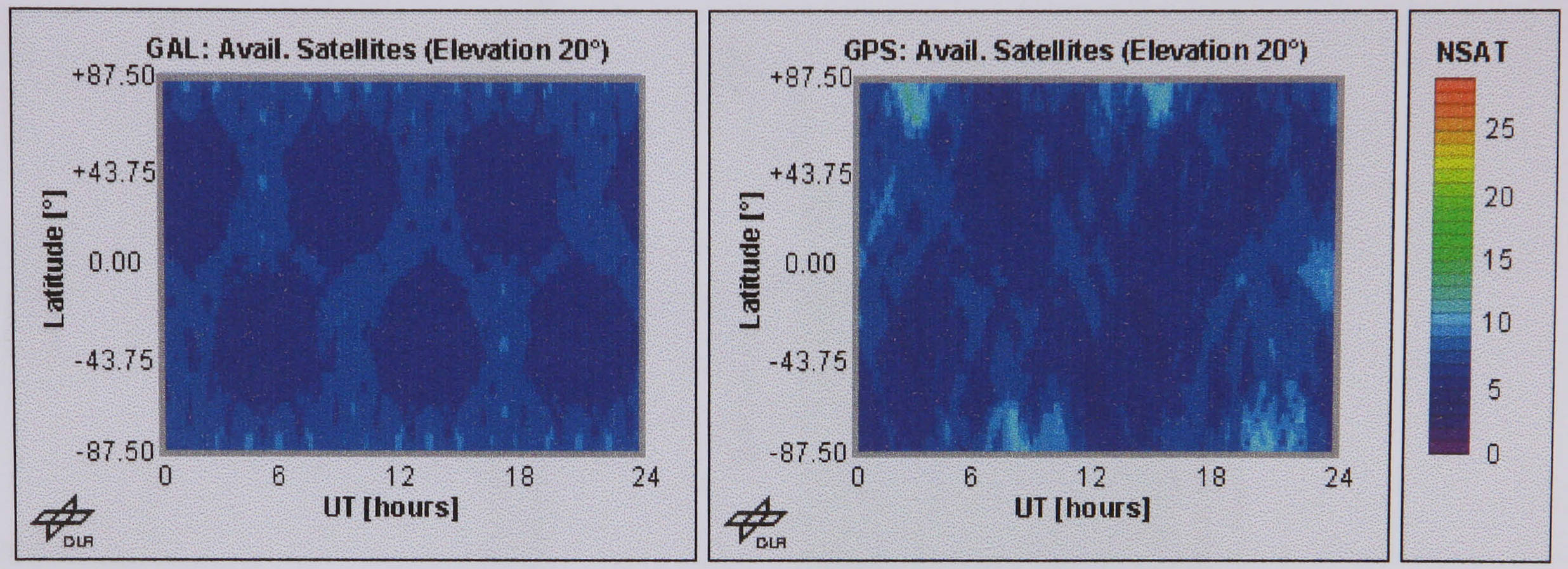

Figure B.2: The number of available satellites for GPS and GALILEO at 17th November 2003, elevation mask 20 degrees (Engler, 2004).

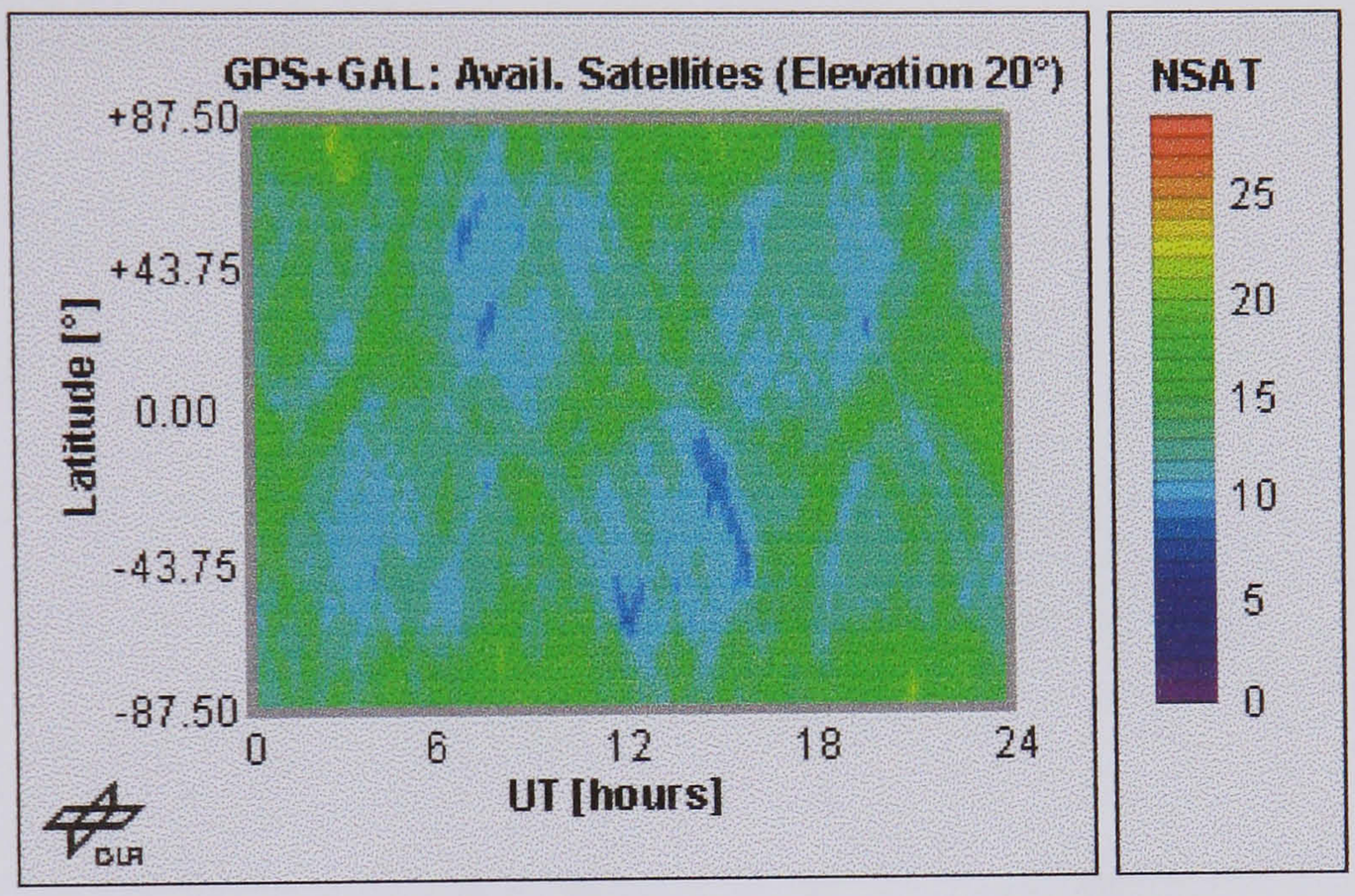

Figure B.3: The number of available satellites for GPS + GALILEO at 17th November 2003, elevation mask 20 degrees (Engler, 2004).

APPENDIX C

Rotation Matrices

After (Moore, 1986), the rotation for a right handed orthogonal coordinate system about the i^{th} axis, through an anticlockwise angle θ (viewed from the positive end of the axis towards the origin) may be expressed by a rotation matrix $R_i(\theta)$ where,

$$R_1(\theta) = \begin{bmatrix} 1 & 0 & 0 \\ 0 & \cos\theta & \sin\theta \\ 0 & -\sin\theta & \cos\theta \end{bmatrix} \quad \text{(C-1)}$$

$$R_2(\theta) = \begin{bmatrix} \cos\theta & 0 & -\sin\theta \\ 0 & 1 & 0 \\ \sin\theta & 0 & \cos\theta \end{bmatrix} \quad \text{(C-2)}$$

$$R_3(\theta) = \begin{bmatrix} \cos\theta & \sin\theta & 0 \\ -\sin\theta & \cos\theta & 0 \\ 0 & 0 & 1 \end{bmatrix} \quad \text{(C-3)}$$

The order of the execution for a number of rotations expressed as a product of the matrices must be strictly followed in order to the rotation matrices do not commute (Moore, 1986).

APPENDIX D

Reduced Dynamic Orbit Determination Technique

The reduced dynamic orbit determination technique is an orbit determination technique based on the Kalman filter theory. The reduced dynamic technique will be explicitly explained through this appendix after (Ashkenazi et al., 1996).

The reduced dynamic technique involved two steps; firstly a predicted orbit is integrated using the force models and an approximate initial starting elements (position and velocity). Secondly, Corrections to the predicted orbit are estimated in real time using the measurement and the statistical properties for both the measurement noise and force model errors.

When the predicted orbit is estimated using approximate initial state vector and force models, the predicted satellite position and velocity errors can be expressed as:

$$X(t)_{j+1} = \Phi_x(t_{j+1},t_j)X(t)_j + \Phi_p(t_{j+1},t_j)p(t)_j + \Phi_y(t_{j+1},t_j)y_j \qquad \text{(D-1)}$$

where; $X(t)$ is a vector including both satellite position and velocity errors.

$p(t)$ is the vector of unmodelled forces in radial, along-track and across track components.

y is the vector of constant parameters (air drag coefficient and solar radiation pressure coefficient).

j and $j+1$ two different epochs.

Φ the corresponding transition matrices.

The constant parameters can be simply modelled as

$$y_{j+1} = y_j \tag{D-2}$$

and the unmodelled force errors $p(t)$ are usually modelled as a first order Gauss-Markov process,

$$p(t)_{j+1} = m_{j+1,j}\, p(t)_j + n_p \tag{D-3}$$

$$m_{j+1,j} = \exp[1-(t_{j+1}-t_j)/\tau_{ij}] \tag{D-4}$$

where; $m_{j+1,j}$ is the noise mapping function.

n_p is the process noise.

τ_{ij} is the time constant of the process.

The variance of the noise n_p can be expressed as,

$$\sigma_p^2 = (1-m_{j+1,j}^2)\sigma_s^2 \tag{D-5}$$

where σ_s^2 is the steady state variance of the process.

The dynamic model for the kalman filter can then be constructed as :

$$\begin{pmatrix} X(t) \\ p(t) \\ y \end{pmatrix}_{j+1} = \begin{pmatrix} \Phi_x(t_{j+1},t_j) & \Phi_p(t_{j+1},t_j) & \Phi_y(t_{j+1},t_j) \\ 0 & m & 0 \\ 0 & 0 & I \end{pmatrix} \begin{pmatrix} X(t) \\ p(t) \\ y \end{pmatrix}_j + \begin{pmatrix} 0 \\ n_p \\ 0 \end{pmatrix}_j \qquad \text{(D-6)}$$

The linearised observation model for the GPS measurements can be formed as

$$l = AX(t) + n_r \qquad \text{(D-7)}$$

If the transition matrices in eqn.(D-6) are determined , the satellite position and velocity errors $X(t)$, together with other parameters can be estimated using a standard Kalman filtering method based on Eqns (D-6) and (D-7). The Kalman filter theory well documented in (Cross, 1982) and the main steps were summarised in appendix-E of this thesis.

In this research, a pseudo-epoch state approach (Bierman, 1977) is used in order to reduce the computational load. The pseudo-epoch state X_j is defined as:

$$X(t)_j = \Phi_x(t_j,t_0)X_j + \Phi_y(t_j,t_0)y \qquad \text{(D-8)}$$

which maps $X(t)_j$ to a initial epoch t_0, or

$$X_j = \Phi_x^{-1}(t_j,t_0)[X(t)_j - \Phi_y(t_j,t_0)y] \qquad \text{(D-9)}$$

After the transformation, the corresponding dynamic and observation equations can be obtained as,

$$\begin{pmatrix} X(t) \\ p(t) \\ y \end{pmatrix}_{j+1} = \begin{pmatrix} I & \Phi_p(j) & 0 \\ 0 & m & 0 \\ 0 & 0 & I \end{pmatrix} \begin{pmatrix} X \\ p(t) \\ y \end{pmatrix}_j + \begin{pmatrix} 0 \\ n_p \\ 0 \end{pmatrix}_j \qquad \text{(D-10)}$$

and

$$I_j = A\Phi_x(t_j, t_0)X_j + A\Phi_y(t_j, t_0)y \qquad \text{(D-11)}$$

$\Phi_p(j)$ can be calculated using,

$$\Phi_p(j) = [\Phi_x(t_{j+1}, t_0)]^{-1}\Phi_p(t_{j+1}, t_0) - [\Phi_x(t_j, t_0)]^{-1}\Phi_p(t_j, t_0) \qquad \text{(D-12)}$$

where $\Phi(t_j, t_0)$ are the corresponding partials from the orbit integration program at epoch j. After X_j has been estimated, the satellite position and velocity error $X(t)$ can be directly calculated using the mapping function eqn. (D-8).

APPENDIX E

Kalman Filtering

The kalman filtering technique is an ideal method for real time orbit determination.

Consider a general linear dynamic system,

$$X(k+1) = C(k+1,k)X(k) + W(k) \tag{E-1}$$

$$Y(k+1) = H(k+1)X(k+1) + V(k+1) \tag{E-2}$$

where, X is the state vector which includes the estimated parameters (satellite position and velocity and the force model coefficients).

Y is the observation vector.

C is the transition matrix which gives the relationship of the state vector in different epochs.

H is the design matrix which represents the relation between the measurements and the state vector to be estimated.

W is the dynamic model noise to define the precision of the dynamic model.

V is the observation noise which gives the precision of the measurements.

The dynamic and observations noises (W and V) are usually described by the normal distribution with the zero mean and the covariance matrices.

$$COV(W) = Q$$

$$COV(V) = R$$

The kalman filtering technique is an optimal estimation method and the optimal a posterior state vector estimation can be computed by the steps given below. The derivation of the kalman filtering equations is well documented in (Cross, 1982) on linear optimal estimation and therefore it is not given here.

Initial Conditions

Kalman filtering is a recursive procedure requiring the specification of the initial state vector $X(0)$ and its variance-covariance matrix $P(0)$. At the starting epoch K, the state vector eqn. (E-3) and the corresponding covariance matrix (eqn. (E-4)) at epoch K+1 can be predicted using eqn. (E-1).

$$X(k+1,k) = C(k+1,k)X(k,k) \tag{E-3}$$

$$P(k+1,k) = C(k+1,k)P(k,k)C^T(k+1,k) + Q \tag{E-4}$$

Filtering

When the external measurements Y(k+1) at epoch k+1 arrives, the estimation of X(k+1,k+1) and the covariance matrix P(k+1,k+1) can be considered as some form of modification of eqns. (E-3) and (E-4) using the new measurement.

$$X(k+1,k+1) = C(k+1,k) + G(k+1)[Y(k+1) - H(k+1)X(k+1,k)] \qquad \text{(E-5)}$$

and

$$P(k+1,k+1) = [I - G(k+1)H(k+1)]P(k+1,k) \qquad \text{(E-6)}$$

where I is the unit matrix and G (k+1) the gain matrix, which can be considered as a projection of the new measurement to the correction of the predicted state vector. Given by,

$$G(k+1) = P(k+1,k)H^T(k+1)[H(k+1)P(k+1,k)H^T(k+1) + R]^{-1} \qquad \text{(E-7)}$$

For orbit determination, the main task for using the Kalman filtering method is to form the dynamic eqn (E-1). The state vector X may include the satellite position, velocity, the errors related to the GPS receivers, such as the clock error, the tropospheric delay factors and ambiguities and the force model parameters such as the drag and radiation pressure coefficients.

The satellite position x and velocity v can be expressed as:

$$x(k+1) = x(k) + v(k)dt + 0.5a(k)dt^2 \qquad \text{(E-8)}$$

and

$$v(k+1) = v(k) + a(k)dt \qquad \text{(E-9)}$$

where a is the acceleration of the satellite.

APPENDIX F

GPS Broadcast Ephemeris Accuracy Statistics

Table F.1: GPS broadcast ephemeris accuracy statistics (compared with IGS final orbit)

Year 2002, Day 202
Overall R.M.S. = 3.73 m

PRN	X [m]			Y [m]			Z [m]			3D [m]		
	min	max	r.m.s	min	max	r.m.s	min	max	r.m.s	min	max	r.m.s
1	-5.329	5.333	2.499	-8.269	6.468	4.340	-3.497	3.546	2.190	1.384	8.543	5.466
2	-3.143	4.065	1.828	-4.321	3.949	1.962	-2.437	3.960	1.654	0.202	5.382	3.151
3	-2.181	1.194	0.784	-1.048	1.607	0.739	-1.212	2.142	0.776	0.327	2.526	1.327
4	-4.418	3.310	1.983	-4.972	6.918	3.285	-5.571	2.652	2.606	0.614	9.336	4.639
5	-3.201	2.306	1.690	-3.052	2.820	1.891	-1.555	1.609	0.860	0.909	4.124	2.678
6	-6.918	7.973	4.686	-4.165	3.059	1.957	-6.292	-0.595	3.220	0.854	10.148	6.013
7	-0.373	1.453	0.495	-2.845	2.386	1.456	-2.265	1.890	0.956	0.101	2.985	1.811
8	-2.181	1.055	1.098	-2.530	1.880	1.041	-1.482	2.255	1.032	0.719	2.883	1.832
9	-1.377	3.820	1.050	-2.788	4.296	1.815	-1.819	2.333	1.129	0.372	4.755	2.381
10	-1.888	2.853	1.275	-1.989	0.795	0.952	-2.664	1.767	1.302	0.638	3.586	2.056
11	-1.789	1.499	1.058	-1.228	1.653	0.575	-1.666	1.483	0.836	0.407	2.279	1.466
12	---	---	---	---	---	---	---	---	---	---	---	---
13	-2.632	2.756	1.359	-1.808	1.897	1.000	-2.720	1.018	1.042	0.176	3.413	1.983
14	-3.218	3.844	2.045	-3.586	3.869	2.084	-2.426	2.300	1.553	2.074	4.650	3.307
15	-5.177	9.822	5.215	-7.758	10.727	5.163	-8.542	6.575	4.530	2.960	11.759	8.624
16	---	---	---	---	---	---	---	---	---	---	---	---
17	-1.836	1.579	1.047	-4.981	2.440	2.077	-5.125	1.721	1.909	0.887	5.984	3.009
18	-5.117	2.694	1.761	-3.447	3.439	1.923	-2.699	3.504	1.626	1.424	5.159	3.073
19	---	---	---	---	---	---	---	---	---	---	---	---
20	-2.009	2.355	1.276	-1.888	0.857	0.806	-1.350	0.665	0.532	0.327	2.651	1.600
21	-4.464	3.068	2.755	-7.869	3.479	3.579	-7.449	6.757	3.654	0.668	10.136	5.809
22	-1.377	2.429	1.061	-2.120	2.714	1.398	-1.650	2.003	1.003	0.579	3.166	2.022
23	-4.317	4.648	2.561	-3.364	2.964	1.798	-3.790	1.269	1.743	1.723	5.382	3.582
24	-2.958	9.950	3.371	-4.994	5.262	2.712	-9.414	2.101	3.995	0.608	12.279	5.889
25	-5.574	4.666	2.826	-3.351	4.862	2.302	-5.955	3.325	3.150	0.654	7.247	4.817
26	-3.135	3.219	1.435	-0.926	2.259	0.761	-2.732	2.078	1.152	0.196	3.413	1.991
27	-6.259	4.135	2.958	-2.428	4.158	2.116	-7.280	6.290	3.536	1.407	7.806	5.072
28	-1.516	1.567	0.943	-1.259	1.552	0.935	-1.902	1.690	1.043	1.440	2.013	1.689
29	-2.015	1.974	0.939	-1.121	0.984	0.574	-1.736	1.329	0.789	0.350	2.271	1.354
30	-1.642	2.955	1.272	-1.402	2.995	1.102	-3.039	2.696	1.627	0.603	3.672	2.341
31	-1.679	2.530	1.283	-2.548	3.184	1.497	-2.316	1.911	1.232	0.139	4.308	2.326
32	---	---	---	---	---	---	---	---	---	---	---	---

University of New Brunswick
Department of Geodesy and Geomatics Engineering

(GPS Lab, 2004)

Table F.2: GPS broadcast ephemeris accuracy statistics (compared with IGS final orbit)

Year 2002, Day 203
Overall R.M.S. = 4.70 m

PRN	X [m]			Y [m]			Z [m]			3D [m]		
	min	max	r.m.s	min	max	r.m.s	min	max	r.m.s	min	max	r.m.s
1	-4.444	4.526	2.203	-7.834	8.197	4.579	-3.875	3.679	2.477	1.717	8.542	5.653
2	-3.212	3.884	1.643	-4.326	2.910	2.028	-2.755	3.418	1.578	0.712	5.336	3.050
3	-1.817	2.191	1.177	-2.326	3.945	1.755	-2.367	3.973	1.575	0.666	4.795	2.636
4	-4.944	3.397	2.452	-3.936	6.529	3.471	-4.099	2.004	1.979	0.458	8.385	4.688
5	-5.021	1.897	2.043	-4.830	4.037	2.353	-4.661	5.619	2.785	1.345	6.094	4.179
6	-5.530	5.712	3.235	-4.173	5.297	2.247	-6.221	1.360	3.401	1.412	6.402	5.204
7	-1.847	1.554	0.933	-2.525	3.006	1.612	-2.151	1.352	0.817	0.356	3.538	2.033
8	-5.297	3.510	1.974	-2.537	4.743	2.265	-1.686	4.570	1.937	0.128	7.175	3.575
9	-2.840	3.112	1.326	-2.918	0.892	0.981	-2.528	3.183	1.619	0.484	4.340	2.311
10	-2.807	3.063	1.639	-1.688	2.280	1.019	-4.184	0.814	1.677	0.776	4.470	2.557
11	-2.720	1.582	1.337	-1.145	1.384	0.623	-1.939	1.688	0.950	0.637	2.831	1.754
12	---	---	---	---	---	---	---	---	---	---	---	---
13	-2.917	1.862	1.553	-2.137	2.179	1.006	-2.322	0.590	0.894	0.638	3.737	2.055
14	-3.114	3.496	2.047	-4.036	4.869	2.374	-2.218	2.346	1.372	2.065	4.943	3.422
15	-18.590	10.178	8.967	-19.360	9.411	6.905	-20.823	11.930	8.420	2.522	26.435	14.106
16	---	---	---	---	---	---	---	---	---	---	---	---
17	-3.103	1.288	1.230	-3.741	3.191	1.934	-4.165	1.502	1.717	0.682	4.966	2.864
18	-2.033	2.204	1.330	-3.376	3.328	1.911	-2.331	1.963	1.086	0.874	3.915	2.569
19	---	---	---	---	---	---	---	---	---	---	---	---
20	-3.413	3.538	2.207	-2.766	2.047	1.728	-2.580	1.487	1.148	1.607	4.599	3.029
21	-4.528	2.929	2.772	-8.500	3.214	3.729	-7.514	6.433	3.417	0.657	10.504	5.768
22	-1.258	2.989	1.198	-2.276	3.283	1.277	-3.252	2.099	1.349	1.009	3.724	2.210
23	-5.232	3.932	2.669	-4.794	2.694	2.167	-3.586	0.975	1.564	1.840	5.860	3.777
24	-20.308	9.880	7.427	-7.693	10.236	5.180	-17.124	6.209	6.592	1.302	22.356	11.201
25	-3.748	4.518	2.617	-2.977	1.747	1.367	-2.588	1.730	1.512	0.654	4.893	3.317
26	-2.446	3.920	1.252	-1.757	1.318	0.642	-1.850	1.636	0.924	0.348	4.146	1.684
27	-3.487	3.348	1.626	-1.041	1.941	0.922	-1.996	3.100	1.516	0.844	4.261	2.407
28	-2.725	1.624	1.657	-3.584	2.263	1.851	-3.462	3.060	1.816	1.881	3.844	3.078
29	-3.039	3.025	1.649	-2.745	6.188	2.805	-3.266	2.445	1.367	1.244	6.771	3.529
30	-2.760	1.954	1.405	-3.377	2.472	1.314	-2.929	3.647	2.099	1.656	3.906	2.847
31	-2.011	2.499	1.279	-2.181	2.345	1.346	-2.455	2.758	1.472	0.521	3.665	2.370
32	---	---	---	---	---	---	---	---	---	---	---	---

University of New Brunswick
Department of Geodesy and Geomatics Engineering

(GPS Lab, 2004)

Table F.3: GPS broadcast ephemeris accuracy statistics (compared with IGS rapid orbit)

Year 2002, Day 202
Overall R.M.S. = 3.73 m

PRN	X [m]			Y [m]			Z [m]			3D [m]		
	min	max	r.m.s	min	max	r.m.s	min	max	r.m.s	min	max	r.m.s
1	-5.338	5.352	2.505	-8.266	6.482	4.342	-3.496	3.546	2.190	1.397	8.541	5.471
2	-3.143	4.047	1.825	-4.325	3.962	1.963	-2.427	3.961	1.657	0.214	5.386	3.152
3	-2.196	1.199	0.785	-1.077	1.617	0.744	-1.204	2.197	0.787	0.322	2.579	1.337
4	-4.433	3.313	1.982	-4.976	6.908	3.287	-5.597	2.645	2.631	0.606	9.348	4.653
5	-3.245	2.326	1.704	-3.062	2.799	1.889	-1.567	1.653	0.876	0.893	4.172	2.691
6	-6.916	7.961	4.685	-4.160	3.032	1.950	-6.280	-0.581	3.211	0.843	10.134	6.005
7	-0.395	1.487	0.507	-2.845	2.381	1.452	-2.251	1.901	0.956	0.095	2.972	1.811
8	-2.155	1.056	1.103	-2.494	1.865	1.031	-1.461	2.230	1.026	0.721	2.852	1.825
9	-1.384	3.825	1.053	-2.773	4.309	1.818	-1.805	2.328	1.127	0.385	4.771	2.384
10	-1.857	2.814	1.252	-1.980	0.824	0.947	-2.626	1.769	1.286	0.648	3.516	2.029
11	-1.784	1.545	1.059	-1.235	1.657	0.574	-1.692	1.486	0.851	0.383	2.295	1.475
12	---	---	---	---	---	---	---	---	---	---	---	---
13	-2.650	2.763	1.364	-1.808	1.889	1.003	-2.679	1.022	1.034	0.233	3.374	1.984
14	-3.228	3.859	2.050	-3.602	3.909	2.087	-2.436	2.287	1.558	2.094	4.656	3.314
15	-5.175	9.825	5.176	-7.790	10.765	5.361	-8.574	6.611	4.538	2.952	11.741	8.725
16	---	---	---	---	---	---	---	---	---	---	---	---
17	-1.805	1.577	1.045	-4.975	2.439	2.080	-5.103	1.740	1.903	0.876	5.971	3.007
18	-5.116	2.725	1.763	-3.455	3.472	1.933	-2.723	3.494	1.639	1.444	5.160	3.087
19	---	---	---	---	---	---	---	---	---	---	---	---
20	-1.983	2.321	1.266	-1.877	0.857	0.798	-1.334	0.683	0.533	0.344	2.624	1.588
21	-4.484	3.089	2.765	-7.893	3.464	3.588	-7.492	6.764	3.669	0.644	10.173	5.830
22	-1.378	2.395	1.054	-2.128	2.711	1.398	-1.622	2.021	1.001	0.570	3.158	2.017
23	-4.275	4.645	2.549	-3.366	2.978	1.803	-3.757	1.274	1.733	1.727	5.389	3.571
24	-3.007	9.631	3.247	-5.270	5.283	2.771	-9.089	2.075	3.905	0.789	11.916	5.785
25	-5.572	4.661	2.824	-3.354	4.873	2.307	-5.961	3.323	3.154	0.661	7.254	4.821
26	-3.130	3.179	1.428	-0.922	2.273	0.765	-2.762	2.083	1.161	0.211	3.415	1.993
27	-6.235	4.122	2.946	-2.377	4.157	2.106	-7.241	6.278	3.524	1.395	7.752	5.052
28	-1.467	1.593	0.935	-1.264	1.535	0.935	-1.876	1.677	1.034	1.415	2.030	1.678
29	-2.006	1.955	0.936	-1.107	0.969	0.574	-1.758	1.344	0.795	0.365	2.248	1.356
30	-1.621	2.955	1.270	-1.426	2.987	1.102	-3.009	2.709	1.626	0.629	3.669	2.339
31	-1.676	2.546	1.283	-2.506	3.203	1.488	-2.287	1.903	1.226	0.164	4.341	2.315
32	---	---	---	---	---	---	---	---	---	---	---	---

University of New Brunswick
Department of Geodesy and Geomatics Engineering

(GPS Lab, 2004)

Table F.4: GPS broadcast ephemeris accuracy statistics (compared with IGS rapid orbit)

Year 2002, Day 203
Overall R.M.S. = 4.69 m

PRN	X [m]			Y [m]			Z [m]			3D [m]		
	min	max	r.m.s	min	max	r.m.s	min	max	r.m.s	min	max	r.m.s
1	-4.462	4.545	2.208	-7.837	8.201	4.580	-3.896	3.689	2.490	1.732	8.543	5.662
2	-3.280	3.787	1.639	-4.381	2.946	2.049	-2.694	3.404	1.563	0.722	5.288	3.055
3	-1.829	2.192	1.182	-2.336	3.915	1.746	-2.336	3.982	1.572	0.652	4.785	2.630
4	-4.921	3.388	2.436	-3.927	6.495	3.438	-4.109	1.985	1.979	0.454	8.356	4.655
5	-5.018	1.902	2.046	-4.858	4.018	2.360	-4.697	5.588	2.783	1.361	6.103	4.184
6	-5.538	5.698	3.238	-4.192	5.281	2.243	-6.229	1.362	3.397	1.419	6.408	5.201
7	-1.807	1.543	0.914	-2.477	3.001	1.597	-2.122	1.359	0.811	0.376	3.474	2.011
8	-5.292	3.497	1.967	-2.498	4.729	2.258	-1.679	4.564	1.931	0.157	7.164	3.563
9	-2.823	3.192	1.332	-2.955	0.869	0.992	-2.519	3.210	1.622	0.459	4.412	2.322
10	-2.801	3.040	1.629	-1.704	2.271	1.018	-4.207	0.787	1.682	0.785	4.487	2.553
11	-2.750	1.633	1.355	-1.216	1.439	0.666	-1.968	1.727	0.969	0.715	2.866	1.794
12	---	---	---	---	---	---	---	---	---	---	---	---
13	-2.904	1.820	1.533	-2.105	2.179	0.998	-2.306	0.595	0.890	0.622	3.718	2.034
14	-3.112	3.494	2.048	-4.021	4.886	2.373	-2.218	2.328	1.380	2.074	4.962	3.424
15	-18.577	10.175	8.965	-19.345	9.381	6.896	-20.813	11.924	8.416	2.527	26.429	14.098
16	---	---	---	---	---	---	---	---	---	---	---	---
17	-3.101	1.300	1.231	-3.720	3.182	1.933	-4.150	1.495	1.712	0.684	4.953	2.860
18	-2.042	2.201	1.327	-3.376	3.347	1.908	-2.339	1.940	1.092	0.893	3.932	2.568
19	---	---	---	---	---	---	---	---	---	---	---	---
20	-3.417	3.512	2.211	-2.764	2.074	1.733	-2.597	1.524	1.161	1.625	4.569	3.040
21	-4.530	2.924	2.777	-8.502	3.218	3.732	-7.533	6.428	3.425	0.676	10.515	5.777
22	-1.266	2.982	1.197	-2.280	3.273	1.273	-3.241	2.116	1.345	1.013	3.712	2.205
23	-5.211	3.923	2.663	-4.768	2.684	2.165	-3.570	0.992	1.558	1.838	5.837	3.769
24	-20.310	9.880	7.446	-7.692	10.251	5.212	-17.144	6.206	6.461	1.290	22.362	11.151
25	-3.744	4.554	2.629	-2.972	1.723	1.369	-2.600	1.737	1.517	0.680	4.934	3.330
26	-2.429	3.897	1.240	-1.761	1.302	0.641	-1.845	1.629	0.922	0.344	4.120	1.673
27	-3.481	3.333	1.628	-1.042	1.922	0.919	-1.993	3.078	1.503	0.825	4.256	2.398
28	-2.707	1.634	1.659	-3.558	2.273	1.859	-3.461	3.074	1.820	1.920	3.809	3.085
29	-3.056	3.030	1.647	-2.738	6.176	2.804	-3.255	2.444	1.365	1.245	6.760	3.527
30	-2.775	1.948	1.410	-3.395	2.460	1.315	-2.932	3.640	2.099	1.646	3.919	2.850
31	-2.008	2.506	1.271	-2.152	2.324	1.327	-2.439	2.762	1.468	0.502	3.660	2.352
32	---	---	---	---	---	---	---	---	---	---	---	---

University of New Brunswick
Department of Geodesy and Geomatics Engineering

(GPS Lab, 2004)

Table F.5: GPS broadcast ephemeris accuracy statistics (compared with IGS predicted (UltraRapid) orbit)

Year 2002, Day 202
Overall R.M.S. = 3.44 m

PRN	X [m]			Y [m]			Z [m]			3D [m]		
	min	max	r.m.s	min	max	r.m.s	min	max	r.m.s	min	max	r.m.s
1	-5.390	5.340	2.512	-8.304	6.457	4.351	-3.498	3.602	2.185	1.434	8.584	5.479
2	-3.225	4.111	1.840	-4.269	3.933	1.990	-2.515	4.124	1.716	0.163	5.405	3.208
3	-1.965	1.154	0.729	-1.027	1.814	0.830	-1.118	2.127	0.772	0.393	2.491	1.348
4	-3.824	2.651	1.444	-4.390	5.830	2.616	-4.904	2.241	2.321	0.979	7.955	3.784
5	-3.173	2.389	1.717	-3.121	2.956	1.976	-1.573	1.574	0.862	0.974	4.152	2.756
6	-6.859	7.872	4.612	-4.083	2.921	1.902	-6.201	-0.604	3.166	0.884	9.915	5.909
7	-0.474	1.702	0.573	-2.825	2.238	1.427	-2.232	1.819	0.890	0.044	2.961	1.776
8	-2.092	0.941	1.096	-2.483	1.829	1.036	-1.430	2.147	1.021	0.680	2.782	1.822
9	-1.437	3.734	1.109	-2.902	4.573	1.949	-1.980	2.437	1.172	0.319	5.021	2.530
10	-2.134	2.199	1.089	-2.358	1.148	0.944	-3.051	2.216	1.414	0.495	3.129	2.019
11	-1.778	1.622	1.075	-1.186	1.553	0.599	-1.682	1.504	0.808	0.125	2.280	1.473
12	---	---	---	---	---	---	---	---	---	---	---	---
13	-2.659	2.921	1.410	-1.920	2.000	1.043	-2.822	1.108	1.069	0.251	3.546	2.054
14	-3.216	3.779	2.023	-3.512	3.840	2.032	-2.441	2.312	1.533	2.066	4.429	3.252
15	-4.775	9.115	4.638	-7.282	9.614	4.789	-7.434	6.201	4.057	2.879	10.346	7.804
16	---	---	---	---	---	---	---	---	---	---	---	---
17	-1.812	1.451	0.952	-4.728	2.368	1.926	-4.997	1.725	1.818	0.851	5.686	2.815
18	-5.453	3.262	2.009	-3.902	3.988	2.216	-3.043	3.704	1.846	1.763	5.506	3.515
19	---	---	---	---	---	---	---	---	---	---	---	---
20	-2.066	2.383	1.305	-2.017	1.084	0.898	-1.425	0.841	0.588	0.496	2.727	1.689
21	---	---	---	---	---	---	---	---	---	---	---	---
22	-1.499	2.532	1.098	-2.169	2.869	1.426	-1.820	1.878	1.021	0.469	3.379	2.069
23	-4.354	4.741	2.584	-3.158	3.062	1.764	-3.859	1.405	1.783	1.707	5.524	3.601
24	-3.323	2.576	1.372	-4.519	6.298	2.685	-4.606	2.013	2.532	0.520	6.434	3.937
25	-5.517	4.762	2.817	-3.547	4.884	2.362	-5.877	3.473	3.198	0.711	7.197	4.872
26	-3.088	3.232	1.421	-0.870	2.288	0.774	-2.808	2.040	1.158	0.198	3.396	1.990
27	-6.367	4.125	2.997	-2.401	4.236	2.132	-7.307	6.293	3.523	1.478	7.850	5.094
28	-1.509	1.627	0.959	-1.266	1.519	0.923	-1.817	1.691	1.029	1.417	2.072	1.683
29	-1.959	2.147	0.954	-1.206	0.922	0.589	-1.724	1.293	0.782	0.447	2.469	1.367
30	-1.650	3.082	1.325	-1.449	3.108	1.139	-3.089	2.781	1.694	0.656	3.861	2.434
31	-1.732	2.584	1.299	-2.618	3.269	1.521	-2.417	1.974	1.273	0.170	4.415	2.371
32	---	---	---	---	---	---	---	---	---	---	---	---

University of New Brunswick
Department of Geodesy and Geomatics Engineering

(GPS Lab, 2004)

Table F.6: GPS broadcast ephemeris accuracy statistics (compared with IGS predicted (UltraRapid) orbit)

Year 2002, Day 203
Overall R.M.S. = 8.22 m

PRN	X [m]			Y [m]			Z [m]			3D [m]		
	min	max	r.m.s	min	max	r.m.s	min	max	r.m.s	min	max	r.m.s
1	-4.500	4.674	2.261	-7.882	8.337	4.618	-3.869	3.669	2.494	1.857	8.685	5.715
2	-3.259	3.885	1.628	-3.981	3.732	2.043	-2.900	3.531	1.570	0.306	5.410	3.048
3	-1.783	2.255	1.161	-2.424	4.034	1.805	-2.404	4.113	1.598	0.633	4.936	2.676
4	-4.731	2.997	2.391	-3.957	6.708	3.358	-4.726	3.091	2.302	0.872	8.741	4.721
5	-5.135	1.952	2.080	-4.828	4.061	2.353	-4.737	5.735	2.833	1.362	6.117	4.230
6	-5.499	5.733	3.228	-4.118	5.278	2.240	-6.269	1.357	3.399	1.454	6.446	5.195
7	-1.670	1.449	0.866	-2.514	2.889	1.553	-1.982	1.242	0.753	0.429	3.408	1.931
8	-5.115	3.458	1.902	-2.449	4.578	2.184	-1.573	4.350	1.868	0.282	6.927	3.447
9	-2.725	2.891	1.244	-2.735	0.822	0.924	-2.428	2.920	1.530	0.404	3.991	2.178
10	-2.785	3.008	1.610	-1.731	2.178	0.985	-4.363	0.763	1.705	0.812	4.645	2.543
11	-2.756	1.695	1.312	-0.790	1.454	0.553	-2.090	1.866	1.002	0.549	2.866	1.741
12	---	---	---	---	---	---	---	---	---	---	---	---
13	-2.716	1.729	1.440	-1.944	2.040	0.910	-2.078	0.573	0.807	0.518	3.429	1.885
14	-3.133	3.591	2.077	-4.048	4.955	2.392	-2.266	2.413	1.390	2.191	5.039	3.460
15	-41.638	16.677	23.246	-49.801	31.320	22.264	-46.370	52.220	22.218	3.674	65.860	39.111
16	---	---	---	---	---	---	---	---	---	---	---	---
17	-3.492	1.306	1.388	-3.417	3.322	2.044	-5.135	2.151	1.827	0.787	5.977	3.073
18	-2.078	2.306	1.384	-3.499	3.498	1.989	-2.377	1.981	1.113	0.871	4.071	2.666
19	---	---	---	---	---	---	---	---	---	---	---	---
20	-3.371	3.518	2.173	-2.770	2.051	1.719	-2.542	1.533	1.138	1.586	4.496	2.995
21	-4.526	2.895	2.742	-8.510	3.196	3.724	-7.435	6.578	3.419	0.636	10.447	5.751
22	-1.172	2.830	1.185	-2.202	3.098	1.234	-3.069	1.984	1.300	0.932	3.510	2.149
23	-5.206	4.056	2.693	-4.745	2.705	2.131	-3.302	1.035	1.439	1.835	5.748	3.723
24	---	---	---	---	---	---	---	---	---	---	---	---
25	-3.911	4.898	2.712	-3.196	1.838	1.425	-2.560	1.671	1.474	0.530	5.256	3.400
26	-2.592	4.028	1.287	-1.857	1.357	0.641	-1.880	1.713	0.972	0.405	4.270	1.735
27	-3.349	3.313	1.600	-1.000	1.868	0.902	-1.871	2.934	1.445	0.697	4.125	2.337
28	-2.605	1.574	1.631	-3.491	2.299	1.834	-3.482	3.066	1.776	1.822	3.715	3.029
29	-2.942	2.783	1.472	-2.664	5.937	2.633	-3.179	1.977	1.238	1.189	6.472	3.261
30	-2.959	2.002	1.462	-3.472	2.534	1.332	-2.953	3.835	2.149	1.670	4.069	2.921
31	-1.992	2.616	1.295	-2.177	2.397	1.366	-2.429	2.912	1.492	0.516	3.821	2.402
32	---	---	---	---	---	---	---	---	---	---	---	---

University of New Brunswick
Department of Geodesy and Geomatics Engineering

(GPS Lab, 2004)

APPENDIX G

Radial Orbital Error Plots

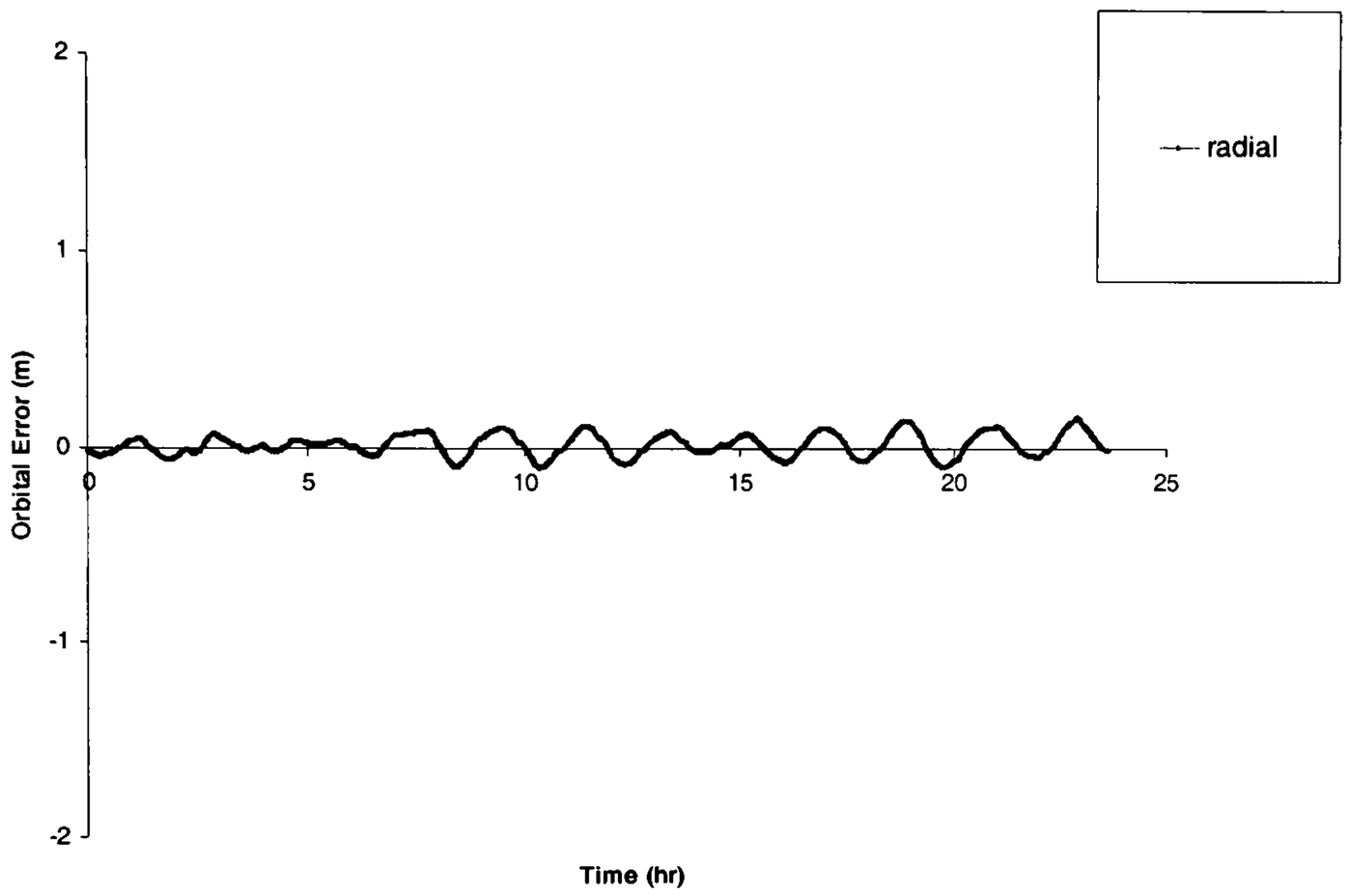

Figure (7.1): Reduced Dynamic Solution for stand alone simulated GPS receiver (GPS Broadcast Ephemeris)

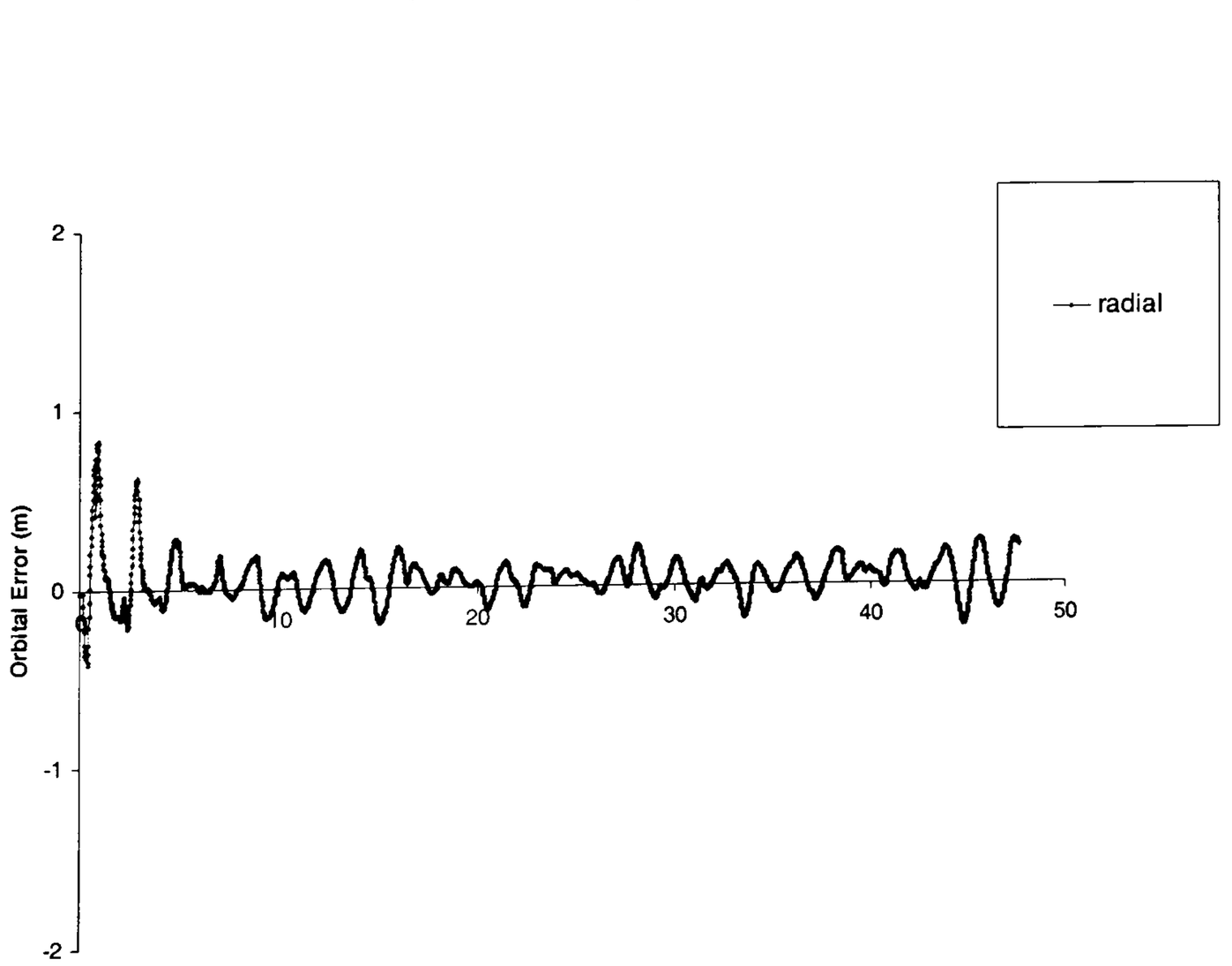

Figure (7.2): Reduced Dynamic Solution for Standalone simulated GPS receiver (GPS Broadcast Ephemeris) (two day arc)

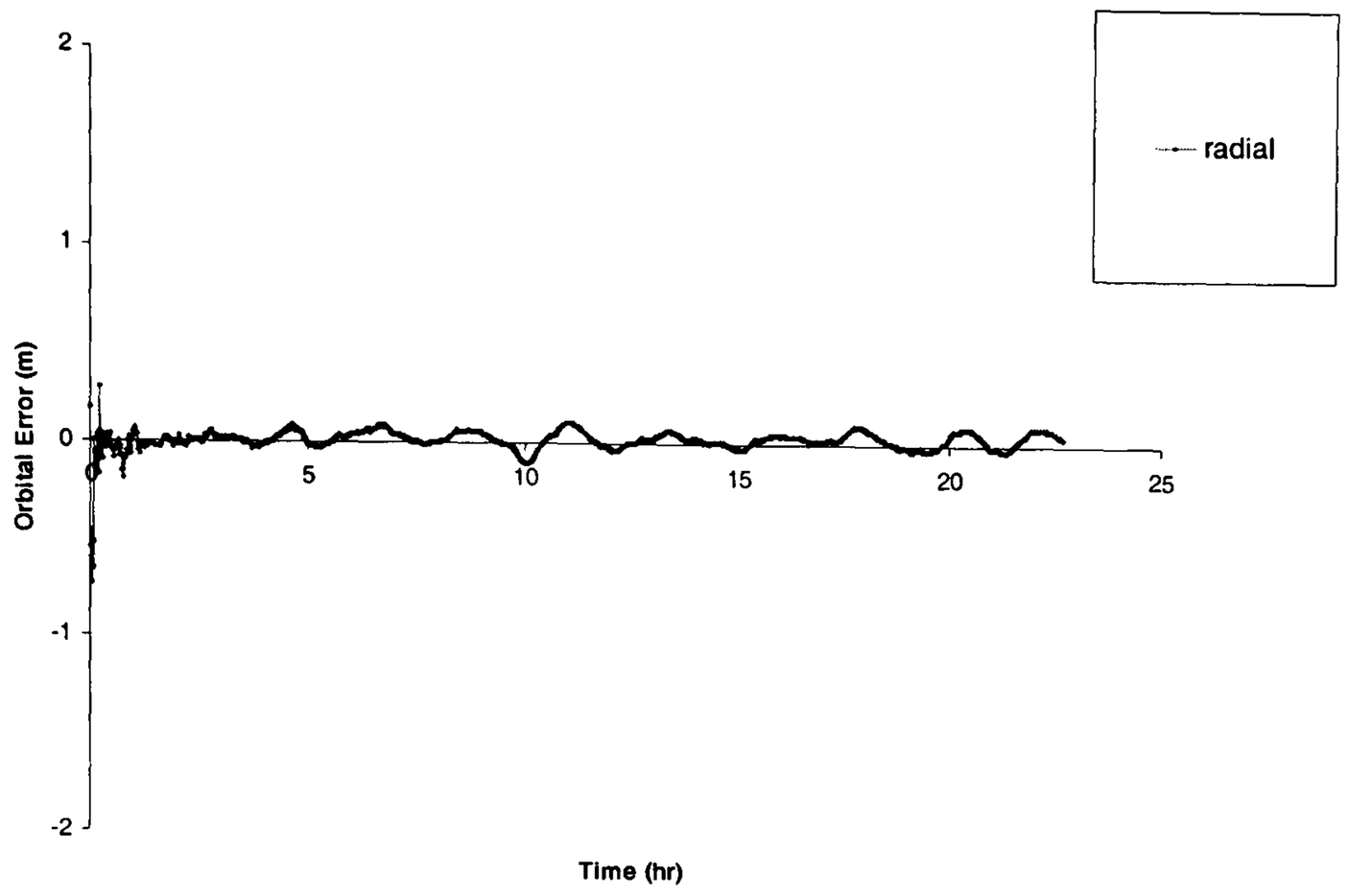

Figure (7.3): Reduced Dynamic Solution for stand alone simulated GPS receiver (IGS UltraRapid GPS Orbits) (one day arc)

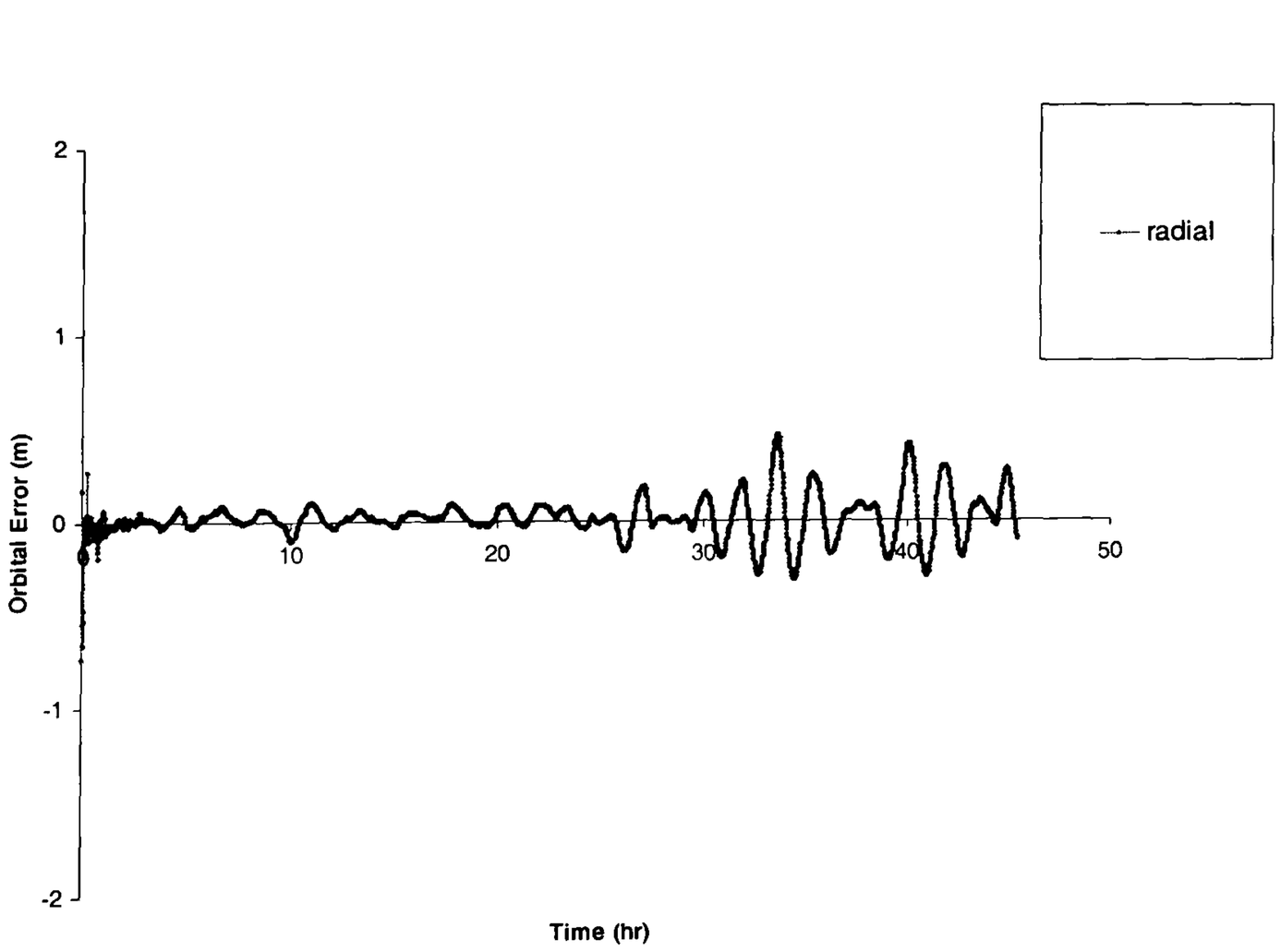

Figure (7.4): Reduced Dynamic Solution for Standalone simulated GPS receiver (IGS UltraRapid GPS Orbits) (two days arc)

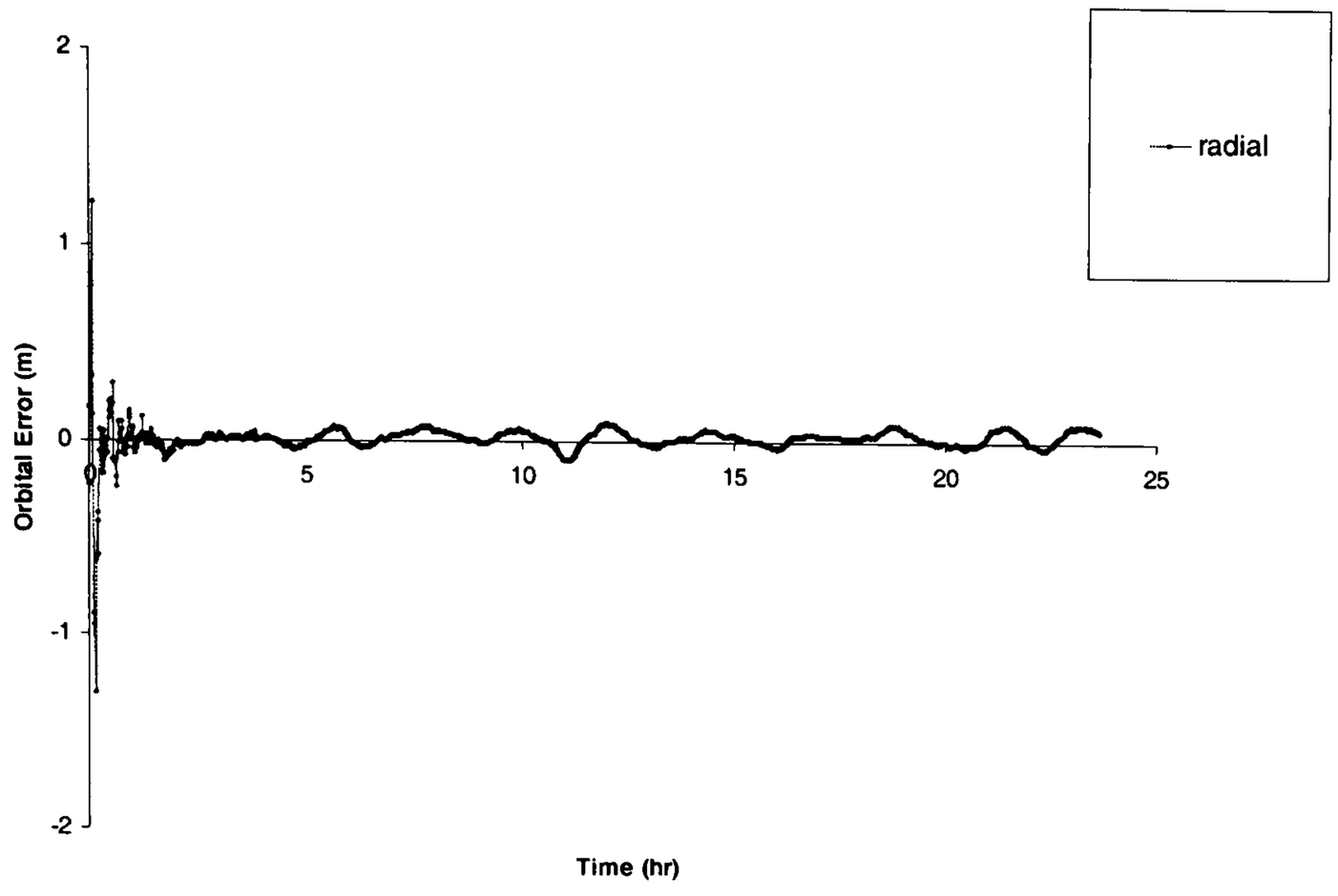

Figure (7.7): Reduced Dynamic Solution for stand alone simulated GPS receiver (IGS Rapid GPS Orbits) (0ne day arc)

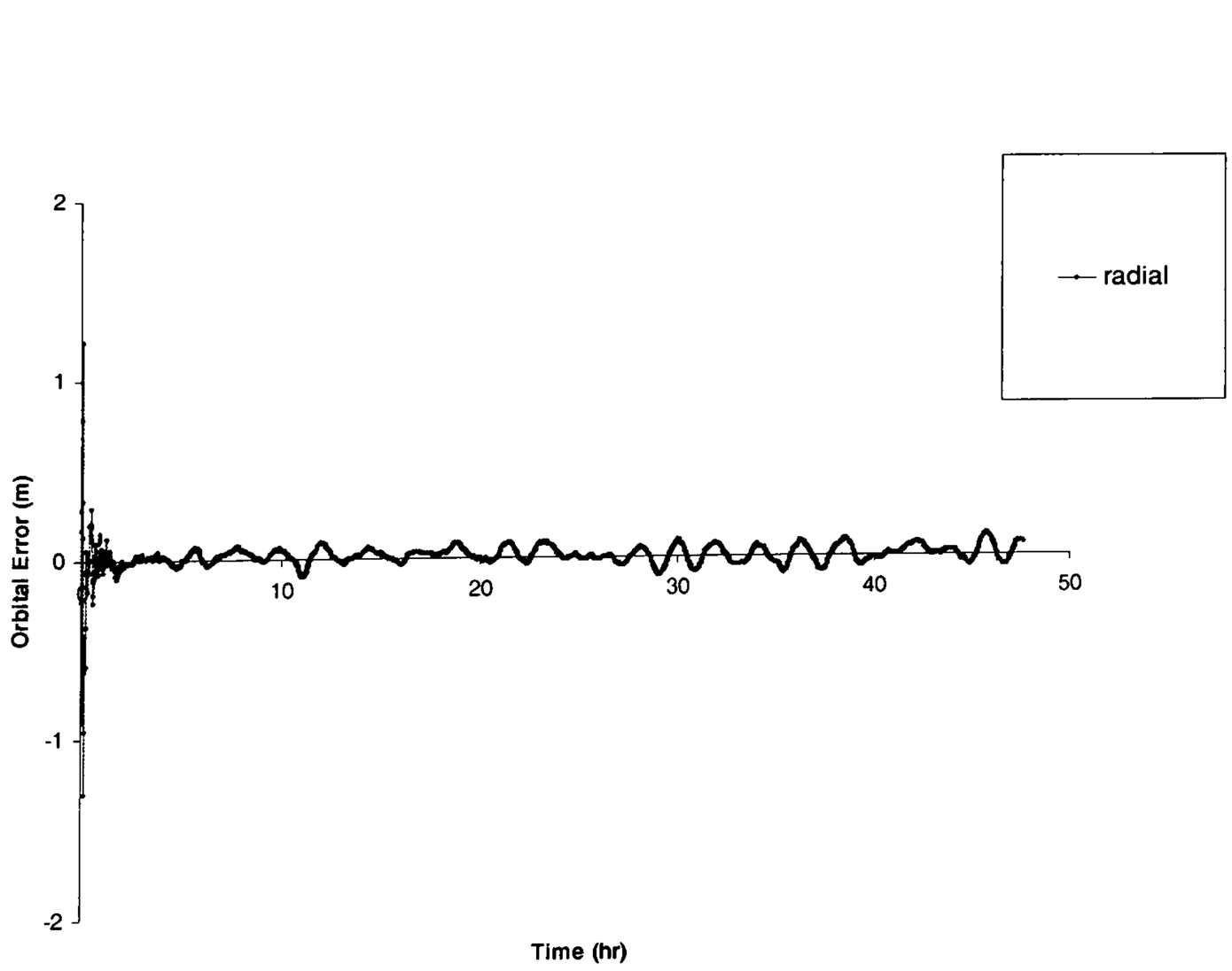

Figure (7.6): Reduced Dynamic Solution for Standalone simulated GPS receiver (IGS Rapid GPS Orbits) (two day arc)

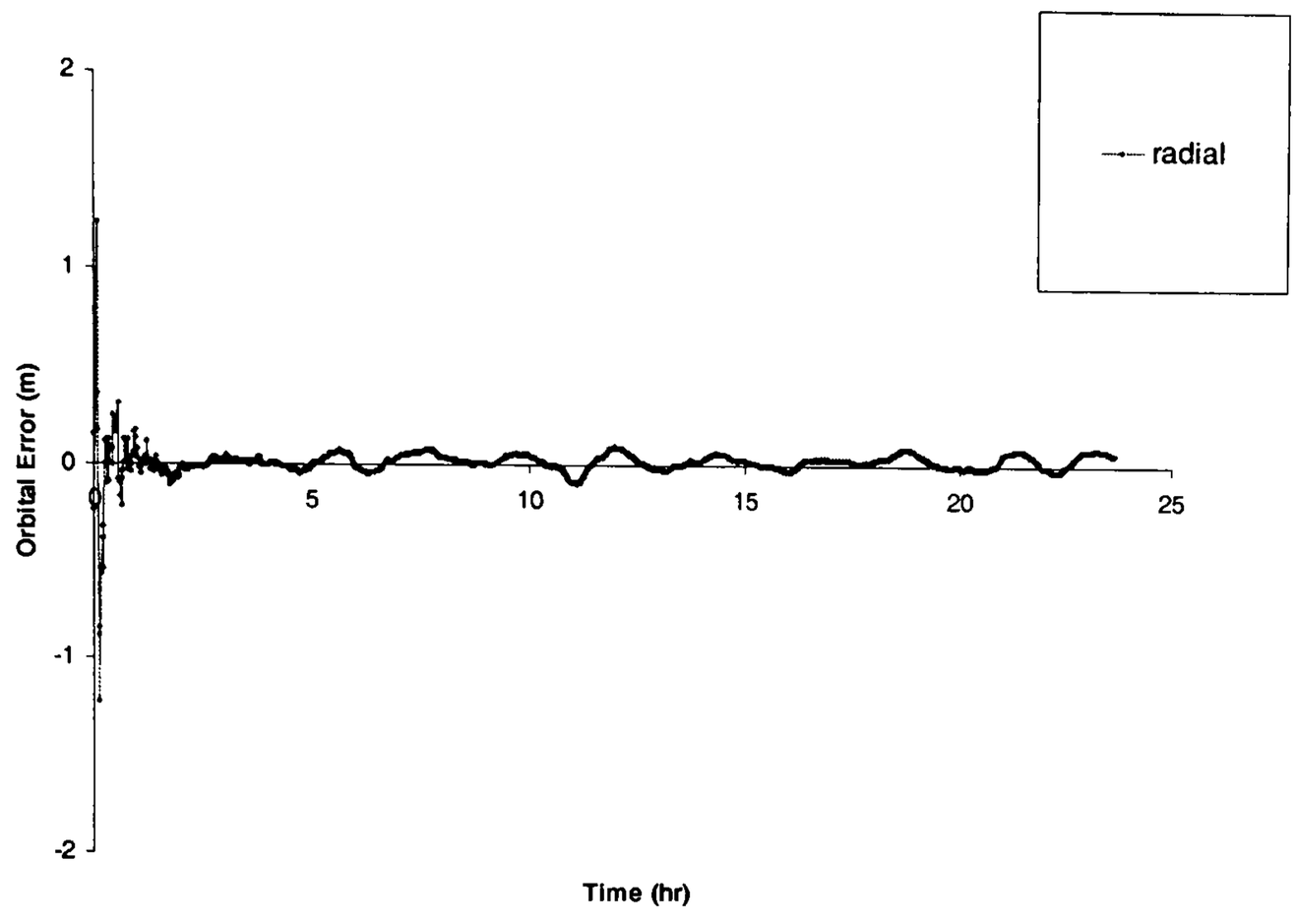

Figure (7.7): Reduced Dynamic Solution for stand alone simulated GPS receiver (Precise Ephemeris)(IGS Final Orbits) (one day arc)

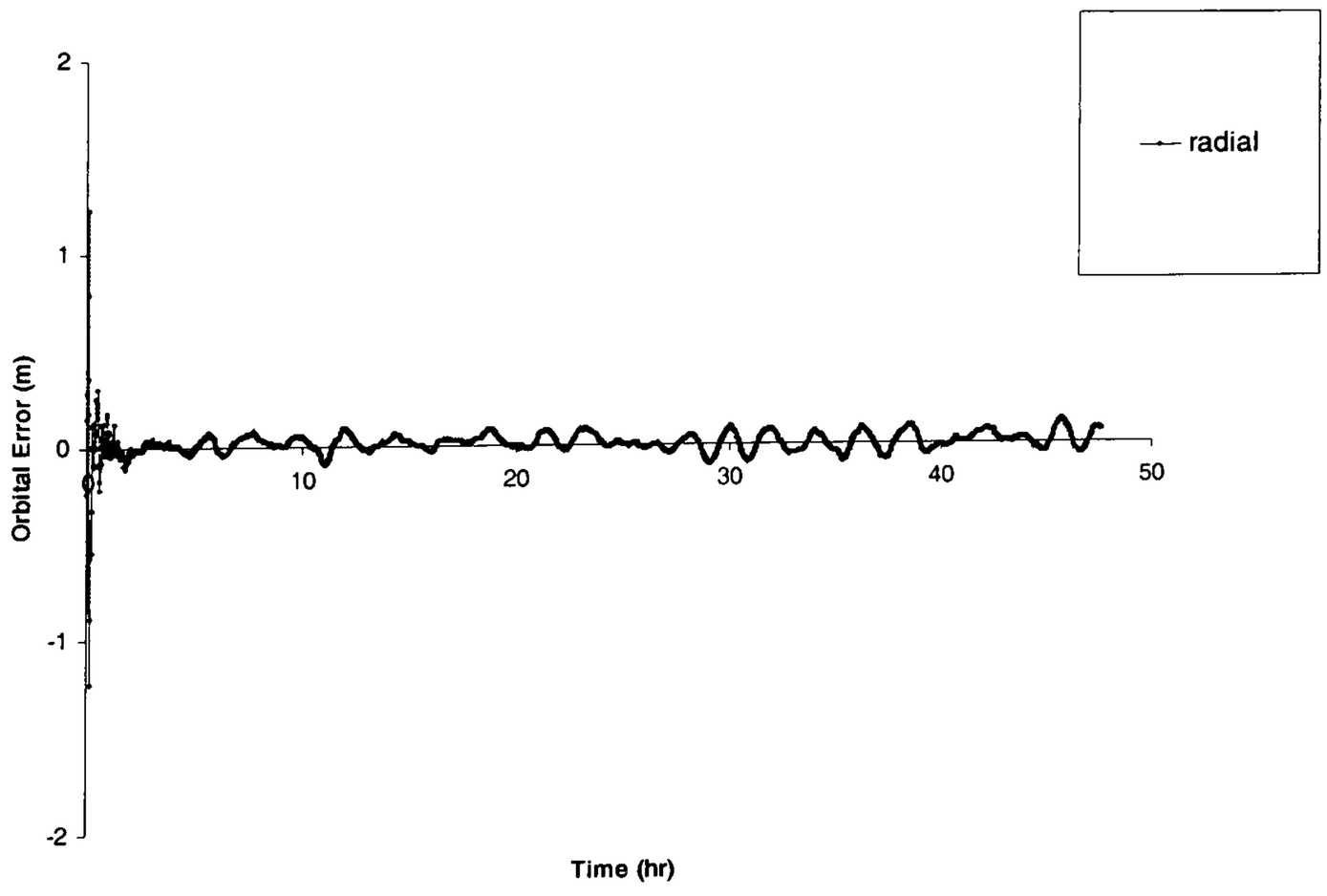

Figure (7.8) : Reduced Dynamic Solution for Standalone simulated GPS receiver (Precise Ephemeris) (IGS Final Orbits) (two day arc)

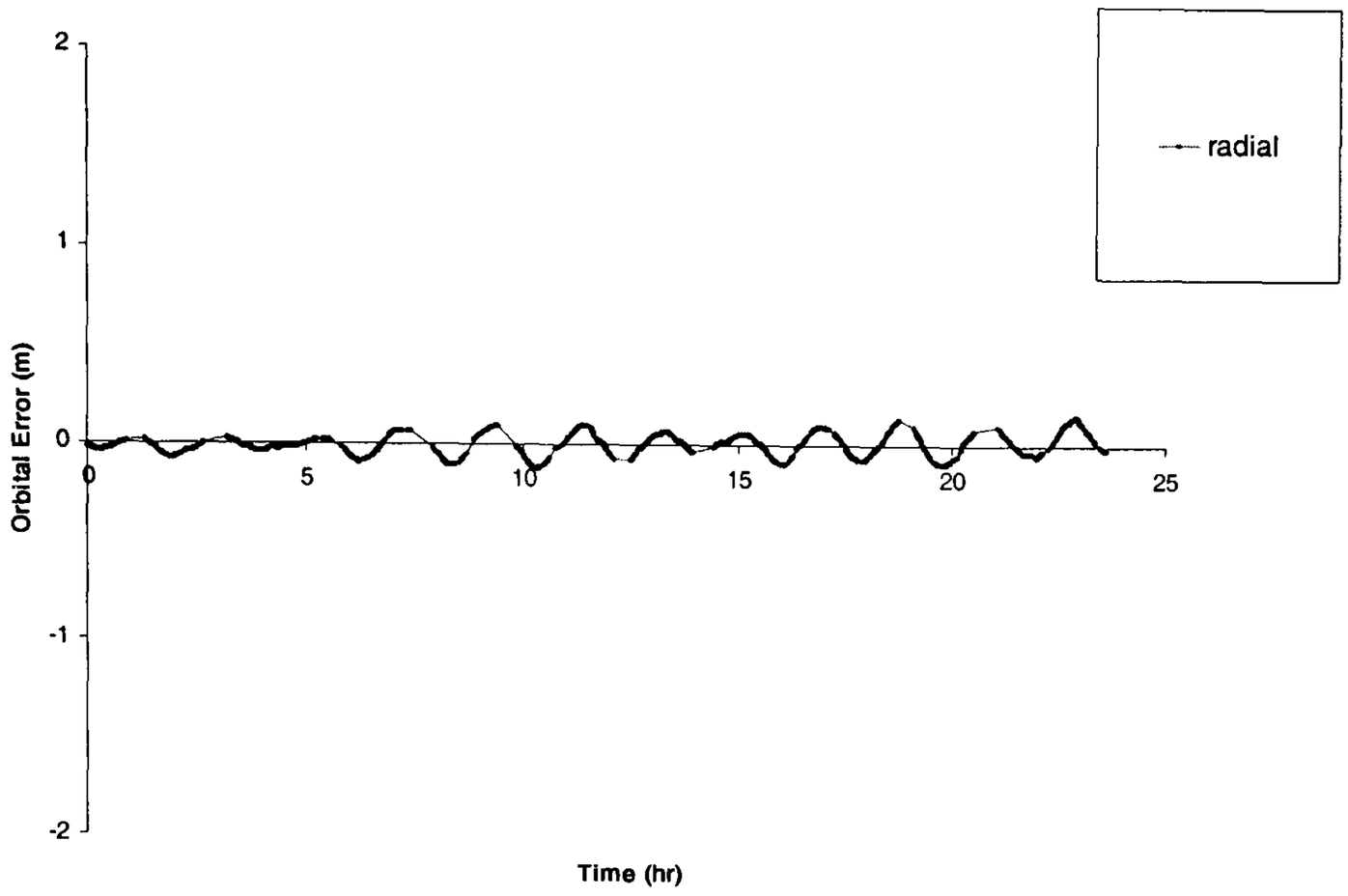

Figure (7.9): Reduced Dynamic Solution for stand alone GPS receiver (Real Data) (one day arc)

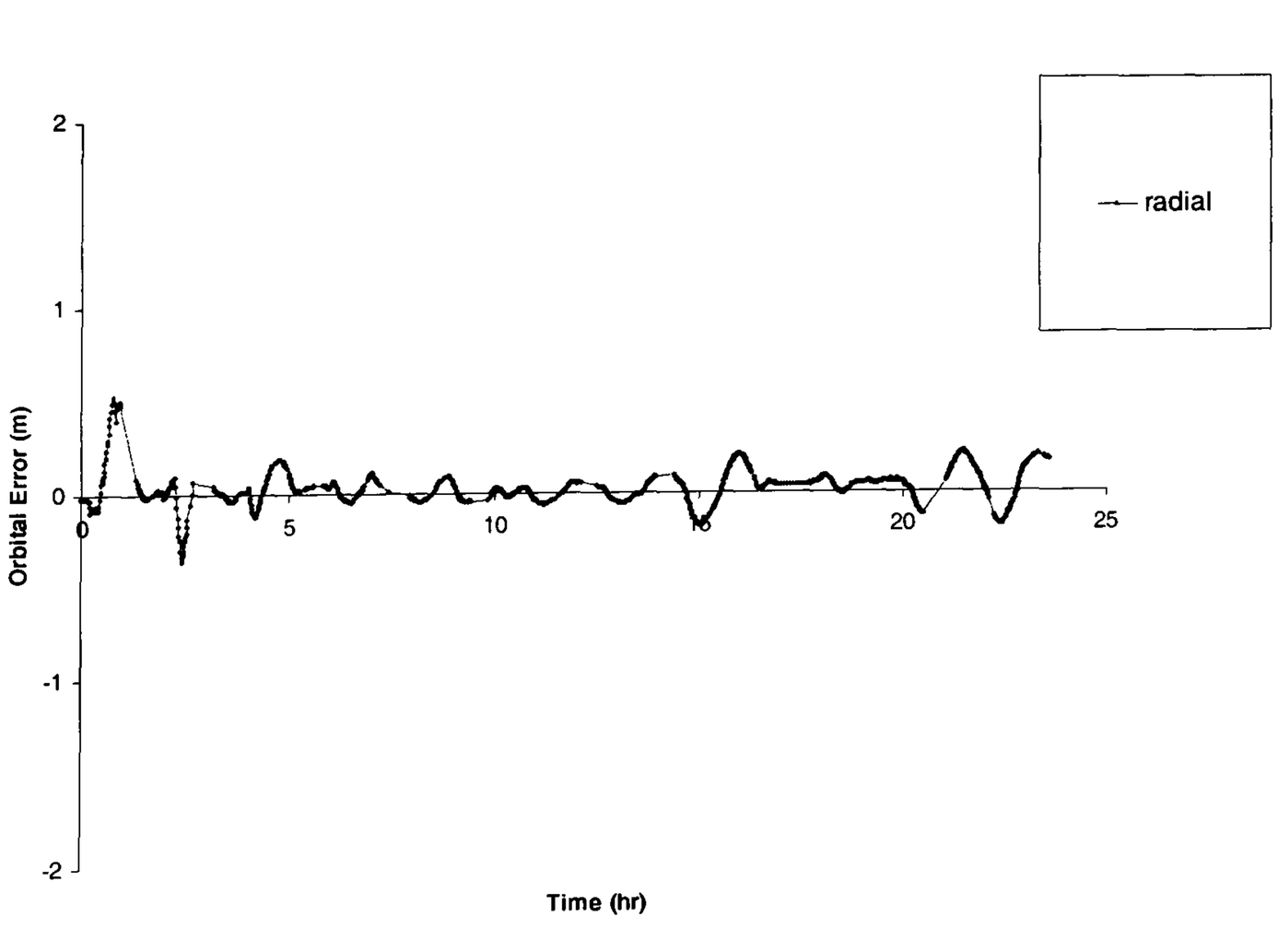

Figure (7.10): Reduced Dynamic Solution for stand alone GPS receiver (Simulated Data) (one day arc)

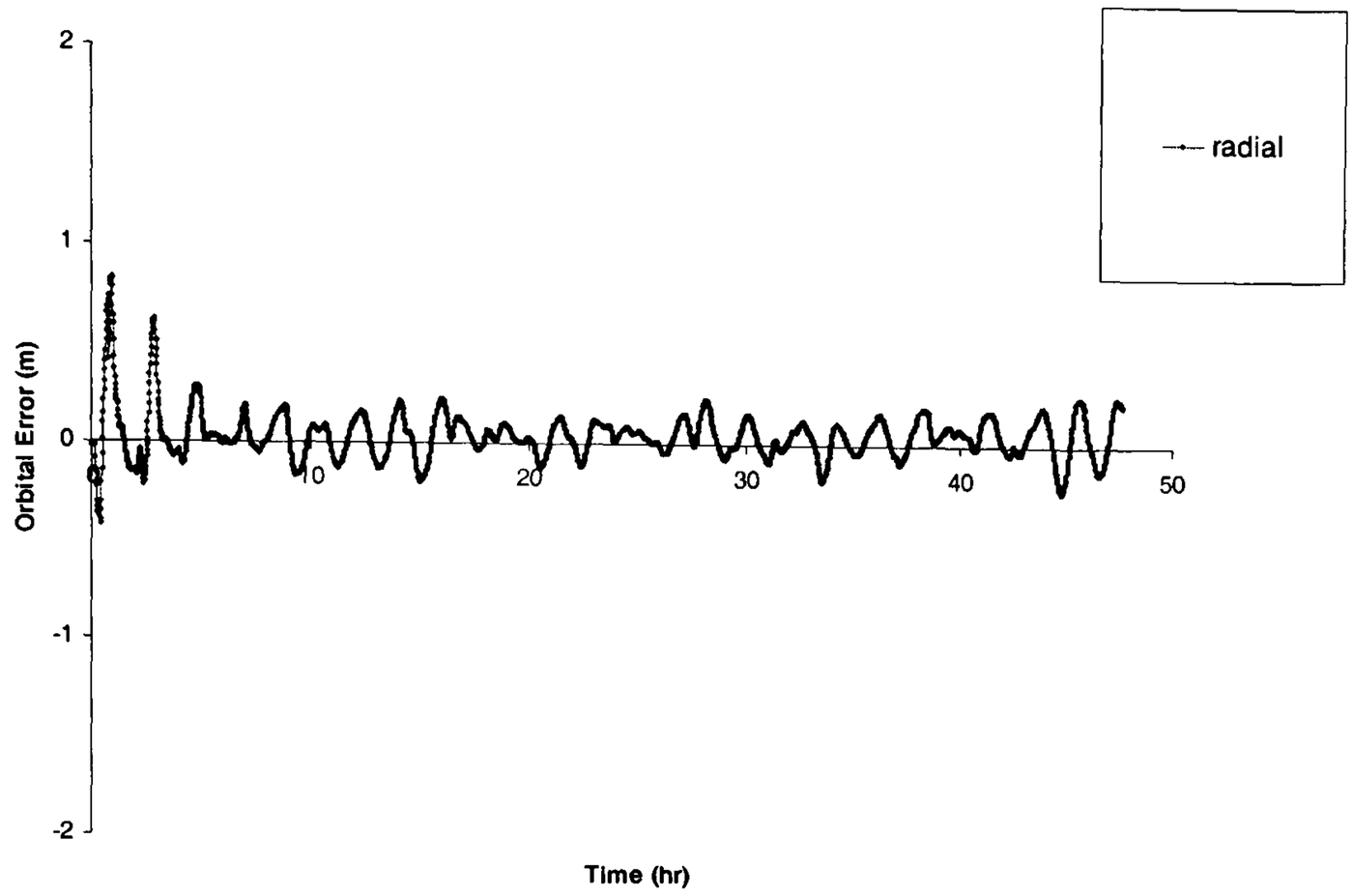

Figure (7.12): Reduced Dynamic Standalone Solution for simulated GPS receiver

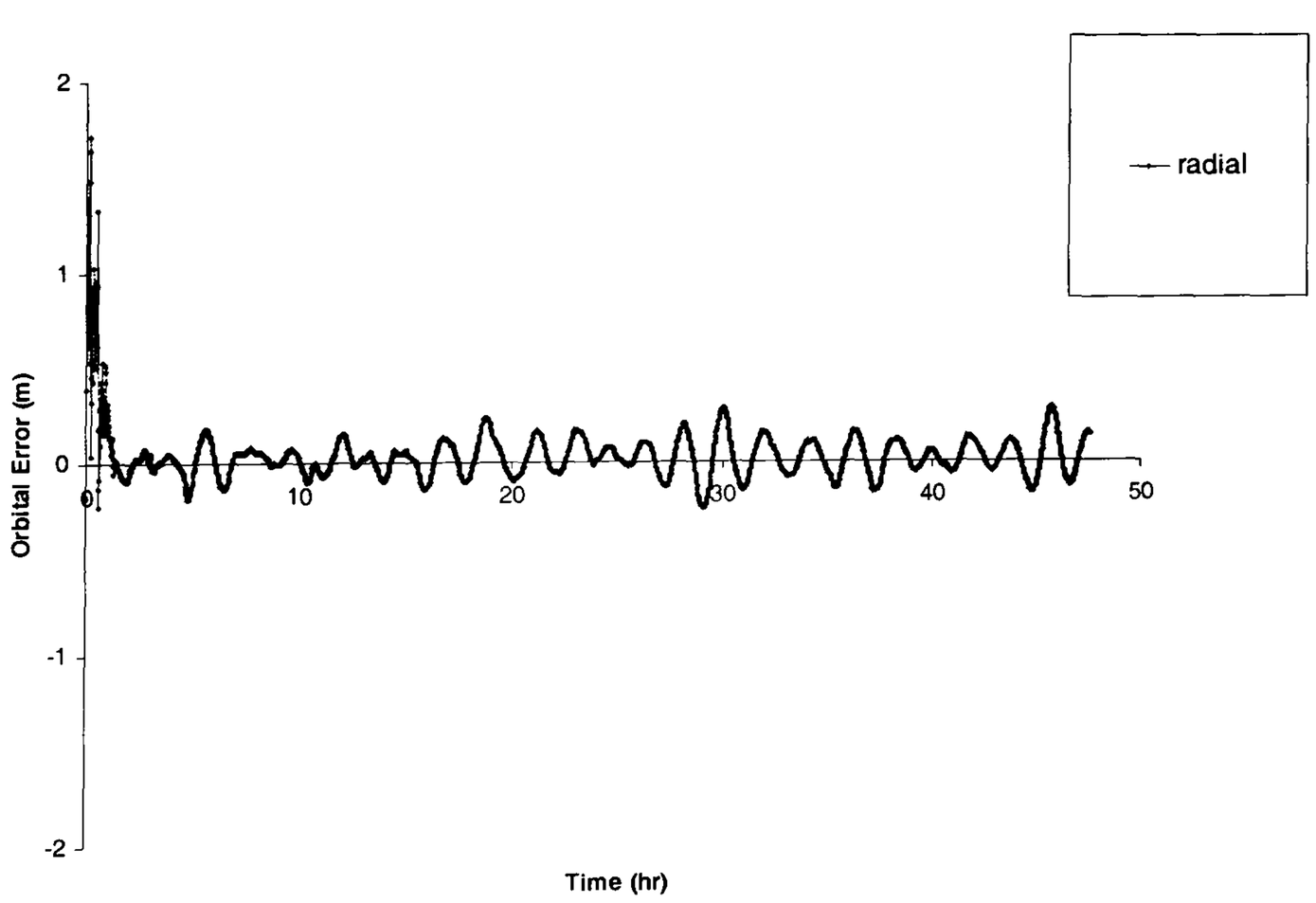

Figure (7.13): Reduced Dynamic Differential Pseudo-range Solution for simulated GPS receiver

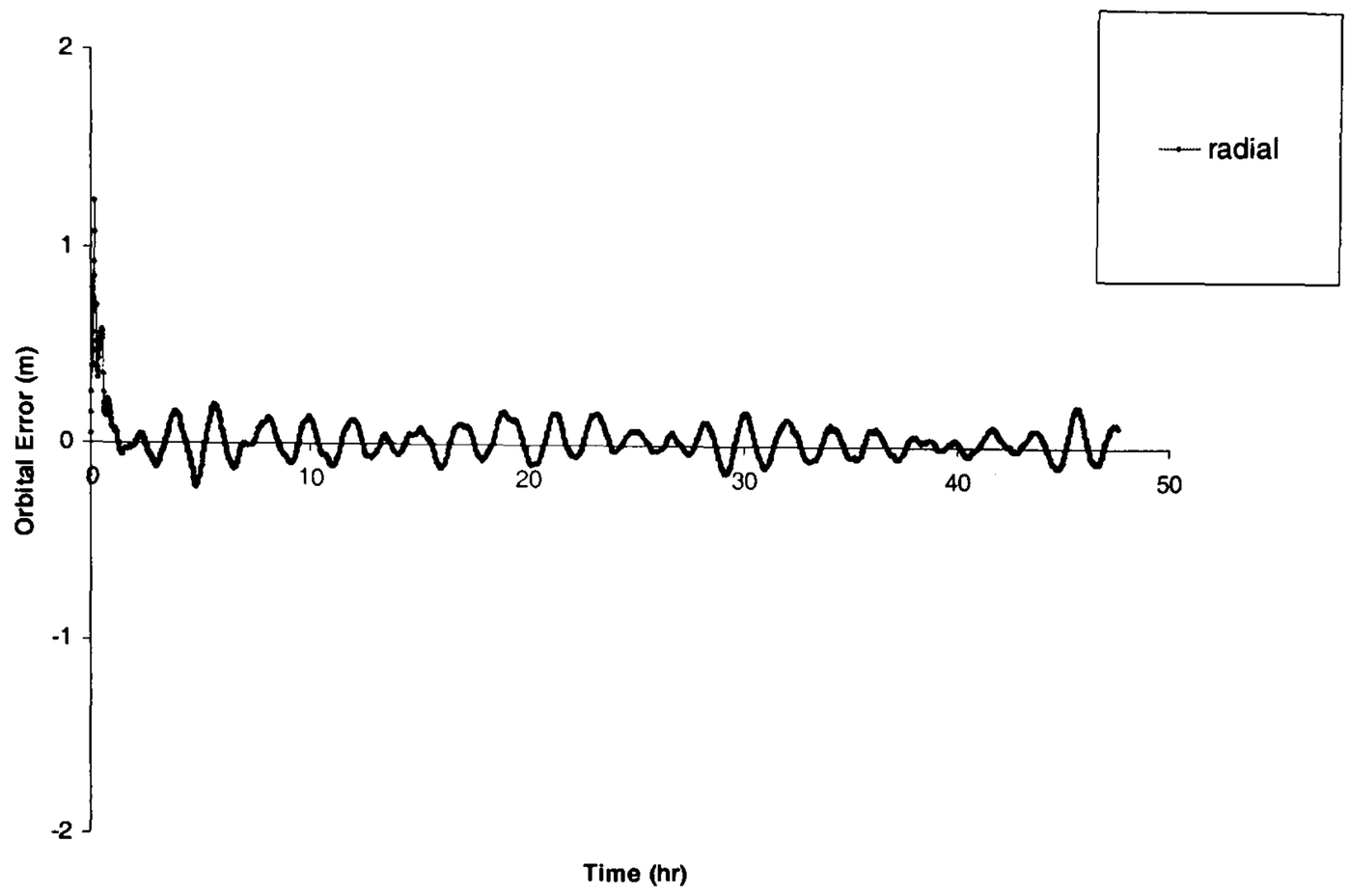

Figure (7.14): Reduced Dynamic Differential Carrier-phase Solution for simulated GPS receiver

Figure (7.15): Reduced Dynamic Standalone Solution for simulated GALILEO receiver

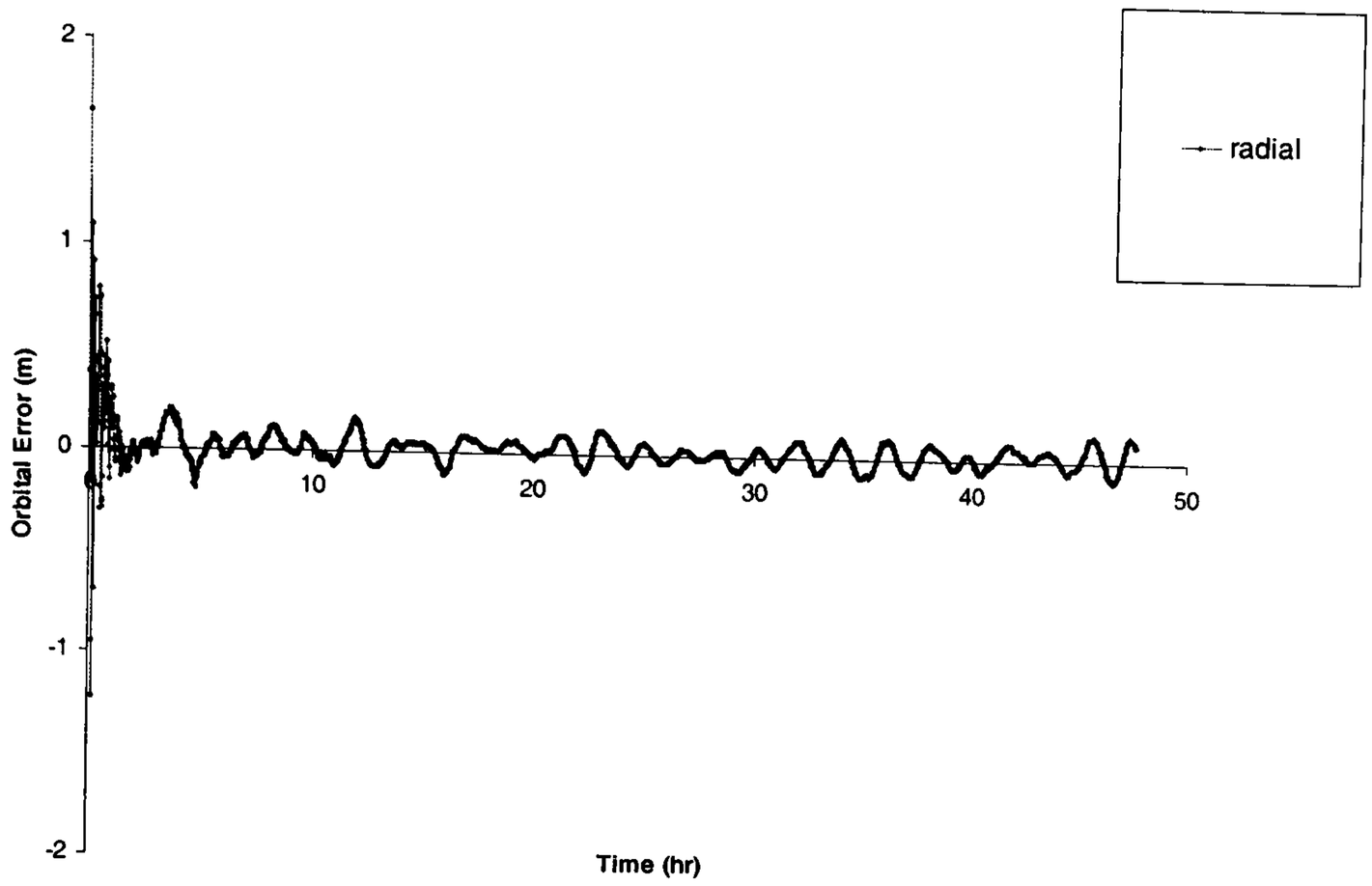

Figure (7.16): Reduced Dynamic Differential Pseudo-range Solution for simulated GALILEO receiver

Figure (7.17): Reduced Dynamic Differential Carrier-phase Solution for simulated GALILEO receiver

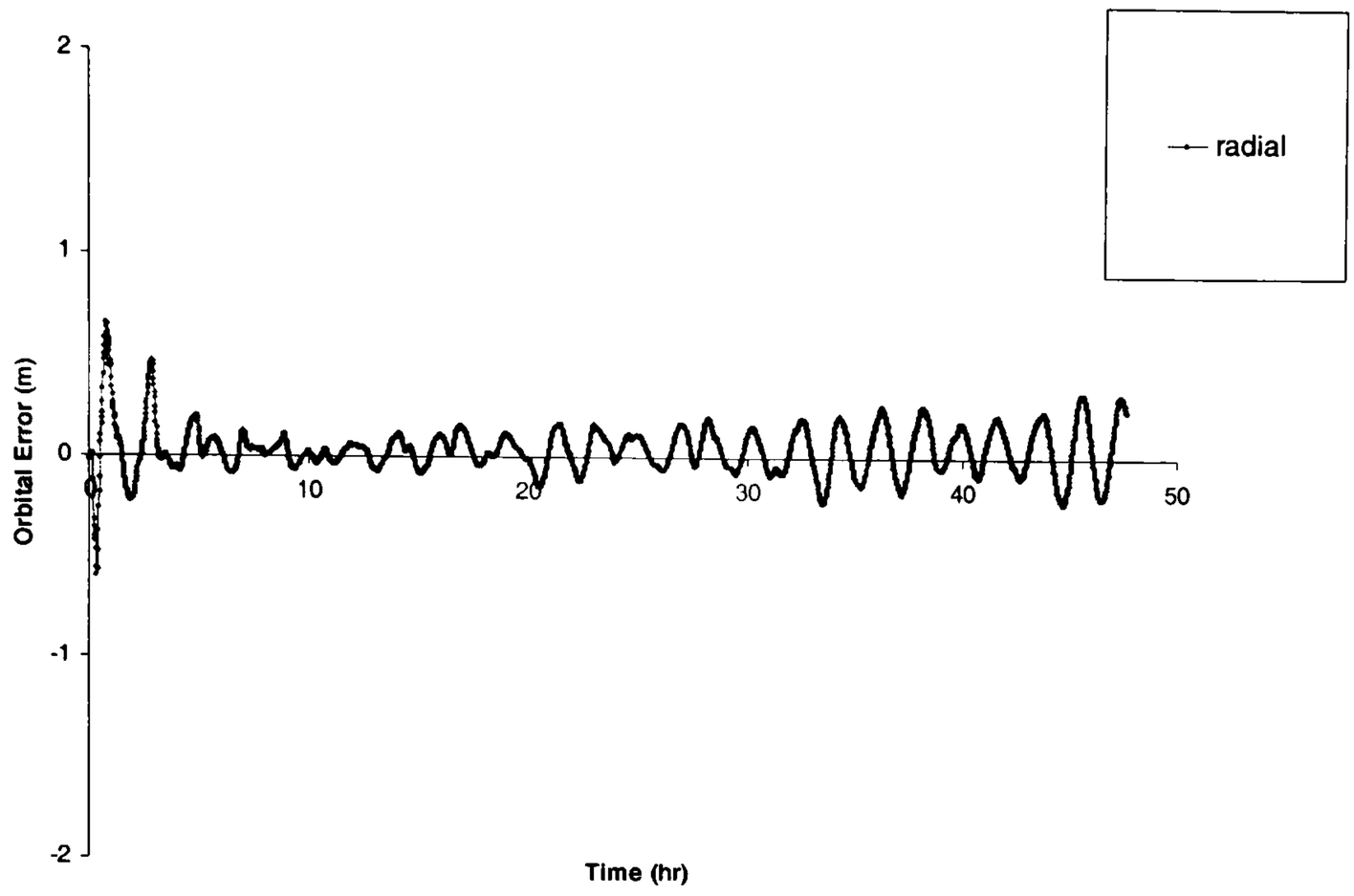

Figure (7.18): Reduced Dynamic Standalone Solution for simulated Combined GPS/GALILEO receiver

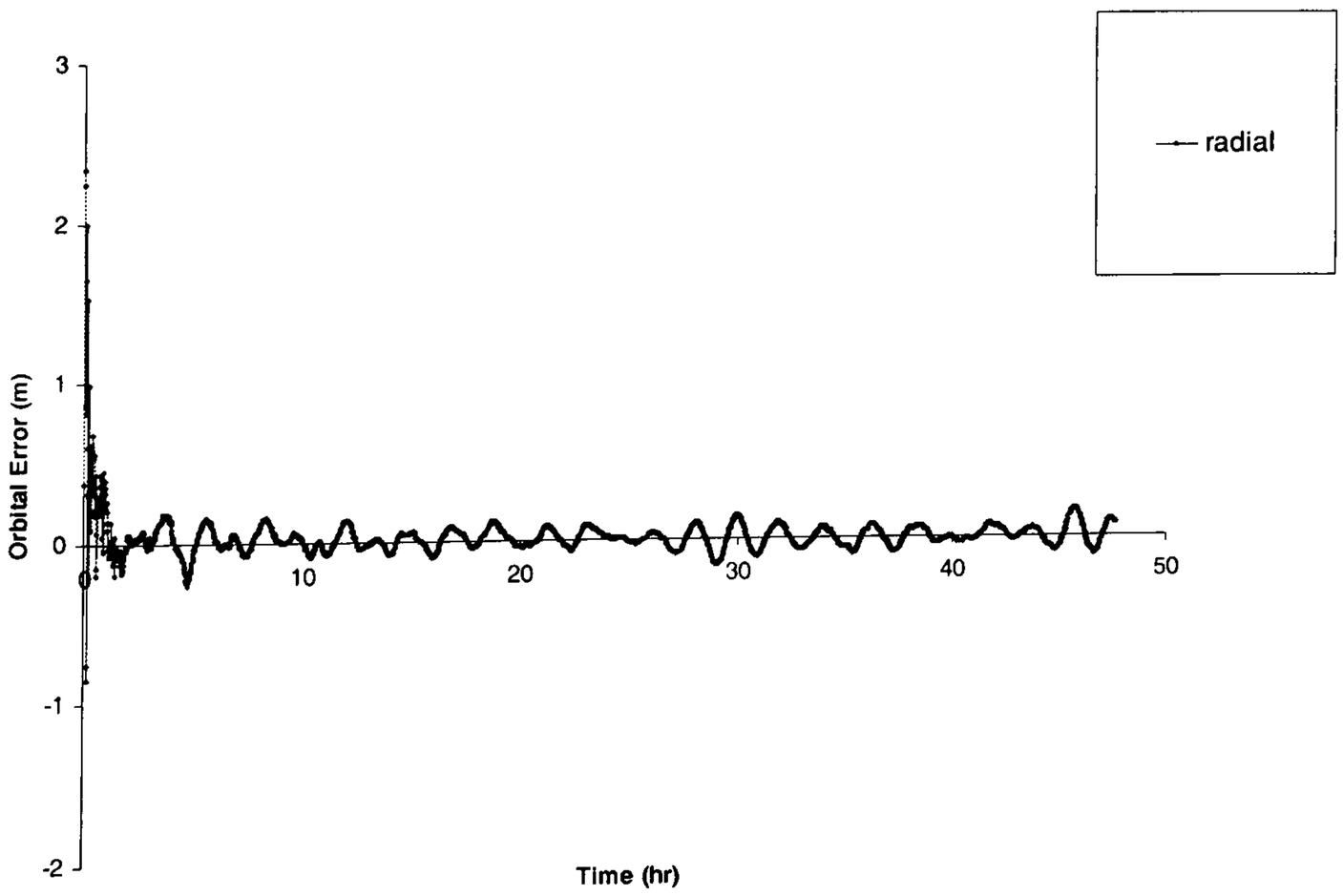

Figure (7.19): Reduced Dynamic Differential Pseudo-range Solution for simulated Combined GPS/GALILEO receiver

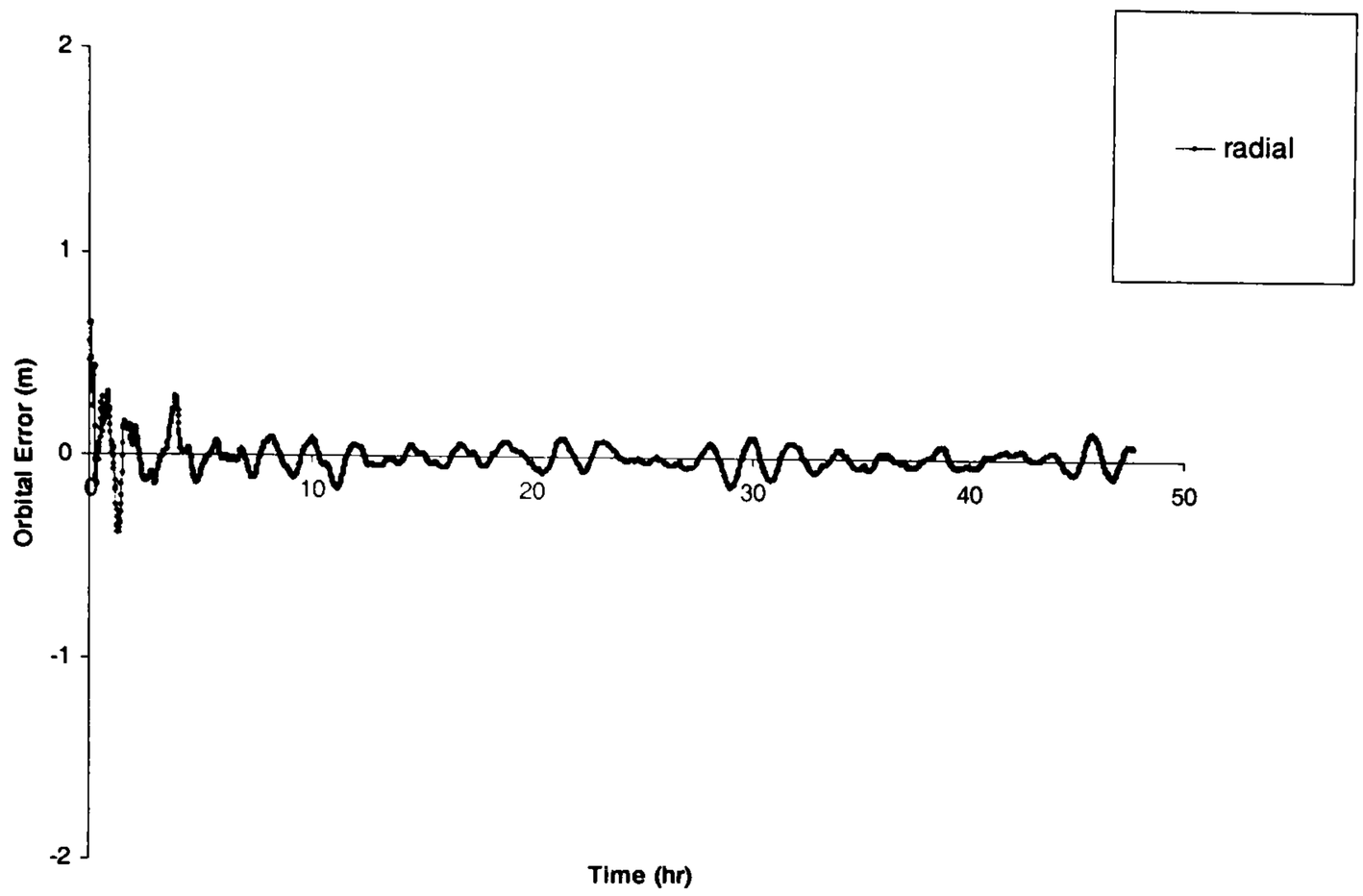

Figure (7.20): Reduced Dynamic Differential Carrier phase Solution for simulated Combined GPS/GALILEO receiver

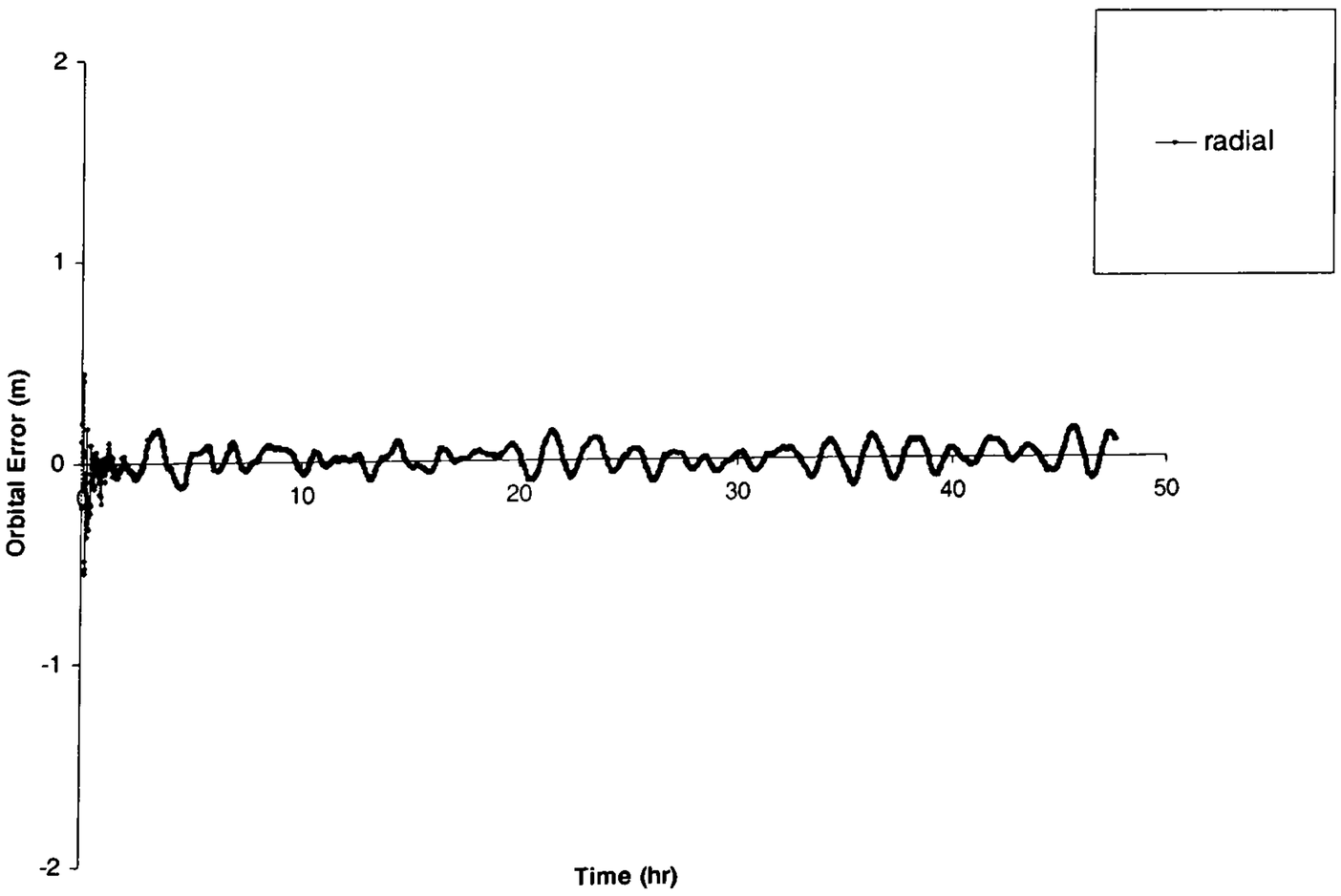

Figure (7.21): Reduced Dynamic Standalone Solution for simulated GPS-modernised/GALILEO receiver

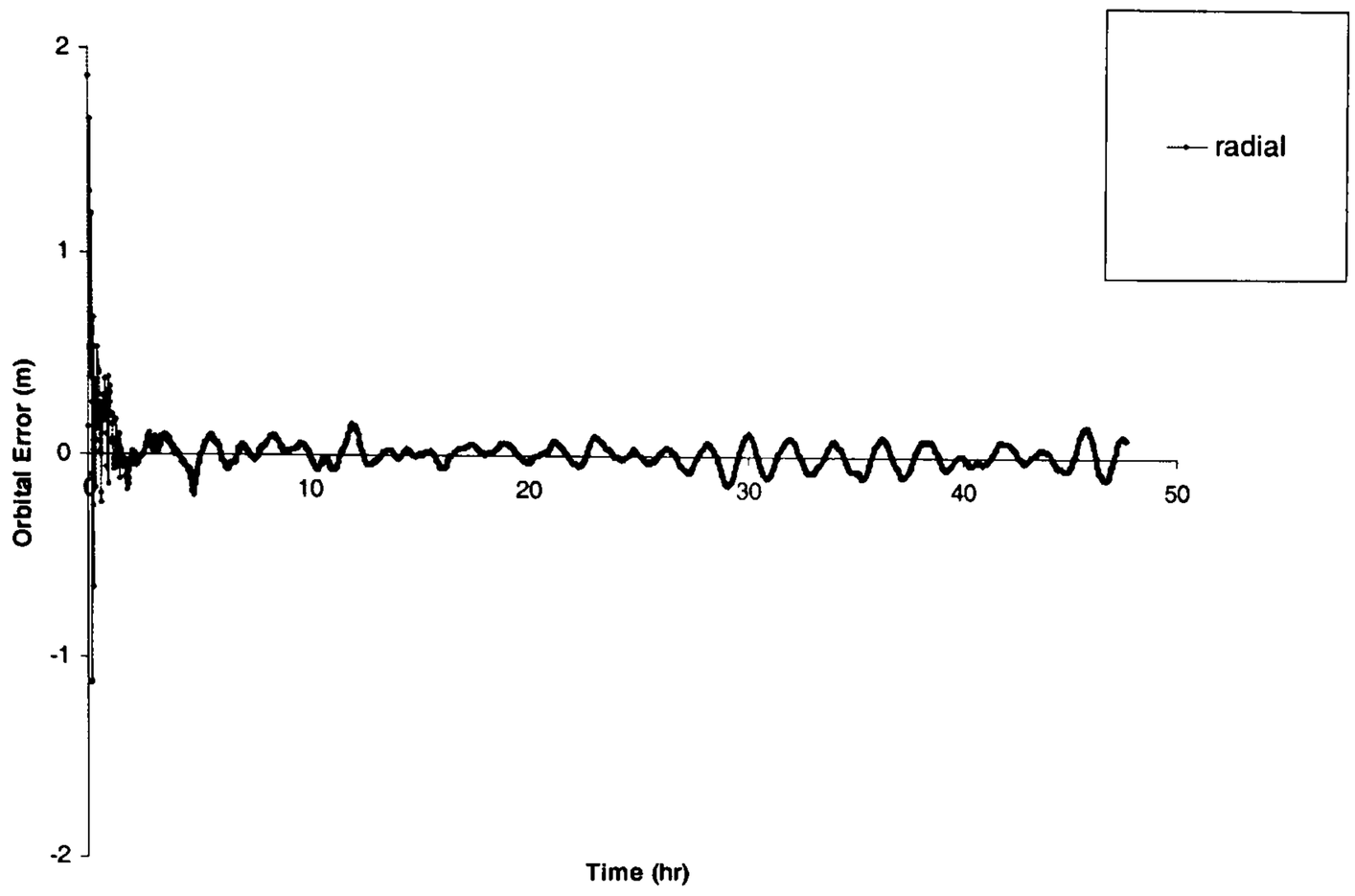

Figure (7.22): Reduced Dynamic Differential Pseudo-range Solution for simulated GPS-modernised/GALILEO receiver

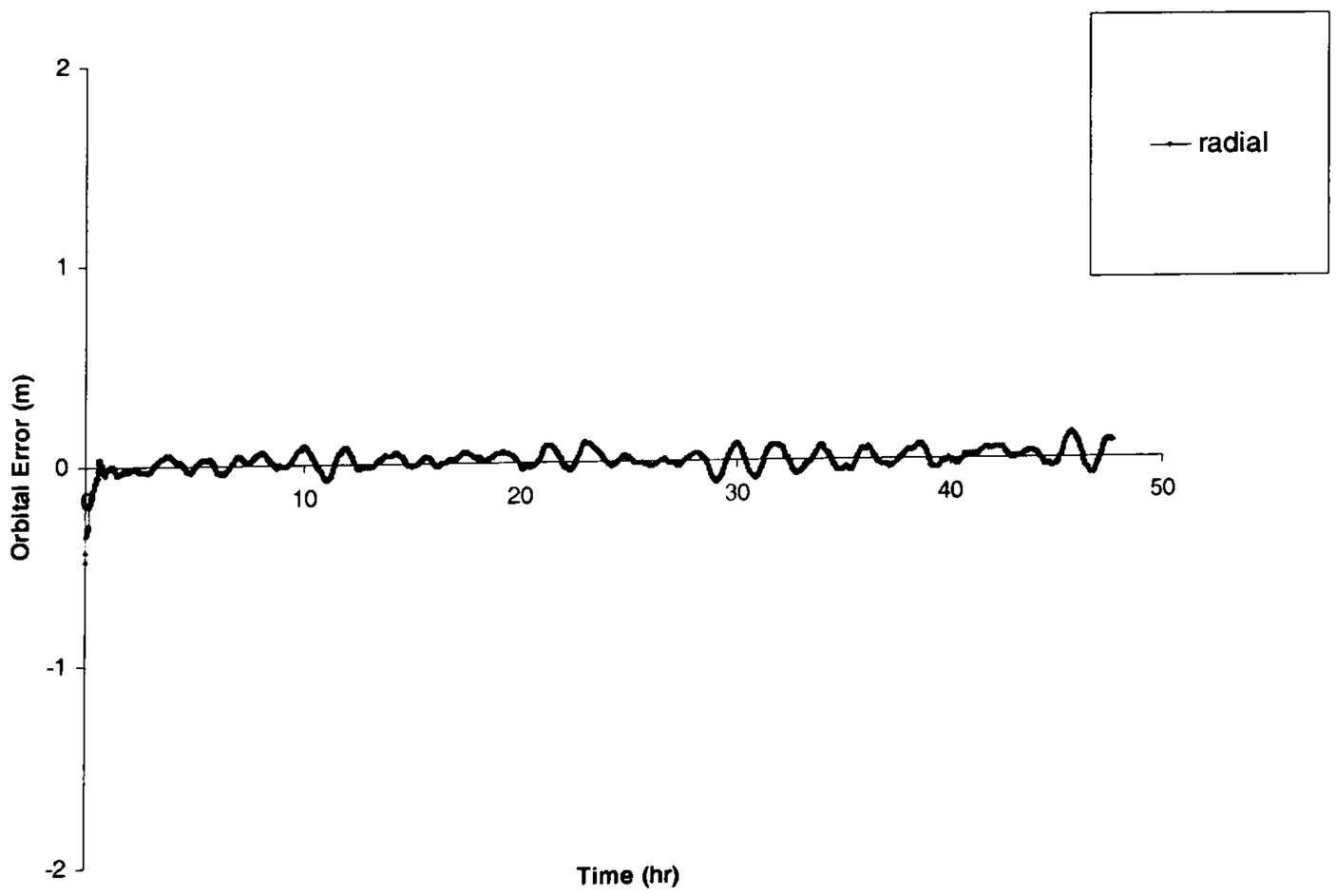

Figure (7.23): Reduced Dynamic Differential Carrier phase Solution for simulated GPS-modernised/GALILEO receiver

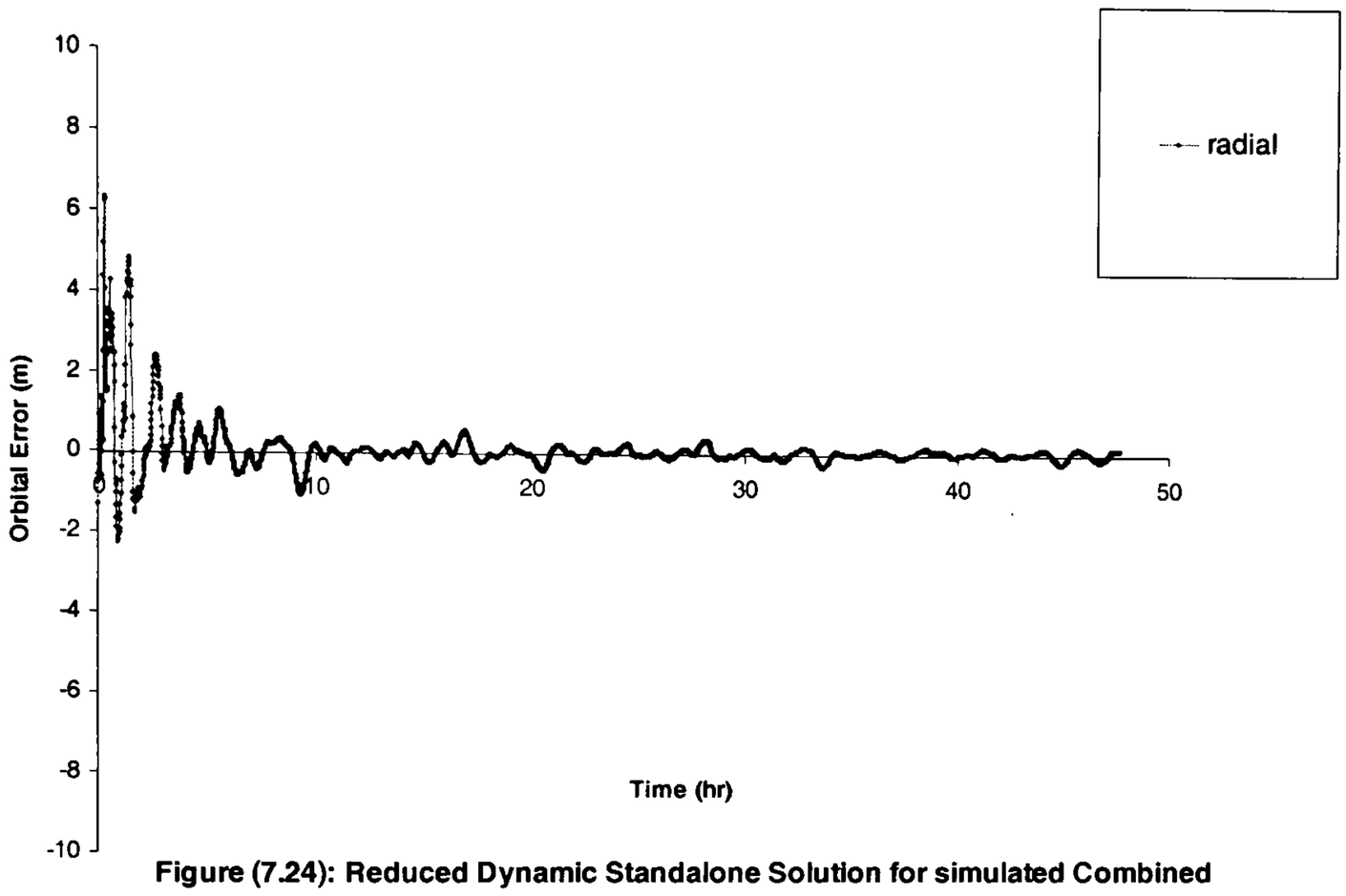

Figure (7.24): Reduced Dynamic Standalone Solution for simulated Combined GPS/GALILEO receiver (21/7/2002-22/7/2002) (Weight towards Observations)

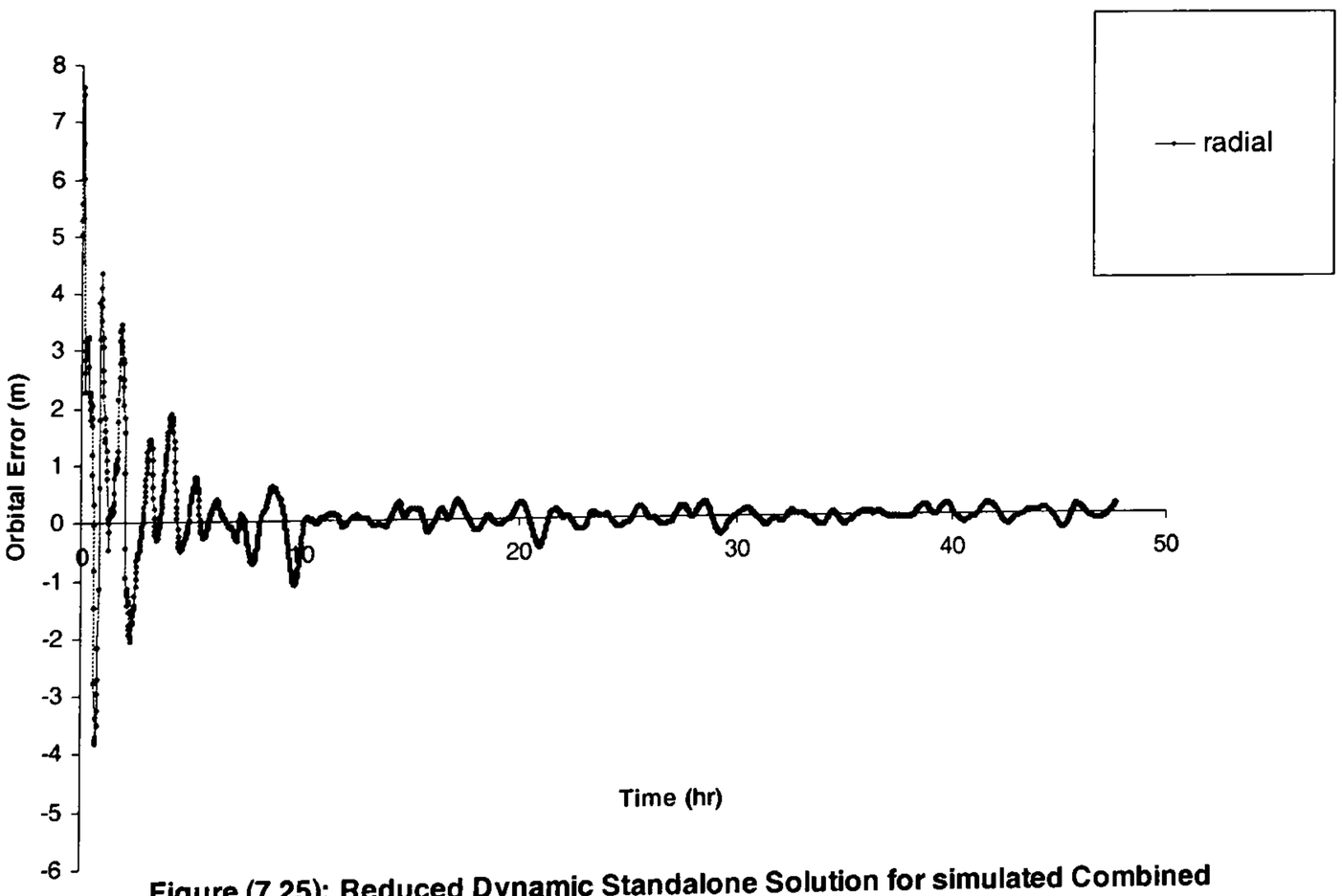

Figure (7.25): Reduced Dynamic Standalone Solution for simulated Combined GPS/GALILEO receiver (22/7/2002-23/7/2002) (Weight towards Observations)

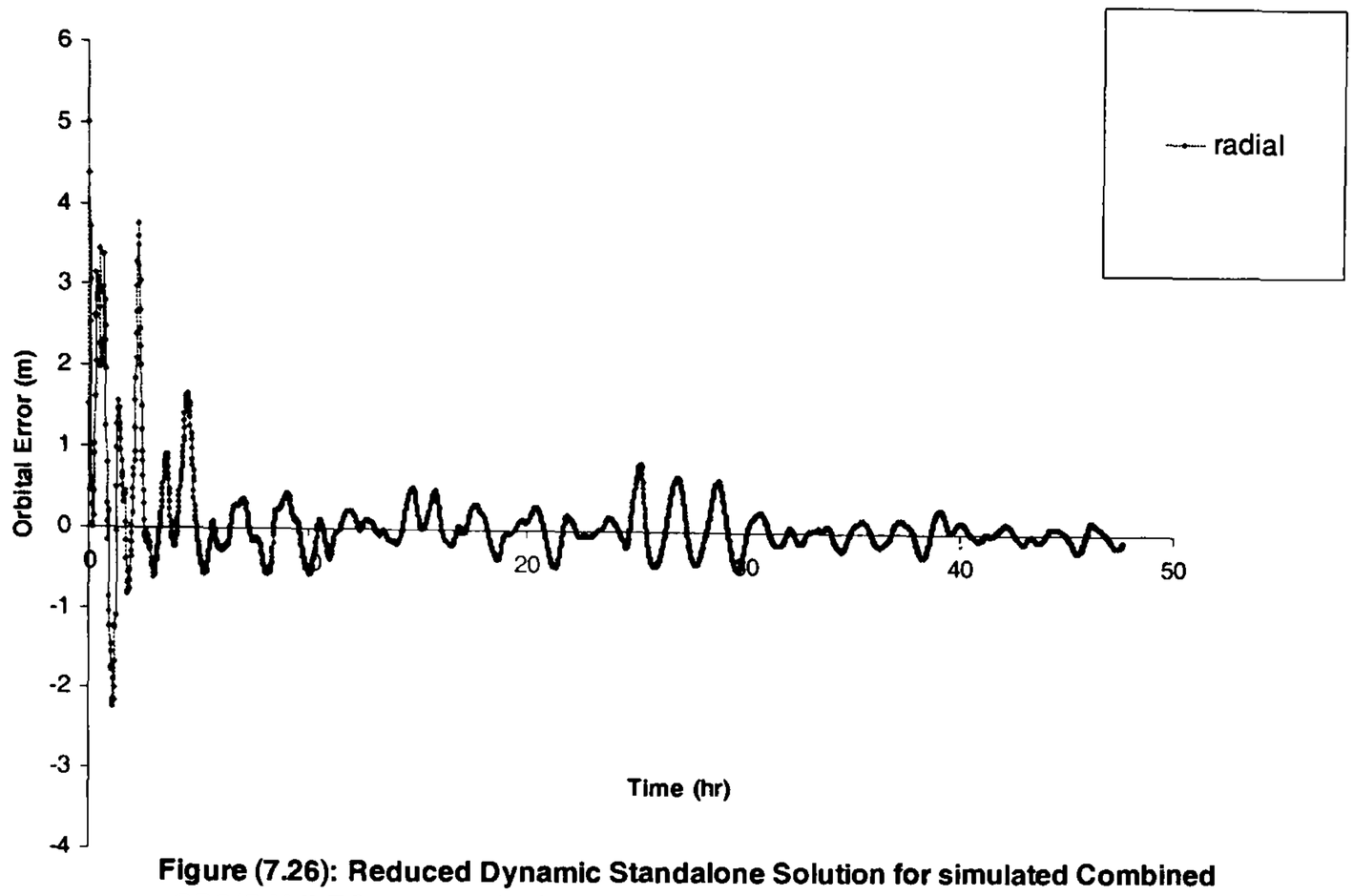

Figure (7.26): Reduced Dynamic Standalone Solution for simulated Combined GPS/GALILEO receiver (23/7/2002-24/7/2002) (Weight towards Observations)

Figure (7.27): Reduced Dynamic Standalone Solution for simulated Combined GPS/GALILEO receiver (21/7/2002-22/7/2002)

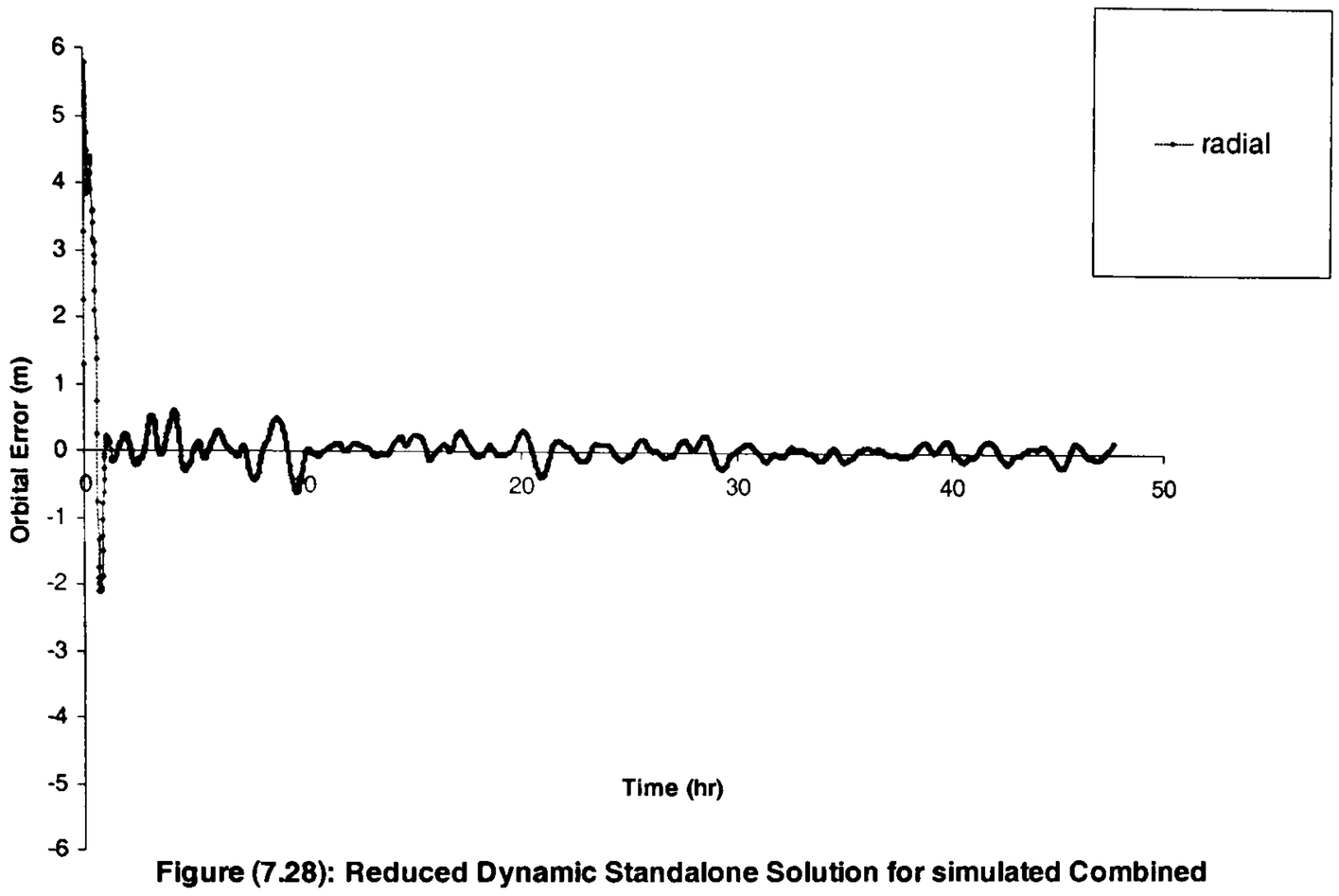

Figure (7.28): Reduced Dynamic Standalone Solution for simulated Combined GPS/GALILEO receiver (22/7/2002-23/7/2002)

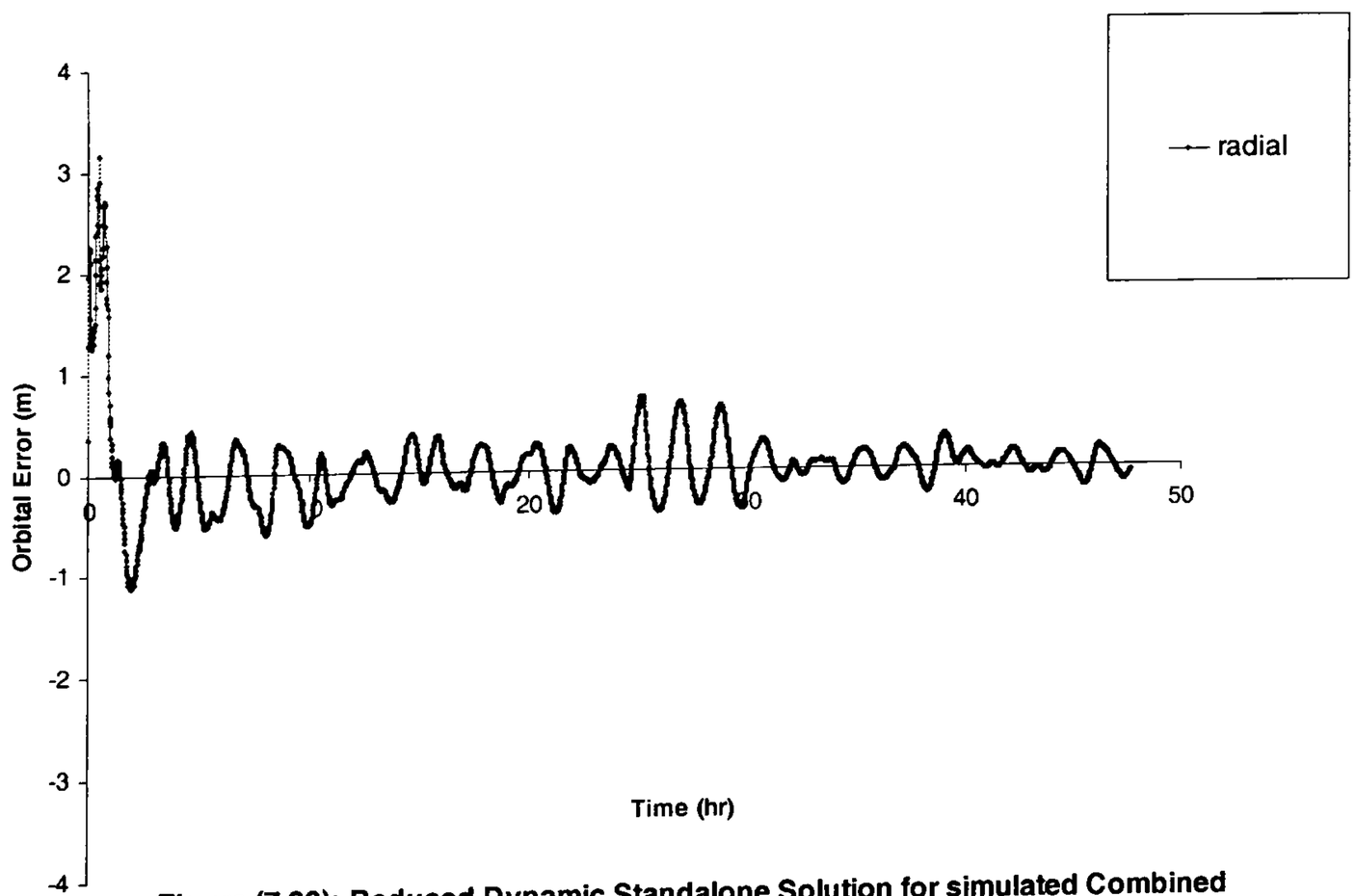

Figure (7.29): Reduced Dynamic Standalone Solution for simulated Combined GPS/GALILEO receiver (23/7/2002-24/7/2002)

APPENDIX H

Publications Based on the Author's Research

Farah, A., (2002). The Ionospheric Delay Effort for GPS Single-frequency Users-Analysis Study for Simulation Purposes. Proceeding of ION GPS-02, The 15th International Meeting of the Satellite Division of the American Institute of Navigation. Portland, Oregon, USA. September (24-27). *(Best Student Sponsored Paper)*

Farah, A., (2002). Ionospheric-Delay Simulation Study for GPS Single-Frequency Users. The 2002 International Symposium on GPS/GNSS. Wuhan, China, November 6 - 8.

Farah, A., Moore, T. and Hill, C. (2003). High Spatial Variation Tropospheric Model for GPS-Data Simulation. Proceeding of ION GPS-03, The 16th International Meeting of the Satellite Division of the American Institute of Navigation. Portland, Oregon, USA. September (9-12).

Farah, A., (2003). A New Ionospheric Delay model for GPS Single-Frequency Data Simulation. 1st International Conference of Civil Engineering Science ICCES1, Assiut University, Assiut, EGYPT, October (7-8).

Farah, A., (2003). A Light on: GPS/GALILEO Data Simulation. The 2003 International Symposium on GPS/GNSS. Tokyo, Japan, November 15 - 18.

Farah, A., (2003). EGNOS Tropospheric Model For GPS-Data Simulation. The 2003 International Symposium on GPS/GNSS. Tokyo, Japan, November 15 - 18.

Farah, A., Moore, T. and Hill, C. (2004). LEO Orbit Determination by GNSS. Proceeding of GNSS-04, The 8th GNSS International Symposium. Rotterdam, Netherlands. May (17-19).